

Simulation of Diffusion in Nanocrystalline Materials: Continuum Approach

Von der Fakultät Chemie der Universität Stuttgart zur Erlangung der
Würde eines Doktors der Naturwissenschaften (Dr. rer. nat.)
genehmigte Abhandlung

Vorgelegt von

Deniss Grjaznovs

aus Riga, Lettland

Max-Planck-Institut für Festkörperforschung, Stuttgart

Universität Stuttgart

2006

Simulation of Diffusion in Nanocrystalline Materials: Continuum Approach

Von der Fakultät Chemie der Universität Stuttgart zur Erlangung der
Würde eines Doktors der Naturwissenschaften (Dr. rer. nat.)
genehmigte Abhandlung

Vorgelegt von

Deniss Grjaznovs

aus Riga, Lettland

Hauptberichter:	Prof. Dr. Joachim Maier
Mitberichter:	Prof. Dr. Ir. Eric Jan Mittemeijer
Mitprüfer und Prüfungsvorsitzender:	Prof. Dr. Emil Roduner

Tag der mündlichen Prüfung: 20.09.2006

Max-Planck-Institut für Festkörperforschung, Stuttgart

Universität Stuttgart

2006

To my family

Acknowledgements

This dissertation has been written at the Max Planck Institute for Solid State Research (Stuttgart) in the department of Prof. Dr. J. Maier. I would like to thank Prof. J. Maier for giving me the great opportunity to be a PhD student in his department. I would like to thank Prof. J. Maier for being my supervisor and for many valuable discussions before and during writing the dissertation. I thank Prof. J. Maier for the care with which he reviewed the original manuscript of the dissertation. Without his important suggestions the dissertation could not have been in this final form.

I would like to express my thanks to Prof. Dr. Ir. E. J. Mittemeijer and Prof. Dr. E. Roduner for accepting my request for being examiners for this work.

I am particularly grateful to Prof. Dr. J. Fleig, who was the first who involved me in the finite element analysis. Discussions with him were particularly important during the initial stages of my work at the Max Planck Institute. His skills to really distinguish positive and negative aspects of the problem still surprise me. I also thank Jürgen for continuous support and many valuable suggestions.

I would like to thank Jacques Morandini, from Simulog, who provided me help in using FLUX-EXPERT in a very beginning of my work with this program and clarified my understanding of some aspects of the finite element analysis.

I would also like to express my gratitude to Dr. R. De Souza (RWTH Aachen), Prof. Dr. D. L. Beke (University of Debrecen), Prof. Dr. V. Kuzovkov (Institute for Solid State Physics in Riga) and Prof. Dr. J. Kalnin (Institute for Solid State Physics in Riga) for having interest in my results, for careful reading my posters presented in the conferences and for interesting discussions on diffusion problems.

I would like to thank Dr. R. Merkle for careful reviewing the german part of the dissertation and Prof. Dr. E. Kotomin, who reviewed the manuscript of the dissertation and provided important comments and suggestions.

Special thanks go to Uwe Traub for providing continuous support in the computer problems and Sofia Weiglein for helping in different problems concerning documents, registrations and PhD students.

I am also greatly indebted to my wife, Jana Lubnevskaja, who assisted me during my stay in Stuttgart. She supported me by a good advice or by simply believing in me. I could not have finished this dissertation without her encouragement and patience. Her contribution to writing the german part of my dissertation is invaluable. I should say ,Thank You‘.

Table of Contents

Symbols and Abbreviations.....	xi
Introduction.....	1
Chapter I. The classical grain boundary diffusion models.....	5
Introduction.....	5
1.1 Grain boundary model. Guggenheim or Fisher?.....	6
1.1.1 Isolated grain boundary model.....	7
1.1.2 Mathematical description of grain boundary diffusion in the isolated grain boundary model.....	8
1.1.3 Transformations made to obtain Fisher's system.....	9
1.1.4 An alternative derivation of Fisher's system.....	12
1.1.5 Whipple's solution.....	13
1.2 Diffusion kinetic regimes.....	14
1.3 Deducing the grain boundary diffusivity from the diffusion profile.....	21
Chapter II. Finite Element Model.....	27
Introduction.....	27
2.1 General aspects with respect to continuum problems.....	28
2.2 Fisher's system expressed in the form suitable for finite element calculation.....	28
2.2.1 Finite element method formulation of space charge layer problem.....	30
2.3 Finite element calculation by using FLUX-EXPERT.....	32
Chapter III. Nonlinearity effect.....	35
Introduction.....	35
3.1 Important definitions.....	35
3.1.1 The C- or B-regime?.....	36
3.2 Integrating Whipple's solution.....	36
3.3 Errors in determining the grain boundary diffusivity.....	43
3.3.1 Nonlinearity and small values of dimensionless parameter w	50
3.3.2 Analyzing the errors of using Le Claire's constant.....	54

3.4	Discussing new procedures for finding the grain boundary diffusivity.....	59
3.4.1	An analytical expression for $\partial \ln C_{av} / \partial w^{6/5}$ at the maximum.....	59
3.4.2	The reason of observing a constant value for $\partial \ln C_{av} / \partial w^{6/5}$. Discussing procedures used in the literature.....	62
3.4.3	On important dependences for finding the grain boundary diffusivity.....	67
	Summary.....	73
Chapter IV. Realistic microstructures.....		75
Introduction.....		75
4.1	Finite Element Calculation. To get started.....	76
4.1.1	Main characteristics of the geometrical model of isolated boundary used in the finite element program.....	77
4.1.2	A comparison of Whipple's solution and FLUX-EXPERT's simulation results.....	78
4.1.3	The accuracy of results obtained in FLUX-EXPERT.....	79
4.1.3.1	The averaging of concentration C_g	79
4.1.3.2	The effect of the finite element mesh.....	81
4.1.3.3	The effect of the time interval.....	82
4.2	Realistic polycrystalline microstructures.....	84
4.2.1	A comparison of the model of parallel boundaries with the model of square grains under conditions of type-B kinetics.....	86
4.2.1.1	The model of parallel boundaries at short diffusion times.....	86
4.2.1.2	The model of square grains at short diffusion times.....	89
4.2.2	General geometrical models.....	94
4.2.2.1	Main characteristics of general geometrical models.....	94
4.2.2.2	Simulation results obtained in the general geometrical models.....	97
4.2.3	A comparison of the model of parallel boundaries with the model of square grains under conditions of type-A kinetics.....	101
4.2.3.1	Analyzing the boundary condition at the bottom.....	102
4.2.3.2	Analyzing Hart's equation and Maxwell-Garnett's equation.....	105
4.2.3.3	Segregation effects under conditions of type-A kinetics.....	110
	Summary.....	116

Chapter V. Space charge layer problems in grain boundary diffusion studies.....	117
Introduction.....	117
5.1 Mathematical model to describe diffusion in a polycrystal including space charge layers.....	119
5.2 Accuracy of the simulated diffusion profiles and effect of coordinate-dependent space charge layer diffusivity.....	121
5.2.1 The finite element mesh and diffusion barrier at the bottom of the geometrical model.....	121
5.2.2 The reason of using constant space charge layer diffusivity.....	126
5.3 How diffusion proceeds in the models of parallel boundaries and square grains.....	128
5.3.1 The model of parallel boundaries under conditions of type-B kinetics.....	130
5.3.2 The model of square grains under conditions of type-B kinetics.....	138
5.3.3 The model of parallel boundaries and the model square grains under conditions of type-A kinetics.....	139
Summary.....	147
Conclusions.....	149
Kurzfassung der Dissertation in deutscher Sprache.....	155
1. Einführung.....	155
2. Physikalische und geometrische Modelle, die in der numerischen Untersuchung benutzt wurden.....	158
3. Ergebnisse und Diskussion.....	164
3.1 Nichtlinearitätseffekt.....	164
3.2 Realistische Mikrostrukturen.....	168
3.3 Probleme durch Raumladungszonen.....	170
4. Zusammenfassung.....	173
References.....	177
Curriculum Vitae.....	185

Symbols and Abbreviations

GB	grain boundary
SCL	space charge layer
FEM	finite element method
D_g	grain diffusion coefficient
D_{gb}	grain boundary diffusion coefficient
$D_{gb,true}$	grain boundary diffusivity value used in the calculation
$D_{gb,app}$	grain boundary diffusivity value obtained by using the conventional model
D_{scl}	space charge layer diffusion coefficient
Δ	ratio of the diffusivities ($= D_{gb}/D_g$)
L_g	diffusion length in the grain (bulk) ($= \sqrt{D_g t}$)
L_{gb}	diffusion length along the grain boundary
δ	grain boundary (core) thickness
δ_{scl}	space charge layer thickness
C_g	concentration in the grain (bulk)
C_{gb}	concentration in the grain boundary
C_{scl}	concentration in the space charge layer
C_{av}	average concentration obtained by integrating C_g along the direction perpendicular to the grain boundary
C_0	constant source concentration
t	diffusion time
Δx	integration interval (step) along x-direction
Δy	integration interval (step) along y-direction

y	real coordinate (depth) along the grain boundary
x	real coordinate perpendicular to the grain boundary
σ	integration constant
s	segregation coefficient
d	grain size, distance between parallel boundaries
g	area fraction of grain boundaries
β	dimensionless diffusion parameter ($= ((\Delta - 1)\delta)/(2L_g)$)
α	dimensionless diffusion parameter ($= \delta/(2L_g)$)
η	dimensionless coordinate along the grain boundary
w	dimensionless coordinate along the grain boundary weighted to $\sqrt{\beta}$
ξ	dimensionless coordinate perpendicular to the grain boundary

Introduction

Grain boundary (GB) diffusion is a particularly important and interesting topic from the viewpoints of technology and basic understanding of diffusion processes in solids. It plays a crucial role in different processes such as sintering, creep, grain growth, or solid state reactions, all of them affecting the properties of a polycrystalline material. GB diffusion is crucial, for example, for corrosion in metals and transport properties of oxides. That is why this phenomenon attracts great attention, leading to a huge number of experimental and (still increasing number of) theoretical works on this subject. Recently, very interesting experimental techniques, like secondary ion mass spectroscopy (SIMS) [Sou04] and Auger electron spectroscopy [WanJ04], were improved in order to understand the diffusion phenomenon on the nanoscale. Simultaneously, the capabilities of theoretical computational methods as well as the performance of modern computers have increased drastically [Nak98]. Both theoretical and experimental approaches help each other in understanding GB diffusion. While the theoretical methods like *ab initio* methods [Liu02] help us to understand the interactions between the diffusing atoms and GBs, it is the phenomenological approach which serves as a bridge between the atomistic methods and the experiment, on the one hand, and

explains physical processes on the basis of macroparameters, on the other hand. The phenomenological (continuum) equations (typically differential equations) are used in the experimental evaluations to provide a desired physical quantity. For GB diffusion, this is, of course, the GB diffusivity (D_{gb}). A very actual question is what happens with diffusion, if the sample reduces in size. Owing to the importance of the problem, the number of phenomenological studies on nanocrystalline materials is steadily increasing. Despite this fact, D_{gb} for nanocrystalline materials is mostly obtained by using the methods suggested several decades ago. The aim of the present phenomenological studies is to analyze „size effects“ caused by the increasing volume fraction of GBs in nanocrystalline materials, to estimate possible errors arising with the application of conventional models to find D_{gb} , and to suggest new methods, if possible.

The first chapter of the present dissertation is devoted to the phenomenological theory for describing GB diffusion. The main ideas and equations comprising the actual phenomenological theory of GB diffusion [Kau95] are considered. The kinetics of GB diffusion is explained on the basis of three main diffusion regimes: type-A, -B and -C as proposed by Harrison [Harr61]. Also a new classification proposed by Mishin [Mis95] is mentioned as far as the small grain sizes are concerned. The main equations which are used to deduce D_{gb} from the measured diffusion profiles in one of the diffusion regimes are discussed as well. The derivation of Fisher's system is given and the important assumptions stemming from this derivation are emphasized. Moreover, Le Claire's equation [Cla63] serving as the main tool for deducing D_{gb} for the measured concentration gradient in the B-regime is discussed in detail. Hart's equation [Hart57], being the more popular equation that allows one to find D_{gb} from the diffusion profile measured under conditions of the type-A kinetics, is also taken account of. The segregation modifications of this equation [Mor60] as well as of Maxwell-Garnett's equation [Kal02] are addressed too.

Chapter two deals with the application of finite element method (FEM) for numerical integration of the diffusion equations for cases where analytical solutions cannot be obtained. In the present study two such cases are met, namely by simulating realistic polycrystalline microstructures and blocking space charge effects. Particularly, the derivation of the equations used in the finite element program is explicitly explained for the problem of GB diffusion. Since the finite element program FLUX-EXPERT [Flu00] is used in the present study, its main structure is discussed in the second chapter.

In the third chapter, the main effects which lead to significant errors of deducing D_{gb} from the diffusion profile measured at extremely short diffusion lengths are discussed in

detail. For this case the diffusion profiles were calculated by using Whipple's solution [Whi54] with varying diffusion times (t) in the range $2 \cdot 10^3 - 10^6$ seconds for different ratios of diffusivities (Δ) between the GB (D_{gb}) and the bulk (grain) (D_g). Consequently, the results of the second chapter correspond to diffusion in the B-regime. It is important to note that the parameter $\beta = [(\Delta-1)\delta]/[2\sqrt{D_g t}]$ was allowed to vary over the orders of magnitude from several thousands to tens (here δ is the GB thickness). The errors in finding D_{gb} by using Le Claire's relation were estimated. The relation itself is discussed rigorously under different conditions, and the reasons of arising errors are explained. New equations for deducing the ratio Δ are suggested on the basis of calculated diffusion profiles. Namely, the equation is proposed to calculate properly the derivative $\partial \ln C_{av} / \partial w^{6/5}$ depending on the diffusion time, which was suggested by Le Claire [Cla63] to be treated as a constant (here w is the dimensionless coordinate). Additionally, a criterion was found deciding on whether the new method is to be preferred or Le Claire's method is still sufficient, based on the knowledge of dimensionless parameter $\alpha = \delta / (2\sqrt{D_g t})$. The main suggestion to improve D_{gb} determination proposed in this study is based on plotting the derivative of the diffusion profile, i.e. $\partial \ln C_{av} / \partial y^{6/5}$, as a function of $y^{6/5}$ (y is the coordinate along the diffusion direction) and to analyze it. The derivative is characterized by the maximum which always gives the correct D_{gb} . The analytical dependences are suggested for the positions of this maximum as well as its value. Additionally, the numerical problems of integrating the Whipple solution used in an integral form [Whi54] are discussed.

How realistic microstructures can be simulated by using FEM is discussed in the fourth chapter. The important issue is the accuracy of finite element calculations with emphasis on the diffusion problems. With respect to the accuracy, mesh of integration and influence of boundaries of geometrical models proposed in this chapter are especially considered. Another parameter considered is the time increment used in the transient kinetics problems. This parameter determines the overall result, if extremely short diffusion times are concerned. A special procedure for simulating GB diffusion at short diffusion times using FEM is proposed. Several microstructures are discussed and different angles between a particular GB of the microstructure to the diffusion direction were probed. The results obtained for these microstructures are compared with those obtained for two main models of polycrystalline materials, i.e. the model of parallel boundaries and the model of square grains. It is shown that the model of square grains is a quite reasonable approximation, if the number of parallel and perpendicular paths is comparable. The area fractions of GBs were varied and the impact on the diffusion profile analyzed. Not only short but also long diffusion times were

studied, i.e. the A-regime of GB diffusion was simulated too. Since the problems of using Hart's equation [Hart57] for increasing GB volume fractions have already been discussed by Belova and Murch [Bel03], in the present study emphasis is laid on the diffusion accompanied with impurity segregation. Both Hart's equation and Maxwell-Garnett's equation (in its improved form suggested by Kalnin *et al.* for the segregation problems [Kal02]) are compared by varying the segregation coefficient from unity to several hundreds. Specifically, the Hart equation gives large errors in D_{gb} due to the linear dependence of the effective diffusivity (which is the only quantity measurable in the A-regime) on the segregation coefficient. For the segregation coefficient only Henry's [Cab91] law is considered.

The conventional GB diffusion models, starting out from Fisher's model [Fis51], completely ignore the existence of space charge regions in ionic solids. However, the role of the space charge effects has already been discussed in many contributions [Mai95]. Recently, it was shown experimentally that the depletion space charge layers (SCLs) can significantly alter the diffusion profile [Sou05], [WanR05]. In this case improved models are necessary. In the fifth chapter the significance of space charge effects is discussed with a focus on the depletion layers [Gou02]. A mathematical model was obtained which takes into account analogous approximations for the GBs as Fisher proposed [Fis51]. The main difference is related to the incorporation of a third diffusivity in order to simulate the space charge effects. Consequently, the mathematical description comprises three differential equations which are needed to simulate space charge effects. Again, FEM is used here to numerically integrate the diffusion equations. Errors in obtaining D_{gb} by means of conventional models (both the Le Claire equation and the Hart equation) were estimated. The calculated diffusion profiles and their properties are discussed. It is shown how the apparent GB diffusivity ($D_{gb,app}$) can be estimated by using new expressions, discussed in the third chapter. However, the use of those is possible in the B-regime only. The diffusion profiles were simulated under conditions of type-A kinetics for the models of parallel boundaries and square grains too. The diffusion times needed to exclude the space charge effects strongly depend on the ratio $\Lambda = D_g/D_{scl}$, where D_{scl} is the diffusion coefficient used in the SCL. This ratio was varied here from 0.1 to 10^3 . In the fifth chapter some numerical problems which can arise when simulating diffusion with blocking SCLs are considered. This is done to demonstrate the accuracy of obtained results and give important hints for future studies.

Lastly, the main results are summarized in Conclusions. In this part the procedures to improve D_{gb} determination are also explained.

Chapter I. The classical grain boundary diffusion models

Introduction

As soon as diffusion along GBs is concerned, idealized GB models need to be introduced. This is done necessarily, because the real GB structure cannot be taken into account on a continuum level. Contrary to the atomistic description, the continuum approach deals with the averaged situation in which D_{gb} becomes the most important characteristic bearing information on the structure and interaction of atoms, including the interaction of diffusing atoms with the host atoms. In some cases, one may consider the diffusivity along a particular GB from the measurements on bicrystals, for example $\Sigma 11$, when the GB structure is determined by one of the high resolution imaging techniques like HRTEM [Höc94], [Leo99] and apply the conventional models to find D_{gb} in this boundary [Lib94]. However, a polycrystalline material consists of GBs characterized by different misorientations between the grains and, as a consequence, different D_{gb} 's. Clearly, the measured D_{gb} in these materials represents some averaged value. There are also evidences that the structure of GBs in nanocrystalline materials is similar to that of coarse-grained materials [Gle89], [Wür03],

[Bar05]. Consequently, the conventional models used to find D_{gb} in coarse-grained materials may be applied to nanomaterials as well.

1.1 Grain boundary model. Guggenheim or Fisher?

There are different interface models in the literature used to analyze and describe various processes related to the interfaces, like diffusion or segregation. One of them was suggested by Gibbs [Def66]. It excludes the real GB thickness, and the concentration change at the interface in this model is step-like. Another model was proposed by Guggenheim [Gug40]. This model is more realistic in comparison with the Gibbs model, because the thickness of GB is taken into account. Fisher [Fis51] was the first who successfully used a similar model to describe diffusion along GBs by means of diffusion equations.

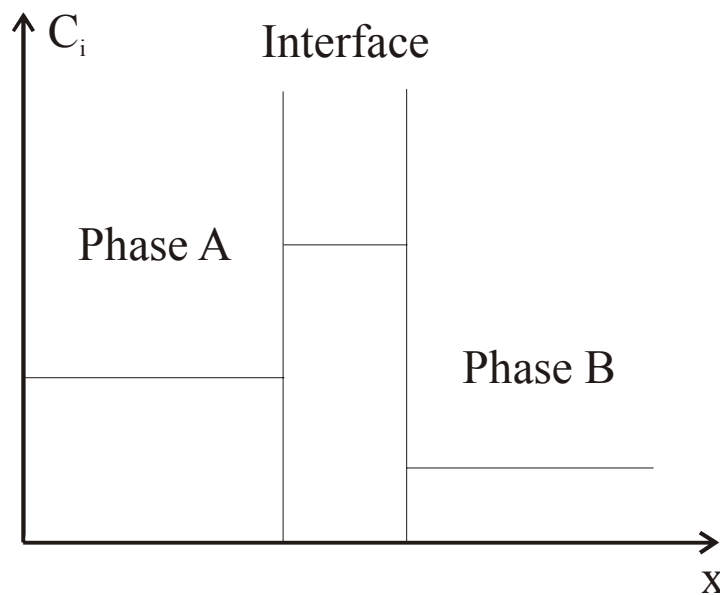


Fig. 1.1 Interfacial model according to Guggenheim [Gug40]. Adapted from [Cab91].

In fig. 1.1 the concentration C_i corresponds to a particular component (i) of a solid solution. The interface is thought to be embedded between two phases A and B. If phase A and phase B are chemically identical materials, the interface is termed a GB. Equilibrium concentration changes are supposed to occur only at the boundaries (interfaces) separating the interface and the adjacent phases, or in the case of a polycrystalline material, the GB and the grain. By supposing that the lateral change of the concentration within the GB (i.e. in the x -direction) is negligible, Fisher could describe diffusion within the GB by one dimensional

Fick's second law [Fis51]. He also supposed that concentrations at the boundaries separating the GB and grains are equal. In this way the segregation effects were excluded. All the approximations introduced by Fisher's model are discussed in the next section on a mathematical level. One should pay attention to the fact that Fisher's model refers to a quasi two dimensional (2D) representation of the GB.

1.1.1 Isolated grain boundary model

The model used by Fisher to describe diffusion along the GBs comprises the free surface carrying the diffusion source and the GB being perpendicular to that surface. The GB has a constant thickness δ (fig. 1.2), i.e. represents a slab, with the diffusion coefficient (D_{gb}) remaining constant along the GB. Therefore, the diffusion coefficients D_{gb} within the GB and D_g within the grain are not functions of concentration, time or positional coordinate. Fisher's model, known also as the isolated boundary model, represents a typical 2D semi-infinite problem. The concentrations and fluxes coincide at the boundaries separating the GB and the grain, i.e. at $x = \pm\delta/2$, allowing the leakage of atoms that exists from the GB into the grain to be taken into account. Consequently, Fisher's model is based on the assumption that $D_{gb} \gg D_g$. One can see from fig. 1.2 that the concentration distribution in this model is symmetrical with respect to the point $x = 0$. The following assumptions are assumed by Fisher's model:

- 1) Fick's laws are obeyed in both the crystal (grain) and the GB slab.
- 2) The diffusion coefficients D_g and D_{gb} are isotropic and independent of concentration, position and time.
- 3) The diffusant flow is continuous at the GB/grain interface (boundary).
- 4) The width of the GB is so small that the concentration variation across it (i.e. in the x -direction) is negligible.
- 5) The condition $D_{gb} \gg D_g$ is fulfilled with the consequence that the mass transport in the bulk is essentially preceded by GB transport (red arrows in fig. 1.2).

All results discussed in the present work were obtained by using these approximations except a modification related to segregation effects. The latter requires supposing that the concentrations at the boundary between the grain and the GB are not equal; however, the continuity conditions are still valid as well all the other assumptions. The segregation effects have been addressed [Bok58], analyzing derivation of D_{gb} in the case of impurity diffusion.

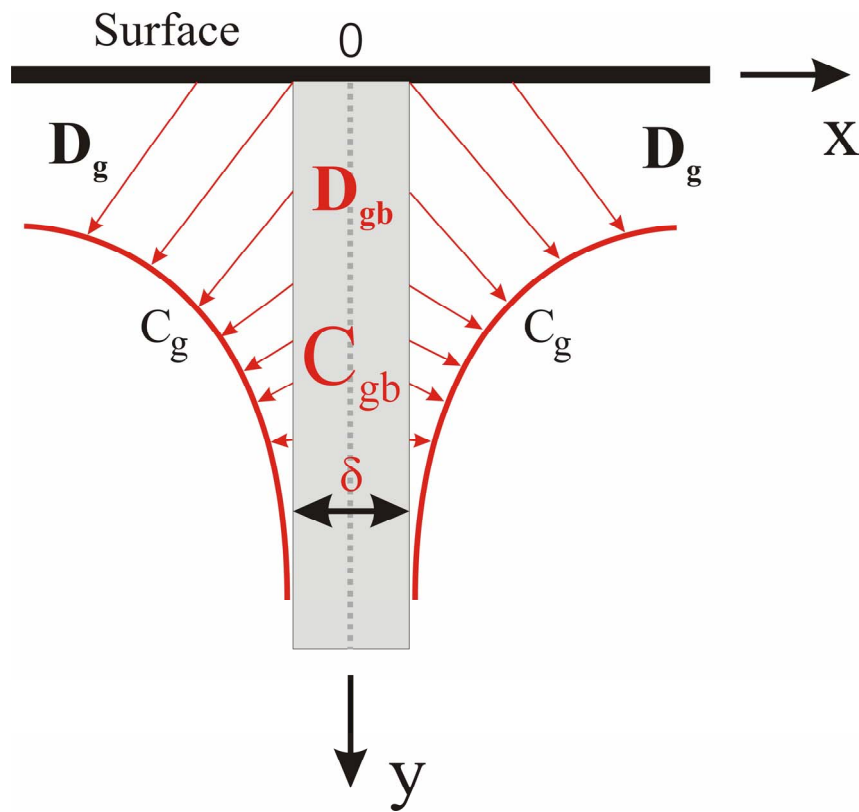


Fig. 1.2 Isolated boundary model.

1.1.2 Mathematical description of grain boundary diffusion in the isolated grain boundary model

Fisher was the first who derived the set of two diffusion equations for the GB diffusion problem and solved them approximately, whereas Whipple [Whi54] gave a rigorous mathematical analysis, including the exact analytical solution to the diffusion equations.

The first diffusion equation represents diffusion within the grain with the diffusion coefficient D_g , the second one diffusion within the GB with the diffusion coefficient D_{gb} (Eq. (1.1)):

$$\begin{cases} \frac{\partial C_g}{\partial t} = D_g \left(\frac{\partial^2 C_g}{\partial x^2} + \frac{\partial^2 C_g}{\partial y^2} \right), & \text{if } |x| \geq \delta/2 \\ \frac{\partial C_{gb}}{\partial t} = D_{gb} \left(\frac{\partial^2 C_{gb}}{\partial x^2} + \frac{\partial^2 C_{gb}}{\partial y^2} \right), & \text{if } |x| \leq \delta/2 \end{cases}, \quad (1.1)$$

where t is the diffusion time. Both Fick's second laws [Fic55] are coupled by applying the boundary conditions of equal concentrations and fluxes at the grain/GB interface (Eq. (1.2)):

$$\begin{cases} C_g(x, y, t) = C_{gb}(x, y, t) \\ J_g(x, y, t) = J_{gb}(x, y, t) \end{cases}, \quad \text{if } |x| = \delta/2. \quad (1.2)$$

These two continuity conditions (Eq. (1.2)) correspond to the conservative property of diffusion [Ghe88] and presuppose the steady state and diffusional equilibrium between the GB and the grain. Obviously, additional boundary and initial conditions are related to the surface. There are two important boundary conditions referring to $y = 0$: constant source and instantaneous source. While Whipple solved the relevant mathematical problem for the case of constant source, Suzuoka [Suz61] found the corresponding solution for the instantaneous source. For both cases the initial and boundary conditions are presented in Eqs. (1.3a) and (1.3b).

Constant source:

$$\begin{cases} C(x, y, t) = C_0 & \text{at } y = 0 \\ C(x, y, t) = 0 & \text{at } t = 0 \\ C(x, y, t) = 0 & \text{at } y \rightarrow \infty \end{cases} \quad (1.3a)$$

Instantaneous source:

$$\begin{cases} C(x, y, t) = C(x, t) & \text{at } y = 0 \\ C(x, y, t) = M\delta(y) & \text{at } t = 0 \\ C(x, y, t) = 0 & \text{at } y \rightarrow \infty \\ \left. \frac{\partial C(x, y, t)}{\partial y} \right|_{y=0} = 0 \end{cases} \quad (1.3b)$$

In Eq. (1.3b) $\delta(y)$ is the delta function and M is the amount of diffusant deposited per unit area of the surface, whereas in Eq. (1.3a) C_0 is the constant concentration of diffusant at the surface. Correspondingly, the mathematical problem of diffusion when both bulk (grain) and GB contribute is to solve the system of differential equations (Eq. (1.2)) subject to the boundary and initial conditions given by Eqs. (1.2) and (1.3).

1.1.3 Transformations made to obtain Fisher's system

In Fisher's model the concentration can be easily expanded into a Taylor series with respect to $x = 0$ [Kau95], [Whi54]. Particularly, the GB concentration can be expanded, since the GB can be considered as a very thin slab, and the concentration within it is

homogeneously distributed [Sut95]. However, this is not the case for the grain concentration. Consequently,

$$C_{gb}(x, y, t) = C_{gb}(x, y, t)|_{x=0} + x \frac{\partial C_{gb}(x, y, t)}{\partial x} \Big|_{x=0} + \frac{x^2}{2} \frac{\partial^2 C_{gb}(x, y, t)}{\partial x^2} \Big|_{x=0} + \frac{x^3}{3!} \frac{\partial^3 C_{gb}(x, y, t)}{\partial x^3} \Big|_{x=0} + \frac{x^4}{4!} \frac{\partial^4 C_{gb}(x, y, t)}{\partial x^4} \Big|_{x=0} + \dots + \frac{x^n}{n!} \frac{\partial^n C_{gb}(x, y, t)}{\partial x^n} \Big|_{x=0} \quad (1.4a)$$

The first derivative of an even function gives an odd function which is zero at the point of symmetry $x = 0$. Hence, one can neglect all the “odd” derivatives:

$$C_{gb}(x, y, t) = C_{gb}(x, y, t)|_{x=0} + \frac{x^2}{2} \frac{\partial^2 C_{gb}(x, y, t)}{\partial x^2} \Big|_{x=0} + \frac{x^4}{4!} \frac{\partial^4 C_{gb}(x, y, t)}{\partial x^4} \Big|_{x=0} + \dots + \frac{x^n}{n!} \frac{\partial^n C_{gb}(x, y, t)}{\partial x^n} \Big|_{x=0}, \text{ where } n = 2m \text{ with } m = 1, 2, \dots \quad (1.4b)$$

Substituting Eq. (1.4b) into the diffusion equation for the GB (Eq. (1.1)), one obtains the following expression

$$\frac{\partial}{\partial t} \left(C_{gb}(x, y, t)|_{x=0} + \sum_{n=2m}^{\infty} \frac{x^n}{n!} \frac{\partial^n C_{gb}(x, y, t)}{\partial x^n} \Big|_{x=0} \right) = D_{gb} \left[\frac{\partial^2}{\partial x^2} \left(\sum_{n=2m}^{\infty} \frac{x^n}{n!} \frac{\partial^n C_{gb}(x, y, t)}{\partial x^n} \Big|_{x=0} \right) + \frac{\partial^2}{\partial y^2} \left(C_{gb}(x, y, t)|_{x=0} + \sum_{n=2m}^{\infty} \frac{x^n}{n!} \frac{\partial^n C_{gb}(x, y, t)}{\partial x^n} \Big|_{x=0} \right) \right], \text{ where } m = 1, 2, \dots \quad (1.4c)$$

The GB concentrations are equal at $x = 0$ and $x = \pm\delta/2$. This property allows one to transform the last expression into a much simpler form, considering the equation at $x = \pm\delta/2$ and, neglecting the higher order terms (i.e. of order δ^2 and higher). Such a simplification is related to the fourth assumption supposed by Fisher's model. This yields

$$\frac{\partial}{\partial t} C_{gb}(0, y, t) = D_{gb} \left[\frac{\partial^2}{\partial x^2} C_{gb}(x, y, t)|_{x=0} + \frac{\partial^2}{\partial y^2} C_{gb}(0, y, t) \right]. \quad (1.4d)$$

The latter equation can be further simplified by substituting Eq. (1.4b) into the boundary conditions (Eq. (1.2)) and keeping in mind that

$$J_{gb} \Big|_{|x|=\frac{\delta}{2}} = -D_{gb} \frac{\partial C_{gb}(x, y, t)}{\partial x} \Big|_{|x|=\frac{\delta}{2}}. \quad (1.4e)$$

In this way, the continuity conditions are rewritten neglecting the higher order terms as:

$$\begin{cases} C_{gb}(x, y, t) \Big|_{x=0} = C_g(x, y, t) \Big|_{|x|=\frac{\delta}{2}} \\ \pm D_{gb} \frac{\delta}{2} \frac{\partial^2 C_{gb}(x, y, t)}{\partial x^2} \Big|_{x=0} = D_g \frac{\partial C_g(x, y, t)}{\partial x} \Big|_{|x|=\frac{\delta}{2}} \end{cases}. \quad (1.5)$$

Finally, Eq. (1.5) allows one to write down the following equations for the GB diffusion

$$\begin{cases} \frac{\partial C_g(x, y, t)}{\partial t} = D_g \left(\frac{\partial^2 C_g(x, y, t)}{\partial x^2} + \frac{\partial^2 C_g(x, y, t)}{\partial y^2} \right), & \text{if } |x| \geq \delta/2 \\ \frac{\partial C_g(y, t)}{\partial t} = D_{gb} \frac{\partial^2 C_{gb}(y, t)}{\partial y^2} + \frac{D_g}{\delta/2} \frac{\partial C_g(y, t)}{\partial x}, & \text{if } |x| = \delta/2 \end{cases}. \quad (1.6a)$$

All terms in the second equation are taken at $x = \pm\delta/2$, so it exactly represents the boundary condition. Eq. (1.6a) is known as the Fisher system. It is important to note, that the solution which can be obtained by solving Eq. (1.6a) reveals the concentration within the grain and neglects the concentration within the GB. If one believes that the assumptions introduced by Fisher's model (see page 3) are reasonable and really reflect the adequate physical situation, the only approximation is related to neglecting higher orders terms in the expansion of C_{gb} .

If there is segregation, the first equation in Eq. (1.5) is replaced by [Her05]:

$$C_{gb}(x, y, t) = sC_g(x, y, t), \quad \text{if } |x| = \delta/2 \quad (1.6b)$$

where s is the equilibrium segregation coefficient or segregation factor. Eq. (1.6b) is known as Henry's isotherm [Cab91], which is valid for dilute conditions. By using this boundary condition Eq. (1.6a) can be rewritten in the following form [Gib66]

$$\begin{cases} \frac{\partial C_g(x, y, t)}{\partial t} = D_g \left(\frac{\partial^2 C_g(x, y, t)}{\partial x^2} + \frac{\partial^2 C_g(x, y, t)}{\partial y^2} \right), & \text{if } |x| \geq \delta/2 \\ \frac{\partial C_g(y, t)}{\partial t} = D_{gb} \frac{\partial^2 C_{gb}(y, t)}{\partial y^2} + \frac{D_g}{s\delta/2} \frac{\partial C_g(y, t)}{\partial x}. & \text{if } |x| = \delta/2 \end{cases} \quad (1.6c)$$

1.1.4 An alternative derivation of Fisher's system

Shewmon [She63] published a more didactic approach to arrive at Fisher's system. Interestingly, his derivation is more elegant in the sense that it allows the straightforward finding of the corresponding equations without rigorous mathematical transformations. Let us consider a 2D slab of the length dy and thickness δ (fig. 1.3). The slab is embedded into the system of two crystals (grains) from both sides, having a different diffusivity. If that slab is an element of a GB, two fluxes are possible from its GB/grain interfaces, i.e. from the GB into the grains, namely the fluxes J_x in fig. 1.3. There is also the flux coming from the top of the slab J_y and leaving some amount of material inside the slab. The amount of material is changed within the slab due to the non-zero difference of fluxes and is given by $(\partial J_y / \partial y) dy$, if dy is very small. The fluxes J_x and J_y are different, because these are determined by the diffusion coefficients D_g and D_{gb} , respectively. The volume of the element is $1 dy \delta$, where the unity corresponds to the length along a z -direction. So the concentration changes with time. Accordingly,

$$dy \delta \frac{\partial C_g}{\partial t} = -\delta \frac{\partial J_y}{\partial y} dy - 2 dy J_x, \quad (1.7)$$

where the negative signs obviously correspond to out-diffusion. Introducing Fick's first law, the following final equation for diffusion along the GB results:

$$\frac{\partial C_g}{\partial t} = D_{gb} \frac{\partial^2 C_g}{\partial y^2} + \frac{2D_g}{\delta} \frac{\partial C_g}{\partial x} \Big|_{x=\frac{\delta}{2}}. \quad (1.8)$$

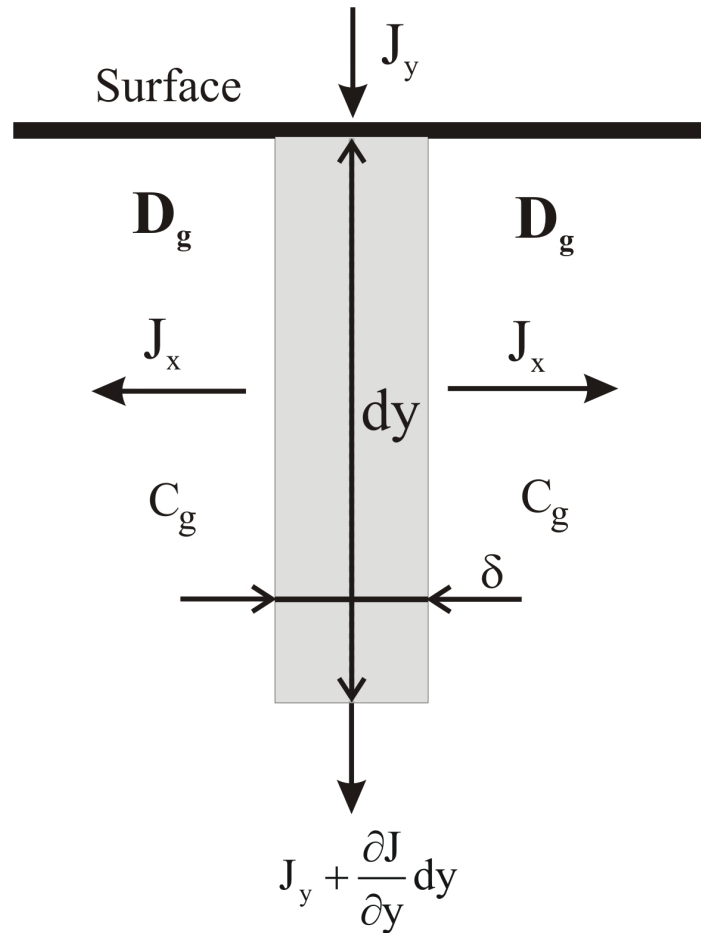


Fig. 1.3 Schematic representation of the GB model for deducing Eq. (1.8). Adapted from [She63].

1.1.5 Whipple's solution

Whipple [Whi54] solved Fisher's system (Eq. (1.6)) by means of the Fourier-Laplace transform [Bee03]. Properties of this solution will be discussed in chapter III. Here only the solution is presented, which reads

$$C_g(\eta, \xi, \beta) = C_0 \operatorname{erfc}\left(\frac{\eta}{2}\right) + \frac{C_0 \eta}{2\pi^{1/2}} \int_1^{\Delta} \frac{d\sigma}{\sigma^{3/2}} \exp\left(-\frac{\eta^2}{4\sigma}\right) \operatorname{erfc}\left[\frac{1}{2} \left(\frac{\Delta-1}{\Delta-\sigma}\right) \left(\frac{\sigma-1}{\beta} + |\xi|\right)\right]. \quad (1.9a)$$

The solution is of integral form with the integral being responsible for GB diffusion. The first term of the solution, obviously, represents diffusion within the grain. Different dimensionless quantities are used in the Whipple solution. The dimensionless quantities η and ξ are, in fact, dimensionless coordinates and given by

$$\eta = \frac{y}{\sqrt{D_g t}}, \quad (1.9b)$$

$$\xi = \frac{x \pm \delta/2}{\sqrt{D_g t}}, \quad \text{if } |x| \geq \delta/2. \quad (1.9c)$$

Eq. (1.9a) differs from original expression by the modulus $|\xi|$. The latter is needed, if the solution is considered at $x \leq -\delta/2$ (see also Eq. (1.9c)). The meaning of the dimensionless parameter β is more complex. According to Kaur *et al.* [Kau95] it characterizes the diffusion process in the sense that a large β -value means that the diffusion along the GBs is greatly pronounced in comparison with bulk diffusion, i.e. the penetration depth along the GB is much larger. It is also related to the inclination angle between an isoconcentration line and the GB. Finally, it is not only high when Δ is large, but also when t is short. The analytical form of β is

$$\beta = \frac{(\Delta - 1)\delta}{2\sqrt{D_g t}} = (\Delta - 1)\alpha. \quad (1.9d)$$

Here the quantity α shows how the diffusion length in the grain ($L_g = \sqrt{D_g t}$) exceeds the GB thickness (δ).

1.2 Diffusion kinetic regimes

Diffusion in an isolated GB (fig. 1.2) can be analyzed or simulated on the basis of Eqs. (1.6c) and (1.9a). In particular, Le Claire [Cla63] could suggest a simple procedure for determining D_{gb} based on integration of Whipple's solution. However, the procedure cannot be used for any experimental condition. It is a purpose of the present study to analyze such conditions when Le Claire's procedure is not valid. GB diffusion goes through different physical situations as the temperature and/or diffusion time increase. Accordingly, Harrison [Harr61] introduced three diffusion regimes and only in one of them the Whipple solution to Fisher's system is valid. The application of Harrison's classification is also discussed in excellent reviews on GB diffusion, for example [Mis97], [Mis99]. Additionally, a new classification introduced by Mishin [Mis95] is used and discussed here in more detail as being

applicable to a variety of materials ranging from coarse grained to nanocrystalline. It should be mentioned that there are also classifications that take into account GB motion [Güt93] or GB diffusion accompanied by diffusion along dislocations [Klin99]. These are not a subject of the present study.

In the aforementioned classification it is supposed that penetration along GBs is deeper than in the remaining grains. As a consequence of the transport coefficient being larger along the GBs, diffusing atoms first move along these paths. For analyzing diffusion regimes surface diffusion is not considered as a rate-limiting process (recently, Preis and Sitte [Prei05], derived analytical solutions for the thin-film problem taking account of rate limiting surface exchange reactions).

In the very beginning of the diffusion process the atoms (traces) move through the GB without a significant contribution to the bulk. It is expected that the overall process is determined by D_{gb} only; it can be described by a complementary error-function solution to the diffusion equation in the case of a constant source. Such a situation was called by Harrison the C-kinetics and later extended by Mishin to an additional C'-regime to take into account the situations when the grain size can be very small. So the conditions of the C and C' – regime (in terms of Mishin's classification) can be written as follows:

$$L_g \ll s\delta/2 \ll L_{gb} \ll d \quad (\text{C-regime}) \quad (1.10a)$$

and

$$L_g \ll s\delta/2 \ll d \ll L_{gb} \quad (\text{C'-regime}). \quad (1.10b)$$

Here L_g , L_{gb} are the grain and GB diffusion lengths, respectively, d is the average grain size and s the segregation factor. The segregation factor (s) is introduced for generality and is set to 1 for self-diffusion. In fig. 4a an example of the C'-regime is given obtained by simulating diffusion using the finite element method (FEM) (the numerically obtained figures serve here as explanation figures. The quantitative analysis will be given in chapter IV). In this figure bright colors represent the enhanced concentration around the interfaces (see also color pattern in fig. 4a). However, the diffusion process is supposed to be confined within the GBs in the C (C')-regime. The existence of the C (C')-regime itself is still questionable, what was already mentioned in [Kau95] and is shortly discussed here. However, this is the only regime, in which D_{gb} (as it is believed) is directly obtained. This fact is used in many experiments to

find s [Her03]. It proceeds typically for a very short time which can be much shorter than in the case of type-B kinetics (fig. 5a, see also discussion below). That is why the C (C')-regime is difficult to verify experimentally, because of short t and/or low temperatures, in which case very small GB concentrations result. Consequently, the usually studied regime is the B-regime. Its evaluation is more reliable, especially for coarse-grained materials.

The exact solution found by Whipple (Eq. (1.9a)) corresponds to the B-regime. The range of validity of this regime is defined as follows:

$$s\delta/2 \ll L_g \ll L_{gb} \ll d \text{ (B-regime according to Harrison [Harr61] or } B_2\text{-regime according to Mishin [Mis95])} \quad (1.11a)$$

and

$$s\delta/2 \ll L_g \ll d \ll L_{gb} \text{ (} B_2'\text{-regime according to Mishin [Mis95]).} \quad (1.11b)$$

For the main results in the present study the common term B - regime is used, because the Whipple solution is valid in both the B_2 - and B_2' -regime. It seems to be that differentiation of the B-regime into the B_2 - and B_2' -regime is interesting only from the point of view of understanding how the diffusion process proceeds. This is also interesting in order to distinguish different types of materials as was proposed by Mishin [Mis95].

The diffusion lengths plotted on the logarithmic scale for different types of materials indicate that the B-regime is suppressed in materials with smaller grain sizes (fig. 5), while the A-regime becomes more prolonged. The plots shown in fig. 5 are very useful from the point of view of understanding diffusion in a polycrystal. These also allow to properly tune numerical experiment, because knowing penetrations is extremely important in order to avoid possible errors. Importantly, bold lines in fig. 5 correspond to the diffusion lengths responsible for the process in a particular regime. For instance, both L_g and L_{gb} can be obtained in the B-regime. All the plots were plotted for $D_g = 2.95 \cdot 10^{-4} \text{ nm}^2/\text{s}$ ($2.95 \cdot 10^{-16} \text{ mm}^2/\text{s}$) and $d = 25 \text{ nm}$. Different ratios $\Delta = D_{gb}/D_g$ were used in order to realize the different types of materials.

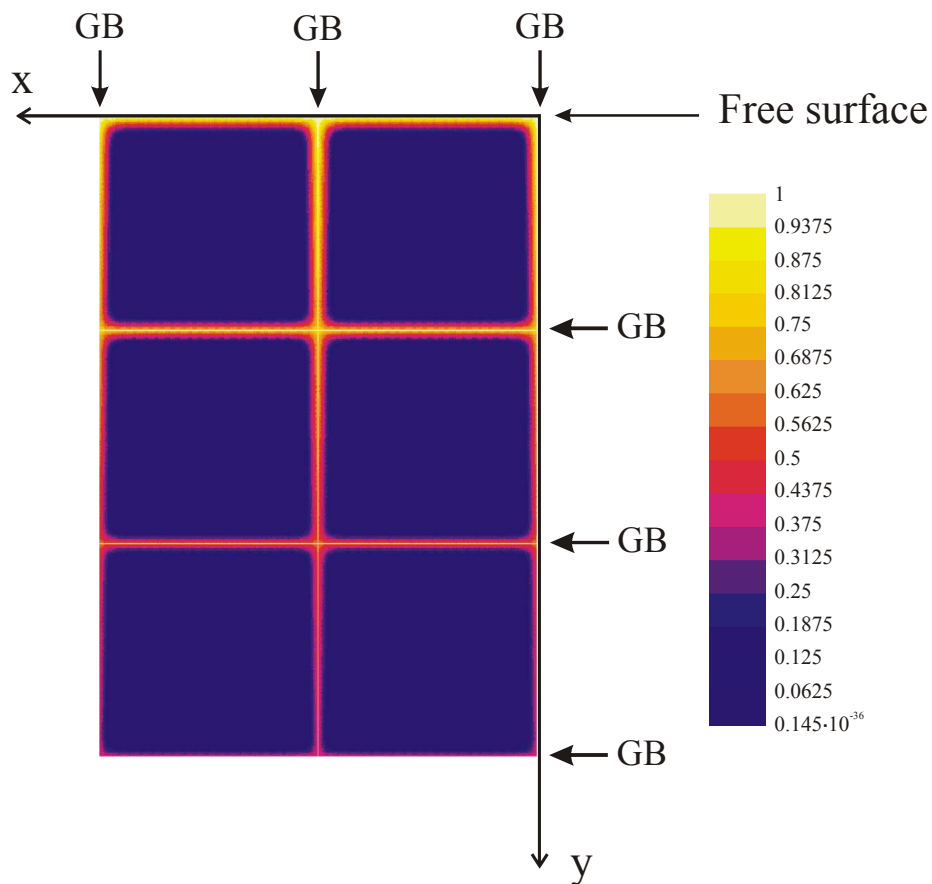
Two diffusion lengths (blue and red lines) shown in fig. 5 have the same slope on the logarithmic scale, as in such cases the same power law $\sim t^{1/2}$ is obeyed which is a typical diffusion dependence. In the B-regime, however, the diffusion length in the GB (green line) follows another law, *viz.* [Kau95]

$$L_{gb} = \frac{\sqrt{s\delta D_{gb}}}{(4D_g/t)^{1/4}}, \quad (1.12a)$$

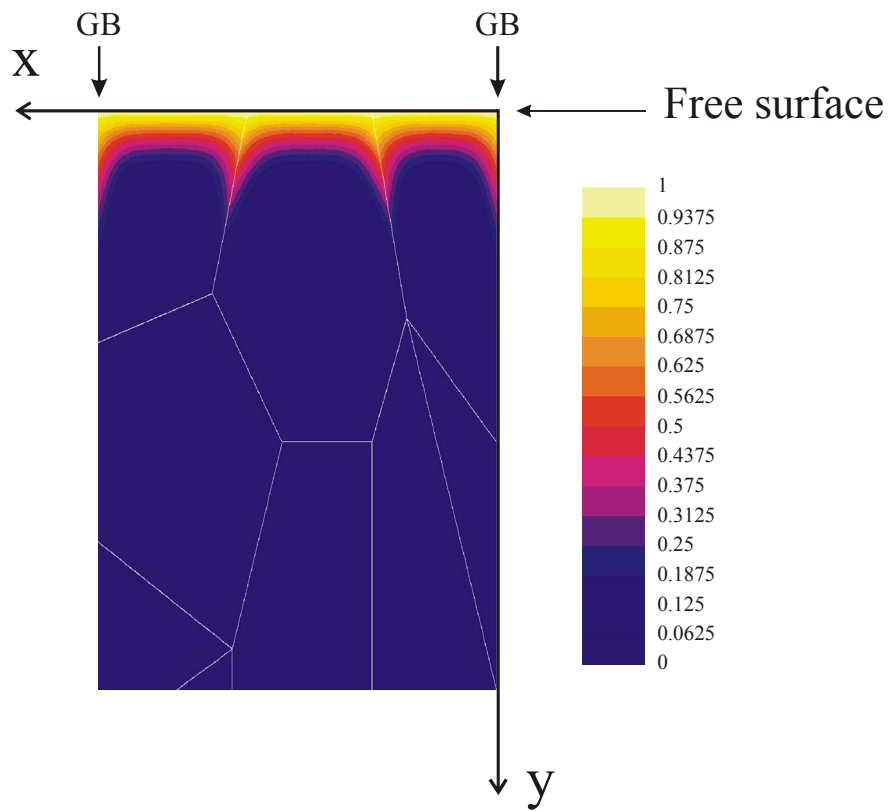
where s is again the segregation factor, t the diffusion anneal time and δ the GB thickness. The effects of segregation are excluded in fig. 1.5, i.e. those are plotted for $s = 1$ only. Moreover, not only L_{gb} , but also the parameter β depends on s as

$$\beta = (s\Delta - 1)\alpha. \quad (1.12b)$$

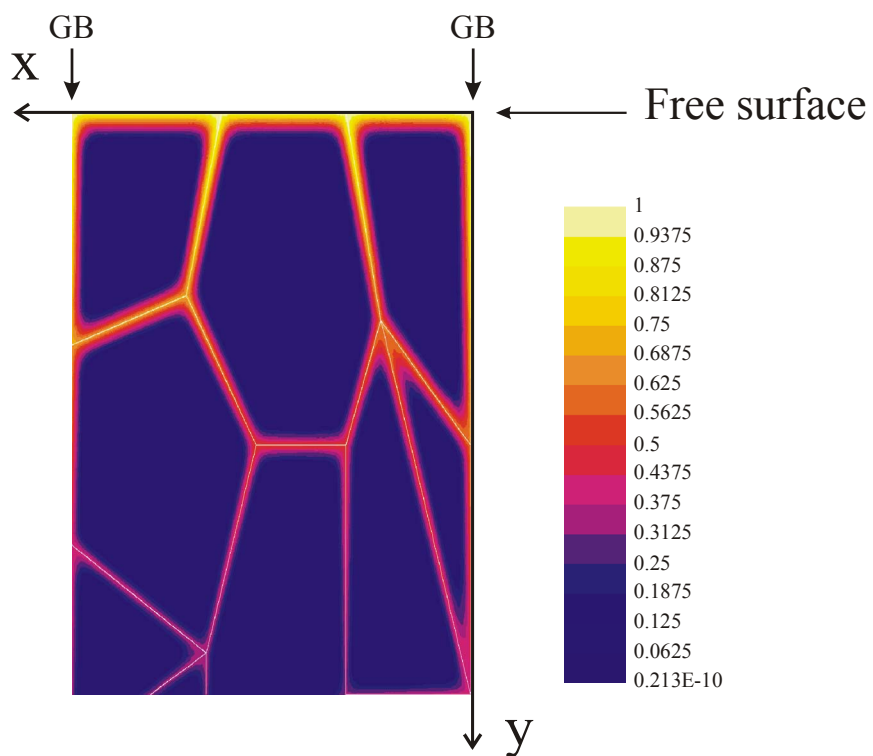
a)



b)



b')



c)

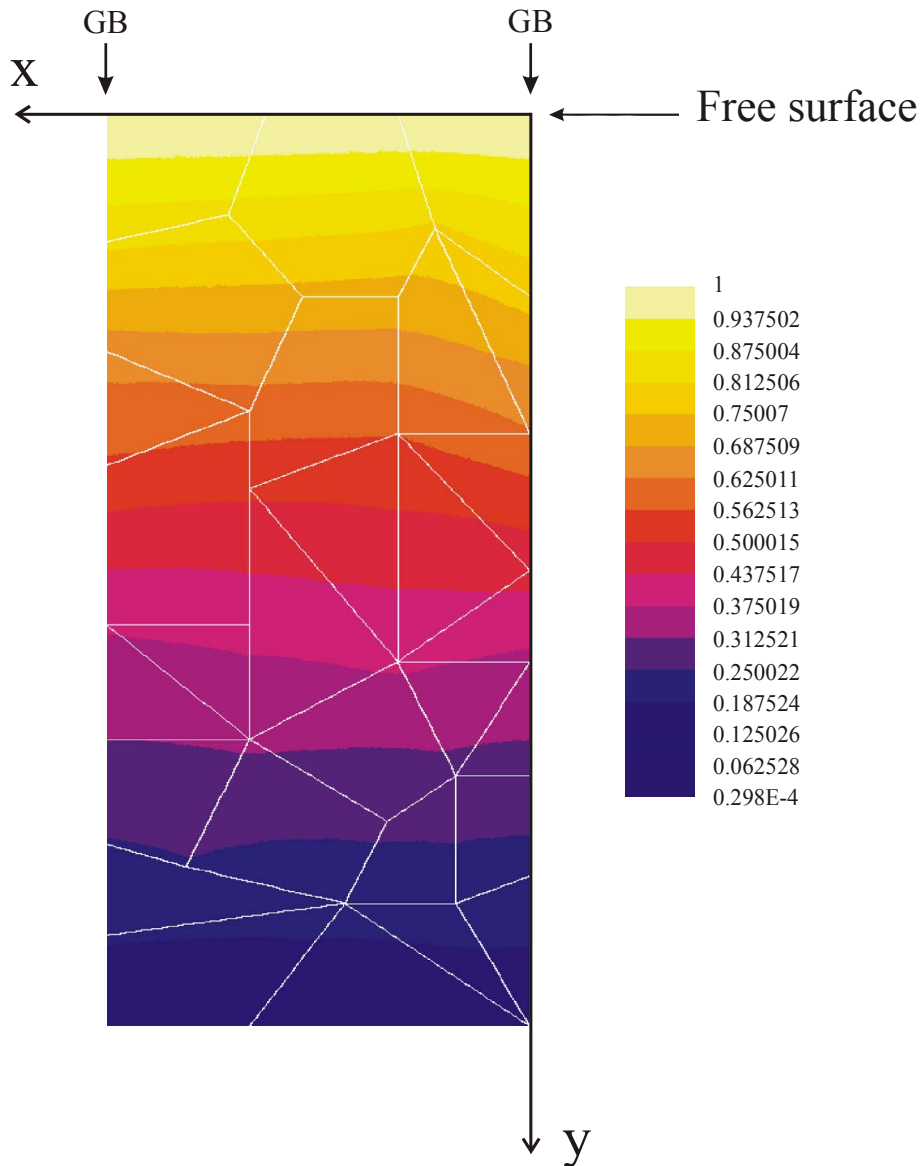


Fig. 1.4 a) Concentration distribution in a square grain pattern under conditions of the C' kinetics regime ($d = 5$ nm). b) A concentration distribution in a general polycrystal under conditions of type-B kinetics for $\Delta = 10^2$ ($d = 25$ nm) b') the same for $\Delta = 2.2 \cdot 10^4$ ($d = 25$ nm) c) A concentration distribution in a general polycrystal for the type-A kinetics for $\Delta = 10^2$ ($d = 25$ nm). All white lines correspond to the GBs. Also shown are relevant color patterns, in which different colors correspond to certain isoconcentration line. Distributions in b) and c) were obtained by using general model 3 used in the present study, for details see chapter IV.

The main difference between the results in figs. 1.4b and 1.4b' does not only lie in the different ratios Δ , but also in the behavior of concentration around the GBs. The inclination angle between a particular isoconcentration line (defined by a line of a particular color) and a GB is larger for smaller ratio Δ . Qualitatively speaking; the result in fig. 1.4b represents a

classical solution (distribution) in the type-B kinetics, corresponding to the B_2 – regime according to the classification of Mishin [Mis95]. Contrary to this, the inclination angle in the distribution in fig. 1.4b' is much smaller, indicating a typical situation for ultrafine-grained (nanocrystalline) materials. Because of this, the diffusion length in the GB (L_{gb} , green line in fig. 1.5) never reaches d for $\Delta = 10^2$, and the A-regime always starts before the diffusion length in the grain (L_g , red line in fig. 1.5) reaches that in the GB for $\Delta = 2.2 \cdot 10^4$, if d is 25 nm (fig. 1.5c).

The A-regime starts when the red and green lines in fig. 1.5 are crossed, or when L_g equals d . In fact, the diffusion length in the A-regime represents some effective diffusion length (not shown in fig. 1.5), which is a combination of D_g and D_{gb} . In this regime the distribution is homogeneous, what allows different theories valid for homogeneous systems to be applicable in the A-regime. High temperatures and/or long diffusion times are needed to observe the A-regime in coarse-grained materials. Contrary, it is suggested that the A-regime is important for ultrafine-grained materials (nanomaterials) due the suppression of B-regime [Bek04] (the condition discussed in reference is too rigorous and the existence of the B-regime is not questionable even for nanomaterials, what is proved in the present study). The effect is just related to the small grain sizes. The conditions for the A-regime are the following:

$$d \ll L_g \approx L_{gb}. \quad (1.13)$$

That is, the main condition for the A-regime is $L_g \gg d$. This starts at the point of equal L_g and L_{gb} (fig. 1.5). However, there is a situation when L_g reaching d is still smaller than L_{gb} . In this case the A' - regime arises. One additional regime is the so called B_4 -regime, in which $L_g \approx L_{gb} \ll d$. This corresponds to the situation that the diffusion fronts from the GB into the grain are not distinguishable anymore and are not overlapping. The inclination angle between the isoconcentration line and the GB is simply 90° in this case. Another possibility is shown in fig. 1.5a, in which L_g reaches d at the same point, where this equals L_{gb} . That is why it can be attributed to both A and B_4 regimes. In the distribution in fig. 1.4c the classical situation is shown, the homogeneous distribution is seen up to a very low level of the concentration. As far as the diffusion process in all of the type A regimes (B_4 , A, A') is obviously described by the solution to diffusion equation in homogeneous media without any exceptions. Accordingly, only one definition is used in the present work, namely the A-regime.

1.3 Deducing the grain boundary diffusivity from the diffusion profile

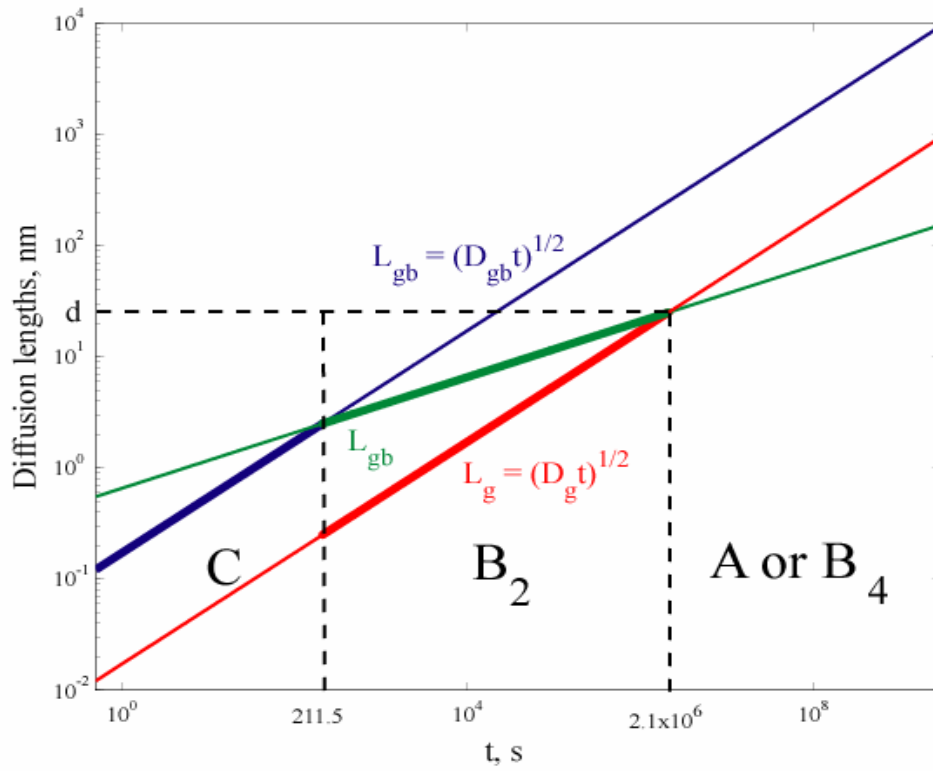
It is to be mentioned, that the diffusion profile is understood as the dependence $C_{av} = f(y)$ or $\ln C_{av} = f(y^{6/5})$ (see discussion below), where C_{av} is an average concentration being a function of time t and penetration depth y . Such a concentration can be found by integrating $C_g(x, y, t)$ along x for the whole range of y , what, in a sense, is a theoretical definition. Experimentally the same quantity can be found, when the sample is cut in slices, and the concentration in each slice is determined, what exactly is the case of tracer measurements [Ask70], [Meh05]. As sectioning methods, including SIMS technique in a depth profiling mode, obtain the average concentration (C_{av}) as a function of y and t , there should be a procedure which allows the grain boundary diffusivity (D_{gb}) to be found. Moreover, since diffusion in a polycrystalline sample passes different kinetic regimes, depending on t or temperature, at least three equations are needed to perform the diffusion profile measurements safely. In fact, such equations exist and intensive literature can be found on applying all the three equations. Nevertheless, these equations are still debated owing due to 1) simplifications made in the models [Chu96a], [Bel01], [Bel03] to find this or that equation and 2) special conditions [Bek04] for studying the GB diffusion and new types of materials [Mis95]. Here we essentially discuss application of two equations due to 1) obvious solution given by the complementary error-function in the type-C kinetics, which need not be explained in detail, and 2) importance of the B-regime and especially A-regime for nanocrystalline materials.

The B-regime has been remaining the most reliable regime for many years, since the grain size of tens of micrometers in the coarse grained materials determines the overall behavior. A procedure to extract D_{gb} from the measured diffusion profile was proposed by Le Claire [Cla63]. The advantage of the diffusion profile measured in the B-regime is in fact, that the bulk and GB diffusion are separable. Following mathematical intuition and knowing that the diffusion profiles are linear functions of $y^{6/5}$ [Lev60], Le Claire came up with the following expression

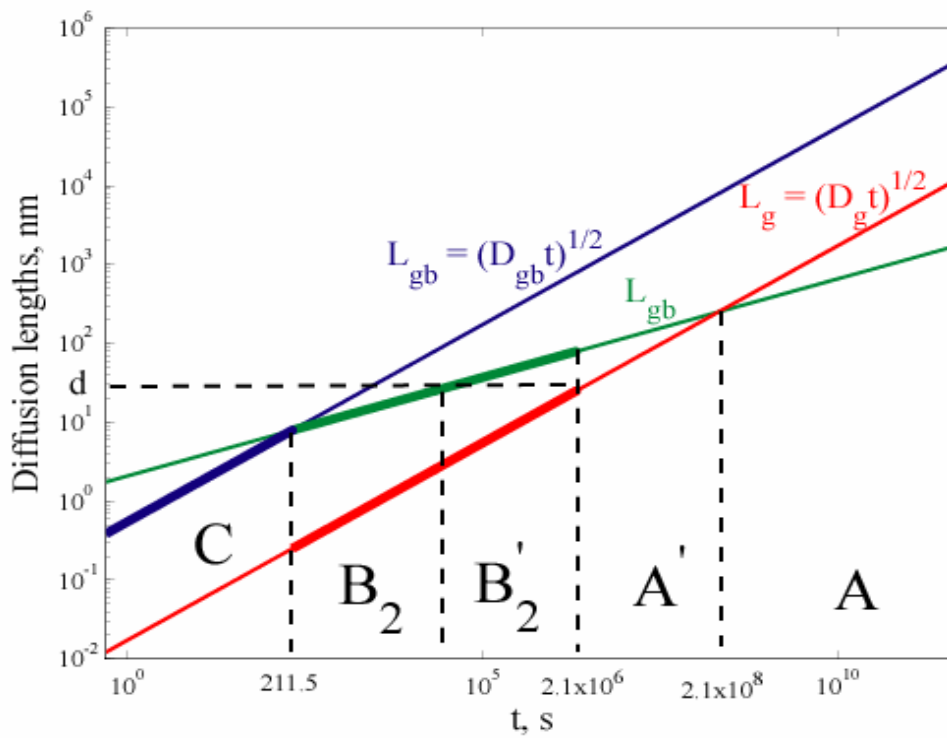
$$\delta D_{gb} = 2\sqrt{\frac{D_g}{t}} \left(-\frac{\partial \ln C_{av}}{\partial w^{6/5}} \right)^{5/3} \left(-\frac{\partial \ln C_{av}}{\partial y^{6/5}} \right)^{-5/3}, \quad (1.14)$$

where w is the dimensionless coordinate, having a very important property of making the diffusion profile plotted as a function of w independent of Δ . This is based on the following

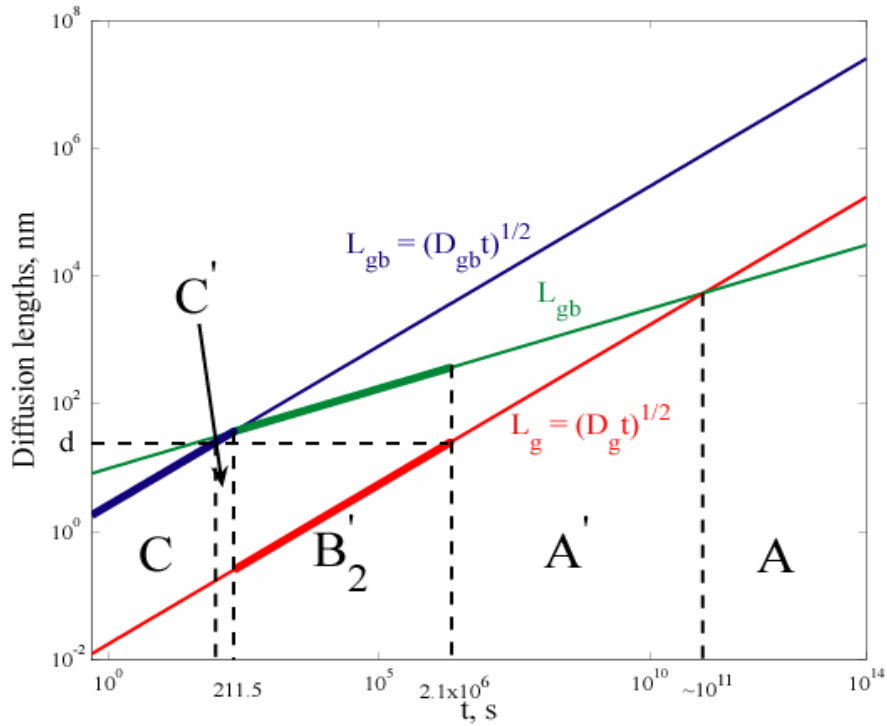
a)



b)



c)



d)

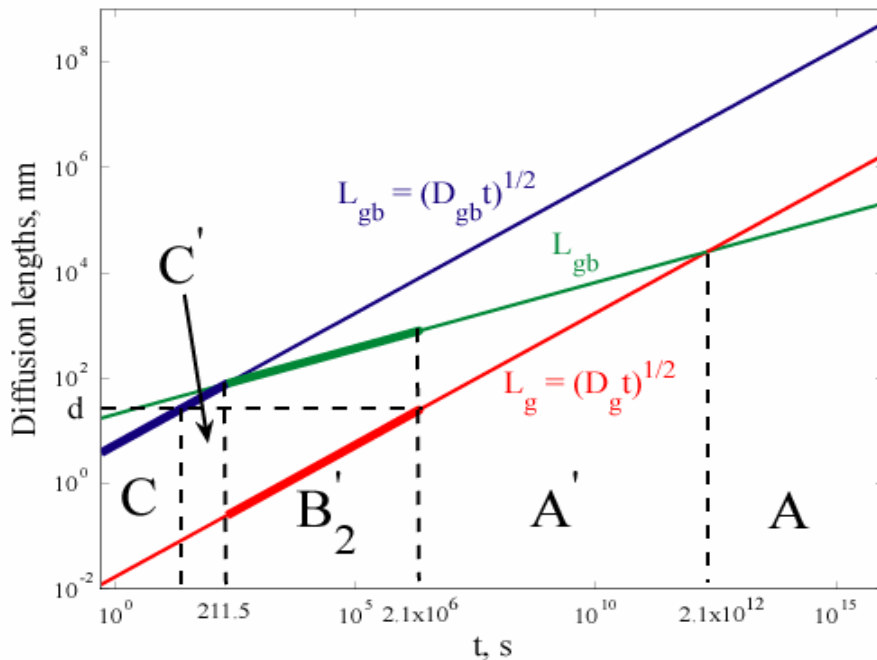


Fig. 1.5 How diffusion lengths along the GBs (L_{gb}) and grains (L_g) vary with the diffusion time (t) for a) $\Delta = 10^2$ (coarse-grained material), b) $\Delta = 10^3$ (fine-grained material), c) $\Delta = 2.2 \cdot 10^4$ (ultrafine-grained material), d) $\Delta = 10^5$ (ultrafine-grained material). The dependences are plotted on the logarithmic scale. In the case of green line L_{gb} is given by Eq. (1.12a).

expression for w :

$$w = \frac{\eta}{\sqrt{\beta}} = \frac{y}{\sqrt{D_g t \beta}} = \frac{y}{\sqrt{\delta D_{gb}}} \left(\frac{4D_g}{t} \right)^{1/4}, \quad (1.15)$$

where η is the dimensionless coordinate weighted to the diffusion length in grain (bulk) and used in the original Whipple solution [Whi54]. While the second derivative in Eq. (1.14) represents an experimentally measurable gradient, the derivative with respect to w can not be obtained without knowing D_{gb} . Le Claire suggested that it can be replaced by a constant value, if $\beta \gg 10$ (Eq. (1.9d)) and $w \gg 2$. Both the quantities are Δ -dependent; therefore these are also unknown for the once measured diffusion profile. However, it is believed that in most cases the conditions are satisfied. If it is really the case, the derivative is replaced by a constant value of -0.78 according to Le Claire [Cla63], giving rise to

$$\delta D_{gb} = 1.322 \sqrt{\frac{D_g}{t}} \left(-\frac{\partial \ln C_{av}}{\partial y^{6/5}} \right)^{-5/3}. \quad (1.16)$$

The latter expression is known as Le Claire's relation, which is the only expression used, when the gradient is measured under conditions of type-B kinetics. Eq. (1.16) is modified, if the segregation of impurities is concerned. The triple product $s\delta D_{gb}$ [Bok58] comes into play in this case. The role of segregation effects in the type-B kinetics is not discussed in the present study. Recently, Chung and Wuensch [Chu96a] observed that the conditions of validity of Eq. (1.16) were not fulfilled in the case of very shallow diffusion gradients. Such situations are discussed in the present study.

Hart's equation is widely used [Hart57], if the diffusion profile was measured at very long t and/or high temperatures. The equation represents a linear combination of diffusivities D_g and D_{gb} weighted to the volume fraction of GBs (g):

$$D_{eff} = gD_{gb} + (1-g)D_g. \quad (1.17a)$$

His equation was modified to take into account segregation by Mortlock [Mor60] and reads:

$$D_{eff} = sgD_{gb} + (1-sg)D_g. \quad (1.17b)$$

The latter expression is known as the Hart-Mortlock equation in which includes the equilibrium segregation factor s is given by Eq. (1.6b). Since this equation is valid only for the model of parallel boundaries, another expression was also suggested to deduce D_{gb} [Kal01]:

$$D_{\text{eff}} = \frac{sD_{gb} [(2-g)D_g + sgD_{gb}]}{(1-g+sg)[sD_{gb}(2-g) + gD_g]} \quad (1.18)$$

This is a modified Maxwell-Garnett, or Maxwell equation [MaxG04], [Max54] which is believed to be valid for realistic polycrystalline microstructures.

All these equations are currently used to deduce D_{gb} from the measured diffusion profiles except Eq. (1.18). Up to now there are no publications demonstrating the use of Eq. (1.18) in diffusion experiments. As these equations do not take into account the conditions of small grain sizes, it is the aim here to check the validity of those theories under conditions of short t . In the next chapters the discussion of such specific conditions will be continued on the basis of numerical evaluations of Whipple's solution as well as numerical integrations of the Fisher system.

Chapter II. Finite element model

Introduction

The finite element method (FEM) is a very useful numerical tool that allows one to effectively integrate differential equations. The physical problems that can be solved by FEM can in general case be discrete or continuum in nature [Com94]. As far as diffusion is concerned, solving continuum problems is relevant in the present work. Consequently, the general definition for the finite element problem is given in this chapter. As diffusion along and across GBs has its own specific features, the integrals that were evaluated to find the physical property at each node of the finite element mesh are also given. Different numerical problems related to FEM and accompanying simulation of GB diffusion by FEM are explained along with discussion of the main results in coming chapters.

Particularly, FEM was chosen as effective tool for numerical integration in such problems that are characterized by complicated geometries. One can find a broad literature on the application of FEM to different mechanical problems. There even exist several serious books on using FEM to integrate conduction type equations [Com94], [Lew96], [Hun02] as

for heat conduction. Moreover, FEM was recently used to describe atoms and diatomic molecules [Kop98], to investigate electronic structure of quantum dots [Qu03] and to make it possible to couple atomistic and continuum approaches [Cur03]. So a broad range of physical problems that can be solved by FEM show its importance and uniqueness.

2.1 General aspects with respect to continuum problems

Two procedures are always associated with FEM, namely discretization and integration. The former is directly related to the transformation of differential equation into a system of algebraic equations which then has to be solved numerically [Com94]. The latter applies to the fact, that in FEM each term of the differential equation is written in integral form, and each integral has to be solved at each point of the mesh. The mesh is a common principle of all numerical integrations. Mostly all numerical difficulties that arise during the calculation are associated with the mesh, especially in transient physical problems. Importantly, in FEM the unknown function (field) is approximated by interpolation at the points of mesh.

The general concept to solve a physical problem by using FEM constitutes of the following:

- understanding the physical phenomenon
- writing down the governing partial differential equation subject to the corresponding boundary conditions
- obtaining the equation in FEM formulation which should be solved, i.e. with the projection polynomials and in integral form
- finding a qualitative and reasonable mesh for the physical problem
- running FEM program

In the case of instationary problems the time interval is also responsible for the accuracy and stability of the obtained results. So, in principle, one has to keep in mind this aspect too [Tho97].

2.2 Fisher's system expressed in the form suitable for finite element calculation

Fisher's system reads

$$\begin{cases} \frac{\partial C_g(x, y, t)}{\partial t} - D_g \operatorname{divgrad}[C_g(x, y, t)] = 0 \\ \frac{\partial C_{gb}(y, t)}{\partial t} - D_{gb} \operatorname{divgrad}[C_{gb}(y, t)] - \frac{2D_g}{\delta} \operatorname{grad}_x[C_g(x, y, t)] = 0 \end{cases} \quad (2.1)$$

The weak formulation [Flu92a] requires to first project the differential equation on the projection polynomials based on Galerkin's projective method. Accordingly, the equation for grain diffusion can be written as [Flu92a]

$$\iint_{\Gamma} \alpha_i \frac{\partial C_g(x, y, t)}{\partial t} dx dy + \iint_{\Gamma} \alpha_i \left(-D_g \operatorname{divgrad}[C_g(x, y, t)] \right) dx dy = 0, \quad (2.2)$$

where α_i is the projection polynomial. The second integral in Eq. (2.2) may also be generalized as

$$\iint_{\Gamma} \alpha_i \frac{\partial C_g(x, y, t)}{\partial t} dx dy + \iint_{\Gamma} \alpha_i \operatorname{div} \left\{ -D_g \operatorname{grad}[C_g(x, y, t)] \right\} dx dy = 0. \quad (2.3)$$

By using the mathematical transformation [Flu92a]

$$\begin{aligned} \alpha_i \operatorname{div} \left\{ -D_g \operatorname{grad}[C_g(x, y, t)] \right\} &= \operatorname{div} \left\{ -\alpha_i D_g \operatorname{grad}[C_g(x, y, t)] \right\} \\ &+ D_g \operatorname{grad}[C_g(x, y, t)] \operatorname{grad}[\alpha_i] \end{aligned} \quad (2.4)$$

Eq. (2.3) becomes

$$\begin{aligned} \iint_{\Gamma} \alpha_i \frac{\partial C_g(x, y, t)}{\partial t} dx dy + \iint_{\Gamma} \operatorname{div} \left\{ -\alpha_i D_g \operatorname{grad}[C_g(x, y, t)] \right\} dx dy \\ + \iint_{\Gamma} D_g \operatorname{grad}[C_g(x, y, t)] \operatorname{grad}[\alpha_i] = 0. \end{aligned} \quad (2.5)$$

According to Gauss-Ostrogradsky's theorem [Flu92a], [Kor68] it follows that

$$\iint_{\Gamma} \operatorname{div} \left\{ -\alpha_i D_g \vec{\operatorname{grad}}[C_g(x, y, t)] \right\} dx dy = - \int_{d\Gamma} \alpha_i D_g \vec{\operatorname{grad}}[C_g(x, y, t)] \vec{n} dl. \quad (2.6)$$

Substituting Eq. (2.6) into Eq. (2.5) gives

$$\begin{aligned} & \iint_{\Gamma} \alpha_i \frac{\partial C_g(x, y, t)}{\partial t} dx dy + \int_{d\Gamma} \alpha_i \left| D_g \vec{\operatorname{grad}}[C_g(x, y, t)] \right| \vec{n} dl \\ & + \iint_{\Gamma} D_g \operatorname{grad}[C_g(x, y, t)] \operatorname{grad}[\alpha_i] dx dy = 0 \end{aligned} \quad (2.7)$$

The equation for GB diffusion in Eq. (2.1) is the boundary condition itself and is taken at $x = \pm \delta/2$ (fig. 1.2). Recalling this boundary condition and using the transformations given by Eqs. (2.4) and (2.6), the final form of Fisher's system used in finite element program is

$$\begin{aligned} & \iint_{\Gamma} \alpha_i \frac{\partial C_g(x, y, t)}{\partial t} dx dy + \frac{\delta}{2} \int_{d\Gamma} \alpha_i D_{gb} \vec{\operatorname{grad}}[C_g(x, y, t)] \operatorname{grad}[\alpha_i] dy + \frac{\delta}{2} \int_{d\Gamma} \alpha_i \frac{\partial C_{gb}(y, t)}{\partial t} dy \\ & + \iint_{\Gamma} D_g \operatorname{grad}[C_g(x, y, t)] \operatorname{grad}[\alpha_i] dx dy = 0 \end{aligned} \quad (2.8)$$

According to standard finite element procedure this final expression is used in the matrix form. In the expression the second and fourth integrals represent the conduction parts, whereas the other two integrals are responsible for the time variation. It should be noted that surface conditions (Eq. 1.3a) that exist in the GB diffusion problem are taken into account in Eq. (2.8). Importantly, segregation problems require the use of the same equation in which the second and the third integral are multiplied by the segregation factor s according to Eq. (1.6c).

2.2.1 Finite element method formulation of space charge layer problem

The space charge layer problem is complex due to additional equations and boundary conditions. Fisher's system was extended in order to take into account the space charge effects. According to the model which will be discussed in chapter V the system of partial differential equations for the space charge problem reads

$$\begin{cases} \frac{\partial C_g(x, y, t)}{\partial t} - D_g \operatorname{divgrad}[C_g(x, y, t)] = 0 \\ \frac{\partial C_{scl}(x, y, t)}{\partial t} - D_g \operatorname{divgrad}[C_{scl}(x, y, t)] = 0 \\ \frac{\partial C_{gb}(x, y, t)}{\partial t} - D_{gb} \operatorname{divgrad}[C_{gb}(y, t)] - \frac{2D_{scl}}{\delta} \vec{\operatorname{grad}}_x [C_{scl}(x, y, t)] = 0 \end{cases}, \quad (2.9)$$

where C_{scl} and D_{scl} are the concentration and diffusivity within the SCL. While the continuity condition at the interface between the GB (or the GB core) and space charge layer (SCL) is reflected in the last equation (as it is supposed by Fisher's system), additional boundary conditions should be written for the interface between the SCL and bulk (fig. 5.1). Supposing equal fluxes and concentration at that interface gives

$$C_{scl}(x, y, t) = C_g(x, y, t) \quad \text{at} \quad \mathbf{x} = \pm \left(\frac{\delta}{2} + \delta_{scl} \right)$$

and (2.10)

$$D_{scl} \frac{\partial C_{scl}(x, y, t)}{\partial y} = D_g \frac{\partial C_g(x, y, t)}{\partial y} \quad \text{at} \quad \mathbf{x} = \pm \left(\frac{\delta}{2} + \delta_{scl} \right).$$

The advantage of using the finite element program is that these boundary conditions together with the boundary condition of zero flux at the bottom of geometry used are automatically included. One needs to slightly modify the equation derived for the more general problem, namely Eq. (2.8). This leads to the following expression:

$$\begin{aligned} & \iint_{\Gamma} \alpha_i \frac{\partial C(x, y, t)}{\partial t} dx dy + \frac{\delta}{2} \int_{dr} \alpha_i D_{gb} \vec{\operatorname{grad}}[C_g(x, y, t)] \operatorname{grad}[\alpha_i] dy + \frac{\delta}{2} \int_{dr} \alpha_i \frac{\partial C_{gb}(y, t)}{\partial t} dy \\ & + \iint_{\Gamma} D \operatorname{grad}[C(x, y, t)] \operatorname{grad}[\alpha_i] dx dy = 0 \end{aligned} \quad (2.11)$$

In the last expression C and D can either correspond to the grain or SCL. This means that the same equation is applied to both regions which have finite dimensions. The difference between these regions (grain and SCL) does not lie only in different diffusivities. Applying Eq. (2.11) for the bulk (grain), D_{gb} is not used or equal to zero. This is achieved in the finite element program, at least in a particular case of FLUX-EXPERT used in the current work, by

creating the regions with different properties when generating the mesh for the problem [Sima95]. The finite element calculations are relevant for chapter IV and chapter V. In the following chapter III we numerically evaluate Whipple's solution by using the program MatLab.

2.3 Finite element calculation by using FLUX-EXPERT

FLUX-EXPERT is based on the Expert-System technique [Mas84] and, consequently, is organized in the way that one has to use different modules [Flu00] in order to obtain the solution. Each module represents a program (or a package) for passing a separate step in solution (fig. 2.1). Usually one has to start with definition of the geometrical model and of the mesh. This is done in the program 'SIMAIL' [Sima95], [Sima97] which only creates the mesh, and the result is saved in the file with the extension 'DAT'. The shape of the elements is also determined in this program. In the present study on GB diffusion the triangular elements were only used.

The program FLUX-EXPERT has several libraries of equations for solving particular physical problems. For example, the diffusion equation, called DIFFUS_2D.EQU [Simu02], is usually supplied once the program is installed. However, this equation exists for solving 2D stationary diffusion problems and simple boundary conditions of Neumann type [Flu95a], [Flu99]. Fisher's system represents Fick's second law subject to a specific boundary condition which represents diffusion along a GB and takes into account a leakage of atoms from a GB into a grain. Thus, to simulate GB diffusion, one needs first to create an equation. This can be done in the module 'Generator' [Flu92b]. The 'Generator' is an important feature of FLUX-EXPERT which suggests much more possibilities for the user [Bau85], [Szt92]. This module makes the use of FLUX-EXPERT very flexible since different equations can be met in real research. When describing the equation, the computation algorithms which can be important for this problem are also defined in 'Generator'. To solve Fisher's system, the transient algorithm is necessary. Consequently, the algorithm called 'RLTDMC' was used. This algorithm is non-symmetric, transient, linear, "ill (poorly)-conditioned", i.e. the Gauss method is used for solving the system of equations [Flu92c]. The operator $\partial/\partial t$ is replaced by the corresponding finite difference scheme [Flu92d]. Importantly, the final system containing the integrals and time differences is implicit in nature. The latter avoids the numerical instabilities associated with finite difference schemes when written in explicit form [For60]. However, before describing the equation all the physical properties should be defined. The module

‘GNOYAU’ allows one to define the physical properties, also called identifiers (for example, D_{gb}), and different operators [Flu00] such as the integrand operators, the operators of differential weights of integrals, the algorithm operators. These operators can then be used in the module ‘Generator’ for a particular equation. In the case of Fisher’s system Eq. (2.8) was incorporated and used along all calculations by FLUX-EXPERT. Another feature of FLUX-EXPERT is that all the physical properties are collected in the data base which can be modified by ‘Generator’, i.e. new necessary physical properties can be added. Therefore, D_{gb}

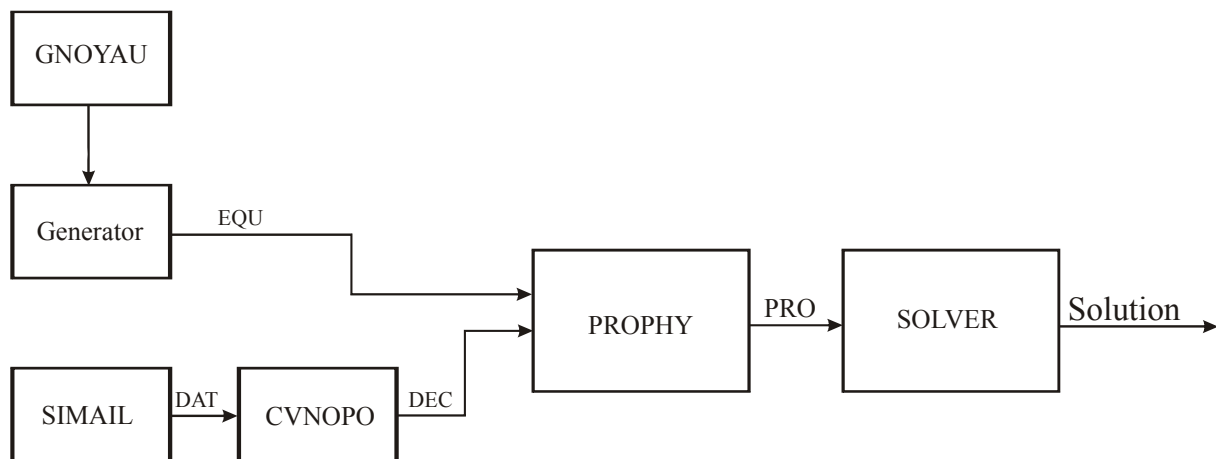


Fig. 2.1 A scheme of steps necessary for obtaining the final solution by using FLUX-EXPERT. Each step represents a module of the program.

was described in order to use it in the equation while D_g and D_{scl} were represented by a diffusion coefficient DC supported by the program [Simu02].

Since the equation and the mesh are defined, these can be used in the module ‘Prophy’ which creates the problem file for integration. Thus, this file contains information on the mesh, the physical properties involved and the equation. The extension of the file produced by ‘Prophy’ is ‘PRO’, and this is usually the biggest file among all the files which are used for solving a physical problem. Finally, the program ‘Solver’ is used to integrate the differential equations and the result of this integration is saved in PRO-file.

Chapter III. Nonlinearity effect

Introduction

Le Claire's relation is still remaining the only one used for the evaluation of GB diffusivity (D_{gb}) from the diffusion profiles measured under conditions of type-B kinetics. The relation is based on the finding of Levine and McCallum [Lev60] that the GB part of $\ln C_{av} = f(y^{6/5})$ plot is a linear function. However, it is very difficult to suggest a scale in which the diffusion profile is exactly a linear function for a broad range of parameters. In this chapter we investigate the validity of such a linear dependence for short diffusion times.

3.1 Important definitions

For that purpose Whipple's solution was integrated, fixing the penetration depth at 500 nm and varying the diffusion time (t) and the ratio of diffusivities (Δ). These are the typical experimental conditions [Mis99] too when measuring the concentration profile and determining the GB diffusivity (D_{gb}), because Δ is unknown. For the integration a sample characterized by a width of 25 nm and a length of 500 nm was used. Such a sample is called

hereafter also as a geometrical model. The value for $D_g = 2.95 \cdot 10^{-4} \text{ nm}^2/\text{s}$ ($2.95 \cdot 10^{-16} \text{ mm}^2/\text{s}$) as well as $D_{gb} = 6.42 \text{ nm}^2/\text{s}$ ($6.42 \cdot 10^{-12} \text{ mm}^2/\text{s}$) were taken from the Arrhenius relations found in [Bro99a] on oxygen diffusion in ultrafine-grained undoped ZrO_2 at 500°C . These values satisfy $\Delta = 2.2 \cdot 10^4$, whereas other ratios in the calculations were obtained by varying D_{gb} and fixing D_g . Most results shown in the present work reflect the behavior of $C_{av}(y, t)$ and the distribution of $C_g(x, y, t)$.

The main aim of the present study is to check the validity of Le Claire's relation for short-time situations and to estimate possible errors of the D_{gb} determination. An apparent GB diffusivity ($D_{gb,app}$) is introduced which can be compared with a true diffusivity $D_{gb,true}$ used in the calculation.

3.1.1 The C- or B-regime?

In order to be able to evaluate D_{gb} by using Le Claire's relation, one should only know that the condition of type-B kinetics is satisfied. The diffusion length in the bulk (grain) (L_g) was allowed to vary from a very small value of 0.77 nm at $t = 2000 \text{ s}$. This implies an extremely short L_g of the order of atomic spacing, and high concentration gradients. Such an extreme situation corresponds to L_g which does not exceed the GB thickness (δ) significantly. One could open the question about the validity of the type-C kinetics under such conditions. In order to understand the diffusion profile calculated for condition of $L_g = 0.77 \text{ nm}$ corresponds more to the B-regime or C-regime, the diffusion profile was fitted by a complementary error-function with D_{gb} . If tentatively the evaluation for type-C is used, the diffusion coefficient is wrong by four orders of magnitude. It is, hence, clear that the diffusion profile does not represent a complementary error function (fig. 3.1) and, consequently, the diffusion process does not correspond to the kinetics of type-C. This also makes generally the existence of the C-regime questionable, although the situations of very small diffusion lengths are of particular interest here. According to this result, it is enough to make several jumps for the atoms moving from the GB into the grain (this is caused by the concentration gradient, what is proposed by Fisher's system (Eq. (1.6a)) to observe the B-regime.

3.2 Integrating Whipple's solution

The integration of Whipple's solution should be done very carefully, because the short t leads to steep gradients and a reduced effective region of integration. The concentrations and

penetrations are smaller. In this case both the density of integration mesh, as far as the numerical integration is concerned, and the limits of integration can be important. The constant intervals (steps) Δx or Δy , depending on the direction, determine the mesh density and are chosen to be important parameters to achieve a very well converged result. In some cases it suffices to find these steps properly. This has nothing to do with the integration step used in the quadrature formula [Pres02] since the integration was performed by using the algorithms worked out in the program MatLab [Kiu05] with applying a function ‘quadl’ [Mat04] based on adaptive Lobatto quadrature [Gan00]. The relevant intervals are due to the 2D nature of the problem of GB diffusion and the integral form of Whipple’s solution.

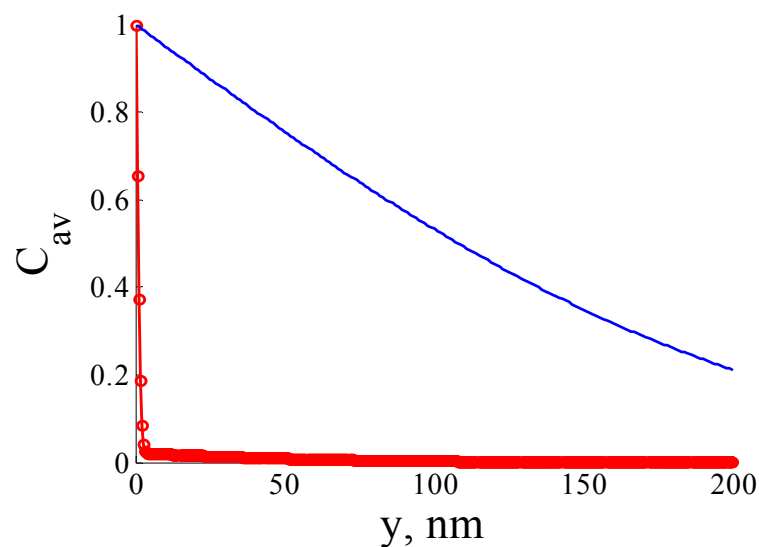


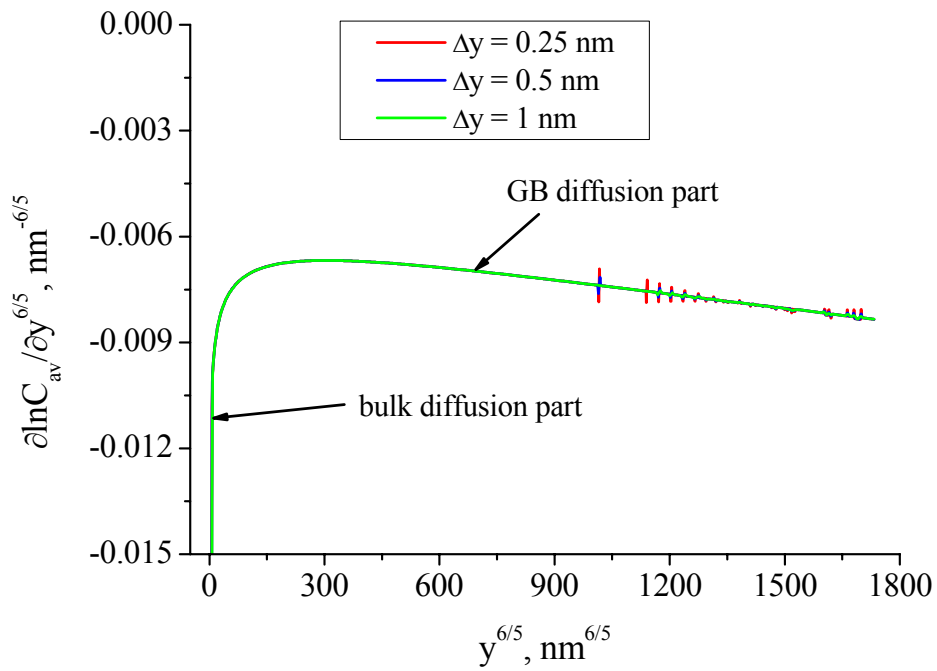
Fig. 3.1 A comparison of the Whipple (red curve) and $\text{erfc}(y/2\sqrt{D_{gb}t})$ (blue curve) solutions for $\Delta = 2.2 \cdot 10^4$ at $t = 2000$ s. The concentration C_{av} is normalized with respect to C_0 (Eq. (1.3a)).

The integration was performed for each x-value along the whole length of 500 nm. Obviously, the interval Δy is of particular importance. The result is much more sensitive to this interval rather than to Δx . For this problem the convergence means that the result remains unchanged when increasing the step of integration and, at the same time, satisfying the necessary error limits. Most of the problems with the integration of Whipple’s solution are related to numerical instability. Additionally, in the analysis we are interested in the derivative of the concentration profile is plotted. The derivative (in some cases the term ‘gradient’ is used in the present work) allows one first to analyze the physical result, and second, to estimate the quality of integration. This is reflected in the strong sensitivity of the derivative with respect to changes of the profile introduced by any numerical factors. Namely, numerical

instabilities are reflected immediately. To estimate the value of the slope of the profile (Eq. (1.16)), the scale of the ordinate ($\partial \ln C_{av} / \partial y^{6/5}$) was changed significantly due to a rapid dependence of the bulk diffusion part of the profile on y in comparison with the GB part of the profile. Thus these two parts obviously have very different rates. At each t the integration scheme (the interval Δy and the limits of integration) was verified separately for all ratios $\Delta = D_{gb}/D_g$ used, whereas the step Δx was once obtained and fixed in the calculations to 0.1 nm. The interval Δy was varied from 40 nm to 0.25 nm for $\Delta = 2.20 \cdot 10^4$ at $t = 2000$ s (fig. 3.2). On the one hand, the GB part of the derivative is not affected significantly when Δy is increased. This is important, because decreasing the step leads to numerical instabilities (spikes in fig. 3.2a). On the other hand, increasing the interval Δy changes the bulk part (fig. 3.2b). This is clear, because the integration of the bulk part requires smaller intervals. Interestingly, the bulk diffusion is observed up to $6 \text{ nm}^{6/5}$ at $t = 2000$ s for $D_g = 2.95 \cdot 10^{-4} \text{ nm}^2/\text{s}$ and $D_{gb} = 6.42 \text{ nm}^2/\text{s}$. At deeper penetrations only the GB diffusion plays a role. The numerical instabilities exist even with $\Delta y = 1.0$ nm, while further increasing the integration step is impossible due to deviations in the bulk part.

The integral published by Whipple [Whi54] contains Δ as the upper limit of integration and σ as the integration parameter (Eq. (1.9a)). All the curves shown in fig. 3.2 were obtained with $\Delta (= 2.2 \cdot 10^4)$ as the upper limit of integration (σ_{\max}). In many cases Δ can be a very large value, making the region of integration too large and leading to very small concentrations. After obtaining the density of mesh ($\Delta y = 1.0$ nm), the upper limit of integration was decreased, because very low concentrations can also lead to the instabilities. Moreover, the values of concentration are so low in such regions that those do not sufficiently contribute to C_g (Eq. (1.9a)). It was observed that the numerical noise arises with σ_{\max} being 15000 (hardly seen in fig. 3.3) for the same parameters that used in fig. 3.2. However, the convergence with respect to the upper limit of integration is reached with $\sigma_{\max} = 20000$. Again the instabilities do not allow for a completely correct result. But, if σ_{\max} , the upper limit of integration, is chosen to be small enough, the function $\partial \ln C_{av} / \partial y^{6/5} = f(y^{6/5})$ becomes even more nonlinear (fig. 3.3). In this sense, fitting the dependences $\ln C_{av} = f(y^{6/5})$ to a straight line would give very large errors in determining D_{gb} . The area under the derivative as well as its value at the maximum decreases with decreasing σ_{\max} . Therefore, it is necessary to use at least $\sigma_{\max} = 15000$ for the parameters $\Delta = 2.2 \cdot 10^4$ and $t = 2000$ s. This means one always has to find reasonable values σ_{\max} , otherwise the slope can be overestimated due to numerical reasons. In fig. 3.4 the integrand of Whipple's solution is plotted as a function of σ for the same diffusion

a)



b)

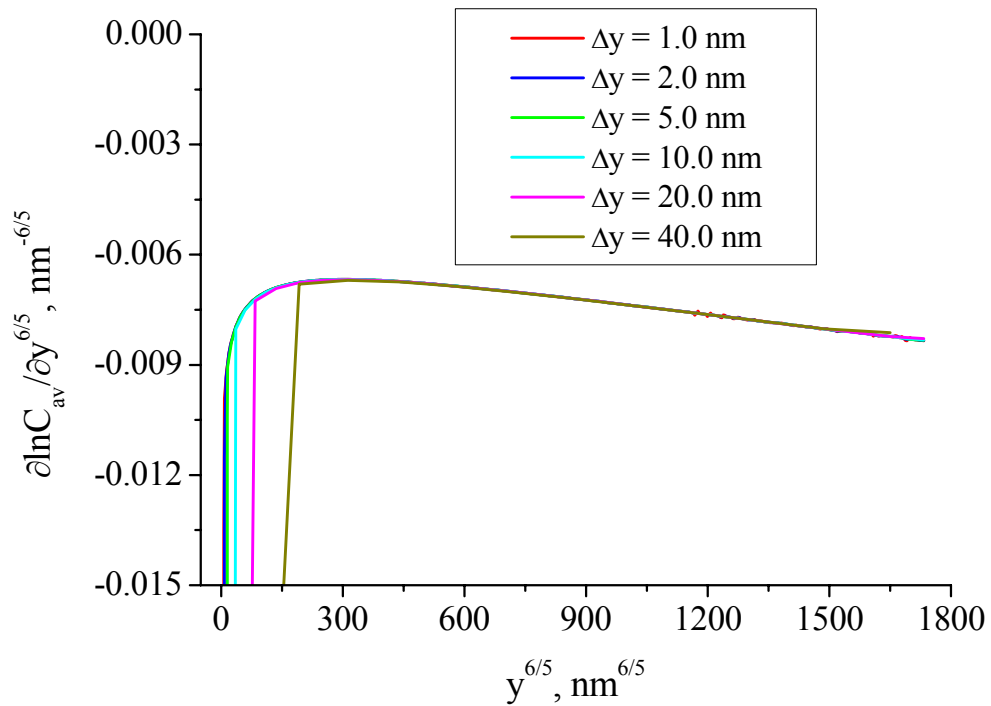


Fig. 3.2 Variation of the derivative $\frac{\partial \ln C_{av}}{\partial y^{6/5}}$ as a function of $y^{6/5}$ obtained for small a) and large b) Δy -steps for $\Delta = 2.2 \cdot 10^4$ and $t = 2000 \text{ s}$.

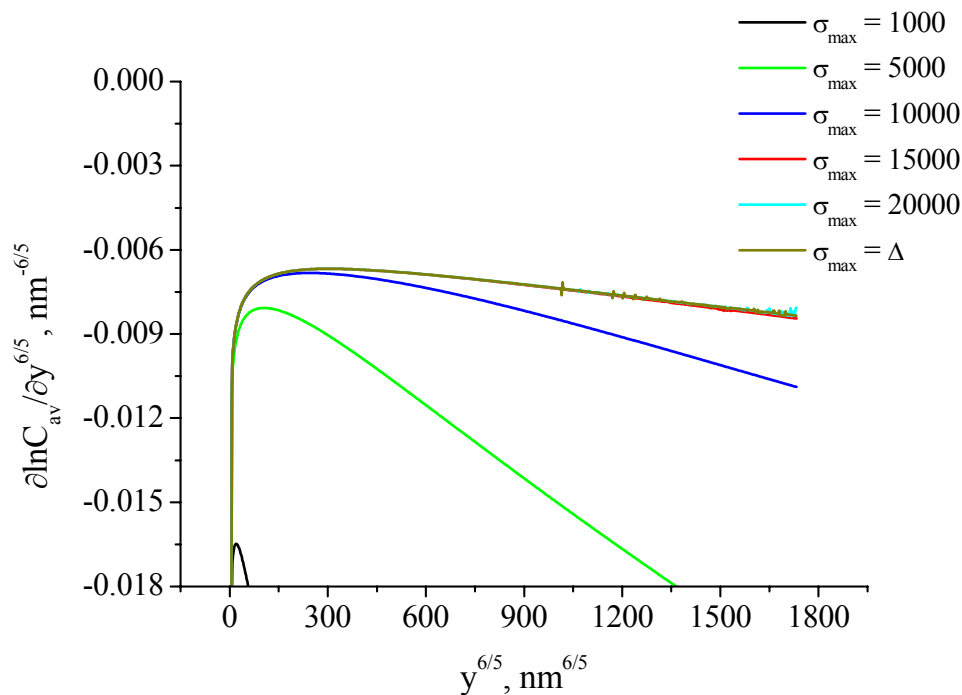


Fig. 3.3 Different upper limits of integration for $\Delta = 2.2 \cdot 10^4$ and $t = 2000$ s.

parameters as in figs. 3.2 and 3.3. It is clearly seen that the integrand has large values at small σ and decreases slowly with σ approaching very small values. One can conclude from this plot, that the reason of the overestimation of the slope for σ being smaller than 15000 (fig. 3.3) comes from the cut-off. In other words, the overestimation is due to lost concentrations at values of σ larger than 1000. The value of the integrand for $\sigma = 15000$ ($\Delta = 2.2 \cdot 10^4$), $y = 10$ nm and $x = 0.25$ nm, i.e. exactly at the GB since the GB thickness is 0.5 nm, is $3.77 \cdot 10^{-9}$. This is one of the highest integrand values which can be observed at these coordinates for $\sigma = 15000$. Such small values should also be taken to effectively integrate Whipple's solution. Consequently, the problem of very large Δ is especially important for integrating Whipple's solution at short t . In such cases, the diffusion length can be much shorter than the length of the sample. So shorter penetrations demand smaller integration limits. Fig. 3.4 shows the influence of increasing coordinates x and/or y . All the changes in the directions parallel with the GB or perpendicular to that lead only to a decreasing area under the integrand. The maximum of the integrand is shifted to larger and smaller σ for the increased coordinates y and x , respectively. It can be mentioned, that all the values discussed are sensitive to parameters such as diffusivities and t . An important consequence coming from fig. 3.4 is that the integral can have a maximum value at rather small y -coordinates.

Finally, different integration intervals were tried in the two parts of the diffusion profile. As it is clearly seen in fig. 3.2 the results for $\Delta y = 0.25$ nm and $\Delta y = 0.5$ nm do not deviate from each other, satisfying the error of 1%. The only problem of those is related to

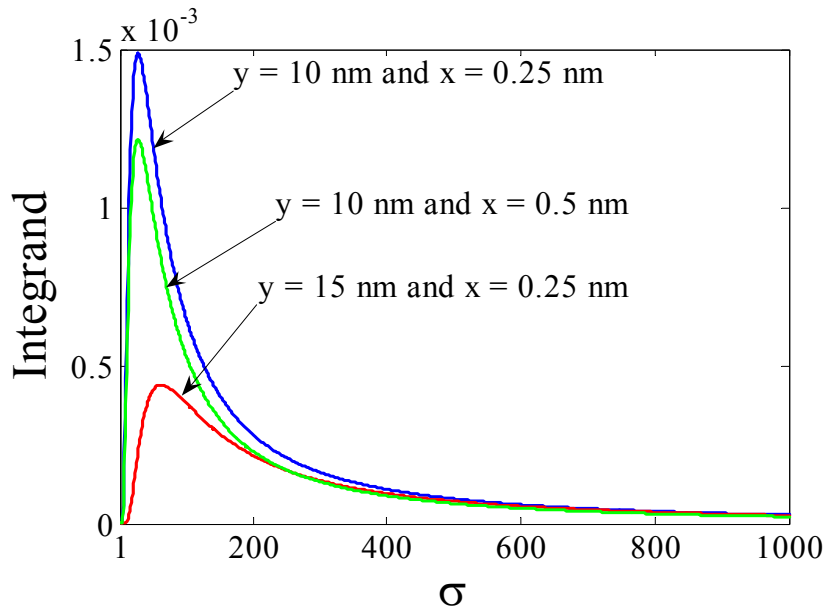
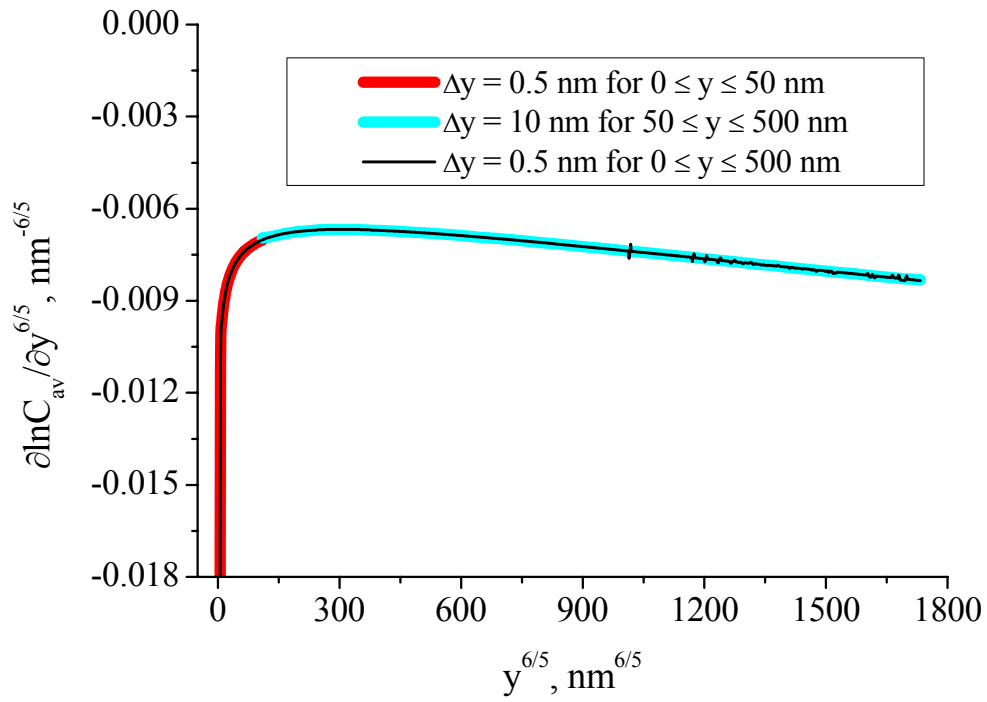


Fig. 3.4 Integrand of Whipple's solution plotted as a function of σ for different coordinates y and x .

instabilities. So $\Delta y = 0.5$ nm can be taken as integration interval in the bulk part. Because the deviations in the GB part arise with Δy being larger than 10 nm, that value is suggested to be a limit of integration in the GB part. In fig. 3.5a the results of integration with different intervals in the two parts of the profile are compared with the result obtained with a constant step. The bulk part was integrated up to a penetration of 50 nm, which exceeds the bulk diffusion length and lies in the region of obvious intermixing between the bulk and GB parts of diffusion. The result of integration with two intervals is in a very good agreement with the result of constant integration interval. Consequently, different integration intervals should be used at $t = 2000$ s in order to exclude any numerical problems and to obtain accurate results.

The increase of t allows the same interval of integration to be used for both parts of the derivative. Thus, the numerical instabilities disappear already at $t = 4700$ s with $\Delta y = 1$ nm due to an increased level of concentration in both the bulk and GB parts of diffusion profile (the length of the sample is fixed). Nevertheless, the deviations in the bulk part with increasing Δy seem to be similar to those observed at $t = 2000$ s up to 13200 s despite the fact

a)



b)

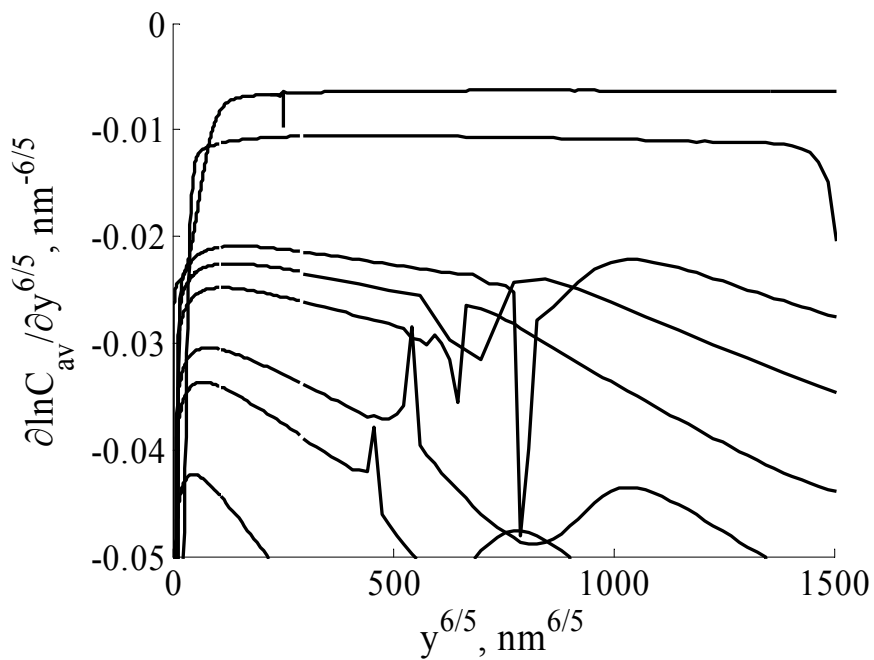


Fig. 3.5 a) A comparison of different integration schemes at $t = 2000 \text{ s}$ and $\Delta = 2.2 \cdot 10^4$, b) An example of the numerical instabilities for $\Delta = 10^3$ at different t (note: the slope decreases with t).

that the derivative of the bulk part changes with t too. Finally, the step in the bulk part was successfully varied in the calculations from 0.5 nm at $t = 2000$ s to 5.0 nm at $t = 500000$ s.

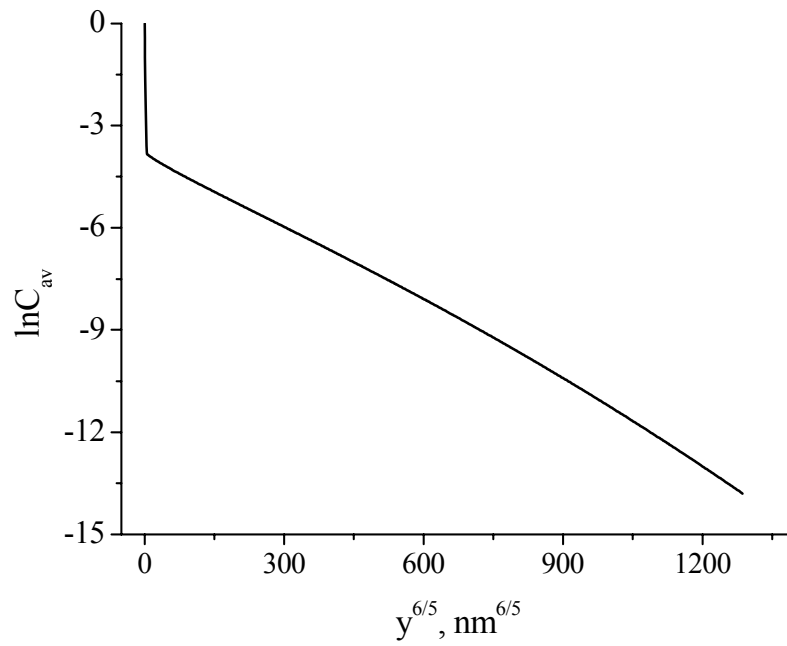
Such a situation is remaining until the interval becomes too small for the integration of the GB part. One can observe similar instabilities as shown in fig. 3.5 for $t = 13200$ s: the problem of low concentrations is replaced by another one, the small changes of the derivative in the GB diffusion part. In this case the variation of σ_{\max} cannot longer improve the result and only integrating with different intervals in different parts of the profile allows again a qualitative result to be obtained. An example of the instabilities arising in the integration is also presented in fig. 3.5b.

3.3 Errors in determining the grain boundary diffusivity

As far as the procedure of integrating the Whipple solution is clear, one can examine different t and Δ . As it was explained above, the length and the width of the sample (geometrical model) were fixed to 500 nm and 25 nm, respectively. This exactly reflects the isolated boundary arrangement (fig. 1.2). Recently, many theoretical works on the evaluation of Whipple's solution were published which are based on the transformation of the solution directly to the average concentration $C_{\text{av}}(y, t)$ [Chu96b], [Eva97], [Sha98]. Such transformations are not used here but will be discussed in the following sections. Also, the integration used in the present work is very similar to what is done experimentally.

The result obtained by simply integrating Whipple's solution is depicted in the following figure for $\Delta = 2.2 \cdot 10^4$ at $t = 2000$ s:

a)



b)

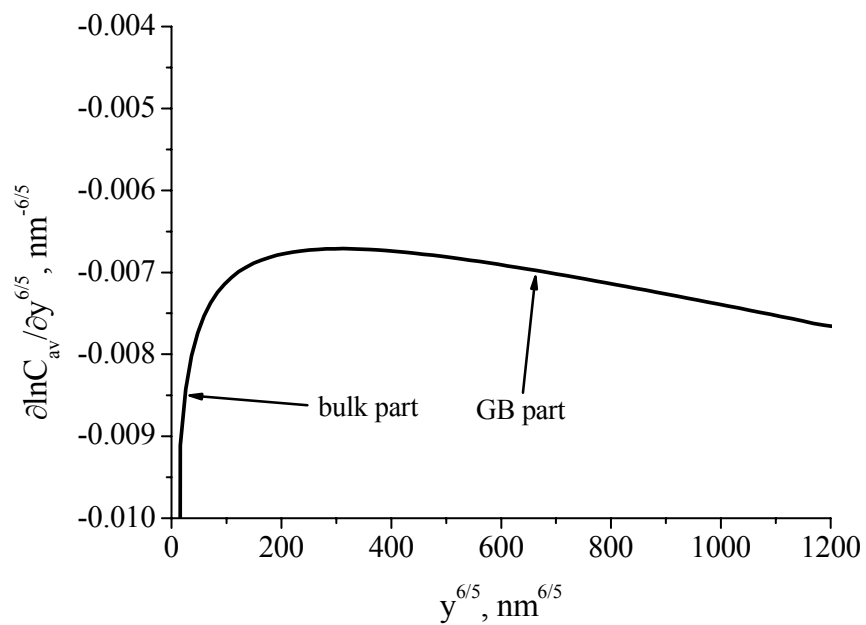


Fig. 3.6 Variation of $\ln C_{av}$ a) and $\partial \ln C_{av} / \partial y^{6/5}$ b) with $y^{6/5}$ calculated for $\Delta = 2.2 \cdot 10^4$ and $t = 2000$ s.

In fig. 3.6a one can see a typical diffusion profile, comprising two distinguishable parts: a near surface part (or so-called bulk part) and a deeper penetration tail due to the GB diffusion. As it was mentioned above, the slope of the GB part gives D_{gb} according to Le Claire's relation (Eq. (1.16)). There are two possibilities to verify such a slope. One of them is to fit the GB part of profile by a straight line subtracting the bulk part. This is usually done in the experiments [Her05], [Yas97], [Kow00], [Bak02]. However, the profile is expected to be a nonlinear function of $y^{6/5}$, and the nonlinearity of its GB part can strongly depend on the depth. Consequently, another possibility might be preferred, namely to plot the derivative of the profile in order to estimate the effect of nonlinearity. Fig. 3.6b shows that indeed the profile is nonlinear, i.e. the derivative simply confirms this.

At some point ($y^{6/5} \sim 300 \text{ nm}^{6/5}$ in fig. 3.6b) the derivative is characterized by a maximum which is close to the bulk part but, in fact, corresponds to the GB part. In the present study it is proved, that this maximum gives the correct slope or, at least, the smallest error to find D_{gb} using Le Claire's relation. To prove this statement, the diffusion profiles were calculated by using Whipple's solution at different t , varying Δ from 10^2 to 10^5 .

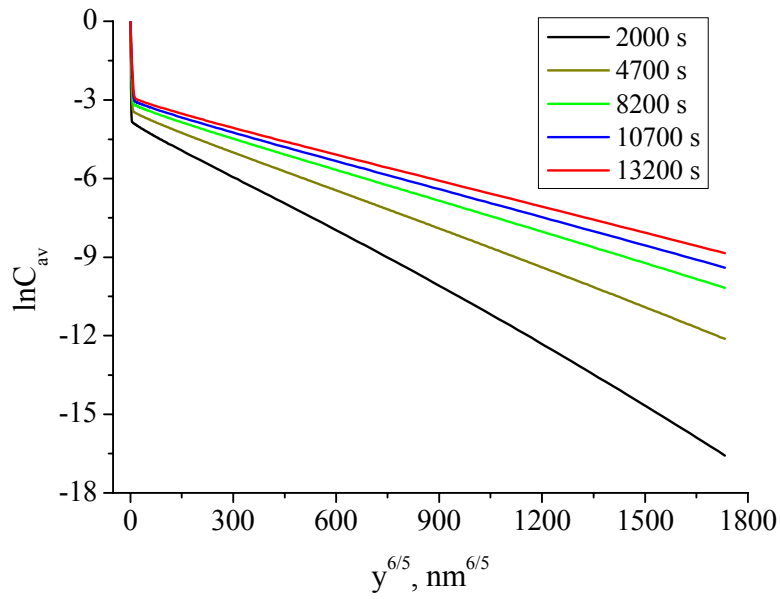
According to fig. 1.5 (the diffusion lengths dependences with t), calculating the profiles up to $t = 500000 \text{ s}$ guarantees the B-regime for different ratios Δ . The slope of the profiles decreases with t , and this is clearly seen in the dependences $\ln C_{av} = f(y^{6/5})$ (fig. 3.7a). The same behavior, obviously, can be observed for all other ratios Δ (fig. 3.8). Importantly, the slope varies with t striving for some saturation at the maximum (figs. 3.7b and 3.8). However, this saturation can never be reached. It means only that having an opportunity to obtain the profiles at very long t , as it is the case for coarse-grained materials; one can observe the values of D_{gb} rather independent of the effects of the GB diffusion nonlinearity. This might be the reason why the effect of nonlinearity has not yet been discussed in the literature. However, the effect of nonlinearity is more pronounced at shorter t . Therefore, the derivative varies with t and along the coordinate y (fig. 3.7b and fig. 3.8). Importantly, all the profiles and their derivatives, shown in figs. 3.7b and 3.8, were calculated for one maximum value of the depth (the length of geometrical model) for Δ being $2.2 \cdot 10^4$ and 10^5 , namely 500 nm. For $\Delta = 10^2$ the maximum depth was 40 nm at $t = 2000 \text{ s}$ and 500 nm at $t \geq 100000 \text{ s}$ in order to exclude the effect of very small concentrations. This is done because C_{av} at $y = 40 \text{ nm}$ for $\Delta = 10^2$ and $y = 500 \text{ nm}$ for larger Δ at $t = 2000 \text{ s}$ is about $0.3 \cdot 10^{-6}$. One may conclude that deeper penetrations than those used in figs. 3.7 and 3.8, can lead to larger errors in determining D_{gb} [Gry05].

The calculated profiles were fitted by a straight line according to the procedure usually used in the experiments and relevant errors in determining D_{gb} were obtained (fig. 3.9, black lines). The error and derivative vary with t . This is reflected in the decreasing error. At longer t the slope is more correct than at shorter ones (again the length of the sample was fixed). It does not mean that the error cannot be larger at long t . The value of the error is only a matter of the nonlinearity of profile. This increases, if deeper diffusion profiles are used. Interestingly, the fitting gives slopes which more strongly deviate from those at the maximum as t shortens. The same can be observed in the case of smaller ratios Δ . The profile is even more nonlinear under conditions of small Δ , giving larger errors. The error is about 45% at 2000 s for $\Delta = 10^2$.

The derivatives plotted in fig. 3.8 demonstrate that the slope is larger at shorter t , decreasing the apparent D_{gb} ($D_{gb,app}$) when applying the Le Claire relation. That is why D_{gb} is underestimated when the diffusion profile is fitted by a straight line, especially in the cases of short t and, as a consequence, short diffusion lengths. The maxima of derivatives of calculated profiles were also put into Le Claire's relation. Taking the values of the derivatives at the maximum allows one to reduce the error (fig. 3.9, red curves). It can be understood in such a way, that the diffusion process developing around and along a GB passes through different conditions, and there is only one situation corresponding to the considered diffusion regime. The deeper the penetration depth the smaller the contribution of GB to diffusion in the grain and the lower the level of concentration around and within the GB. Therefore, the whole process is becoming to be concentrated within the GB. In other words, the contribution of GB is not simply a linear process of $y^{6/5}$ or any other power law.

Interestingly, the error for $\Delta = 2.2 \cdot 10^4$ and 10^5 (fig. 3.9b) increases at longer t . In these cases the maximum was not reached for the used length of the sample (for example, the curve for $t = 500000$ s in fig. 3.8c), although the diffusion profile itself still comprises the two distinguishable parts. This opens a question about an additional effect related to the nonlinearity. One may conclude that the length of the whole geometrical model may be too great giving the slope affected by the new conditions along the depth or too short giving the slope affected by the bulk part of the diffusion profile [Kau95]. In both cases the concentrations and derivatives are smaller than those at the maximum. In these cases the derivative does clearly show how the profile is affected. The discussion of short lengths of the sample will be continued in the next section.

a)



b)

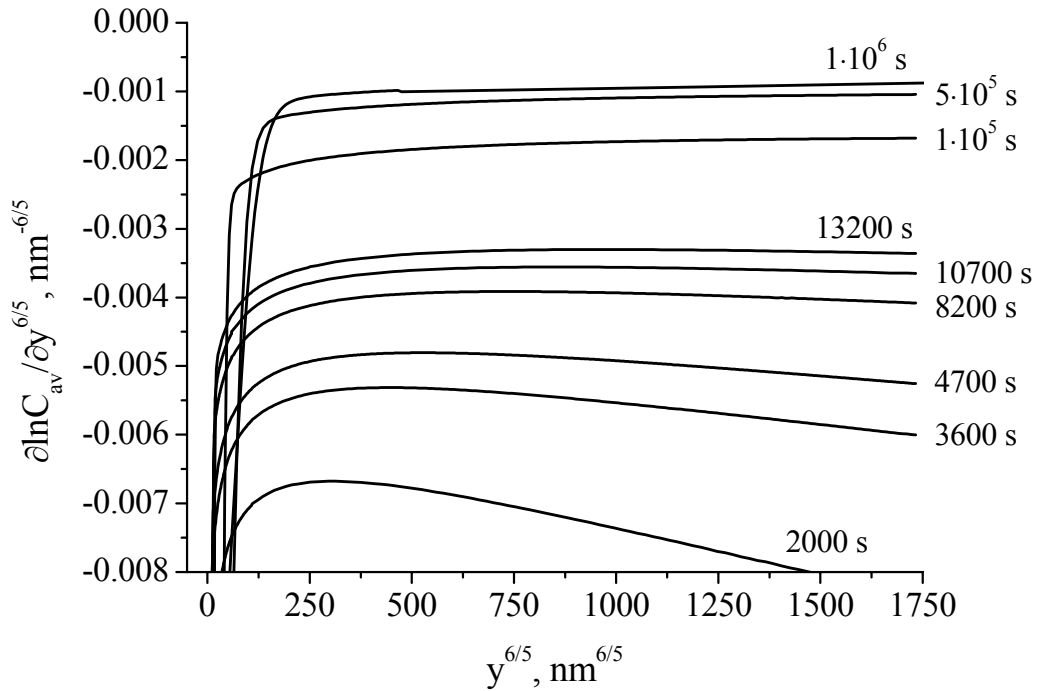
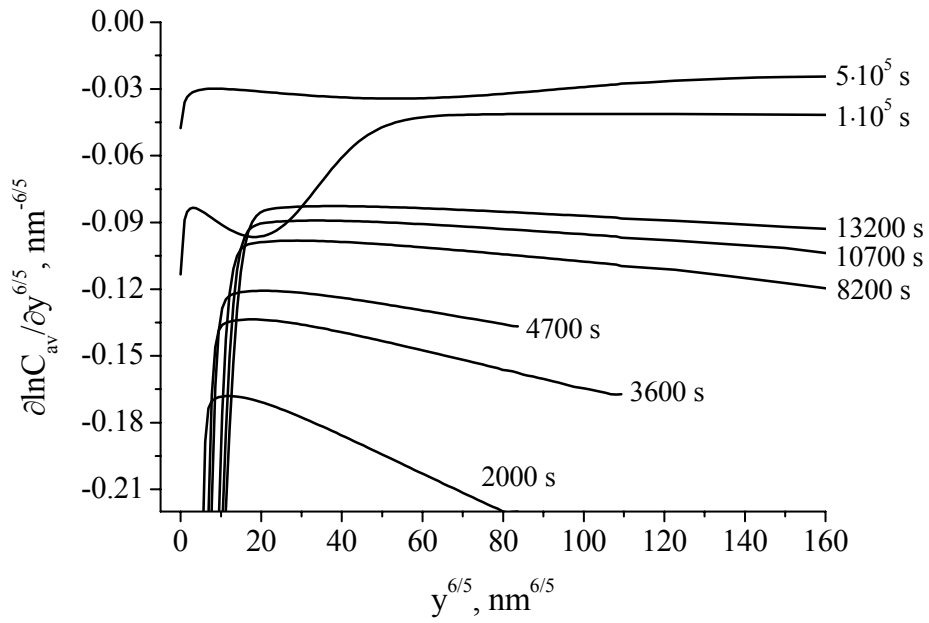


Fig. 3.7 Variation of $\ln C_{av}$ for $t = 2000 \text{ s} - 13200 \text{ s}$ a) and $\partial \ln C_{av} / \partial y^{6/5}$ for $t = 2000 \text{ s} - 1 \cdot 10^6 \text{ s}$ b) with $y^{6/5}$ calculated for $\Delta = 2.2 \cdot 10^4$.

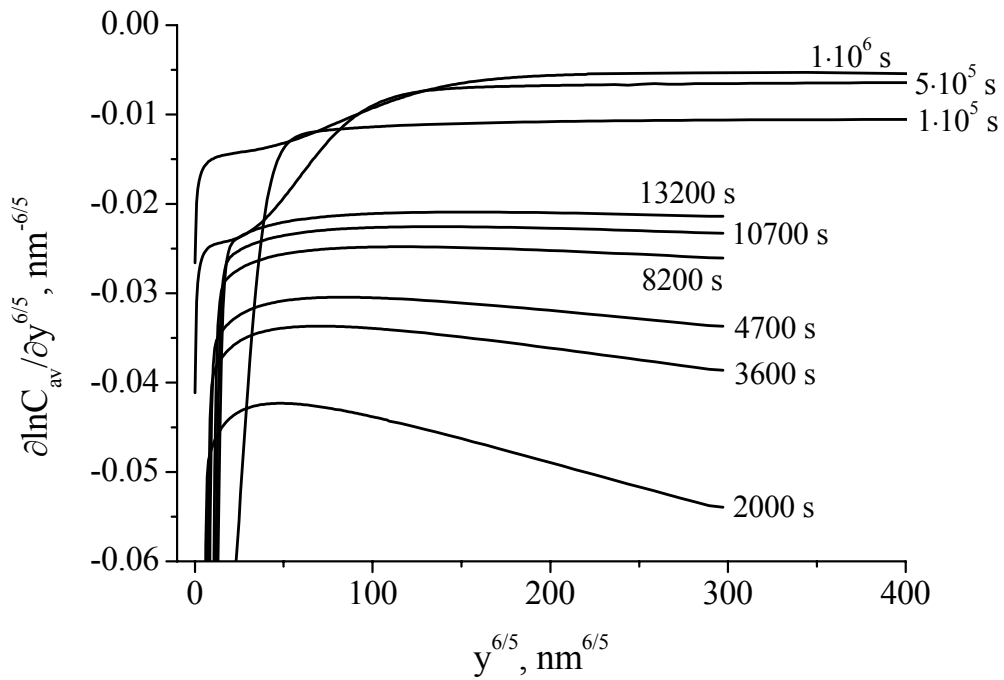
When the positions of the maxima are known, one would compare them with a criterion, which has already been discussed in the literature [Moy91], but very often ignored in the evaluation of experiments. The criterion is based on the relationship between y and L_g . According to this criterion, the determination of D_{gb} should be done from those parts of measured diffusion profile, which satisfy $y \geq 5L_g$. In the calculations L_g is the same for all ratios Δ used and depends only on t , because D_g was fixed. However, the ratio Δ increases, and the position of maximum goes from $y_{\max}^{6/5} \sim 12 \text{ nm}^{6/5}$ for $\Delta = 10^2$ at $t = 2000 \text{ s}$ (the corresponding diffusion length $L_g \sim 0.77 \text{ nm}$) to $y_{\max}^{6/5} \sim 1732 \text{ nm}^{6/5}$ for $\Delta = 10^5$ at $t = 500000 \text{ s}$ (which is, in fact, not the position of maximum, but simply corresponds to the depth of 500 nm, $L_g \sim 12 \text{ nm}$). The positions satisfy the criterion by being 10 times larger than L_g for $\Delta = 10^2$ at $t = 2000 \text{ s}$ and 42 times larger than L_g for $\Delta = 10^5$ at $t = 500000 \text{ s}$. So the criterion is very rough. It only reminds one that the GB part of diffusion profile is influenced by the bulk diffusion part. The criterion is still not absolutely correct and even misleading when the profile is fitted by the straight line.

It is interesting to analyze here how the maximum appears. In fig. 3.10 solutions given by pure bulk diffusion (a complementary error-function in the case of a constant source) and by Whipple's solution excluding bulk diffusion (pure GB contribution) are presented separately for $\Delta = 10^5$ at $t = 500000 \text{ s}$ and $t = 2000 \text{ s}$. A sum of both contributions gives C_{av} obtained by integrating Eq. (1.9a), also shown in fig. 3.10. The bulk diffusion solution decreases rapidly in comparison with the GB diffusion part. Whipple's solution coincides with purely bulk diffusion at very small coordinates and then is influenced by both contributions, and for larger y -coordinates dominates by the GB part. The GB contribution becomes predominant at around $110 \text{ nm}^{6/5}$ in fig. 3.10a, what is much smaller (by a factor of 16 in this nonlinear scale) than the position of the corresponding maximum ($y_{\max}^{6/5} \sim 1732 \text{ nm}^{6/5}$). Normally, for the parameters involved one needs a length of the sample larger than 500 nm in order to reach the maximum at long t . The maximum can correspond to the beginning of the B-regime since the diffusion regimes change each other not only with time but also along y [Kau95]. This regime finishes when the derivative goes down. The position of the maximum for $\Delta = 10^5$ at $t = 2000 \text{ s}$ (fig. 3.10b) is about $763 \text{ nm}^{6/5}$, what is 100 times larger (on the nonlinear scale) than the coordinate at which the GB part becomes the solution determining part. The longer t obtains a much more slowly varying function, suggesting the slope to be very small, whereas shorter t gives higher derivatives. In both the cases the overall solution is determined by the bulk diffusion part only at extremely small depths, i.e. of the order of several nanometers.

a)



b)



c)

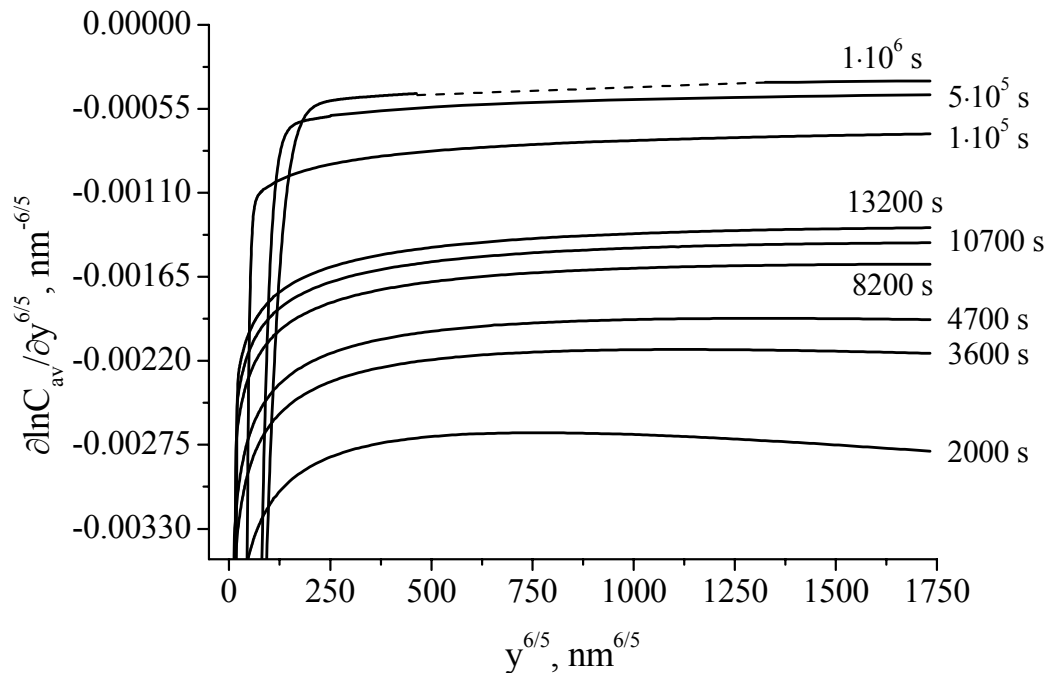
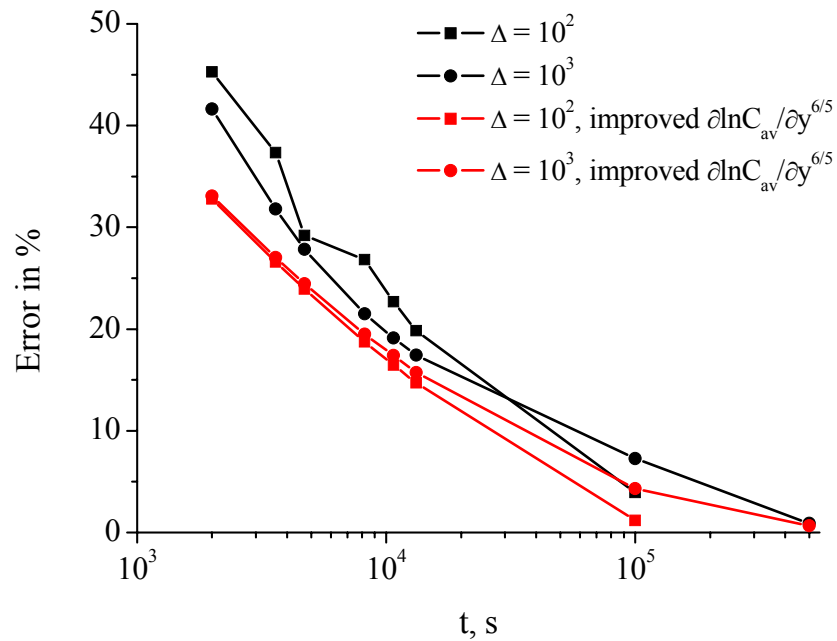


Fig. 3.8 Variation of the derivative $\partial \ln C_{av} / \partial y^{6/5}$ with $y^{6/5}$ obtained for a) $\Delta = 10^2$, b) $\Delta = 10^3$, c) $\Delta = 10^5$. The dashed line means that the integration in this region was very unstable and, therefore, impossible.

3.3.1 Nonlinearity and small values of dimensionless parameter w

The parameter w (Eq. (1.15)) is a very helpful quantity as regards understanding the conditions of the developing diffusion process. The problem of this parameter is in fact that its knowledge requires the knowledge of the diffusion coefficient D_{gb} . Meanwhile, the parameter makes the diffusion profiles plotted as a function of w for fixed t independent of the ratio of diffusivities Δ . This seems to be one of the main reasons, why Le Claire suggested the derivative $\partial \ln C_{av} / \partial w^{6/5}$ to be constant [Cla63]. Moreover, Le Claire mentioned that w should be larger than 2 to use his relation. On the other hand, the condition of $w \ll 2$ can be understood, if the gradient $\partial \ln C_{av} / \partial y^{6/5}$ is analyzed. As it was mentioned above, the contribution of bulk diffusion to the concentration profile is very restricted, because of interference of bulk diffusion with GB diffusion. The interference starts at surprisingly small values of y . The reason is that the derivative changes its value going slowly through the maximum and then decreasing due to the GB contribution only. In fig. 3.11 the dependence of

a)



b)

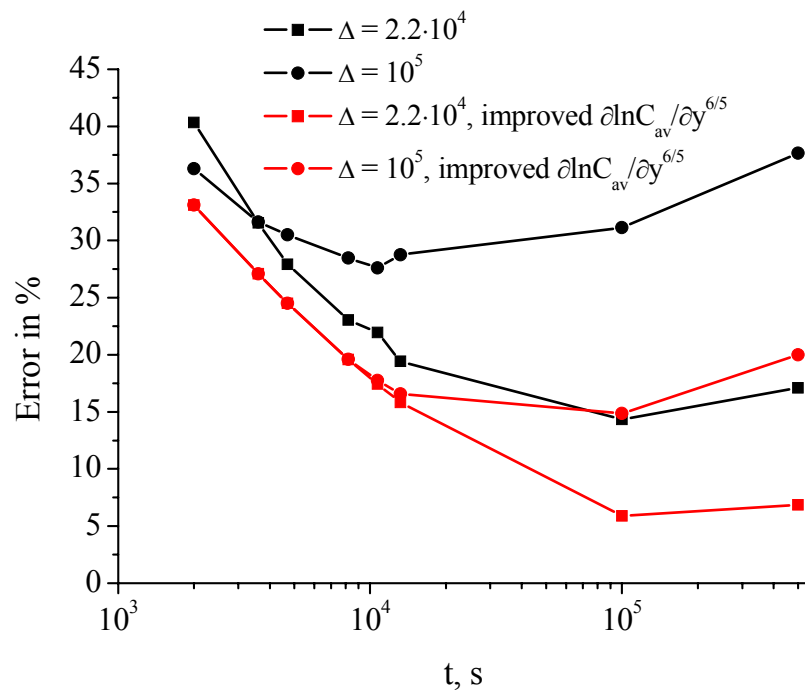
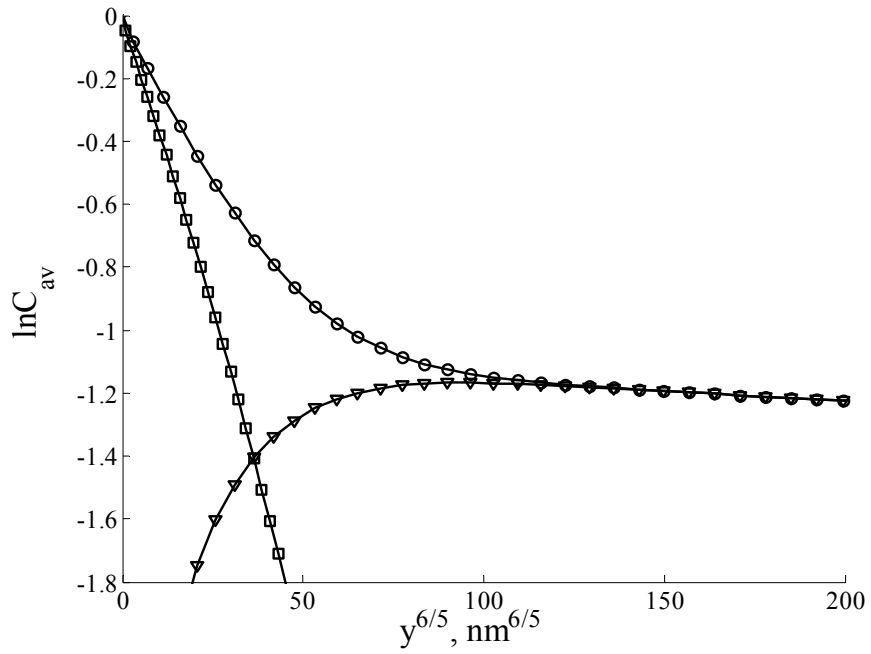


Fig. 3.9 Variation of the errors in determining D_{gb} with time ($D_{gb,app}$ was obtained by using Le Claire's relation): a) $\Delta = 10^2$, $\Delta = 10^3$, b) $\Delta = 2.2 \cdot 10^4$, $\Delta = 10^5$. Errors were estimated according to $\left(|D_{gb,app} - D_{gb,true}| / D_{gb,true} \right) \cdot 100\%$.

a)



b)

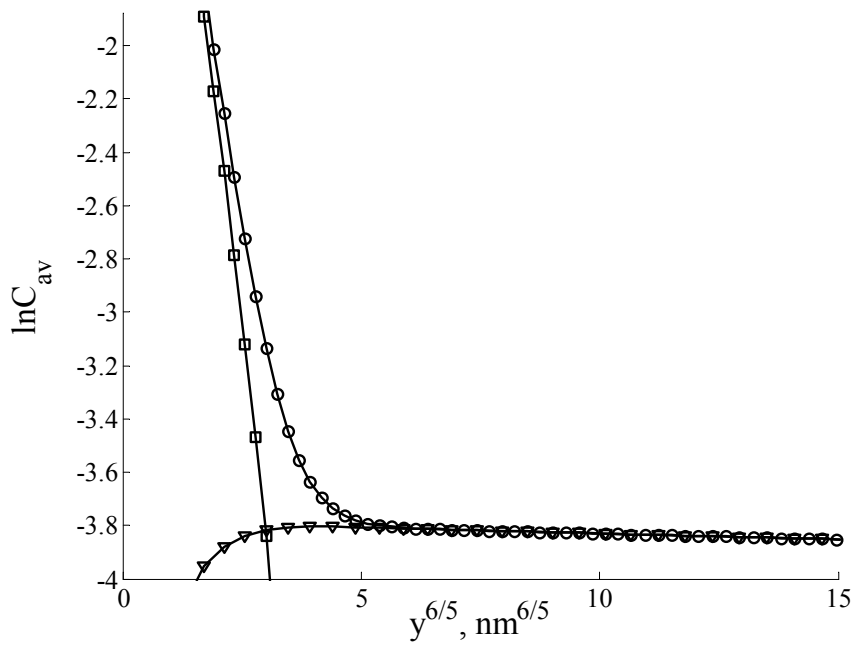


Fig. 3.10 Whipple's solution (circles) compared with its bulk part (squares) and GB part (triangles) at $t = 500000$ s a) and 2000 s b) for $\Delta = 10^5$.

the dimensionless parameter w on the real coordinate y is shown for different t , where the domain of inapplicability of Le Claire's relation is determined by values of w less than 2. Despite the fact of very different t , 2000 s and 500000 s, the values of w can be either smaller or larger than 2. In the dominator of w is the square root of $D_g t \beta$. While the β - parameter (Eq. (1.9d)) decreases with the diffusion time as $t^{-1/2}$, the positional coordinate y can be increased – both facts lead to the compensated values of w . The value of 2 is reached at smaller y , if t is decreased, because the shown linear dependences have different slopes. This looks like that there is a higher probability to arrive to the conditions of $w \ll 2$ for longer t , because the range of y is larger than for shorter t . One should keep in mind that the increase of t is only possible for a polycrystalline sample having larger grains, and deeper penetrations are needed to observe the nonlinearity. Particularly, at higher t the position of maximum is shifted to larger values of y . Correspondingly, the values of w larger than 2 for $t = 500000$ s arise at sufficiently larger values of y in comparison with $t = 2000$ s. An interesting question to be addressed is about the shape of diffusion profile at different w .

In order to analyze the diffusion profiles for different values of w , y was varied from 0 to 500 nm for $t = 2000$ s and $\Delta = 2.2 \cdot 10^4$. It is clear, that small values of w correspond to those parts of the diffusion profile, which are mostly influenced by bulk diffusion (fig. 3.12a). If the dimensionless parameter (w) increases, the profile changes from steep part to the interference part. Such a behavior continues until the maximum of the derivative is reached as it was observed for the dependences on the real coordinate. The corresponding diffusion profiles were plotted for considered w -values (fig. 3.12b). Surprisingly, the shape of those profiles in the dependence $\ln C_{av} = f(y^{6/5})$ represents classical, usually expected, diffusion profiles, comprising two distinguishable parts due to bulk diffusion and GB diffusion separately. Consequently, D_{gb} can be found from such dependence by applying Le Claire's relation. However, this would cause errors since the maximum is not reached. Thus the qualitative estimation of the profile leads to the situation when D_{gb} is found according to the procedure, which is not straightforward. This also allows the problems discussed in [Chu96a] to be better understood. In the latter paper, errors of the order of 70% were observed. However, an explanation of those errors was not given. Instead, they suggested a new expression for the δD_{gb} -product which requires the knowledge of new fitting parameters summarized in this paper. According to the present analysis, the maximum of the gradient gives an accurate result and many problems of using the conventional procedures are related to the nonlinearity.

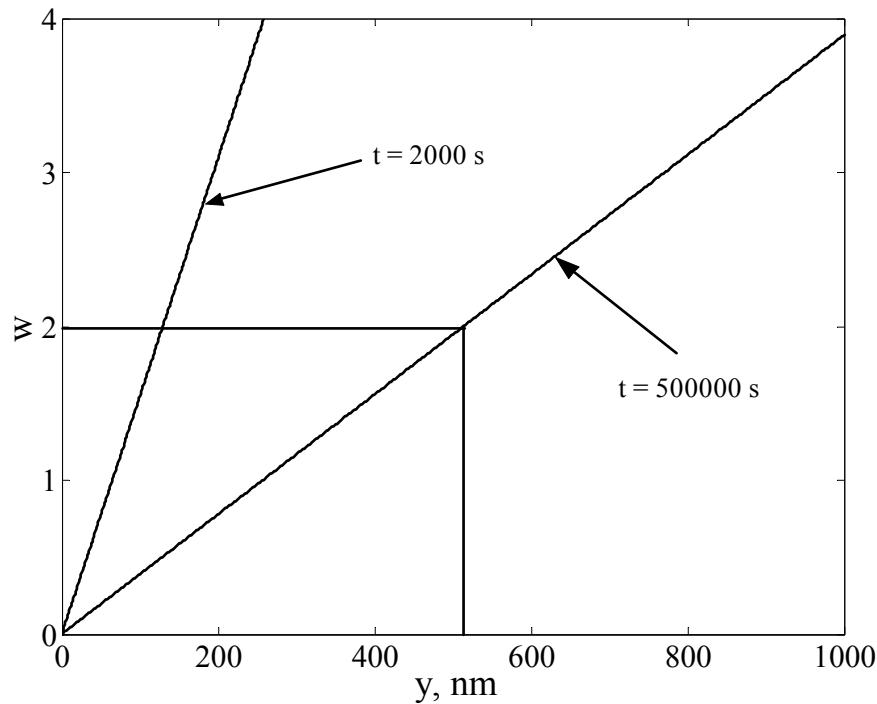


Fig. 3.11 Dependence of the dimensionless quantity w on real positional coordinate y for $t = 2000$ s and $t = 500000$ s.

3.3.2 Analyzing the errors of using Le Claire's constant

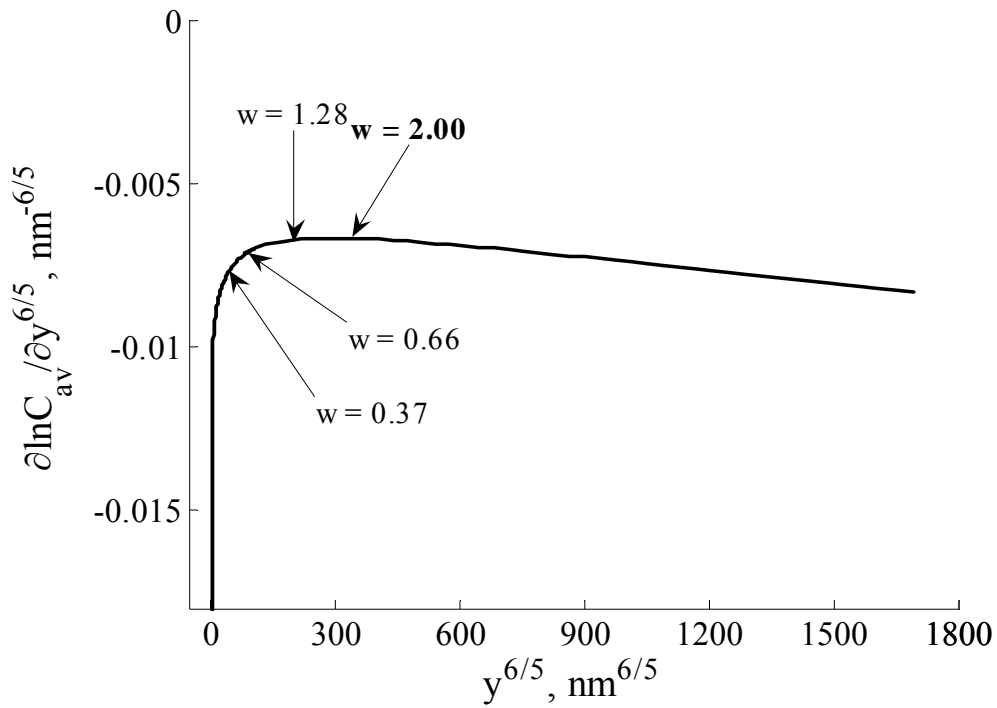
In fig. 3.9 the errors of finding the GB diffusivity (D_{gb}) remained high, even after using the maximum of the derivative. It was supposed that an additional problem is related to Le Claire's constant ($\partial \ln C_{av} / \partial w^{6/5} \approx -0.78$, Eq. (1.14)) as being the only quantity, which was not discussed up to now. As far as the diffusion profiles were obtained for different ratios Δ and t , the derivatives of those as functions of dimensionless coordinate w were also plotted. The deviations of the derivative from Le Claire's constant were observed and estimated. In fig. 3.13 the derivatives are depicted for the same ratios Δ and t as in fig. 3.8. The qualitative picture is similar, but the meaning is different. Interestingly, the derivatives for different Δ have the positions of maxima at the same w which vary from 2 to 6, depending on t . For the smallest ratio $\Delta = 10^2$ Le Claire's constant is reached at $t = 100000$ s due to β close to 1 in contrast to other ratios. This is an exception case which refers to small Δ which is unlikely in diffusion experiments, unless small angle grain boundaries are concerned. Thus, for the ratios Δ larger than 10^2 it takes at least 500000 s to reach Le Claire's constant for the diffusion parameters used in the present study. An important property of the dependences in figs. 3.13c and 3.13d is in fact that these become more and more restricted with t . Comparing the dependences for $\Delta = 2.2 \cdot 10^4$ and $\Delta = 10^5$ demonstrates that the values of w are twice as large

as in the former case, while the positions of maxima are approximately the same. This is related to the values of β and the length of the sample remaining constant. Large values of w always mean very deep profiles characterized by nonlinearity, what was also considered in the theoretical study of Le Claire [Cla63]. The nonlinearity in his profiles is obvious, but Le Claire did not discuss this property properly. Therefore, the tendency is that the position of maximum shifts to higher values of w , and that the maximum value of derivative tends to Le Claire's constant as t grows. Both facts make the dependence more and more parallel to the abscissa, i.e. tending to a constant value for a fixed length of the sample. In this sense one may expect that there can be situations depending on the parameters in which the derivative is, to some extent, a constant value. Consequently, high temperatures and/or long diffusion times lead more or less to Le Claire's constant.

The Le Claire constant is reached for very different values of β , varying from 2 for $\Delta = 10^2$ at $t = 100000$ s to 2000 for $\Delta = 10^5$ at $t = 500000$ s. These values cover a wide β -range in comparison with Le Claire's work. Consequently, the values of β do not really determine the accuracy of the result. However, y and t are relevant for the deviations from Le Claire's constant. It is very likely that diffusion in ultrafine-grained materials (or nanocrystalline materials) is studied under conditions of short t and penetrations. That is why the measured diffusion profile can be obtained for $w \ll 2$. This effect has already been observed by Chung [Chu96a] when measuring the diffusion profile for MgO bicrystal. The latter point is discussed below. Importantly, the maxima of the derivatives correspond only to values of w larger than 2 according to fig. 3.13.

As the maxima of the derivatives on the real coordinate are known from fig. 3.8, then one may estimate the maxima of derivatives on the dimensionless coordinate and put both into the original expression of Le Claire (Eq. (1.14)). Following this procedure, the evaluation of errors for finding D_{gb} was continued (fig. 3.14). The errors are greatly reduced at shorter times, namely from 35% to very small errors not exceeding 1%. Nevertheless, the errors for larger ratios Δ and longer t are still high and increase with t . The reason comes from the $\partial \ln C_{av} / \partial w^{6/5}$ values taken at the maximum, while the length of geometrical model (500 nm) gives shorter values of w . These values were taken at the maxima to be in accordance with procedure used for shorter t . The dashed curves in figs. 3.13c and 3.13d show how the length was increased to reach the maximum for longer t . However, these values obviously give larger errors. By using the values found at the depth of 500 nm being the length of geometrical model, the error was decreased (red and blue points in fig. 3.14).

a)



b)

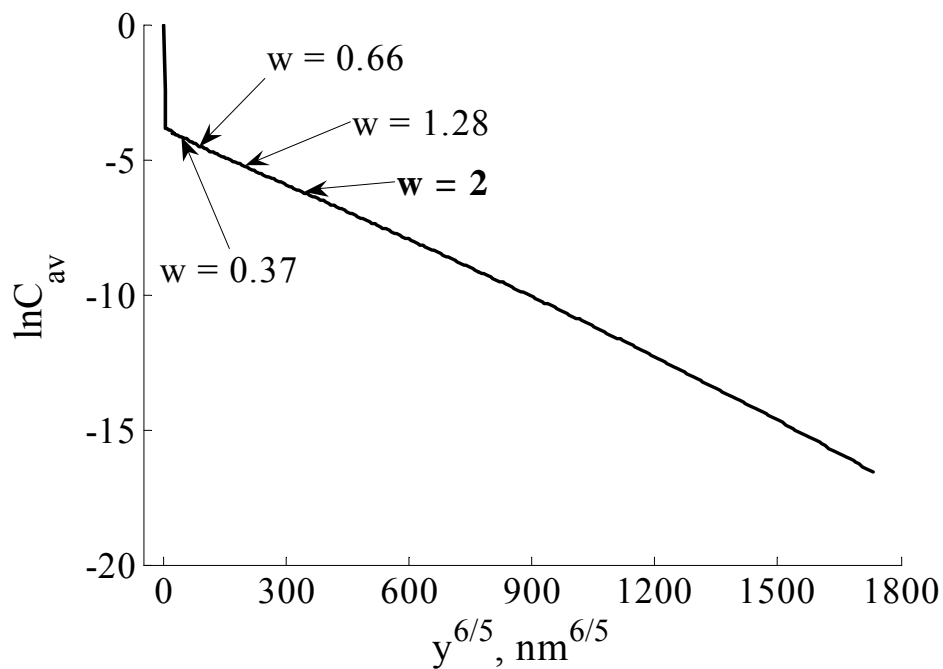
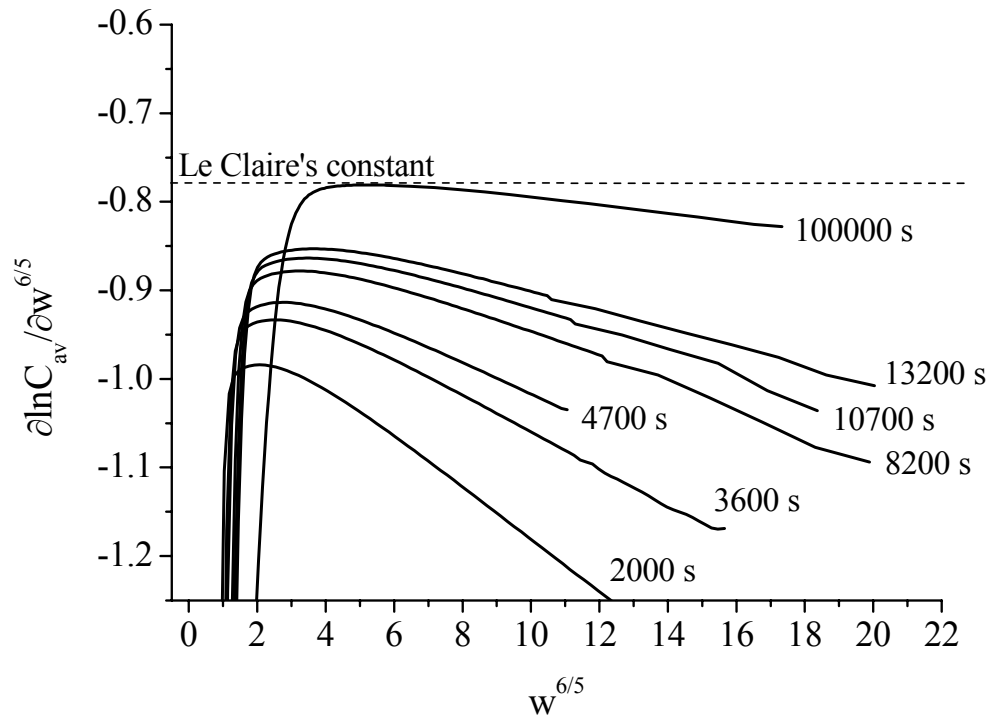
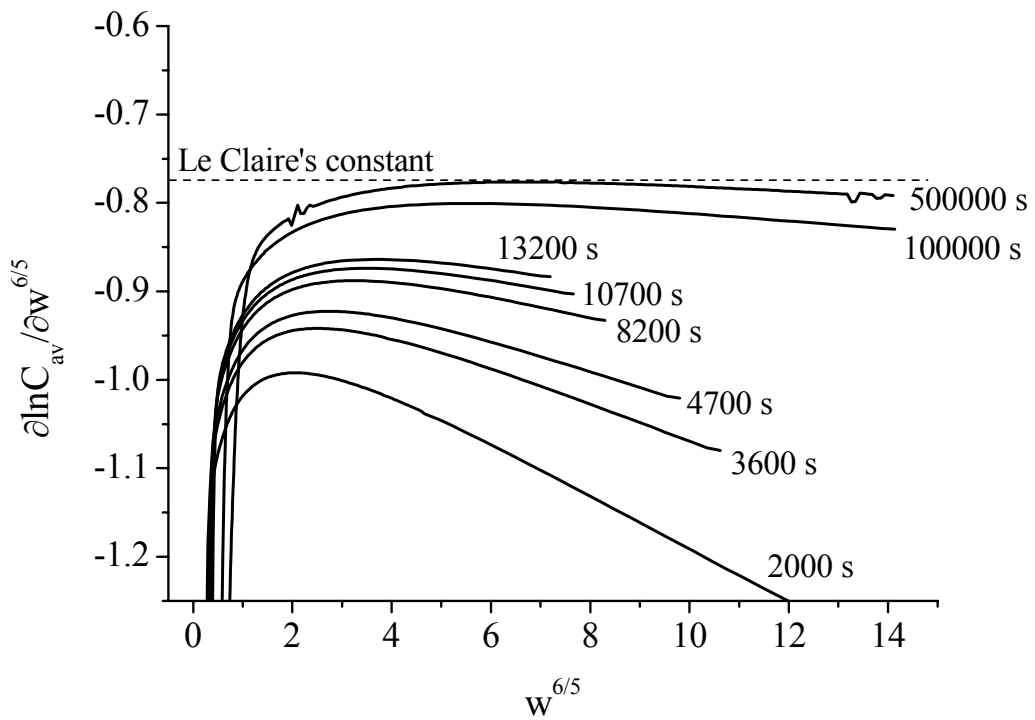


Fig. 3.12 Variation of the dimensionless quantity w as a function $y^{6/5}$ along the derivative of the diffusion profile a) and the diffusion profile b) calculated for $\Delta = 2.2 \cdot 10^4$ at $t = 2000$ s.

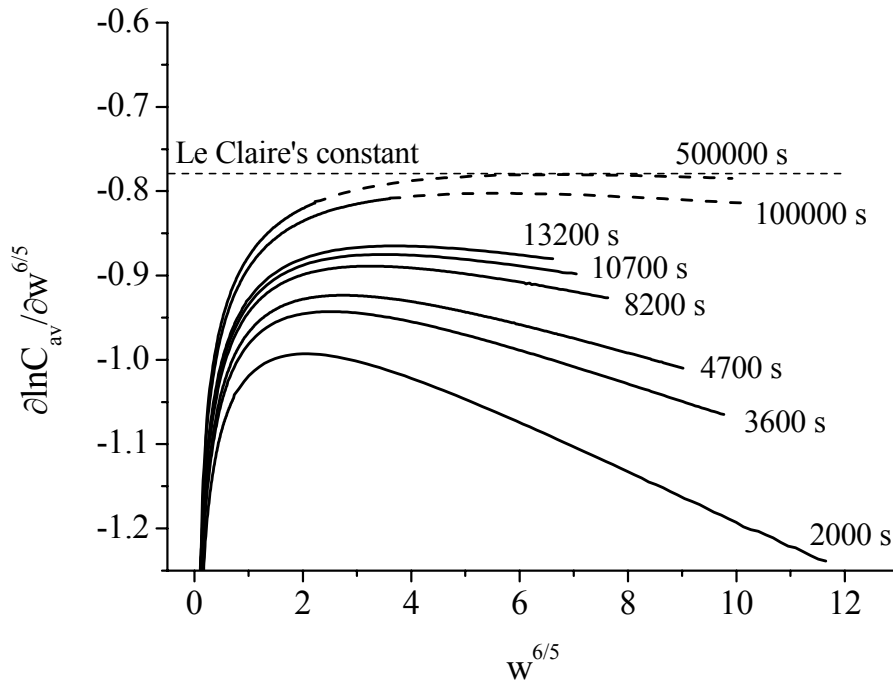
a)



b)



c)



d)

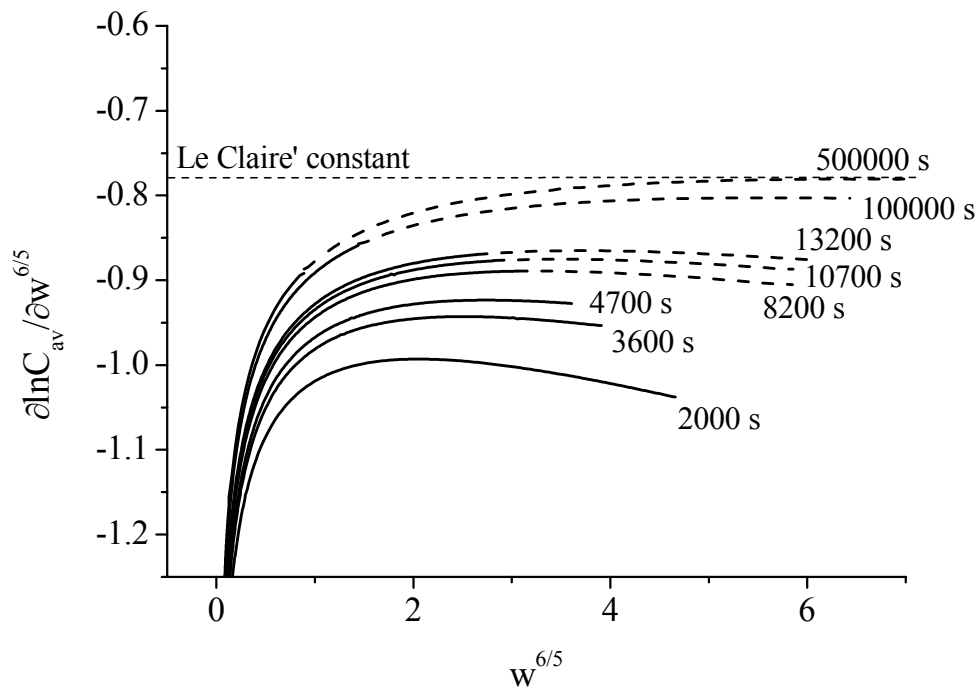


Fig. 3.13 Variation of the derivatives $\partial \ln C_{av} / \partial w^{6/5}$ with $w^{6/5}$ for a) $\Delta = 10^2$, b) $\Delta = 2.2 \cdot 10^4$, c) $\Delta = 10^3$ and d) $\Delta = 10^5$ at different diffusion times. Le Claire's constant is also indicated. The dashed curves were obtained by increasing the length of the sample and indicate restriction due to this finite length.

All the points discussed so far give a clear explanation of how the errors arise when extremely small diffusion lengths come into play. These situations very likely occur in nanomaterials with very small grains. As D_{gb} needs to be obtained, such an error analysis must be done as far as experimental evaluation is concerned. However, it is difficult to take account all the effects observed in the preceding sections. Obviously, improved procedures to deduce D_{gb} are necessary.

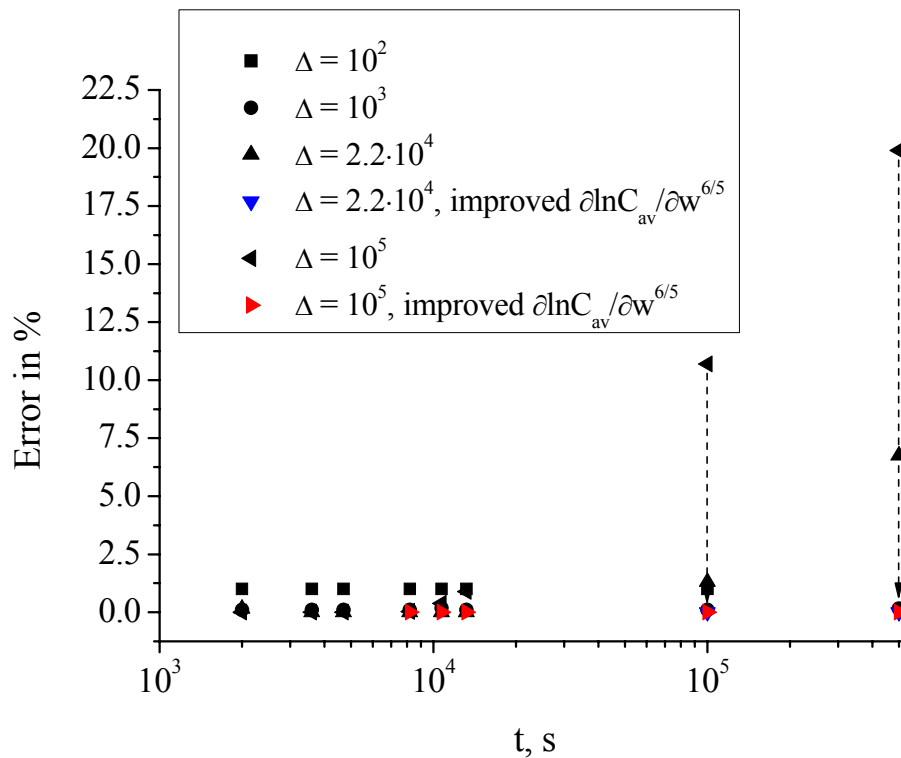


Fig. 3.14 Errors in determining D_{gb} calculated by putting both maxima on $y^{6/5}$ and $w^{6/5}$ into the original Le Claire expression. The dashed arrows show how the error is reduced after using the improved derivative.

3.4 Discussing new procedures for finding the grain boundary diffusivity

3.4.1 An analytical expression for $\partial \ln C_{av} / \partial w^{6/5}$ at the maximum

First of all, a very useful expression can be suggested for the derivative $\partial \ln C_{av} / \partial w^{6/5}$. Plotting the maxima found in the preceding section from the dependences $\partial \ln C_{av} / \partial w^{6/5} =$

$f(w^{6/5})$ as functions of another dimensionless parameter α (Eq. (1.9d)), it was observed that they almost linearly dependent on α (fig. 3.15). A small curvature, seen in this figure, cannot introduce a large error. As it can be expected, and was mentioned above, the maxima for $\Delta > 10^2$ almost coincide, and only the result for $\Delta = 10^2$ is slightly different from all the others. Despite that fact, one can see the slopes of all of the lines being the same. The values of α vary from 0.02 at longer times to 0.32 at shorter times. The large values of α as 0.32 can be attributed to the so-called B₁-regime [Mis95], [Mis92a] – the transition between the B- (B₂- or B₂'-) and C- regimes. This regime can be relevant for discussion here. Consequently, the result in fig. 3.15 shows that the B₁-regime especially important for the cases of shallow penetrations.

Fitting the lines shown in fig. 3.15 to a straight line yields the following expression

$$\frac{\partial \ln C_{av}}{\partial w^{6/5}} = -0.77 - 0.71\alpha, \quad (3.1)$$

neglecting the difference which exists between the line for $\Delta = 10^2$ and the others. This expression is very helpful (at least in the range of α used) since one can simply estimate the value of α , which only requires D_g to be known. According to fig. 3.15, $\alpha > 0.02$ requires Eq. (3.1) to be used to find the derivative $\partial \ln C_{av} / \partial w^{6/5}$ properly. If it is not the case, Le Claire's constant should be put into the original expression for the δD_{gb} – product.

According to what was discussed before, there are some cases when the derivative taken at the maximum also leads to significant errors (this is concerned only the derivative on w , if the length of the sample is too short to arrive exactly at the maximum). On the other hand, by plotting the derivative $\partial \ln C_{av} / \partial w^{6/5}$ it can be found out whether or not the maximum is reached. For the accurate determination of D_{gb} , it is suggested to increase the penetration depth (if not the length of the sample) until the maximum is reached despite these errors. This is, because the value of $\partial \ln C_{av} / \partial w^{6/5}$ at the depth corresponding to the length of the sample is impossible to find. Table 2.1 compares the values of $\partial \ln C_{av} / \partial w^{6/5} = f(w^{6/5})$ at the maximum taken from the calculated dependences (fig. 3.13) with those found by using Eq. (3.1).

It should be emphasized that Szabo *et al.* [Sza90] in their discussion of how to find the segregation coefficient (s) and D_{gb} separately, observed deviations of the apparent parameters from the true ones if α increases. The explanation of this effect is given here and, moreover, an improved procedure to deduce D_{gb} is suggested.

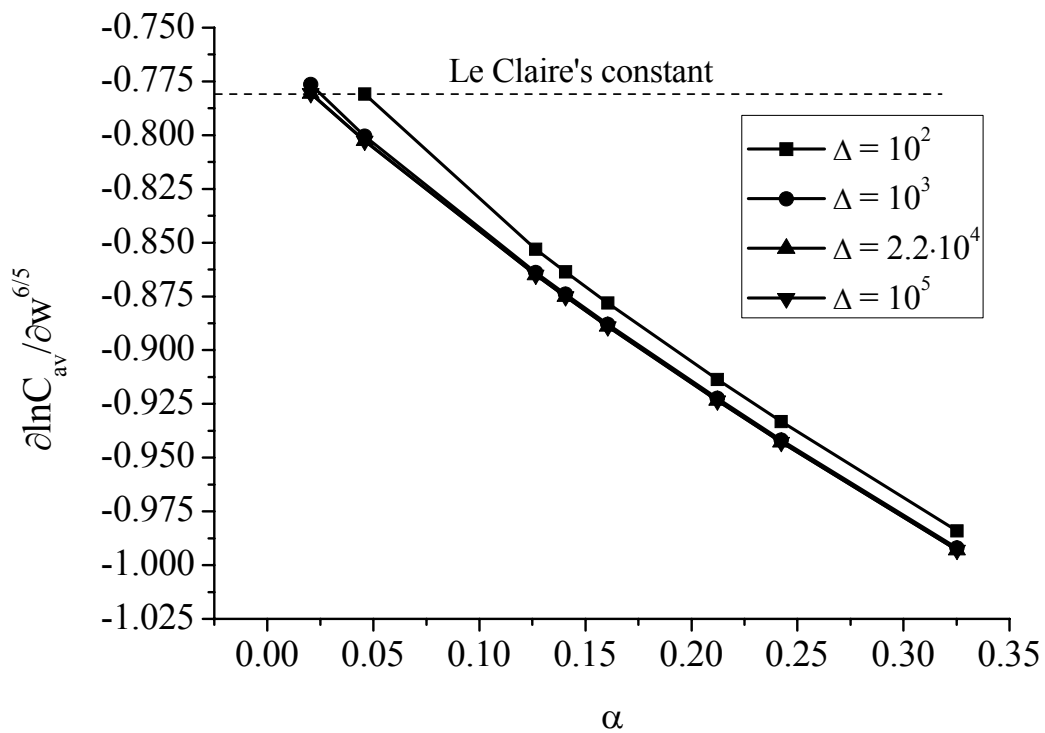


Fig. 3.15 Maxima of the dependences $\partial \ln C_{av} / \partial w^{6/5} = f(w^{6/5})$ plotted against the dimensionless parameter α for different ratios Δ .

Table 3.1 A comparison of the derivatives at the maximum found by using calculated dependences and Eq. (3.1) for $\Delta = 2.2 \cdot 10^4$.

t, s	$\partial \ln C_{av} / \partial w^{6/5} = f(w^{6/5})_{\text{true}}$	$\partial \ln C_{av} / \partial w^{6/5} = f(w^{6/5})_{\text{Eq. 2.1}}$
2000	-0.99	-1.00
3600	-0.94	-0.94
4700	-0.92	-0.92
8200	-0.89	-0.88
10700	-0.87	-0.87
13200	-0.86	-0.86
100 000	-0.80	-0.80
500 000	-0.78	-0.78

3.4.2 The reason of observing a constant value for $\partial \ln C_{av} / \partial w^{6/5}$. Discussing procedures used in the literature

It is believed that there are certain cases when the exact Whipple's solution can be transformed to a simpler mathematical form. These cases have been for the first time introduced by Whipple [Whi54] and Le Claire [Cla63] and were explicitly discussed later in the book of Kaur *et al.* [Kau95]. The origin of those transformations lies in a fact that the ratio of diffusivities (Δ) can be very large, typically, of the order of 10^5 or so for metals. The expression for C_g (used in the cited paper of Le Claire) then reads:

$$C_g(\eta, \xi, \beta) = \operatorname{erfc}\left(\frac{\eta}{2}\right) + \frac{\eta}{2\pi^{1/2}} \int_1^{\infty} \frac{d\sigma}{\sigma^{3/2}} \exp\left(-\frac{\eta^2}{4\sigma}\right) \operatorname{erfc}\left[\frac{1}{2}\left(\frac{\sigma-1}{\beta} + \xi\right)\right]. \quad (3.2)$$

The meaning of the dimensionless quantities η and ξ was given in chapter I (Eqs. (1.9b) and (1.9c)). By comparing with Eq. (1.9a) the upper limit Δ is replaced by infinity, and the term $\left(\frac{\Delta-1}{\Delta-\sigma}\right)^{1/2}$ under the complementary error-function is simply ignored. After Le Claire, the same transformation was applied by Chung and Wuensch [Chu96a], [Chu96b], and it is important to discuss this once more in order to prevent possible errors. As it has been explained [Kau95], the approximation $\Delta \rightarrow \infty$ may be used when $\beta \ll \Delta$ with β remaining finite. In the present study β was varied from 2 ($\Delta = 10^2$, $t = 100000$ s) to 32518 ($\Delta = 10^5$, $t = 2000$ s), always being smaller than Δ . Strictly speaking, the ratio Δ/β is 50 at longer times and only 3 at shorter times for all Δ used. Additionally, η (Eq. (1.9b)) varies from 41 to 650 in all the calculations in the present study. These values of η are smaller than Δ , except for Δ as small as 10^2 . Since η is weighted by the diffusion length L_g , the ratio y/L_g is exactly of the order of several hundreds or smaller; otherwise extremely deep penetrations come into play. Unrealistic situations, when $\eta \gg \Delta$ were supposed by Le Claire when suggesting Eq. (3.2). On the other hand, such an approximation allows the contribution of bulk diffusion to be neglected, and Le Claire transformed Eq. (3.2) to a special mathematical form for C_{av} , neglecting the bulk diffusion part. One can also think of this approximation in terms of w . If η is much larger than Δ which itself is much larger than β , then w increases to values of tens or even hundreds. Nevertheless, the maximum of $\partial \ln C_{av} / \partial w^{6/5}$ lies in the region of w from 2 to 6 and not larger. In fig. 3.16 two derivatives are shown, calculated under condition $\beta < \Delta$. The

first of them was obtained by using a convenient mathematical form to better integrate Eq. (3.2), published in [Kau95], excluding bulk diffusion. The second one was found by using the same mathematical form, taking into account bulk diffusion. The equation used for integration is

$$C_{av} = \operatorname{erfc}\left(\frac{w\beta^{1/2}}{2}\right) + \frac{4(D_g t)^{1/2}}{L\pi^{1/2}} \int_0^{\beta^{1/2}} \exp\left(-\frac{w^2\tau^2}{4}\right) \left[\frac{1}{\pi^{1/2}} \exp\left\{-\frac{1}{4}\left(\frac{1}{\tau^2} - \frac{1}{\beta}\right)\right\} - \frac{1}{2}\left(\frac{1}{\tau^2} - \frac{1}{\beta}\right) \operatorname{erfc}\left\{\frac{1}{2}\left(\frac{1}{\tau^2} - \frac{1}{\beta}\right)\right\} \right] d\tau, \quad (3.3)$$

where τ is a new integration variable related to σ through $\tau = \left[\left(\frac{\Delta - \sigma}{\Delta - 1}\right) \frac{\beta}{\sigma}\right]^{1/2}$; L is the width of the sample or the distance over which C_g is averaged. The difference between Eq. (3.3) and the one originally suggested in [Kau95] lies in the use of bulk diffusion part. Comparison of both equations shows that the maximum is not influenced by neglecting bulk diffusion (fig. 3.16, dashed lines). This again confirms that the bulk part is confined within a very tiny region, what is also shown in fig. 3.10. So the maximum lies far enough from the bulk part and corresponds only to the GB diffusion. Interestingly, Eq. (3.3) was integrated successfully by using MatLab without any serious numerical problems. One may conclude here that, in principle, bulk diffusion may be excluded but not because $\eta \gg \Delta$ which is an unrealistic condition. Interestingly, the maximum of the calculated derivatives is slightly higher than Le Claire's constant.

More important is another condition, *viz.* $\beta \ll \Delta$. The ratio $\Delta/\beta = 50$ leads to Le Claire's constant, according to the results of the present study. Comparing this with what was discussed by Chung and Wuensch [Chu96a], $\Delta/\beta \geq 50$ looks much more realistic. They used the condition $\Delta/\beta (\approx 2L_g/\delta) \geq 10^3$ in order to apply $\Delta \rightarrow \infty$. In this case $\beta \approx \Delta/10^3$. For small ratios Δ , say 10^2 or 10^3 , the condition is never fulfilled, giving the values smaller or equal than 1. This would mean that the measurements on small angle boundaries could not be evaluated.

Continuing the discussion started in [Kau95] with respect to the reasons leading to $\Delta \rightarrow \infty$, the *erfc*-term in Whipple's solution (Eq. (1.9a)) was plotted against σ for two extreme cases: $\Delta = 10^5$ and $\Delta = 10^2$ (fig. 3.17). The diffusion time (t) was varied from 2000 s to 500000 s not only because exactly these times were used in the present study, but also

because these cover the values of β which can be met in the measurements. The values of $\beta \geq \Delta$ would mean $L_g \leq \delta$, what corresponds to the type-C diffusion kinetics. Consequently, another criterion for the C-regime is $\beta > \Delta$, which is the same as $L_g < \delta$ and leads to complex C_g . Otherwise, L_g is larger than δ , and the B-regime becomes responsible for the diffusion process, regardless we refer to the classical B-regime or B_2 , B_2' , or B_1 .

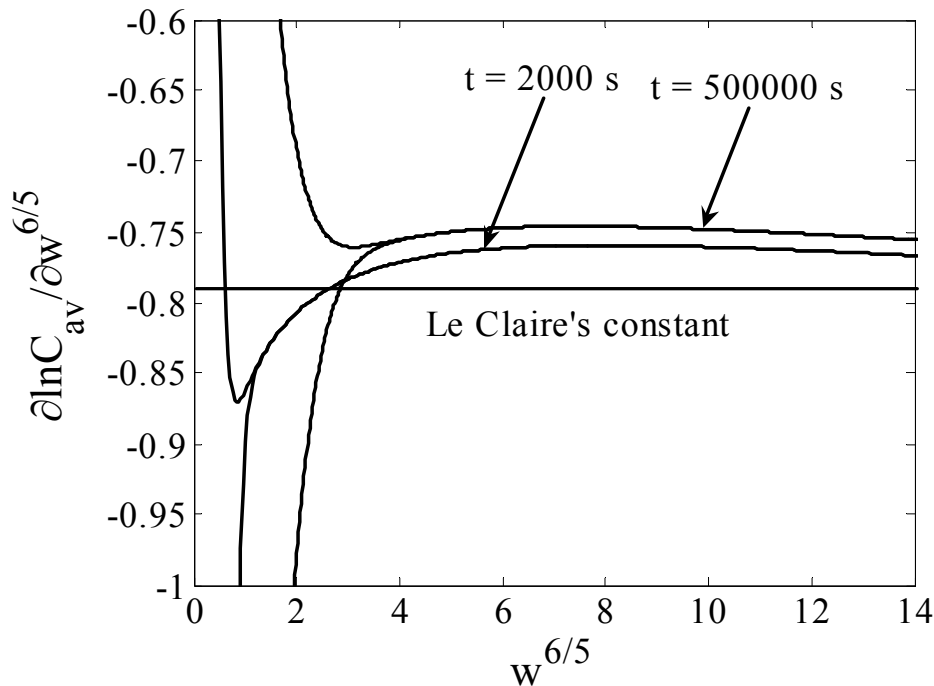
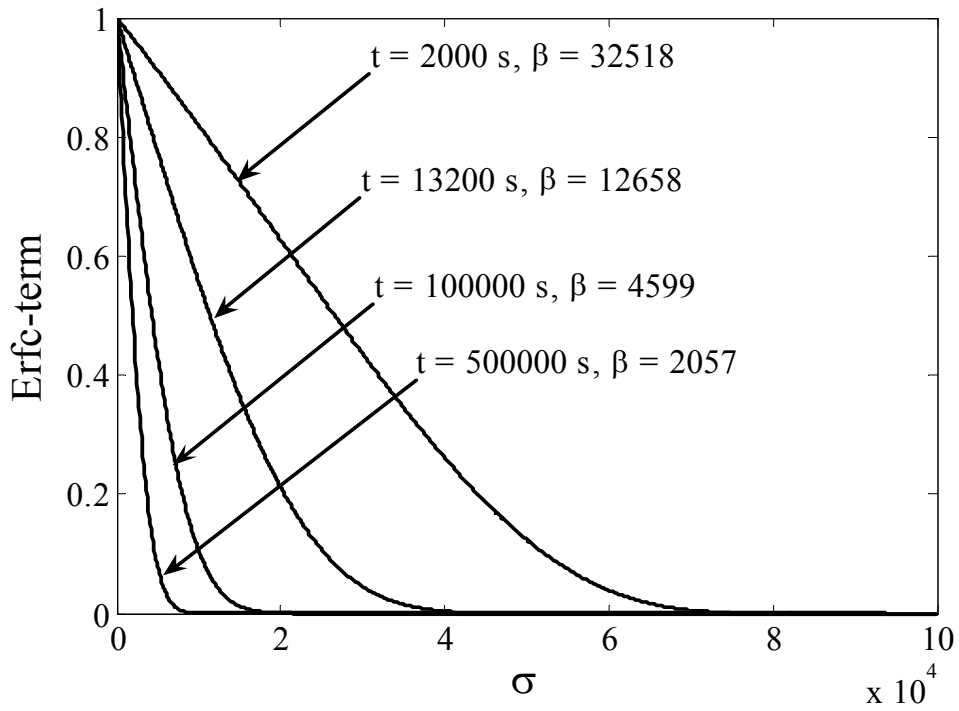


Fig. 3.16 Variation of the derivatives with $w^{6/5}$ calculated for $\Delta = 10^2$ by using Eq. (3.3) excluding (dashed curves) and including (solid curves) the bulk diffusion part.

Appreciable values of the erfc-term are possible, if β is close to Δ . In these cases the upper limit of integration should be exactly Δ . If β decreases, the upper limit can be taken smaller and at $t = 500000$ s it can surely be replaced by infinity (fig. 3.17). In fact, it is a very restricted region of β , when $\Delta \rightarrow \infty$ may be used for nanomaterials. The restriction is defined by L_g , because increase of t leads finally to the A'-regime as it is the case for $\Delta = 10^5$ with the average grain size of 50 – 100 nm or so (fig. 1.5d). This is the typical situation for nanomaterials when we proceed to the A-type regimes at large β . The new criterion for using $\Delta \rightarrow \infty$, suggested in the present study, is that α should be smaller than 0.02. Interestingly, if it is not taken into account, the integration of Eq. (3.3) gives Le Claire's constant, even if $\alpha > 0.02$ (fig. 3.18). This, of course, can be misleading. This is the aim of the experiment to find β , while α can be estimated, knowing D_g . Consequently, the analysis in terms of α is more convenient and allows one to make all necessary conclusions.

a)



b)

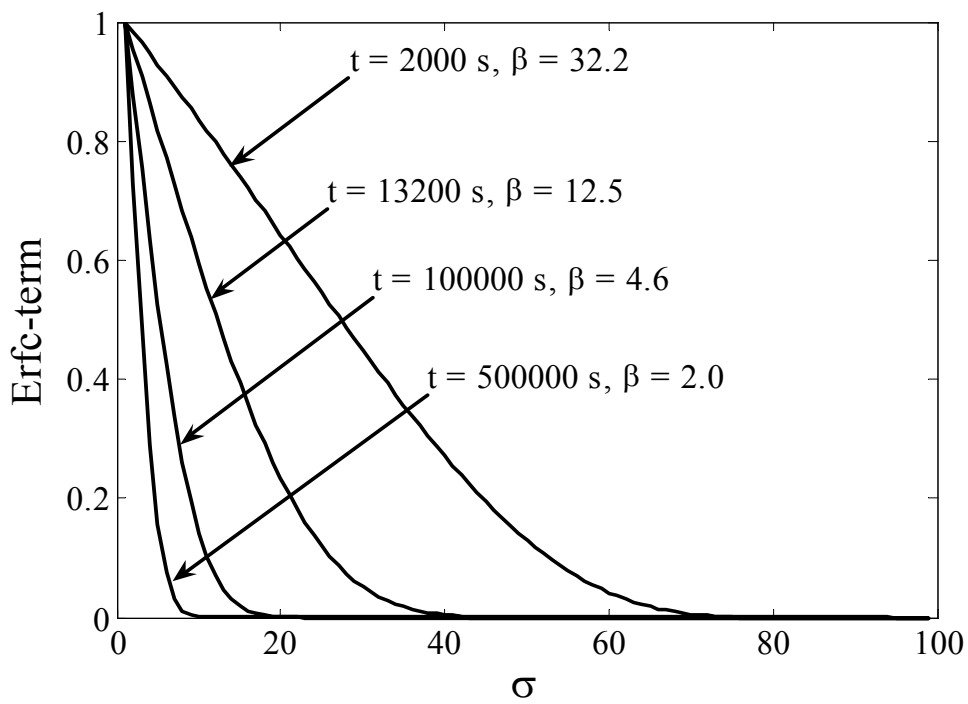
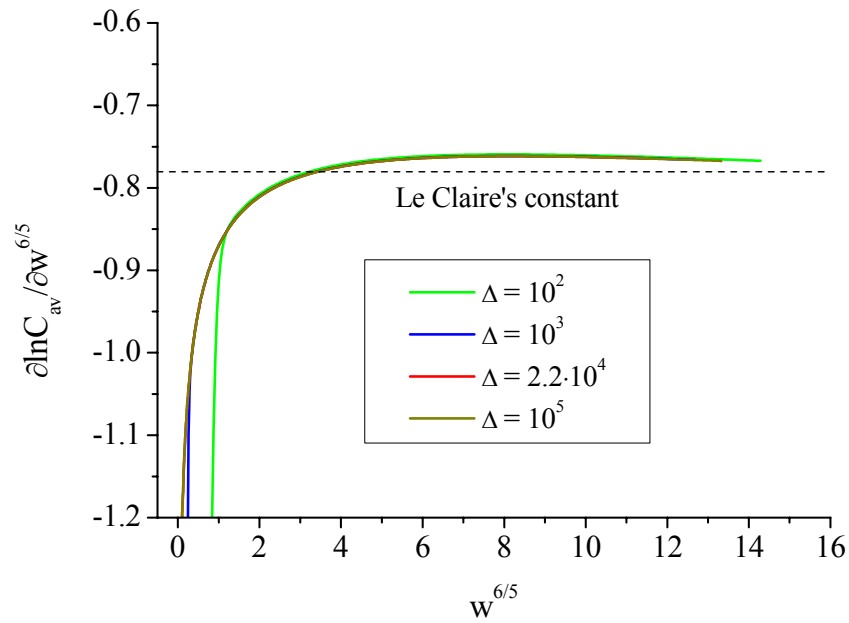


Fig. 3.17 The term $\text{erfc}[\dots]$ taken directly from Whipple's solution (Eq. (1.9a)) is calculated at $\xi = 0$ for $\Delta = 10^5$ a) and $\Delta = 10^2$ b).

a)



b)

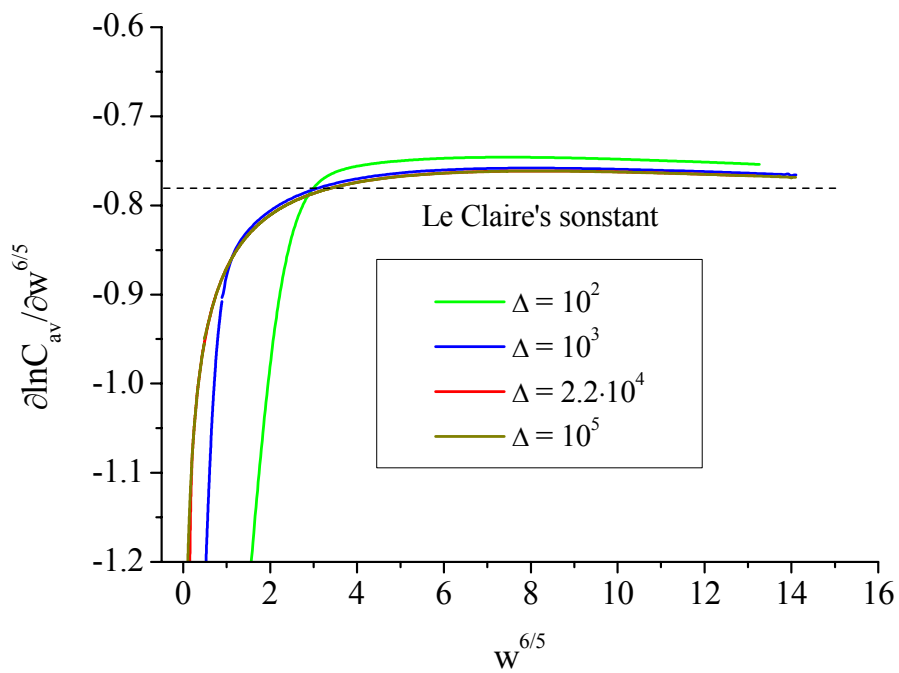


Fig. 3.18 Variation of the derivative $\frac{\partial \ln C_{av}}{\partial w^{6/5}}$ as a function of $w^{6/5}$ calculated by using Eq. (3.3) for different ratios Δ at $t = 2000$ s a) and $t = 500000$ s b).

An additional and important comment is that similar results can also be obtained, say for $\Delta = 10^2$, if in the exact Whipple solution $\Delta = 10^5$ (the upper limit of integration) is used instead of Δ with β corresponding to $\Delta = 10^2$. This is, of course, an artificial point, which is nothing but only a mathematical trick to get to Le Claire's constant, because the range of varying σ is increased in this case. In this sense the following question arises. Is the result obtained for a very short time correct under these conditions? Probably, it would be enough to increase the range for σ . The answer is very nicely given by comparing the exact Whipple solution with the result of FEM. By using numerical method to integrate Fisher's system (Eq. (1.6)), one observes the solution independent of Whipple's solution and, consequently, of $\Delta \rightarrow \infty$. The corresponding result is discussed in chapter IV (fig. 4.1). Here it is only important to mention that the results of both integrations coincide within a very small error even at 2000 s.

3.4.3 On important dependences for finding the grain boundary diffusivity

Summarizing the previous sections, the following procedure could be suggested for nanomaterials: 1) Measure the diffusion profile and determine D_g by simply fitting the near surface part to the complementary error-function solution or Gaussian function depending on boundary conditions. 2) Plot the derivative of the measured diffusion profile and identify its maximum, $(\partial \ln C_{av} / \partial y^{6/5})_{\max}$ (it is recommended to reach this maximum). 3) Calculate the parameter α . 4) If $\alpha > 0.02$, use Eq. (3.1) to find the derivative $(\partial \ln C_{av} / \partial w^{6/5})_{\max}$ and put the derivatives into Eq. (1.14), or if $\alpha < 0.02$ use the standard Le Claire constant. The disadvantage of this procedure is in fact, that plotting the derivative can be a serious problem for the experimental profile due to, for example, scattering of the experimental points [Kow00]. An alternative procedure which further improves the determination of D_{gb} and is more sufficient for ionic materials (as it will be shown in chapter V) is discussed now.

As far as the maximum is responsible for the accuracy of determined diffusion coefficient D_{gb} , it would be better to find the derivative at the maximum as accurately as possible. It seems to be the only possibility to find D_{gb} accurately. Because of this, it would be particularly interesting to analyze how the position of the maximum depends on t . In fig. 3.19 the positions for different Δ are plotted as functions of t on the logarithmic scale. It is very likely that the positions are linearly dependent on t on the logarithmic scale, what is very well seen for smaller ratios Δ . The points for $\Delta = 2.2 \cdot 10^4$ and 10^5 at long t are affected by the finite length of geometrical model (500 nm), reflecting that the necessary maximum is not reached.

That is why, the maxima for these large ratios Δ were taken at one point of 500 nm, beginning from 13200 s for $\Delta = 10^5$ and 100000 s for $\Delta = 2.2 \cdot 10^4$. The following relationship for $y^{6/5}$ at the maximum is found:

$$\log(y_{\max}^{6/5}) = \log(K) + H \cdot \log(t)$$

or

$$y_{\max}^{6/5} = K \cdot t^H,$$
(3.4)

where t is as usually the diffusion time, K is a normalizing coefficient which depends on Δ and, in general, on D_g and D_{gb} . However, the most useful information comes from the parameter H which is found out to be independent of D_g and D_{gb} , at least in the considered range of parameters. The parameter H determines the slope of the lines in fig. 3.19 and allows one to know t needed to reach the maximum, if the diffusion profile once measured is too shallow. This power law is not surprising since it reflects the typical diffusion property – dependence as a power law on t . In order to realize the long times (10^7 s – 10^{10} s) for large ratios Δ , the width as well as the length of the sample was increased (fig. 3.20), and Eq. (3.2) was integrated since β is much smaller than Δ . Consequently, the parameter H was determined by fitting the lines in figs. 3.19 and 3.20 to a straight line and is summarized in table 3.2. The perfect linear dependences were observed for short and very long times (red lines, reflecting the fitting in fig. 3.20, show this very clearly). Comparing the results of integration of the exact Whipple solution and Eq. (3.2) at $t = 500000$ s shows that the latter slightly overestimates the maximum positions (not shown here). The exact Whipple solution could not be integrated at so high t properly leading to very strong numerical instabilities. The dependencies in fig. 3.20 are characterized by a nonlinearity which is also seen for $\Delta = 10^3$ and 10^2 in fig. 3.19. The width of 5157 nm ($\sim 5.16 \mu\text{m}$) was applied for $\Delta = 10^5$, what demonstrates that a micrometer regime is already relevant here. However, this gives huge diffusion times which will never be realized in the experiments at least for the parameters D_g , D_{gb} used in the present study; however the temperature can be increased. More importantly, the slopes for all Δ used are very well comparable for short t (table 3.2). In these calculations the β – parameter was varied up to $\sim 10 - 15$ for all Δ . The most reasonable value of H is 0.6, because it suggests that $y_{\max} \sim t^{1/2}$ – the expected dependence. As the diffusion time grows up, the process slowly develops with time in a comparison with short t giving rise to the nonlinearity in figs. 3.19 and 3.20 (this can be the second reason explaining the effect of nonlinearity discussed in the preceding sections).

A similar behavior was observed for the maximum of the derivatives. When plotting the absolute values of maxima for relevant ratios Δ from $t = 2000$ s up to 500000 s, straight lines arise on the logarithmic scale (fig. 3.21). Again and importantly, similar slopes were observed for all the ratios Δ . In the dependence for the position of the maximum the values K are Δ -dependent, and to analytically calculate the position one needs to know this parameter. However, the most important is the maximum which can directly be put into Eq. (1.16). The general expression for the lines in fig. 3.21 is represented as follows:

$$\log \left| \frac{\partial \ln C_{av}}{\partial y^{6/5}} \right|_{\max} = \log(A) + B \cdot \log(t), \quad (3.5)$$

where B is the slope of the dependence $\log \left| \frac{\partial \ln C_{av}}{\partial y^{6/5}} \right|_{\max} = f(\log(t))$, A is the parameter which is Δ -dependent and also depends on t . In table 3.3 the values of the slopes are summarized for various Δ . These are very close to each other, indicating that single slope of approximately -0.34 may be used when calculating the derivative $-\partial \ln C_{av} / \partial y^{6/5}$ at the maximum, at least for $D_g = 2.95 \cdot 10^{-4}$ nm²/s. This conclusion is not very much different from the analysis performed by Atkinson and Taylor [Atk79], since they supposed that the gradient $-\partial \ln C_{av} / \partial y^{6/5}$ should be proportional to $t^{-0.3}$. However, an analytical relation to find the slope was not suggested.

All the quantities in Eq. (3.5) do not bear enough information on the diffusion coefficients. These quantities are dependent on the parameters and vary with both Δ and absolute values of D_g and D_{gb} . In this form Eq. (3.5) is difficult to use for finding Δ . However, it could be particularly important, since in many cases the measured diffusion profile can be influenced by additional processes accompanying diffusion of a solute in the material. Even though the quantities A and B are known, it is unclear how to relate them to Δ . If the quantity B is supposed to be a constant, there should be a relation between the quantities A and Δ . The later comes from the fact that the lines in fig. 3.21 are shifted up with increased Δ .

Consequently, the values of A found by fitting the functions in fig. 3.21 to the straight line were plotted against Δ . The corresponding result shown in fig. 3.22 suggests that there is a linear dependence of $\log(A)$ on $\log(\Delta)$ also on the logarithmic scale. This is a particularly important result, because it directly relates the slope (the maximum of the derivative) of the diffusion profile with the ratio Δ . According to this plot and in the fashion of Eq. (3.5) $\log(A)$ can be found by using

$$\log(A) = \log(C) + F \cdot \log(\Delta). \quad (3.6)$$

In this equation the quantity C can be different depending on D_g and t, and finally, the general expression for the slope is

$$\log \left| \frac{\partial \ln C_{av}}{\partial y^{6/5}} \right|_{\max} = \log(C) + F \cdot \log(\Delta) + B \cdot \log(t) \quad (3.7)$$

or

$$\left| \frac{\partial \ln C_{av}}{\partial y^{6/5}} \right|_{\max} = C \cdot \Delta^F \cdot t^B$$

All the dependencies (Eqs. (3.5) and (3.6)) reflect the fact that the maximum of derivative follows a single law when increasing the ratio Δ or time t. Further details on using Eq. (3.7) will be discussed in chapter V.

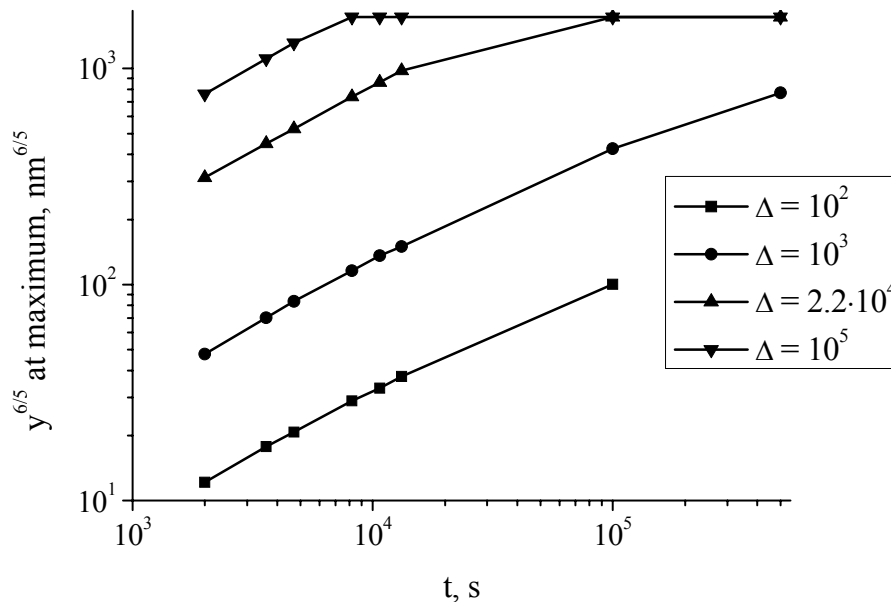


Fig. 3.19 Variation of $y^{6/5}$ taken at the maximum of the derivatives $\partial \ln C_{av} / \partial y^{6/5}$ with t for different Δ on the logarithmic scale. The length of the geometrical model is 500 nm.

Table 2.2 Different slopes H varying t ($y_{\max}^{6/5}$).

Δ	H(t)		
	$2 \cdot 10^3 \text{ s} \leq t \leq 1.32 \cdot 10^4 \text{ s}$	$1 \cdot 10^5 \text{ s} \leq t \leq 2.1 \cdot 10^6 \text{ s}$	$2.1 \cdot 10^6 \text{ s} \leq t \leq 10^{10} \text{ s}$
10^2	0.59	0.53 (up to $1 \cdot 10^5 \text{ s}$)	-
10^3	0.58	0.50 (up to $5 \cdot 10^5 \text{ s}$)	-
$2.2 \cdot 10^4$	0.60	0.42 (0.50)	0.29
10^5	0.61	0.42	0.30

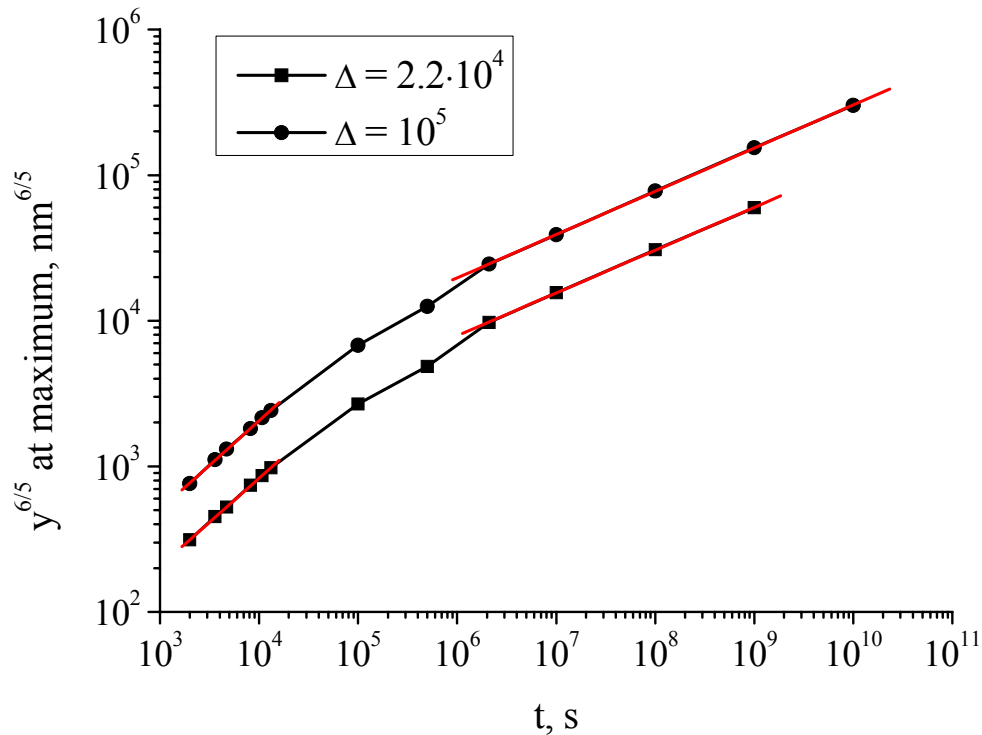


Fig. 3.20 Variation of $y^{6/5}$ taken at the maximum of the derivatives $\partial \ln C_{av} / \partial y^{6/5}$ with t for different Δ on the logarithmic scale. The width and the length of the geometries were increased to reach small values of β : the length of about 40 000 nm is needed to integrate Eq. (3.2) for $\Delta = 10^5$ at $t = 10^{10}$ s. Red lines correspond to the fitting.

Table 3.3 The values of the slope B for various Δ ($D_g = 2.95 \cdot 10^{-4} \text{ nm}^2/\text{s}$).

Δ	B
10^2	-0.32
10^3	-0.33
$2.2 \cdot 10^4$	-0.34
10^5	-0.36

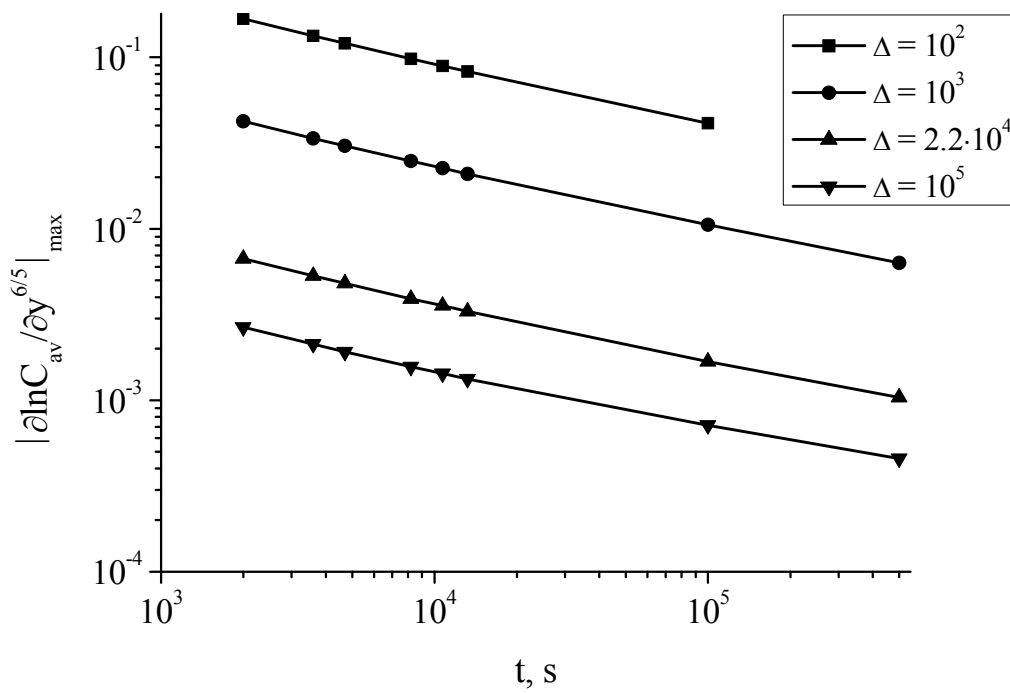


Fig. 3.21 Variation of the modulus of the maximum with t for different Δ . The result is performed on the logarithmic scale.

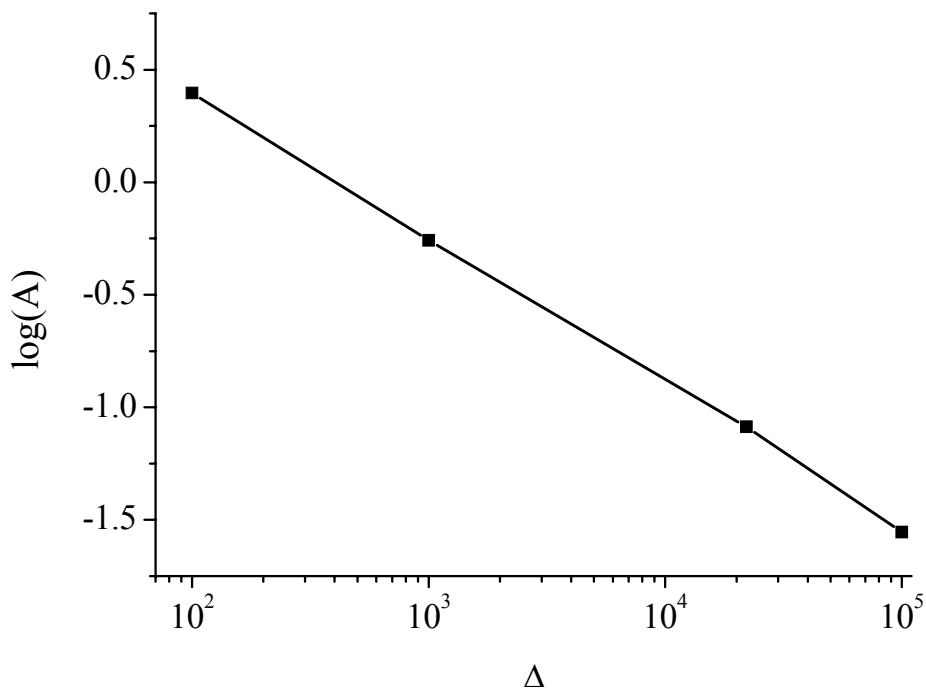


Fig. 3.22 Variation of $\log(A)$ in Eq. (3.5) with Δ .

Summary

It is shown that the nonlinearity of the diffusion profile $\ln C_{av} = f(y^{6/5})$ has to be analyzed, especially at short diffusion times. The maximum of the diffusion profile can be used to find the GB diffusivity accurately under such conditions. This maximum corresponds to the diffusion kinetics which is relevant under certain conditions. The use of Le Claire's relation requires type-B kinetics, and the maximum reflects that situation. Application of Le Claire's constant of 1.322 leads to errors at very short diffusion times. In order to improve the determination of the GB diffusivity, an equation is suggested to find the derivative $(\partial \ln C_{av} / \partial w^{6/5})$ at the maximum. The improved procedure is explained in detail. Additionally, new dependences are derived on the basis of integrations of the exact Whipple solution for the maximum value of $(\partial \ln C_{av} / \partial y^{6/5})$ and its position. For the dependence of the gradient $(\partial \ln C_{av} / \partial y^{6/5})$ at the maximum the quantity B is found to be ~ -0.34 . The value of the gradient at a certain diffusion time can be directly used in the Le Claire relation, if the quantities F and C are known.

Chapter IV. Realistic microstructures

Introduction

A polycrystal consists of GBs differently oriented with respect to each other and the diffusion direction. Even though it is important to take these orientations into account, conventional GB diffusion models ignore this effect. In this chapter realistic microstructures are discussed, and the conventional analysis is applied to the diffusion profiles calculated in both the B-regime and the A-regime. The influence of the crystallographic misorientations of the grains is neglected [Lea57].

It is important to mention that the reliability of the model of isolated boundaries (fig. 1.2) as a representation of a polycrystal is partly based on sufficiently small values of the parameter β (see discussion below and [Kau95]) and/or large grain sizes. In this case the grain shape and the GBs orientations do not play a significant role. On the other hand, as the diffusion time (t) shortens, the diffusion process in a polycrystal is mostly determined by the GB contribution. This is the typical situation in materials with small grain sizes.

Different theoretical methods were recently applied in order to analyze the diffusion behavior under realistic conditions. Attempts were undertaken to analyze GB diffusion in realistic microstructures by using Potts model [Swi97] and phase field approach [Zhu01]. Moreover, attempts were also undertaken to obtain some analytical solutions to describe diffusion in real polycrystals [Bed05]. However, the model of parallel boundaries (the same as the isolated boundary model in the B-regime) and the model of square grains are very often considered when simulating diffusion in polycrystalline materials by using the Monte-Carlo method [Bel03]. Also the model of spherical grains is convenient for analytical evaluations [Harr61] as well as for numerical considerations [Sak90]. The analysis of GB diffusion in realistic microstructures is mostly restricted to the extreme cases of the A- or C-regime. Consequently, both the model of parallel boundaries and the model of square grains are analyzed in the present study in the B- as well as A-regime but with an eye to more realistic (general) microstructures, developed here by using the finite element approach. Further literature and ideas on simulating diffusion in the realistic microstructures are discussed in the following sections.

4.1 Finite Element Calculation. To get started

As already mentioned the finite element method (FEM) is a very useful tool for studying different physical processes [Sim06]. Application of the FEM to problems of diffusion and heat conduction was discussed in the literature due to the importance of these processes and the possibility to model these by means of classical differential equations (for example, [Com94]). That is, a linear partial differential equation of the second order of parabolic type is treated in the case of mass transfer (heat conduction) [Wei65]. Moreover, a numerical study of such processes can serve as a model simulation of instationary problems for the finite element calculations. However, problems such as GB diffusion have never been studied intensively by FEM. The paper of Whipple [Whi54] was published in earlier 50's of the last century. Since that time, Whipple's solution has been remaining the only exact solution of diffusion equations to the GB diffusion problem, and there was no need to solve the Fisher system by means of numerical methods. Only a single paper, by Z. Knesl *et al.* [Kne74], was dealing with FEM for interacting GBs in the model of square grains. Even though, numerical methods can help to obtain the concentration distribution for such geometrical situations. As a result of this simulation they simply compared the diffusion profiles obtained for the isolated boundary model to those for the square grains for the

interacting GBs. Despite this fact, it was a pioneering work as regards on the application of FEM to the problems of GB diffusion.

There is always a numerical aspect relating to the integration of differential equations. The accuracy of integration defines the quality of simulating concentration profiles, which is reflected in the parameters obtained from simulated profiles. The integration can become very critical in the cases of extremely small diffusion lengths, because the diffusion process in the bulk (grain) is concentrated closely to the surface where the gradients are very high. This is specifically important for GB diffusion, because of two interrelated processes: the GB diffusion rates can be significantly different from the bulk diffusion rates. The GB contribution to the overall process is prolonged along the y-coordinate (fig. 1.2) at short t and is strongly concentrated around the GB. This implies that high densities of integration meshes are required in those regions in order to get accurate results. Otherwise, the simulated diffusion profiles could either be inaccurate or even physically inadequate by giving negative concentrations. It is the purpose here to show: 1) how the GB diffusion problem can be resolved by using FEM, 2) which problems arise when integrating Fisher's system (Eq. (1.6a)) by FEM, 3) what conclusions can be drawn from numerical analysis.

4.1.1 Main characteristics of the geometrical model of isolated boundary used in the finite element program

The typical t used in the present work is 2000 s for $\Delta = 2.2 \cdot 10^4$. In this case $L_g \approx 0.77$ nm, i.e. it is comparable with the interatomic spacing, whereas $L_{gb} \approx 64.61$ nm. Let the whole length of geometrical model be 500 nm and the width 40 nm. The length of 500 nm is mostly used, if not stated otherwise. That is, the geometry is represented by a rectangle box with the diffusant applied at the free surface. The diffusant moves into the box under the concentration gradient until a whole space is filled up by the diffusant. This problem is again two-dimensional with reflecting boundaries at all sides of the geometrical model, if a special property is not defined, for example, the GB or the free surface. The GB thickness (δ) is neglected as it is supposed by Fisher's model. The latter means that the GB is represented by a line with neglecting the GB concentration within it. The relevant geometrical model is equivalent to that used to integrate Whipple's solution. The only difference between the two solutions is the influence of reflecting boundaries in the FEM model. Consequently, Eq. (1.3a) should be added by the zero-flux condition at the bottom of geometry. However, our main analysis is related to the maximum of the derivative of $\ln C_{av} = f(y^{6/5})$. If the maximum is not

affected by the boundary, the solution is valid for infinite systems as well. The role of this condition for simulation of diffusion in the A-regime is discussed in section 4.2.3.1.

4.1.2 A comparison of Whipple's solution and FLUX-EXPERT's simulation results

To compare Whipple's solution with FLUX-EXPERT's result, a consideration of single GB is necessary. The two results are shown in fig. 4.1. These coincide within an error of 1% until the influence of the zero-flux boundary condition becomes significant at larger coordinates (the derivative goes to zero). This demonstrates that the model applied in FLUX-EXPERT (the geometrical model, mesh as well as the derived Eq. (2.8)) can be used to integrate the Fisher system. This is particularly important because diffusion is studied here under extreme conditions: short t and diffusion lengths, leading to high derivatives. In the next sections the results of the integration in FLUX-EXPERT for different geometrical models and parameters are discussed. All these results were obtained with a very high accuracy, what is, however, computationally costly.

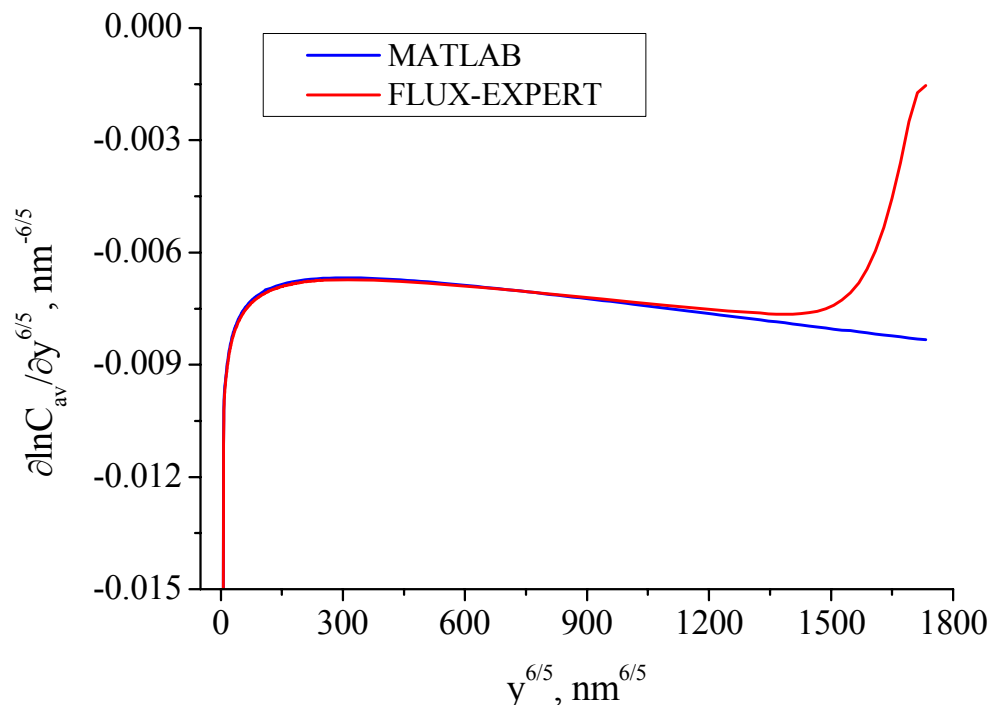


Fig. 4.1 A comparison of the integration by FEM (FLUX-EXPERT) with Whipple's solution (MATLAB). The ratio $\Delta = 2.2 \cdot 10^4$ and $t = 2000$ s.

4.1.3 The accuracy of results obtained in FLUX-EXPERT

4.1.3.1 The averaging of concentration C_g

It is reasonable to discuss here how, using FLUX-EXPERT, the concentration $C_g(x, y, t)$ is integrated along the direction perpendicular to the GB. The diffusion parameters are found from the profile of concentration $C_g(x, y, t)$ averaged along the x-direction (fig. 1.2), which reveals the concentration $C_{av}(y, t)$ as a function of coordinate y only. This is done in the same manner as in real diffusion experiments by using, for example, tracer measurements [Ask70]. FLUX-EXPERT gives the concentration distribution over all mesh points. One can also plot the concentration along different paths of the geometrical model [Flu92e]; however, the averaging is not realized in the program specifically. The special script was written by using the programming language Perl in order to obtain C_{av} .

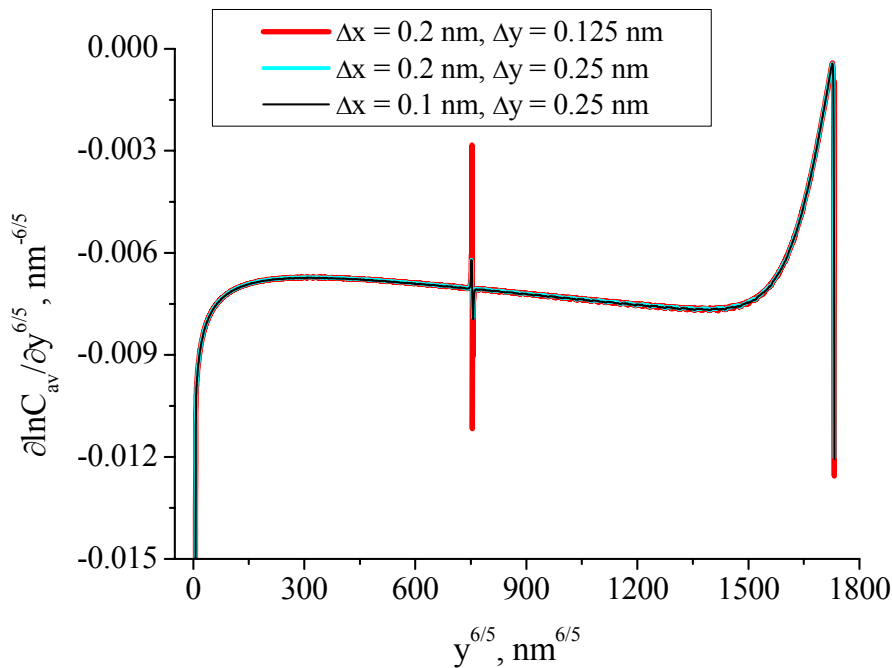


Fig. 4.2 Variation of the derivative $\partial \ln C_{av} / \partial y^{6/5}$ with $y^{6/5}$ calculated with different intervals Δx and Δy .

The script runs the module XPLOIT [Flu92e], in which the concentration is calculated along the paths of constant y-coordinates in the automatic mode. The module allows one to calculate the integral itself; however the averaging is done by dividing that integral by $(x_{max} - x_{min})$, i.e. the width of the geometrical model used. Consequently,

$$C_{av}(y, t) = \frac{1}{x_{max} - x_{min}} \int_{x_{min}}^{x_{max}} C_g(x, y, t) dx \quad (4.1)$$

The steps of integration are controlled in this script along both directions, but the interval along the x-direction (Δx) is, of course, an important parameter. In the present work the only intervals used to obtain C_{av} are $\Delta x = 0.20$ and 0.25 nm. If the interval Δx is decreased, say by a factor of 2, the derivative does not change and, in principle, the same result can be obtained (fig. 4.2, black line). The step along the y-direction can influence the result as well, leading to numerical instabilities similar to those observed by integrating Whipple's solution (see section 3.2). The instability is reflected in noise and spikes, for example at $y^{6/5} \sim 750 \text{ nm}^{6/5}$ in fig. 4.2. Such spikes are enhanced when the interval Δy decreases.

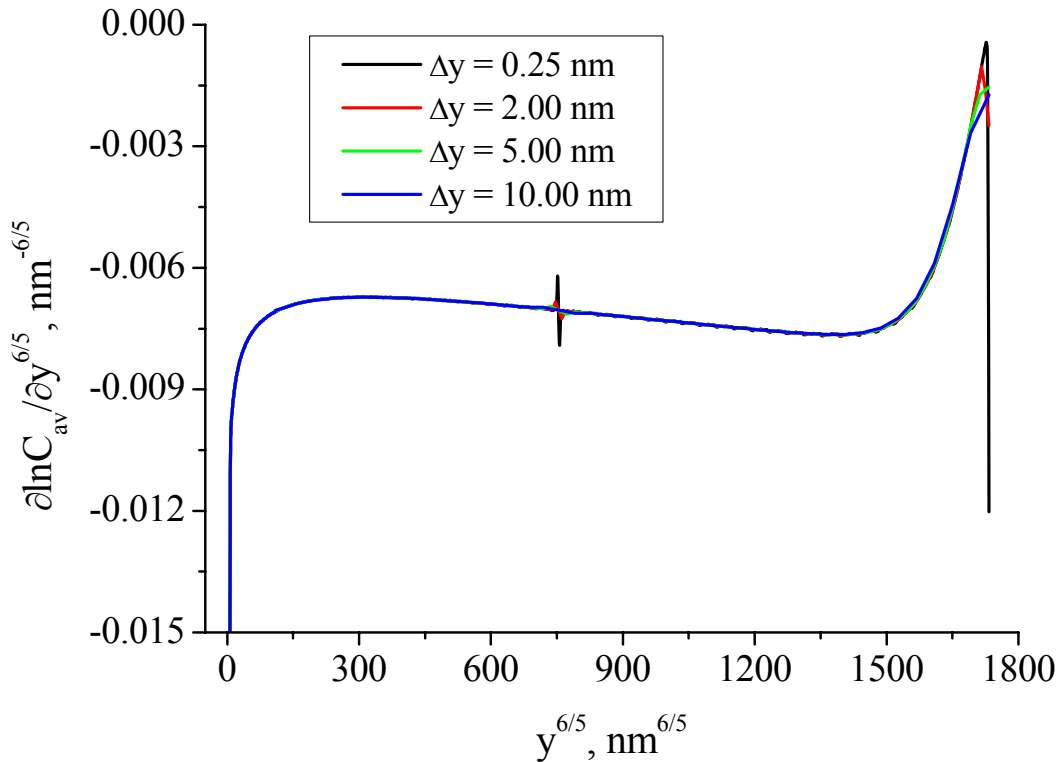


Fig. 4.3 Variation of the derivative $\partial \ln C_{av} / \partial y^{6/5}$ with $y^{6/5}$ calculated with different steps Δy in the GB part.

Consequently, the following Δy -intervals were tested in the GB part of the diffusion profiles (i.e. in the region $50 - 500$ nm for $\Delta = 2.2 \cdot 10^4$ at $t = 2000$ s): 0.25 , 2.00 , 5.00 , and 10.00 nm, while the interval in the bulk part of the profile was fixed to 0.25 nm. The derivatives of the corresponding diffusion profiles are presented in fig. 4.3. In this way one

can show that increasing the interval of integration (Δy) in the GB part leads to derivatives without instabilities. In order to get a similarly smooth profile of the derivative three steps were finally adapted according to three parts of the diffusion profile: bulk part, GB part and the reflecting boundary. The example of this profile is shown in fig. 4.1 obtained with the Δy -steps 0.25, 20.0, 5.0 in the bulk, GB and reflecting boundary parts, respectively.

4.1.3.2 The effect of the finite element mesh

Diffusion has a specific feature which should be taken into account for numerical integration of the diffusion equations by FEM. The diffusion gradients vary with time striving for zero until the equilibrium is achieved. On simulating diffusion in different kinetic regimes, the problem of the mesh becomes very important. One would thus presume different density meshes in different parts of geometry and/or at different t . This also complicates the numerical integration of diffusion equations. However, it would be useful to find a universal mesh for certain diffusion parameters, sufficiently dense to use it under different conditions. Moreover, there is always a trade-off between mesh density and time interval (Δt). Several calculations are typically needed to get a final diffusion profile, which depends on the parameters (diffusivities, t) used in the numerical experiment. Unfortunately, it is not possible to simply increase the density, because it would greatly increase the computational time. Moreover, the finite element program used has limits too. In particular, FLUX-EXPERT has a maximum number of elements of one million (!), at least for the version of the program used in the present work [Flu00]. One can imagine that this maximum number is fixed for the whole geometry, and once the geometry was defined, satisfying the accuracy, it is not possible to increase its length further. One should pay attention that these numerical problems become specifically important when simulating diffusion in nanocrystalline materials due to small diffusion lengths.

The mesh density for the concentration profile plotted in fig. 4.1 is as follows: 0.25 nm along the x-direction and about 0.24 nm along the y-direction. Hereafter this mesh is called mesh 1. Such a mesh density implies the number of triangle elements to be 657729 for the geometry of 40 nm in width and 500 nm in length (40x500 nm²). The same density for the geometry of 25 nm in width gives 409940 triangle elements. This is the most dense mesh used in the present work (except the space charge layer problems discussed in the next chapter), for which the number of elements is already half of the program's limit (see also other examples in table 4.1). The result obtained by using this mesh is consistent with that obtained by

integrating Whipple's solution (fig. 4.1). This allows mesh 1 to be a model mesh and to skip a comparison of that with more dense meshes. In fig. 4.4a the profile for mesh 1 (red curve) is compared with that for smaller number of elements. The density was also decreased to 0.5 nm and about 0.48 along the x- and y-direction, respectively. This is a mesh, called mesh 2, with ~164884 elements for the sample: 40x500 nm². It is very important to note that for a mesh of smaller density the reflecting boundary leads to larger values of the concentration $C_{av}(y, t)$, especially at deeper y-coordinates. In this case the derivative looks more like a straight line in the GB part artificially, but this is purely the effect of the mesh only (green and blue lines in fig. 4.4a). In the worst case, the decrease of the mesh density could lead to a vanishing of the GB part, affecting the maximum so strongly that the slope of the diffusion profile could not be obtained.

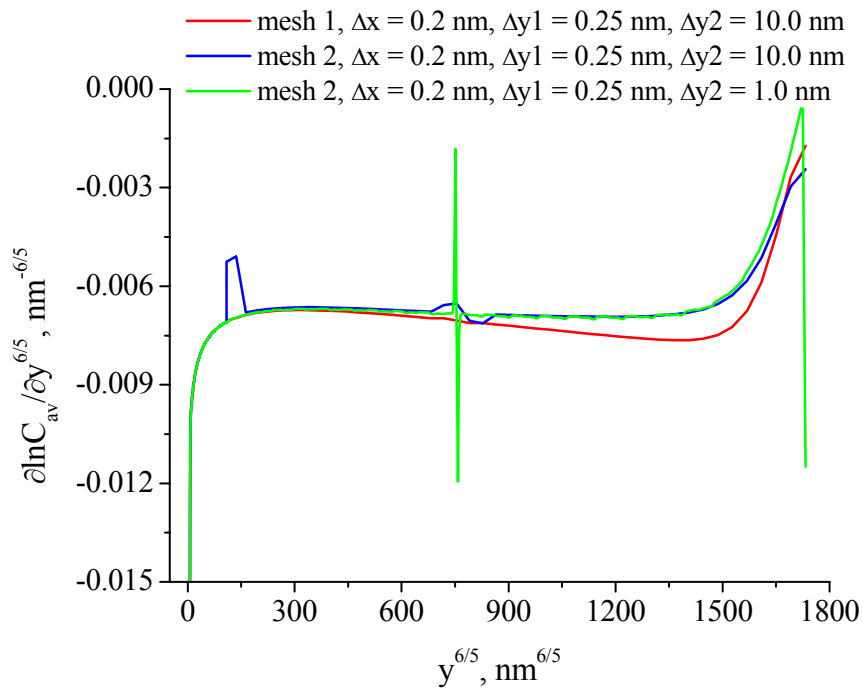
The integration parameters (the interval Δy , see discussion above) differ for both mesh 1 and mesh 2. The interval $\Delta y = 10$ nm and smaller along the GB part leads to the instabilities for mesh 2 (blue and green curves). In fig. 4.4b the comparison of mesh 1 is made with additional new meshes for the same geometry (40x500 nm²) at longer t in order to get a preliminary impression of the introduced errors. Additionally, decreasing mesh density does not really allow one to start the calculation with short time of 200 s, as it was done with mesh 1. Consequently, the starting times are 200 s for mesh 3 and 7000 s for mesh 4 (table 4.1). In fig. 4.4b the noise (green curve) is related to a very small step integration Δy of 0.25 nm. Obviously, such intervals together with small densities are not advisable. The results for mesh 1 and mesh 3 coincide at $t = 10700$ s, demonstrating that one can use the meshes of smaller densities for simulating diffusion at higher t only. However, the main choice is made for mesh 1 is preferred as satisfying the necessary accuracy at short t and allowing t to be increased as well as the ratio of diffusivities (Δ).

Table 4.1 Parameters of different test meshes.

Name	Density along x/y direction	Number of triangle elements (40x500 nm ²)
mesh 1	0.25/0.24	657729
mesh 2	0.50/0.48	~164864
mesh 3	1.00/0.97	41391
mesh 4	2.00/1.95	10445

4.1.3.3 The effect of the time interval

a)



b)

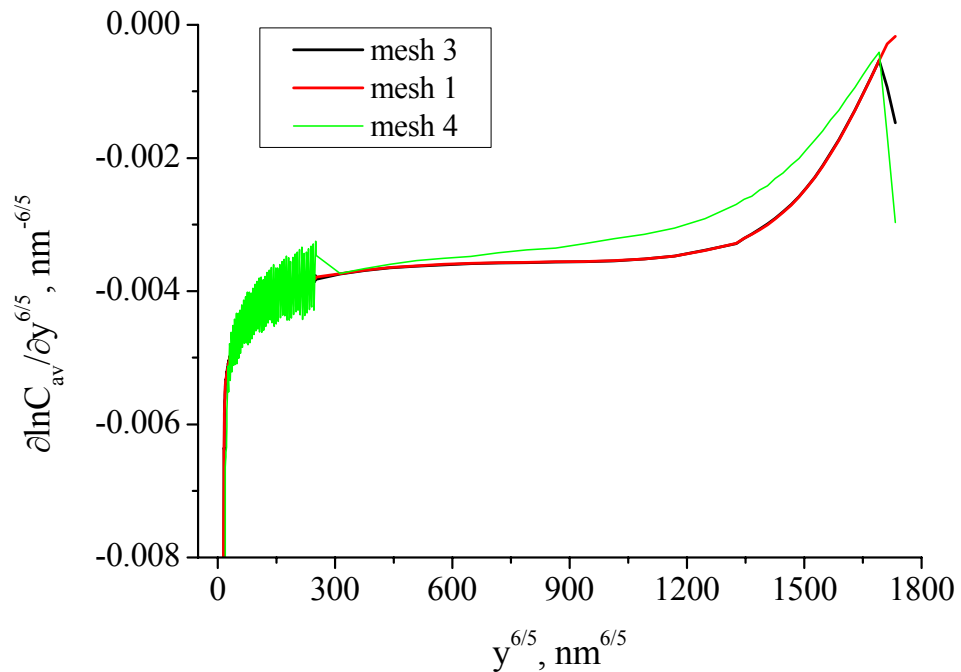


Fig. 4.4 A comparison of different meshes at a) $t = 2000$ s and b) $t = 10700$ s. The steps Δy_1 and Δy_2 mean the intervals in the bulk part and GB part of the profile, respectively.

As we deal with transitory problems, the solution strongly depends on the time interval used. The smaller the interval Δt the more accurate the solution. Because very small values Δt leads to time-consuming calculations, an appropriate computational procedure should be found with respect to that parameter too. In order to check its effect, various Δt were used, simulating the diffusion profile for conditions $\Delta = 2.2 \cdot 10^4$ at $t = 2000$ s. The interval Δt was varied from 600 s to 6.25 s, starting the calculation with t of 200 s. In all the calculations under conditions of the type-B kinetics (see section 1.2), this starting time was taken as 200 s, if not otherwise stated. Consequently, the largest Δt suggests 3 computational steps, whereas the smallest one 288 steps.

The profiles for various Δt are presented in fig. 4.5. One can see that there is a very little difference in the derivatives calculated for $\Delta t = 6.25, 12.5$ and 25 s. Finally, $\Delta t = 12.5$ s was used in all the calculations up to 13200 s. It was observed, that after 13200 s Δt can be increased and, consequently, in the A-regime the time interval of 20000 s was used.

The starting time value can affect the accuracy of a particular result, especially at very short t . That is why, Δt should be tuned every time, beginning a new calculation with a new geometry (or mesh) and parameters. In fig. 4.5 it is demonstrated that large $\Delta t = 600$ s leads to the vanishing of the maximum. Fitting the corresponding profile by a straight line does not give a correct slope.

4.2 Realistic polycrystalline microstructures

In GB diffusion studies the isolated boundary model (fig. 1.2) has been serving as a good approximation of a real microcrystalline structure for many years. However, a real microcrystalline structure comprises many GBs differently oriented to each other and to the diffusion direction. Ignoring the GBs orientations seems justified by the fact that in coarse-grained materials the influence of a GB orientation on a concentration profile is negligible, because of the possibility to study diffusion under conditions of high temperatures and/or long t . The type-B kinetics is considered for the coordinate developing process. In the case of coarse-grained materials L_{gb} is also less than d [Kau95], i.e. the condition given by Eq. (1.11a) is fulfilled. It is believed that the diffusion process changes with time and along a GB oriented perpendicularly to the surface. One would expect that the role of GBs, which are not parallel to the diffusion direction increases, if the β -parameter increases (Eq. (1.9d)), i.e. the larger ratio Δ or significantly shorter t (and/or smaller d) are considered. The former would lead to the condition $L_{gb} \gg d$, whereas the latter tends to the specific type-B kinetics in which all the

properties discussed so far are valid (chapter III) and the condition $L_{gb} \gg d$ can be recalled also. Interestingly, L_g can reach d earlier than L_{gb} , what would exactly mean that one faces the type-B₄ kinetics (fig. 1.5a, imagine that $d > 25$ nm) but this is only possible for coarse-grained materials.

There is another interesting finding of Mishin [Mis92b] that plotting the diffusion profile versus $y^{6/5}$ or simply y gives, in principle, similar errors of determining D_{gb} in a coarse-grained polycrystal when only the orientation of a GB to the surface is taken into

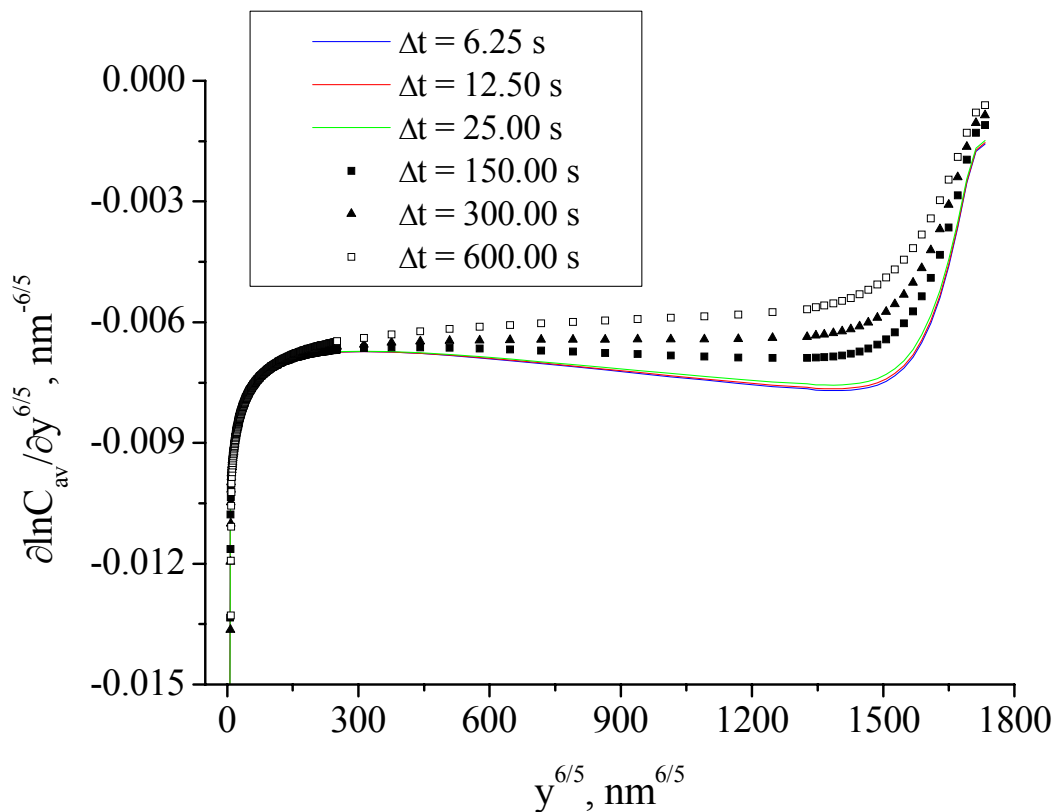


Fig. 4.5 A comparison of the derivatives of concentration profiles calculated by the FEM with different time intervals (Δt) at $t = 2000$ s.

account and analyzed. This is not true for a bicrystal, or an idealized system of parallel boundaries, because the profile is more nonlinear in this case according to Mishin. However, this opens the question about the validity of both methods (i.e., $\ln C_{av} = f(y^{6/5})$ and $\ln C_{av} = f(y)$) for polycrystals, what is also mentioned in [Kau95]. The other possible situations for L_{gb} being larger than d are discussed in the present work (fine-grained or ultrafine-grained materials [Mis95]). Nanocrystalline materials, characterized by grains of ten-hundreds of nanometers, have L_g of several or tens nanometers, what gives rise to β -values of the order of several thousands. The problems discussed above concerning the application of Le Claire's

relation (Eq. (1.16)) come into play together with the GBs orientations. The problems of GB orientations make the diffusion studies more complicated. In this sense the effects of small grain sizes are *size effects* – a term that arises particularly when discussing properties of nanocrystalline materials [Mai03], [Mai04a].

Two important points are taken into account now. First, the orientation of a GB to the surface is not analyzed. According to [Kau95], after the pre-diffusion anneals the GBs will tend to maximize the inclination angles with the surface in a way that most of their values will be around 90°. Moreover, the diffusion profile for real polycrystalline specimen represents an averaged resultant of the influence of different GBs orientations.

4.2.1 A comparison of the model of parallel boundaries with the model of square grains under conditions of type-B kinetics

The model of square grains used to analyze the corresponding diffusion effects represents a 2D pattern with GBs being simple lines perpendicular or parallel to the diffusion direction. Consequently, the concentration within the GBs is neglected. Each GB forms a side of square (fig. 4.6). Also the zero flux condition is used at the sample's bottom as a boundary condition. The typical grain sizes are 10, 25, 50 and 100 nm. Correspondingly, the grain size for the model of parallel boundaries simply means the distance between two neighboring GBs. The diffusion time was varied to cover different kinetic regimes, going from the B-regime to the A-regime. This allows one to apply different procedures used to deduce D_{gb} . The typical ratio of diffusivities Δ is $2.2 \cdot 10^4$, however in some cases smaller ratios are also used (it is indicated). Such ratios fit very well to all important requirements needed to be taken into account for the accuracy and convergence when simulating diffusion by FEM.

4.2.1.1 The model of parallel boundaries at short diffusion times

It is reasonable to start the analysis of the B-regime at short t with the model of parallel boundaries. Let us consider the variation of the distance between the boundaries from 10 nm to 100 nm. The diffusion process is analyzed at 2000 s. The values of diffusion parameters are the same as explained in chapter III. Under these conditions the contribution of GBs leads to the same slopes independently of d , whereas the bulk contribution (given by a complementary error-function) intermixed with the GB contribution changes. Because the average concentration (C_{av}) represents the grain concentration averaged along the direction

perpendicular to the GB, the GB part of the concentration is larger for smaller distances. This is confirmed by the result shown in fig. 4.8.

The GB part of the concentration reduces to a constant value when the distance is doubled (the results for $d = 12.5, 25, 50$ and 100 nm in fig. 4.7). Consequently, smaller deviations of the concentration C_{av} in the bulk part of the profile result for the larger distances. For larger d the bulk parts of the profiles are better determined by a complementary error-function solution (red curve in fig. 4.7). The strongest deviation appears, of course, for $d = 10$ nm, suggesting that this result will lead to serious errors in determining D_g from the corresponding profile. This is ascribed to an additional effect related to the small grain sizes. In order to emphasize the effect, the concentration profiles for the same parameters were calculated for the micrometer regime (fig. 4.7).

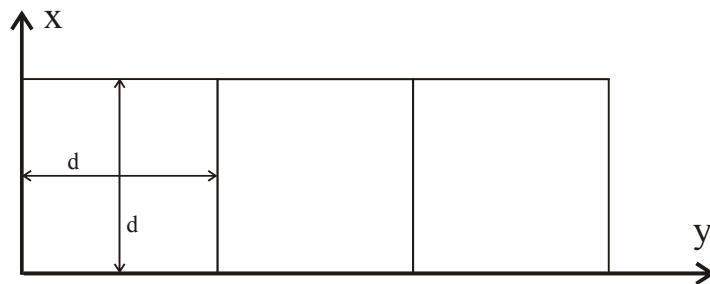


Fig. 4.6 Schematic representation of the square grain model.

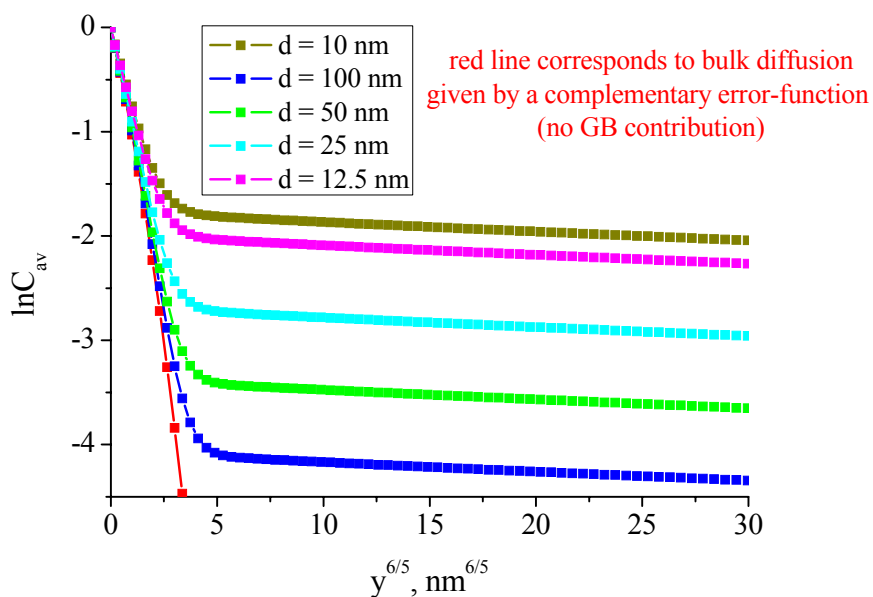


Fig. 4.7 Variation of $\ln C_{av}$ with $y^{6/5}$ calculated for the model of parallel boundaries for different distances between the boundaries (d).

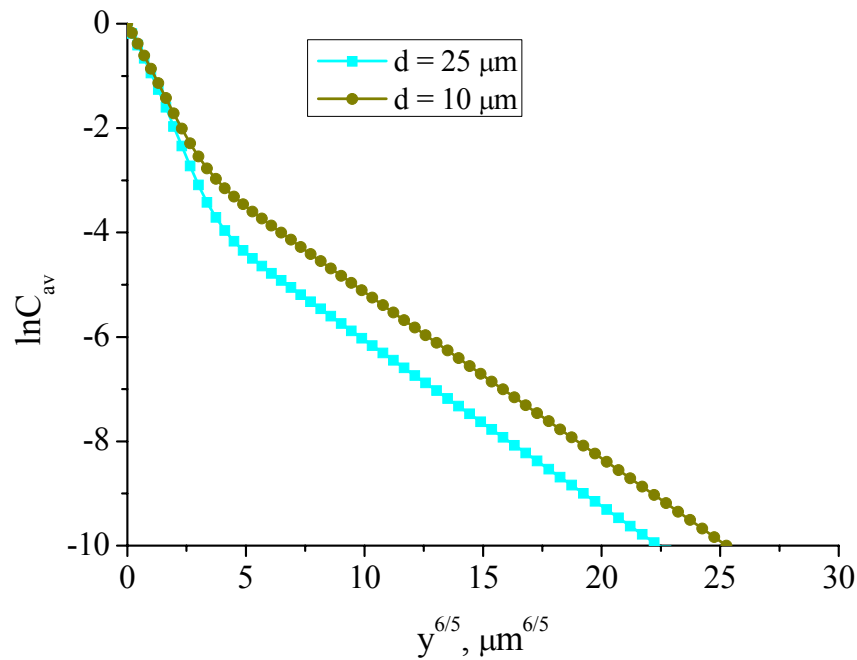


Fig. 4.8 Variation of $\ln C_{av}$ with $y^{6/5}$ calculated for $\Delta = 2.2 \cdot 10^4$ at $t = 2.04 \cdot 10^9$ s for the model of parallel boundaries.

The diffusion length in the grain (L_g) at $t = 2.04 \cdot 10^9$ s is about $0.78 \mu\text{m}$ for the profiles in fig. 4.8. This is exactly by three orders of magnitude higher than that at $t = 2000$ s. The deviations in the bulk parts for the profiles for different d are smaller in comparison with the nanometer regime. The GB part is affected in a way the two distinguishable parts of the profiles disappear with time (very small values of β arise). The profiles are less acute (between the two parts of the profiles) in fig. 4.8 in comparison with fig. 4.7. The slopes of the GB parts of the profiles shown in fig. 4.7 or in fig. 4.8 are the same for varying corresponding d . Clearly, the slope can then be changed only by varying t , if Δ is fixed. Yet, the profile in a nanoregime is more sensitive to the distance d . The process in the grain has not enough time to adopt a complementary error-function at very short t . In fig. 4.9 the diffusion profiles as shown in fig. 4.7 and fig. 4.8 for $d = 25$ and 10 nm and $d = 25$ and $10 \mu\text{m}$ are presented again together with the corresponding complementary error-function solutions to analyze the transition from the bulk diffusion parts to the GB parts of the profiles on different scales. The deviation of the result for $d = 10$ nm from its bulk diffusion profile is larger than that for $d = 10 \mu\text{m}$. Interestingly, the profiles in fig. 4.9b correspond mostly to bulk diffusion and only partly to the intermixture of the bulk and the GB parts, whereas on the nanoscale the GB part is very distinguishable despite the reduced values of y .

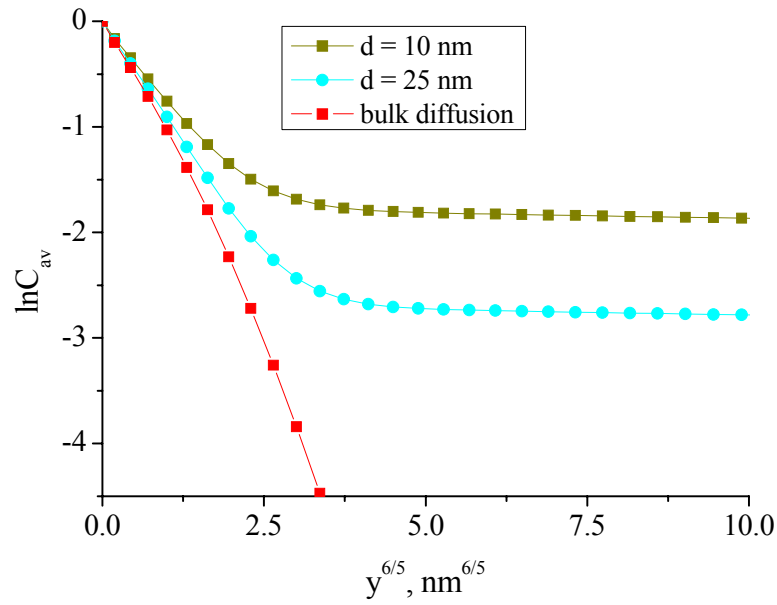
Understanding the diffusion process at different time scales allows one to analyze the role of GBs in the model of square grains or in one of the general representations of a polycrystal. The short times lead to an artificial prolongation of the process along GBs and, as a result, the GBs orientation can play a role. In these cases L_{gb} is typically much larger than d , and the kinetics are slightly different in comparison with the coarse-grained materials.

4.2.1.2 The model of square grains at short diffusion times

Let us *first* compare the profiles calculated for the square grains with the corresponding profiles for the parallel boundaries at fixed t . In fig. 4.10 the profiles are performed for these two models for $\Delta = 2.2 \cdot 10^4$ at $t = 2000$ s and for $d = 25$ nm and 100 nm. The profile for the square grains comprises two types of diffusion paths, namely parallel and perpendicular ones. The perpendicular GBs lead to spikes clearly seen in fig. 4.10. The number of these perpendicular paths is 19 for $d = 25$ nm and 4 for $d = 100$ nm for the fixed total length of the sample (geometry) of 500 nm. Each of them contributes to the profile changing the slope of it. It is seen that the discrepancy between the two models is more pronounced for smaller d . Moreover, one can recall here the effect of nonlinearity discussed in chapter III. When increasing the volume fraction of GBs (g) or decreasing d , the effect of nonlinearity is further induced, especially at very deep parts of the profiles (figs. 4.10b and 4.11).

When, *second*, analyzing the effect of g , one should be especially careful with the slope of the profile. The slope increases with decreasing d (fig. 4.11). The atoms move through the perpendicular and parallel boundaries in the model of square grains, and their concentration should be decreased in comparison with the motion of those along the parallel paths only. Surely, if the number of perpendicular GBs is higher, the concentration reduces. Consequently, two effects characterize the diffusion profile. One is related to increasing/decreasing d and leads to larger concentrations for smaller distances d , especially at coordinates close to the surface (fig. 4.11). Another one also depends on d and with decreasing d leads to smaller concentrations in comparison with the parallel boundaries. If the distance d is 25 or 10 nm, there is a convex curvature of the profile, because the perpendicular boundaries do not allow the number of atoms to be increased. This is in contrast to $d = 50$ or 100 nm, when the concentration increases at the deeper parts of the profile for the fixed length of the sample. If one believes that the model of square grains indeed represents a general polycrystal, then the GBs orientations can change the values of $D_{gb,app}$ applying Le Claire's

a)



b)

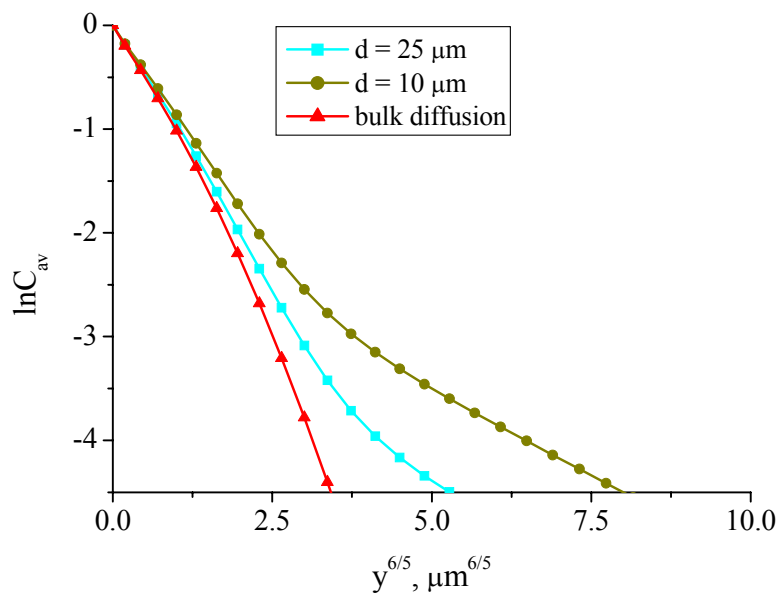


Fig. 4.9 A comparison of the diffusion profiles calculated at $t = 2000 \text{ s}$ a) and $t = 2.04 \cdot 10^9 \text{ s}$ b) for different distances between the parallel boundaries (the same profiles as performed in figs. 4.7 and 4.8, but for another scale of $y^{6/5}$).

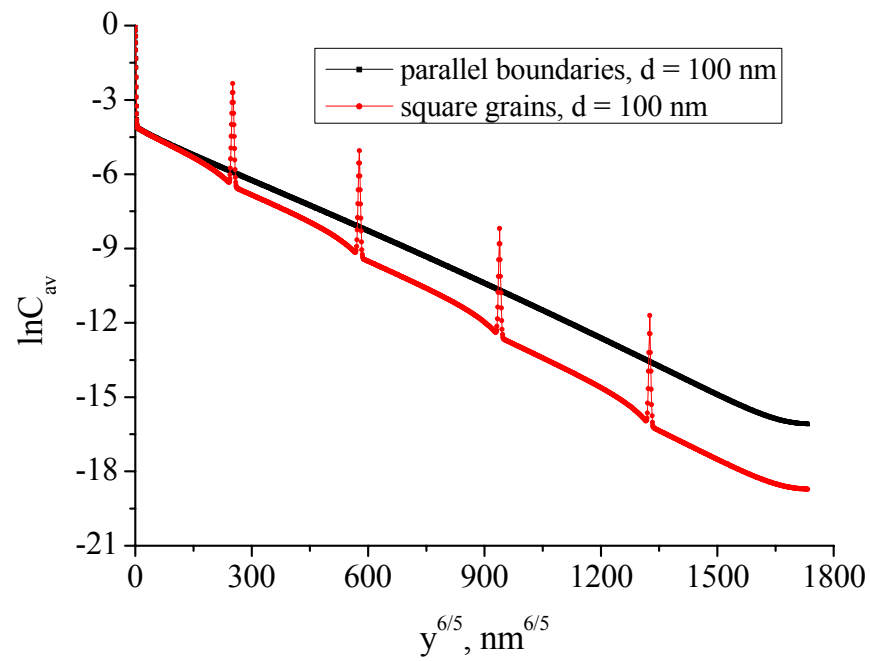
relation (Eq. (1.16)). The larger the slope the smaller the value of $D_{gb,app}$. Such an underestimation of D_{gb} is very typical for short t in the model of square grains in the type-B kinetics. The slope of the profile varies with t as well as with d . In order to estimate possible errors all the profiles presented in fig. 4.11 were fitted by straight lines. Accordingly, table 4.2 contains information on varying $D_{gb,app}$ determined by applying Le Claire's relation. Also the results of fitting the profiles calculated for the parallel boundaries are presented. As it is expected, all the slopes for the square grains are larger than for the parallel boundaries. It is important to notice that the slopes presented in table. 4.2 may only be compared with the slope of -0.00675 , giving $D_{gb,app} = 4.22 \text{ nm}^2/\text{s}$ which itself is erroneous ($D_{gb,true} = 6.42 \text{ nm}^2/\text{s}$). The latter value includes the corrected Le Claire's constant, but is affected by the effect of nonlinearity. Consequently, $D_{gb,app}$ can be three times smaller than the true value applying the conventional analysis when the effects of GBs orientations are not taken into account. The underestimation can be even larger, if the profile is measured (or calculated) for deeper coordinates influenced by larger number of perpendicular GBs.

Analyzing the derivatives of the profiles in the grain closest to the surface (fig. 4.12) reveals that the maximum is not reached even for $d = 100 \text{ nm}$ due to the perpendicular boundaries, since the position of maximum $y_{max}^{6/5} \approx 300 \text{ nm}^{6/5}$ at $t = 2000 \text{ s}$ for $\Delta = 2.2 \cdot 10^4$. The positions of perpendicular GBs are $15.85, 47.59, 251.19 \text{ nm}^{6/5}$ for $d = 10, 25, 100 \text{ nm}$, respectively. Moreover, the effect of perpendicular GBs is reflected in the increasing derivative in fig. 4.12. The peaks (spikes) in the diffusion profiles are broadened (red curve in fig. 4.12), i.e. their contribution can be characterized by certain widths.

Table 4.2 The slopes and values of $D_{gb,app}$ calculated by fitting the diffusion profiles by straight lines for different d . The values of $D_{gb,app}$ should be compared with the value of $4.22 \text{ nm}^2/\text{s}$.

d, nm	Square grains		Parallel boundaries	
	-slope	$D_{gb,app}, \text{ nm}^2/\text{s}$	-slope	$D_{gb,app}, \text{ nm}^2/\text{s}$
10	0.0113	1.79	0.00713	3.85
25	0.01095	1.88	0.00714	3.84
50	0.0101	2.15	0.00715	3.83
100	0.00892	2.65	0.00716	3.82

a)



b)

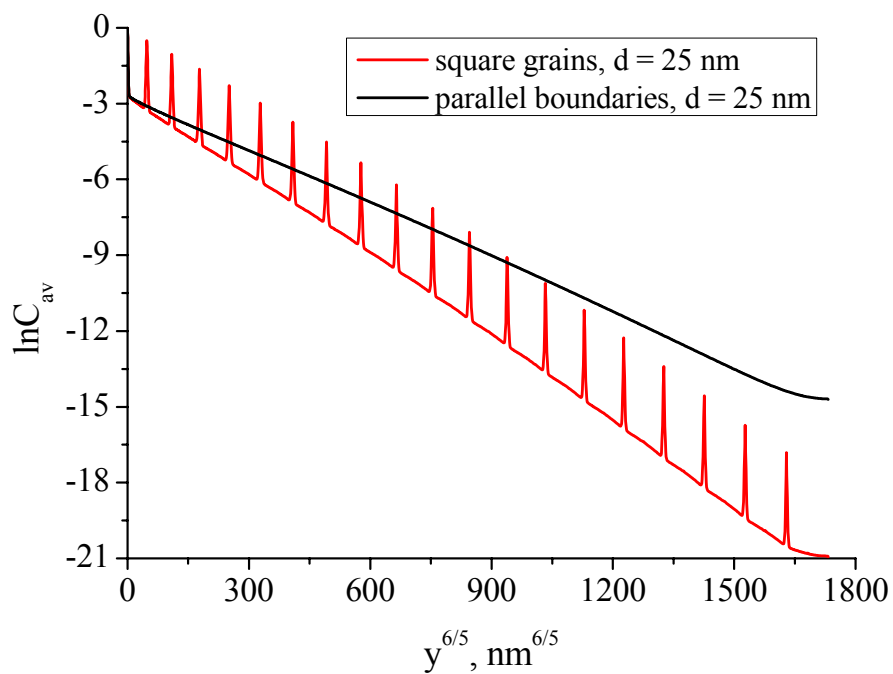


Fig. 4.10 Variation of $\ln C_{av}$ with $y^{6/5}$ calculated for two models with $d = 100$ nm a) and $d = 25$ nm b).

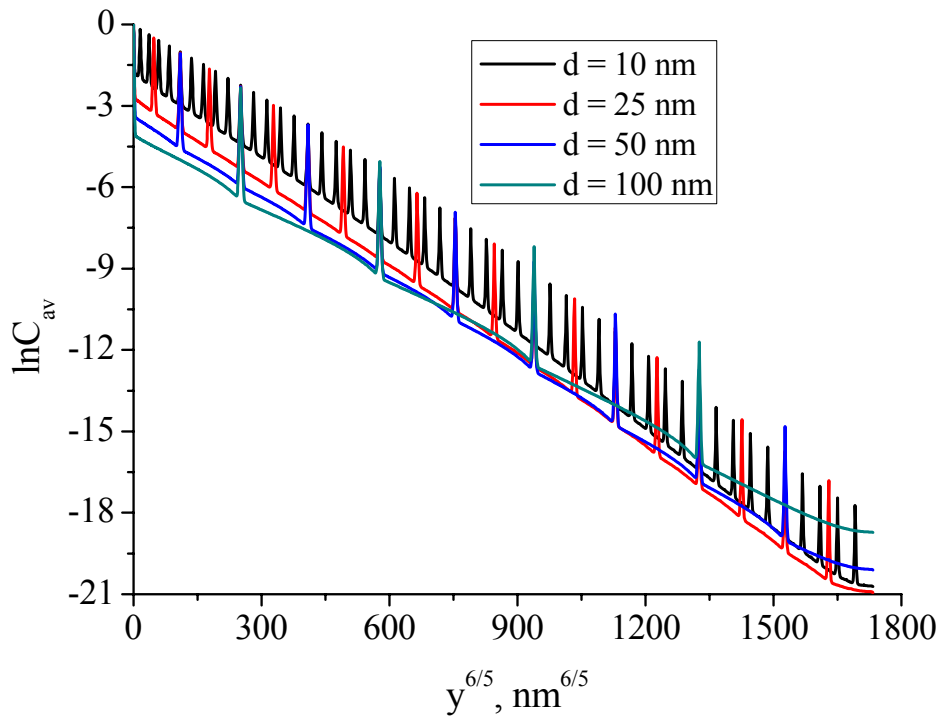


Fig. 4.11 A comparison of the diffusion profiles calculated for the model of square grains with different volume fractions of GBs.

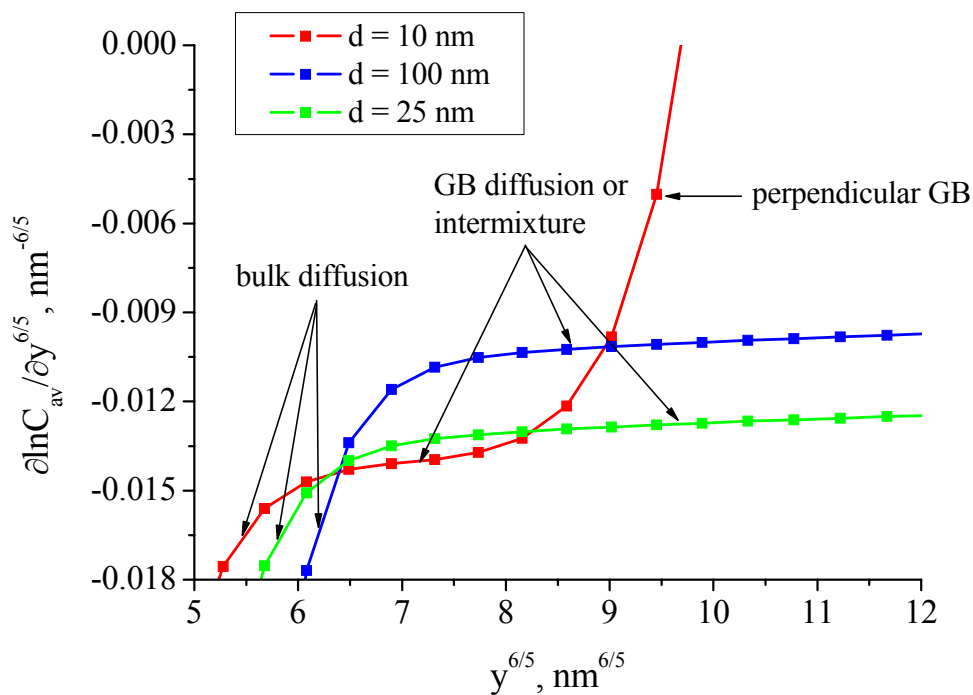


Fig. 4.12 A comparison of the derivatives $\partial \ln C_{av} / \partial y^{6/5}$ calculated for the model of square grains (only the first grain is taken into consideration) with $d = 10, 25$ and 100 nm.

A logical question arises when the model of square grains is used to simulate the diffusion profiles in a real microstructure, namely the question concerning different spatial orientation of GBs. The disadvantage of the model of square grains is that it comprises only perpendicular or parallel GBs. Can this model represent a realistic situation? In order to answer this question new models were proposed consisting of differently oriented GBs, i.e. GBs being not necessarily perpendicular to the diffusion direction. The models represent specific cases and may not exactly correspond to real polycrystals. However, the results obtained for these models give an important hint on the behavior of the diffusion process in realistic situations.

4.2.2 General geometrical models

4.2.2.1 Main characteristics of general geometrical models

Let us define the first general model (denoted here as general geometry 1) comprising a unit with 17 GBs (6 parallel boundaries and 11 all others) of different orientations and lengths. The length (depth) of that unit is 250 nm, while the width is 40 nm. The unit was reflected once with respect to $y = 250$ nm for simulating diffusion at different time scales. Finally, the geometry used to simulate diffusion was 40 nm in width and 500 nm in depth. The unit is presented in fig. 4.13a, where also the length of all GBs are shown which vary from 20.6 to 70 nm (= the longest parallel boundary). All parallel boundaries in this geometry are situated at $x = 0$ only. In this way the half of the real grains was realized, because the number of triangle elements in the mesh used is already about 710000. When creating the mesh, some grains were divided into rectangular and triangular parts (see a snapshot in window in fig. 4.13a) in order to have a mesh of high quality. The former always gives a mesh of the high quality, while the latter suffices from sharp angles between the boundaries. One can estimate that $d = 30.5$ nm in this geometry by summing the lengths of all boundaries and dividing the sum by the number of boundaries (see discussion below). The lengths of GBs being closer to the surface are about 25 nm. Diffusion was simulated at rather short t , not exceeding 13200 s for $\Delta = 2.2 \cdot 10^4$, and the results obtained can be compared to a real polycrystal having $d = 25$ nm, or a little bit larger. The angles between the GBs and the diffusion direction vary from 14° to 78.7° in the general geometry 1 except for the parallel boundaries having 0° . Varying GBs lengths and angles in a wide range allows the general geometry 1 to be adapted to a quite generalized situation.

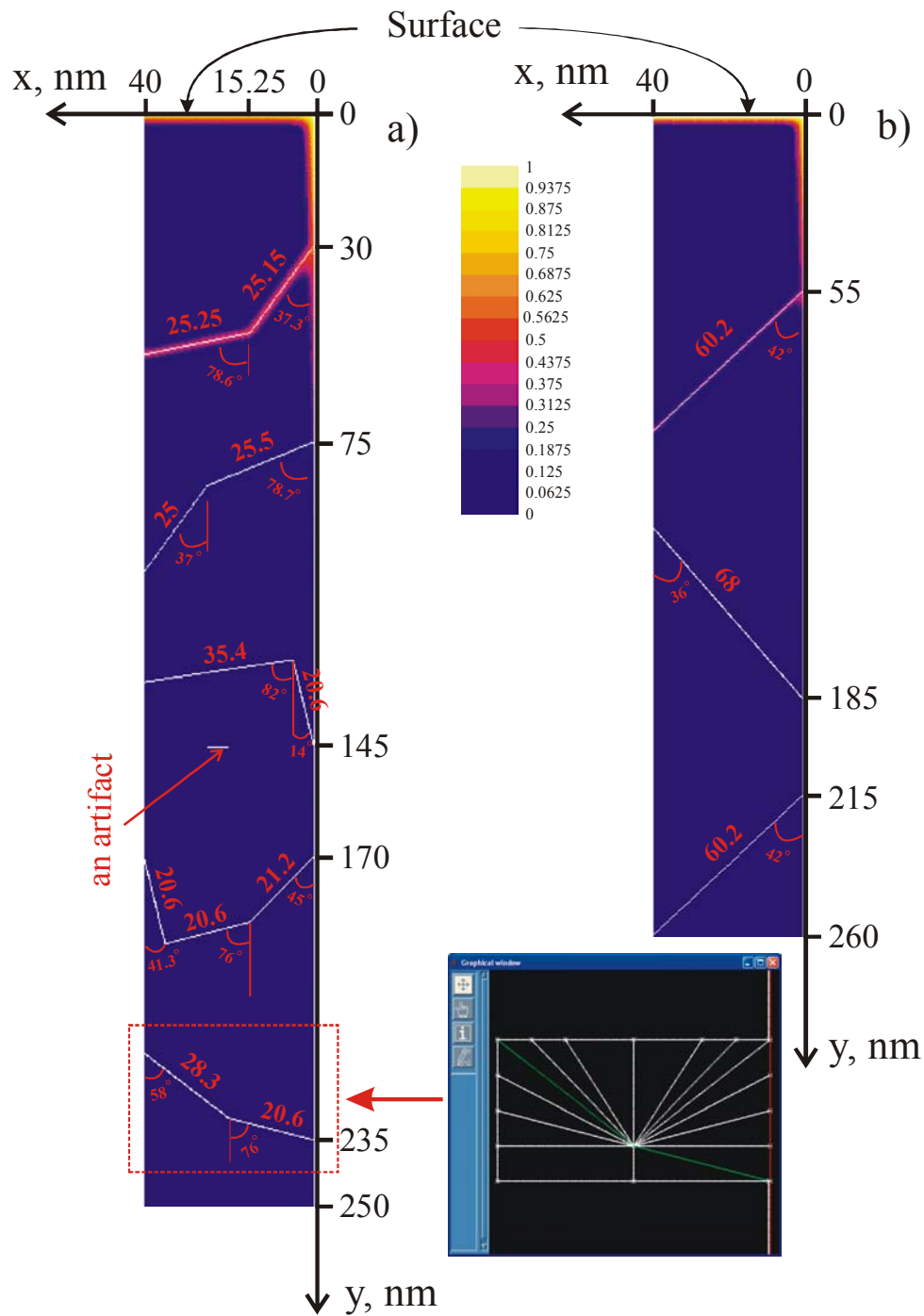


Fig. 4.13 Concentration distribution in the general geometry 1 (a) and general geometry 2 (b) at $t = 8200$ s for $\Delta = 2.2 \cdot 10^4$. The distribution is shown in colors, see explanation on the color pattern. White lines are GBs. In the window the fragment of the geometry drawn in the program SIMAIL [Sim95] is presented (red and green lines are GBs, white lines are additional lines used to make the quality of the mesh higher, i.e. the corresponding triangle and rectangular parts). Also the lengths of GBs in nm and their angles in degrees with respect to the diffusion direction are shown. An artifact means that in fact there is no GB at this place.

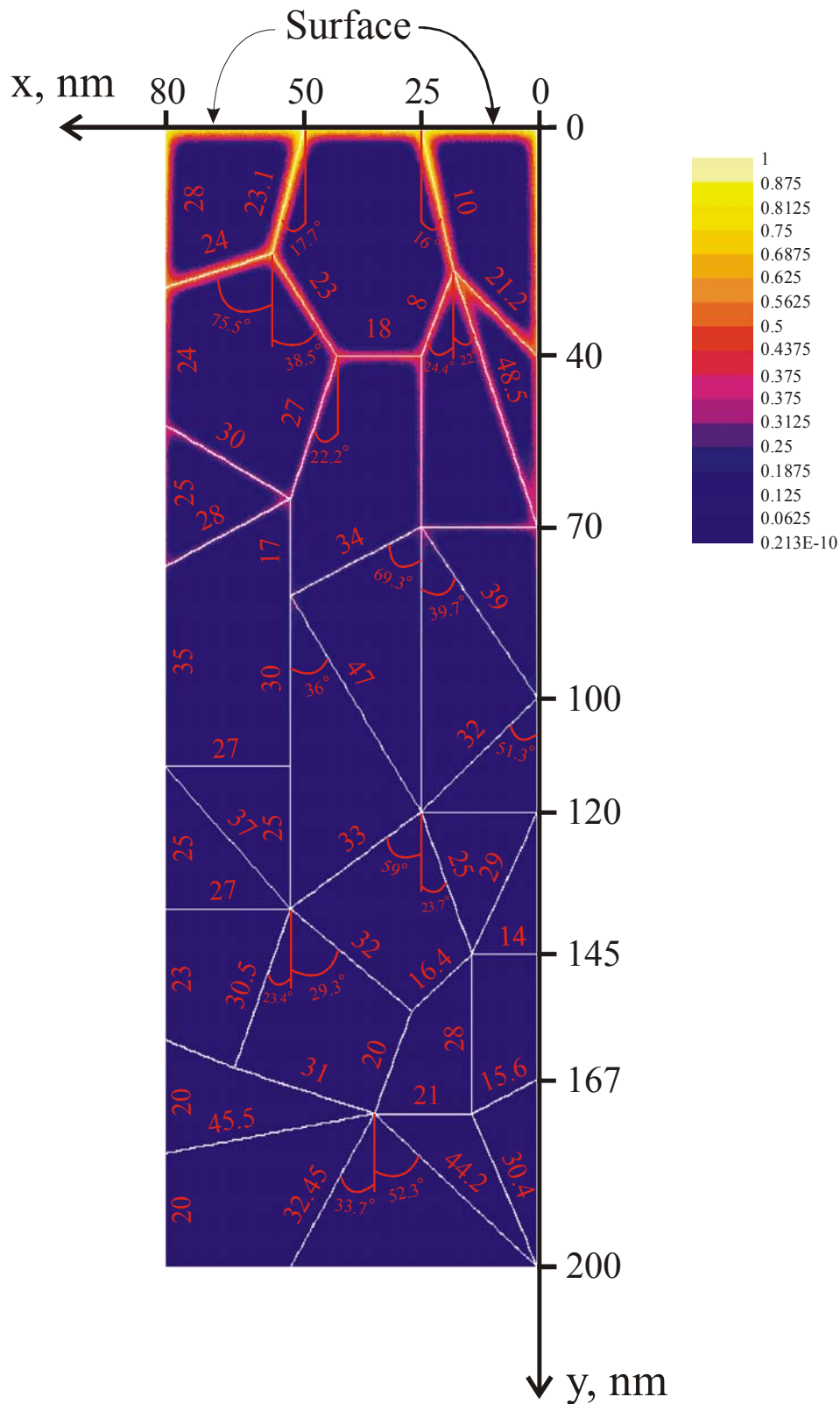


Fig. 4.14 Concentration distribution in the general geometry 3 at $t = 8200$ s for $\Delta = 2.2 \cdot 10^4$. The distribution is shown in colors, see explanation on the color pattern. White lines are GBs. The lengths of GBs are also shown. Only some angles with respect to the diffusion direction are indicated.

The general geometry 2 presented in fig. 4.13b is used for the same objective of analyzing the profile affected by different orientations of GBs. The unit is reflected at $y = 260$ nm. However, in this case $d = 64$ nm. The geometry is characterized by 4 parallel boundaries and 3 boundaries having the angles 42° and 36° to the diffusion direction.

One more general model (general geometry 3) was used with a larger number of grains and GBs in comparison with general geometries 1 and 2. The unit of this geometry is shown in fig. 4.14. The geometry consists of 57 GBs, including 21 parallel GBs. The lengths of GBs vary from 8 to 50 nm. The average grain size (d) was estimated to be 29.1 nm. So the results obtained for such a geometry should be comparable with those for $d = 25 - 30$ nm. As one can see, the geometry is twice as wide as for the general geometries 1 and 2. The problems of creating the mesh for this geometry become more serious than for the general geometries 1 and 2. Consequently, the number of triangle elements for this geometry is 355537 for the unit in fig. 4.14 and 710722 for the final geometry of the length 500 nm and of the width 160 nm. Using the general geometry 3, one should clarify the error introduced by the mesh of the smaller density. Advantage of this geometry is that the angles are very different, suggesting the contributions of very different boundaries. Additionally, some grains are very small, and these would be filled by diffusant in a very short t . This is a particular property of general geometry 3, which is important.

4.2.2.2 Simulation results obtained in the general geometrical models

All the geometrical models described so far were used to analyze the effects of GBs orientations. The lengths of the samples (geometrical models) were fixed to about 500 nm depending on the geometry, and the diffusion profiles were calculated at $t = 8200$ s for $\Delta = 2.2 \cdot 10^4$. The corresponding model of square grains exhibits 8 perpendicular GBs for $d = 60$ nm, if the GB at $y = 540$ nm (the length of the sample) is modeled as a reflecting boundary with the flux of atoms at this boundary being zero. As it was explained, the perpendicular boundaries lead to steeper diffusion profiles having spikes. That is why C_{av} was decreased in comparison with the model of parallel boundaries. However, the spikes themselves reflect increased concentrations around the perpendicular GBs. This effect is also confirmed in fig. 4.15, plotting the profile for square grains with $d = 60$ nm together with the profile calculated for the general geometry 2. The profile for the general geometry 2 has also the spikes slightly prolonged along the depth and, in principle; the profile is very close to that calculated for square grains. One GB in this model is oriented like having the angle with the parallel

boundary larger than 90° (the boundary of 68 nm in fig. 4.13b). It should be noted that the boundary gives a contribution to the profile with the angle 36° , because the concentration C_g is integrated along the x-direction varying y-coordinates from $y = 0$ nm to 520 nm. The difference of that boundary is reflected in the increasing concentration along the depth until its end is reached. The general geometry 1 has also several boundaries with the same effect. If the number of GBs is increased, this leads to further reduction of C_{av} , what increases the slope of the profile (black line in fig. 4.15, general geometry 1). Consequently, different slopes for general geometries 1 and 2 were observed despite the fixed t of 8200 s.

The profile calculated for the general geometry 1 could also be compared with that calculated for the square grains with $d = 30$ nm, because of similar grain size ($d = 30.5$ nm). The latter point is particularly important. As it is immediately seen in fig. 4.16, the profile for the general geometry 1 is characterized by the concentrations which are smaller than those for the square grains. This is related to the fact that the geometry under consideration has larger grain areas, which suggests reduced concentrations in the parts of the profiles close to the surface. Nevertheless, the slope of the profile for the general geometry 1 is slightly increased in comparison with the square grains of 30 nm. On the one hand, an increase of the slope is only possible, if the number of perpendicular GBs is larger. On the other hand, for the general geometry 1 the increase is related to the fact that the number of parallel boundaries in this geometry is smaller than the number of the others. The contribution of parallel boundaries exists but is not significant enough, i.e. mostly the other orientations affect the profile. Such situations are very difficult to predict, because the orientations can be different. Moreover, it is difficult to estimate d in such situations. Interestingly, d can also be estimated by taking the square root of the average grain area. According to this procedure, d was found to be about 40 nm for the general geometry 1. However, the larger grain size (in comparison with the square grains) would lead to a decrease of the slope.

Consequently, the slope of the concentration profile increases, if the number of parallel boundaries is smaller than all the others comparing these profiles with those for the square grains or when similar numbers of the two types of boundaries (parallel and perpendicular) comprise the geometry. Additionally, the profile for the general geometry 2 is not very much different from that for the square grains (fig. 4.15). In order to check this point further, the profile calculated for the general geometry 3 was analyzed, because this geometry comprises a large number of different GBs. In fig. 4.17 three profiles are compared, namely the profile for general geometry 1, the square grains with $d = 25$ nm and the general geometry 3. In the latter the number of GBs is by about a factor of 3 larger than in the general geometry

1. The number of parallel boundaries is extremely smaller than that of the others (there is no contribution of parallel diffusion paths at all). It is very significant, because the concentration once increased cannot be decreased sufficiently. This distinguishes the geometry from the general geometry 1. Additionally, some grains in the geometry are very small. These two facts cause some nonlinearity of the profile. Interestingly, the profile for the general geometry 3 is close to the profile for the model of square grains (both the profiles have d around 25 nm) and the slopes of those are believed to be similar. The decrease of the concentration at the coordinates close to the surface is similar in the two models. Because the model of square grains comprises the two extreme orientations, namely 0° and 90° with respect to the diffusion direction, it is supposed that the model of square grains is a good averaged representation of the real microcrystalline structure.

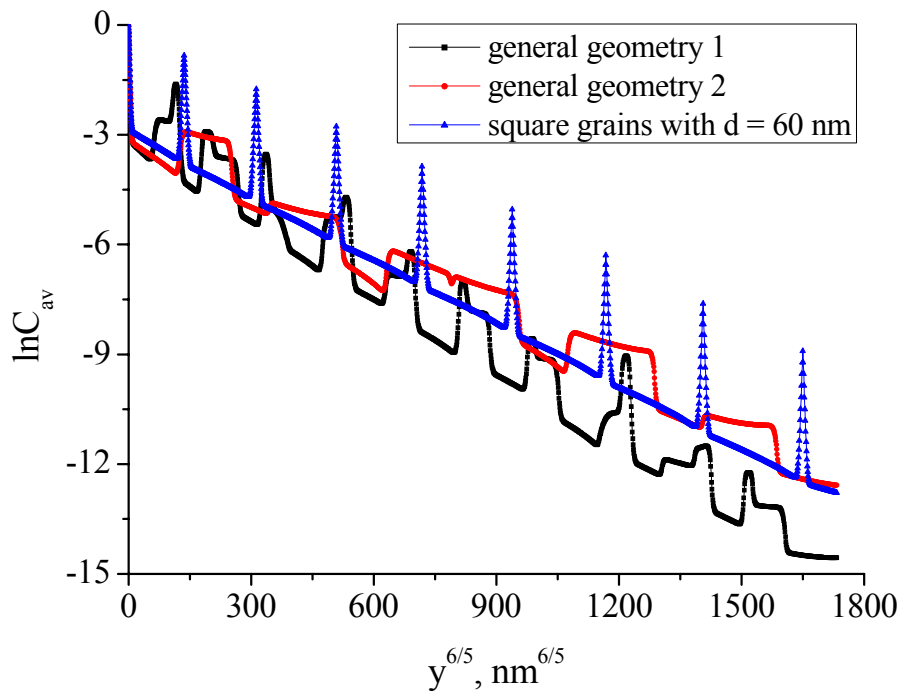


Fig. 4.15 A comparison of the diffusion profile of general geometry 2 with the profile of the model of square grains and general geometry 1. All the three profiles were calculated at $t = 8200$ s for $\Delta = 2.2 \cdot 10^4$.

The role of perpendicular boundaries is not the same at different t . It is, of course, related to the decreasing value of the parameter β (Eq. (1.9d)) with t . Thus, the parameter β yields information on the role of GBs orientations in the case of $L_{gb} \gg d$. Of course, small values of β allow the contributions of perpendicular boundaries to be excluded (see discussion

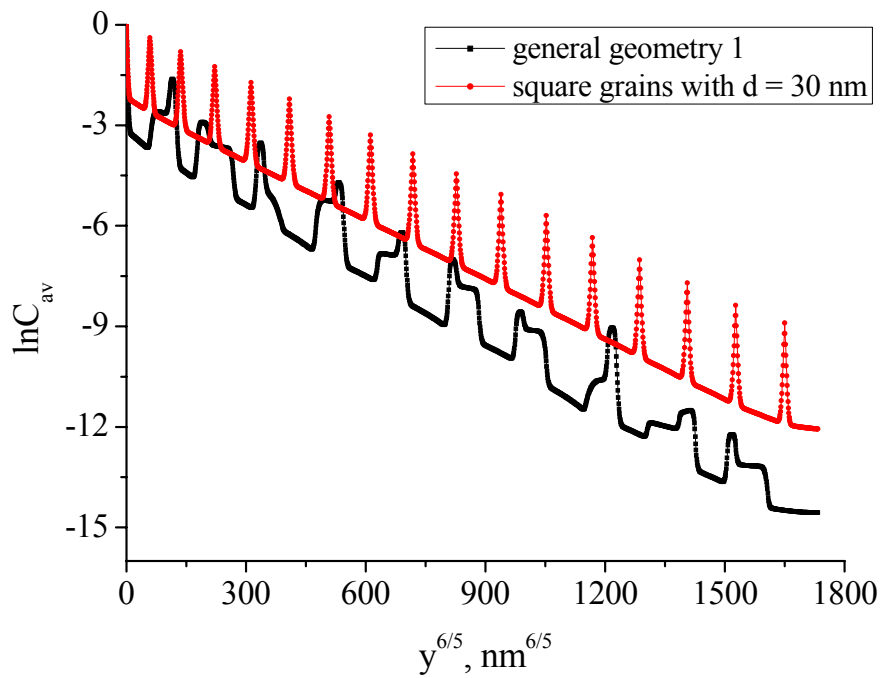


Fig. 4.16 A comparison of the diffusion profile of general geometry 1 with the profile of the model of square grains with $d = 30$ nm. All the profiles were calculated at $t = 8200$ s for $\Delta = 2.2 \cdot 10^4$.

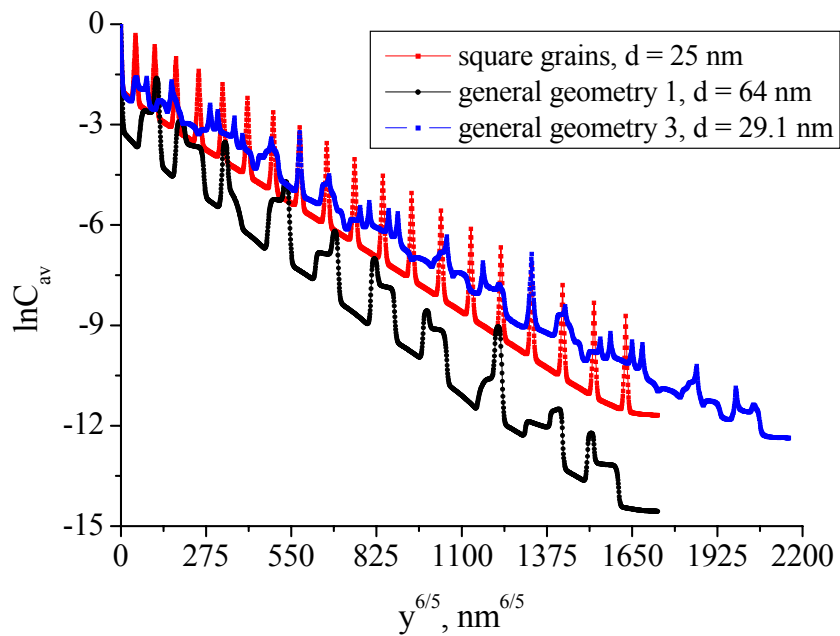


Fig. 4.17 A comparison of the diffusion profile of general geometry 3 with the profiles of the model of square grains with $d = 25$ nm and general geometry 1. All the three profiles were calculated at $t = 8200$ s for $\Delta = 2.2 \cdot 10^4$.

above). However, the A-regime starts when L_g is comparable with d , and in nanomaterials β remains high even when $L_g \approx d$. Nonetheless, the condition for starting the A-regime in nanomaterials is the same, and the contribution of perpendicular boundaries is negligible when $L_g \approx d$. This is confirmed by the result in fig. 4.18. The parameter β is around 182 at $t = 3 \cdot 10^6$ s and, for comparison, 3488 at $t = 8200$ s for $\Delta = 2.2 \cdot 10^4$. It is seen the two profiles for parallel boundaries and square grains coincide at long t . Below is given further analysis on the role of perpendicular boundaries.

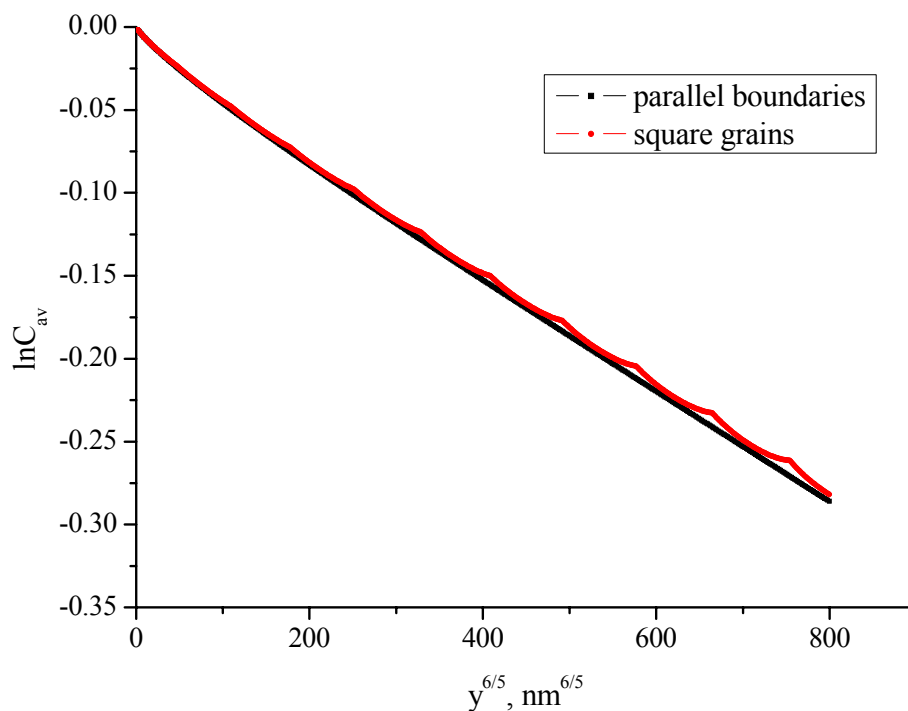


Fig. 4.18 A comparison of two profiles obtained for the model of square grains and the model of parallel boundaries at $t = 3 \cdot 10^6$ s for $\Delta = 2.2 \cdot 10^4$ ($d = 25$ nm, $L_g \approx 30$ nm). Parameters: $\beta = 182$, $\alpha = 0.17$.

4.2.3 A comparison of the model of parallel boundaries with the model of square grains under conditions of type-A kinetics

As the model of square grains is a good representation of a realistic microstructure, the results for this model can be compared to those obtained for the model of parallel boundaries in the A-regime. Such a comparison would allow one to better understand the role of different evaluation equations in terms of extracting D_{gb} from the diffusion profiles measured in the A-regime. The A-regime is particularly important for nanocrystalline materials due to small grain sizes. One may simply define the A-regime to be observed, if L_g exceeds d (no matter to

which extent), while L_{gb} can be larger (nanomaterials) or smaller than d (coarse-grained materials). According to Monte-Carlo simulations of Belova and Murch [Bel01], the A-regime is observed when $d/(2L_g) \leq 0.4$. The role of GBs orientations is not sufficient in the A-regime due to the result in fig. 4.18. In order to better clarify this point the diffusion profiles were calculated for both the model of parallel boundaries and square grains at high t . The different equations (Eqs. (1.17)-(1.18)) were used in order to compare $D_{gb,app}$ with the true one. On the one hand, analysis of the equations has been started recently by Belova and Murch [Bel03], [Bel04]. Also a very interesting mathematical analysis was performed by Mishin [Mis92c] in order to suggest the expression for the effective diffusivity (D_{eff}) in heterogeneous media. On the other hand, the problem of D_{eff} has a very strong analogy with those problems dealing with conductivity in heterogeneous media which are discussed, for example, in [Lan78], [Gar95], [Harte04], [Kab05]. Most of these contributions concern Maxwell's (Maxwell-Garnett's) equation (Eq. (1.18)). However, Hart's equation (or Hart-Mortlock's equation for studying diffusion with segregation) is still remaining the only equation used for determining D_{gb} in the A-regime. Up to now one cannot find any experimental paper on D_{gb} measurement where Maxwell's or similar equation is used. It should also be noted, that Kalnin *et al.* [Kal02] modified Maxwell-Garnett's equation for the problems of segregation. Consequently, there is the purpose here to compare all these equations. Segregation is also studied varying the segregation coefficient (s) from very small to very large values. This implies the possibility to analyze D_{eff} under these different conditions, i.e. different values of s and geometries.

4.2.3.1 Analyzing the boundary condition at the bottom

The problem of the reflecting boundary becomes particularly important when simulating diffusion by FEM in the A-regime for a semi-infinite sample. However, for finite systems, for example, thin films, the reflecting boundary is a necessary condition [Gil76]. It is reasonable to analyze the boundary effect in order to estimate possible errors in determining D_{gb} . The increased diffusion lengths, especially L_{gb} , lead to the increase of concentration at the bottom of the sample and, thus, the concentration profiles affected by the reflecting boundary.

In fig. 4.19 the derivatives are performed for different lengths of the sample (the model of parallel boundaries) at $t = 7 \cdot 10^5$ s. The result corresponds to the B-regime, because

of $d/(2L_g) \approx 0.87$ at that time for $\Delta = 2.2 \cdot 10^4$. As one can see, the length of 500 nm may not be used for the analysis in the B-regime at so a high t , because the effect of the reflecting boundary becomes very strong – the maximum of the derivative is suppressed by this influence. The maximum appears, if the length is increased to 3200 nm. Interestingly, Shewmon [She63] explained that for an accurate experimental determination of the diffusivity (D) the concentration should decrease at least by an order of magnitude, what means a minimum penetration $y \approx 3\sqrt{Dt}$ (D is the diffusivity of a solute and t has its usual meaning). The diffusion length L_{gb} of 279.46 nm for $\Delta = 2.2 \cdot 10^4$ at $t = 7 \cdot 10^5$ s is only about twice as small as the length 500 nm. One needs to increase the length of the sample to guarantee several diffusion lengths and to calculate the diffusion profiles at appropriate times by using the FEM. The concentration profiles were also calculated in the A-regime for different lengths of the sample (fig. 4.20). It could be expected, that the boundary effect, arising in the B-regime, can alter the profile sufficiently in the A-regime too. For the length 1000 nm (fig. 4.20) C_{av} is about 0.70 at the bottom of the sample, while it is about zero at $y = 3200$ nm. Table 4.3 comprises the calculated diffusion lengths in the A-regime (L_{eff}) and the values of C_{av} at the bottom of the sample of different lengths for ratios Δ from 10^2 to 10^5 at $t = 5 \cdot 10^6$ s. The value of C_{av} at the bottom reflects the minimum concentration in the sample ($C_{av,min}$) except the point at the GB. The diffusion length L_{eff} was calculated according to $\sqrt{D_{eff}t}$, where D_{eff} was found by using Hart's equation (Eq. (1.17a)). The following three lengths of the sample are compared in table 4.3: 500 nm, 1000 nm and 3200 nm. Depending on the ratio Δ , the length can be chosen very long to exclude the boundary effect, keeping in mind the cost issue of computational time. In order to find the most suitable length for a particular case of $\Delta = 2.2 \cdot 10^4$, the values of $D_{gb,app}$ were calculated. According to table 4.3, the concentrations of about 0.90, 0.70 or even 0.30 (the corresponding $D_{gb,app}$ is not shown in the table) at the bottom may not be used, leading to significant errors. For instance, D_{gb} is overestimated by a factor of 26 for the length 1000 nm, because L_{eff} is larger than 1000 nm for $\Delta = 2.2 \cdot 10^4$ at $t = 5 \cdot 10^6$ s. The length of the model should be 3-4 times larger to obtain a reasonable result. If the ratio Δ is small ($= 10^2$), the length may be surely 500 nm to find D_{gb} accurately. The value of $C_{av,min}$ for $\Delta = 10^2$ and the length of 500 nm is so small, that D_{gb} is very accurate (not shown in the table), providing an error less than 1%. In a sense, this analysis confirmed suggestions of Shewmon for the experiment. If the profile is affected by the boundary in the B-regime, what is very possible with L_{gb} being only twice smaller than the length of the sample, $D_{gb,app}$ can be extremely large. In the present study, t was increased up to $50 \cdot 10^6$ s!

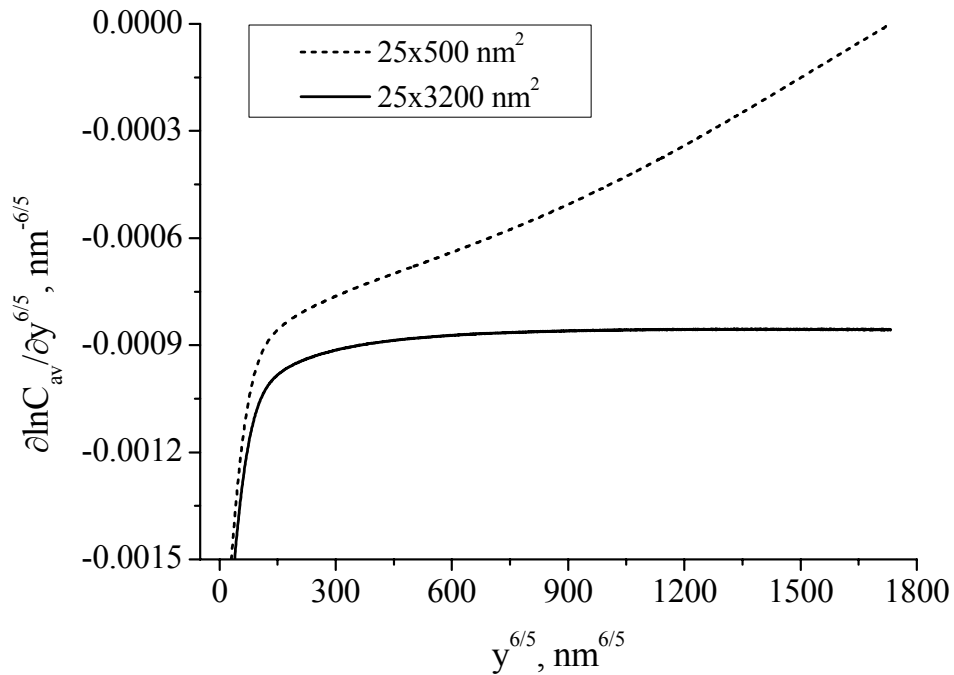


Fig. 4.19 Variation of the derivative $\partial \ln C_{av} / \partial y^{6/5}$ with $y^{6/5}$ calculated at $t = 7 \cdot 10^5$ s for $\Delta = 2.2 \cdot 10^4$ for the model of parallel boundaries of two lengths: a) 500 nm, b) 3200 nm.

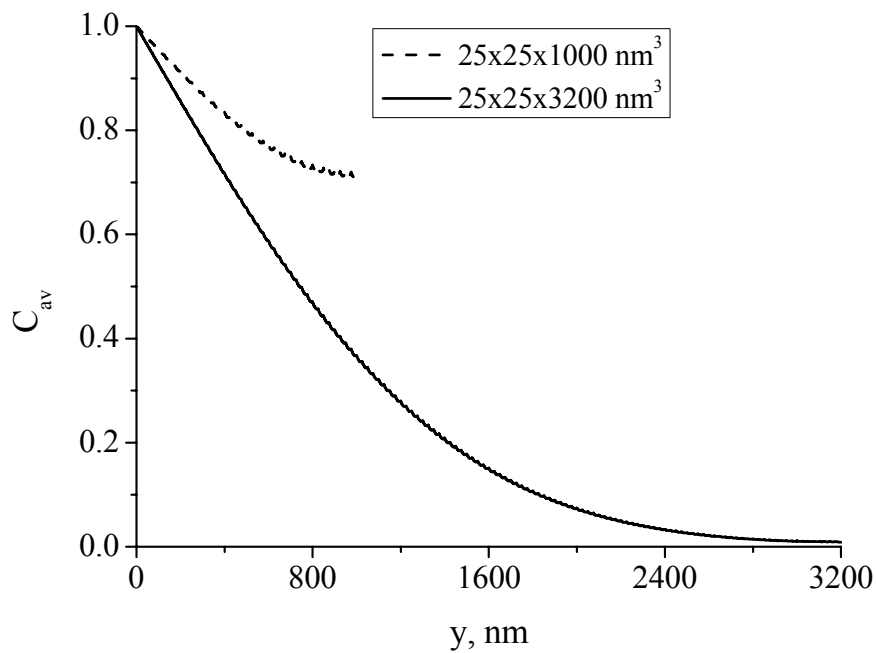


Fig. 4.20 Variation of C_{av} with y calculated at $t = 5 \cdot 10^6$ s for $\Delta = 2.2 \cdot 10^4$ for the model of square grains of two lengths: a) 1000 nm, b) 3200 nm.

For such high t much longer samples (geometries) are needed. Finally, the model of the length of 13000 nm was chosen as an appropriate one for different ratios Δ and t except $\Delta = 10^2$ for which the length was 1000 nm and 2000 nm for studying segregation effects (see discussion below).

Table 4.3 The minimum values of the average concentration ($C_{av,min}$) and diffusion lengths L_{eff} (Hart's equation, Eq. (1.17a)) calculated for different ratios of the diffusivities (Δ) and lengths of the sample (the model of square grains) at $t = 5 \cdot 10^6$ s. The average grain size (d) is assumed to be 25 nm. Also are presented the values of $D_{gb,app}$ calculated for $\Delta = 2.2 \cdot 10^4$ by using Hart's equation, i.e. these values should be compared with the true one of $6.42 \text{ nm}^2/\text{s}^*$.

Δ	$L_{eff}, \text{ nm}$	$C_{av, min}$			Type of material
		500 nm	1000 nm	3200 nm	
10^2	84	$4.68 \cdot 10^{-7}$	-	-	Coarse-grained
10^3	240	$8.05 \cdot 10^{-2}$	$1.81 \cdot 10^{-4}$	$2.45 \cdot 10^{-26}$	Fine-grained
$2.2 \cdot 10^4$	$1.11 \cdot 10^3$	$9.94 \cdot 10^{-1}$	$7.20 \cdot 10^{-1}$	$8.91 \cdot 10^{-3}$	Ultrafine-grained
10^5	2370	-	-	$3.47 \cdot 10^{-1}$	Ultrafine-grained
$D_{gb,app}, \text{ nm}^2/\text{s}$		$2.26 \cdot 10^4$	$2.61 \cdot 10^1$	6.31	

*The values of $D_{gb,app}$ were calculated by using an improved procedure, see discussion below.

4.2.3.2 Analyzing Hart's equation and Maxwell-Garnett's equation

The A-regime is characterized by the fact that both the Hart equation and the Maxwell-Garnett equation suppose the steady-state condition of diffusion to be fulfilled. The area under the diffusion profiles calculated by FEM varies as t increases (fig. 4.21). This would imply slightly different diffusivities, found by Hart's or Maxwell's (Maxwell-Garnett) equation. As it will be shown below the latter discrepancy is insufficient. Moreover, as t is $50 \cdot 10^6$ s, the variation becomes extremely slow. In the present study the concentration profiles were calculated at very long t for the model of square grains and parallel boundaries leading to the conditions very close to the steady-state. The overall process is called here a quasi-steady-state diffusion.

The diffusion time was varied from $2 \cdot 10^6$ s to $50 \cdot 10^6$ s. However, the value of $50 \cdot 10^6$ s corresponds to 19 months and would unlikely be realized experimentally. Clearly, large absolute values of t are related to the temperature, since the diffusivities used in the simulation were quite small as being taken at 500°C according to the Arrhenius dependences found in [Bro99a] for undoped ZrO_2 . Increasing the temperature would allow one to decrease t . Anyway, as the A-regime is concerned one can think of the interacting GBs in the sense that

the atoms move between different boundaries, and one can apply the corresponding equations for D_{eff} .

Calculating the values of D_{eff} as a function of t for different Δ , different kinetic regimes were covered as proposed by Mishin [Mis95], namely the A- and A'-regimes. Since the GB and grain contributions are not separated in the A-regime, and the overall diffusion process is described by single diffusion equation with D_{eff} , the diffusivity D_{eff} was found by fitting the concentration profiles with a complementary error-function solution to diffusion equation using the program MATLAB. In this program a special toolbox was used for the fitting, namely the Optimization toolbox [Mat03], [Mat06]. The default values of optimization parameters of the standard function of the Optimization toolbox "lsqcurvefit" based on the nonlinear least-squares method [Ger03] were used for fitting. For instance, the total number of iterations was 400, whereas the absolute and relative errors were fixed to 10^{-6} .

The models of square grains and parallel boundaries are compared in fig. 4.22 for different Δ , $t = 10 \cdot 10^6 - 50 \cdot 10^6$ s, fixed area fraction (2D geometry) of GBs (g) and fixed D_g . The larger ratio Δ yields increased values of D_{eff} . This can be understood by the fact, that D_{eff} is more determined by D_{gb} which is increased along the simulation for larger Δ . Moreover, increasing g (decreasing d) makes D_{eff} determined by D_{gb} only, as it is discussed in [Kau95]. In other words, the increase of D_{gb} leads to the same effects as the increase of g . The value of g was calculated as $S_{\text{gb}}/S_{\text{total}}$, where S_{gb} and S_{total} are the area given by GBs and the total area of 2D geometry (sample), respectively. Consequently, g for the model of square grains is twice as large as that for the model of parallel boundaries, if d is the same in both cases. For $d = 25$ nm g is about $1.96 \cdot 10^{-2}$ for the parallel boundaries and $3.84 \cdot 10^{-2}$ for the squares, if the length of the sample is 13000 nm. One has also to pay attention to the fact that D_{eff} is the same in the two models (fig. 4.22). It is related to the finding in fig. 4.18. According to these results, the role of perpendicular boundaries is negligible, if diffusion is studied in the type-A kinetics. Then it is interesting to compare the corresponding concentration distributions in order to clarify the latter point.

In fig. 4.23 a fragment of the concentration distribution in the model of parallel boundaries as well as in the model of square grains at $t = 3 \cdot 10^6$ s for $\Delta = 2.2 \cdot 10^4$ is shown in color. The concentration variation from 0.6 to 0.3 corresponds to a depth range from 475 nm to 800 nm. Because the difference between the two models increases along the depth y (the diffusion regimes change with the depth), this range of the concentration was chosen as the most interesting one for the analysis of the role of perpendicular boundaries. The distributions for the two models completely coincide at higher concentrations. Similar values of

concentration were obtained in both models at the same depths. This confirms the idea about the negligibility of perpendicular GBs in the A-regime. The distributions are only slightly different at the points of the concentration level change. For instance, the concentration 0.375 arises at $y \approx 730$ nm in the model of parallel boundaries, whereas it arises at $y \approx 755$ nm in the model of square grains. What one is eventually interested in is the value of a calculated apparent GB diffusivity ($D_{gb,app}$).

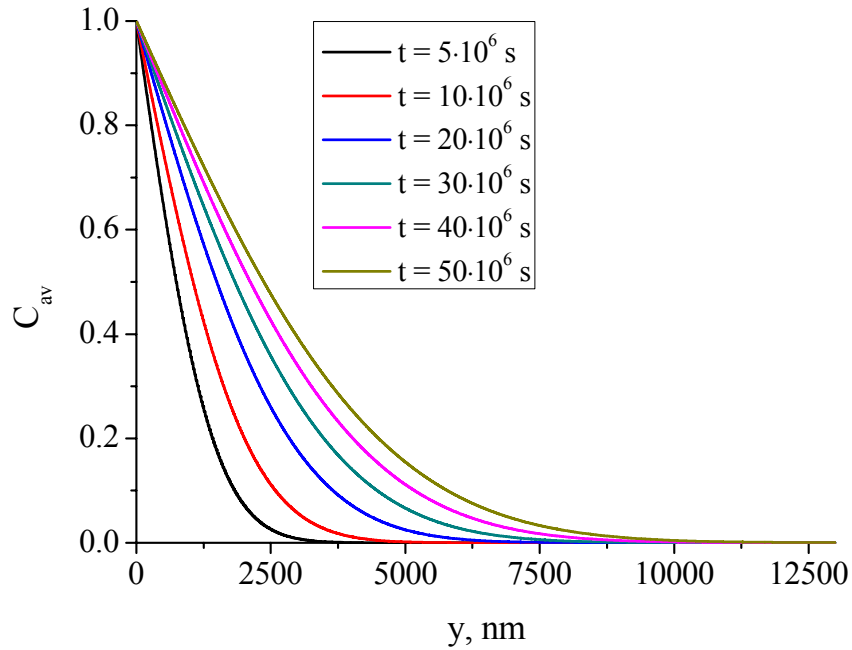
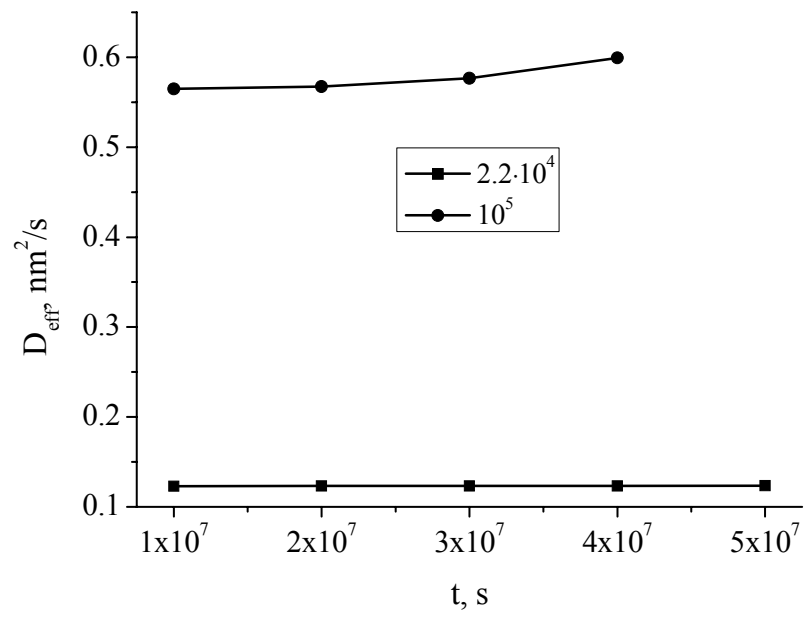


Fig. 4.21 Variation of C_{av} with y calculated at different t for $\Delta = 2.2 \cdot 10^4$ for the model of square grains.

Moreover, very recently Belova and Murch [Bel04] posed the question about the transition from the type-B kinetics to the type-A kinetics for the model of square grains. The answer to this question is given here due to the results in figs. 4.22 and 4.23: the condition for the transition in both the model of square grains and the model of parallel boundaries is the same (the condition $d/(2L_g) \leq 0.4$ was suggested by Belova and Murch for the model of parallel boundaries [Bel01]), since the role of perpendicular boundaries vanishes at high t . However, segregation of impurity atoms leads to another effect. In order to make a comparison of $D_{gb,app}$ with the true value, used in the simulation, for GB diffusion accompanied by segregation, two equations will be used: Hart's equation and Maxwell-Garnett's equation.

a)



b)

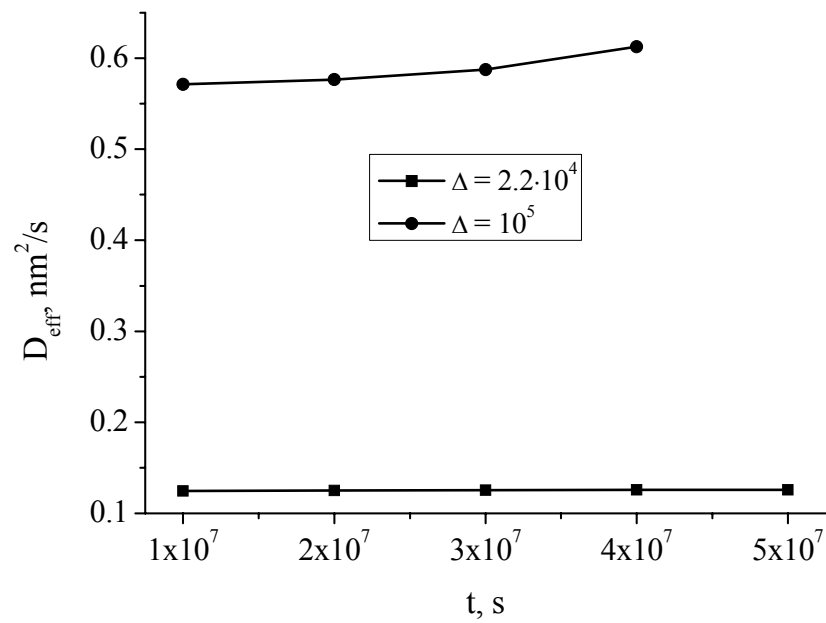


Fig. 4.22 Time evolution of D_{eff} for different ratios Δ : a) square grains, b) parallel boundaries.

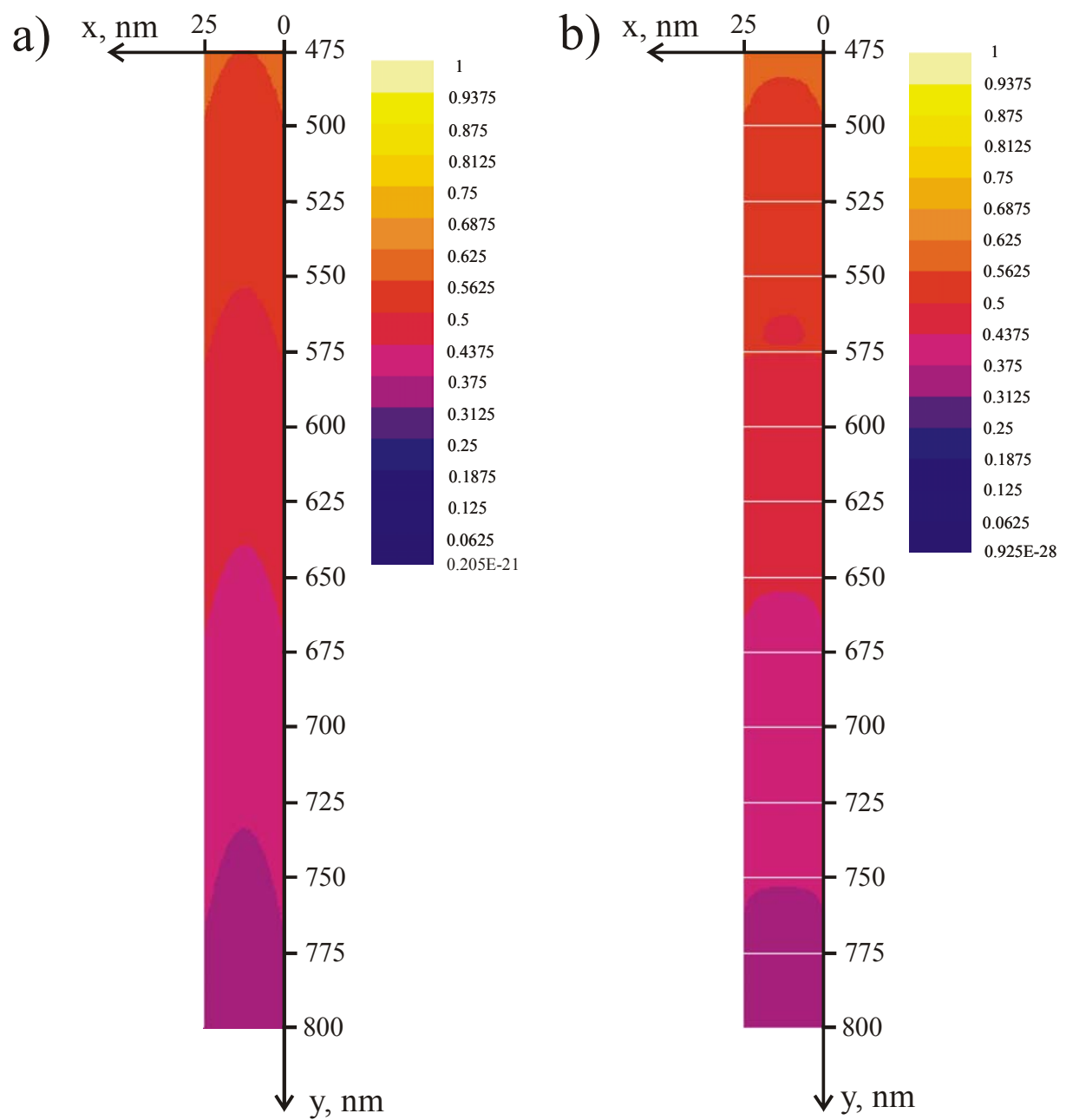


Fig. 4.23 A fragment of the concentration distribution at $t = 3 \cdot 10^6$ s: a) parallel boundaries, b) square grains. White lines represent to the perpendicular GBs with respect to the diffusion direction. The parallel boundaries in both distributions are at $x = 0.0$ and 25.0 nm. The corresponding color pattern is also shown.

4.2.3.3 Segregation effects under conditions of type-A kinetics

The Hart equation and its extended version for diffusion of impurities, known as Hart-Mortlock's equation (Eq. (1.17b)), is widely used to deduce D_{gb} , if the diffusion profile is measured under conditions of the kinetics of type-A. As Belova and Murch [Bel03] showed, the Hart-Mortlock equation leads to errors of deducing D_{gb} , when simulating diffusion in the model of square grains varying g and fixing the segregation factor (s). In the present work another important point is addressed, namely the influence of segregation. Very often s is obtained by measuring the triple product $s\delta D_{gb}$ in the B-regime, if D_{gb} is known from the measurements in the C-regime [Her03]. However, the measurements in the C-regime are not always possible. Then one could combine the measurements in the B- and A-regime. When knowing the product sD_{gb} from the measurements in the B-regime, the only unknown parameter in the Hart-Mortlock equation or the Maxwell-Garnett equation is s . Can the Hart-Mortlock equation provide reasonable values for s ? It is supposed that s can be used as the ratio of the corresponding concentrations in the GB and in the grain (Eq. (1.6b), very dilute conditions). The question of the validity of Hart-Mortlock's equation with respect to segregation has not been analyzed yet. Contrary, the Maxwell-Garnett equation was recently analyzed theoretically, extended to the problems of segregation and chemical diffusion [Kal02], [Jam06]. In the study of Belova and Murch [Bel03], it was proved that the Maxwell-Garnett equation gives smaller errors than Hart-Mortlock's equation varying g . Nevertheless, segregation imposes new conditions, i.e. suppresses the type-B kinetics. This is why it can be particularly interesting to analyze the equations under the conditions induced by the segregation.

Diffusion profiles were simulated in the model of parallel boundaries and in the model of square grains by using the modified Fisher system (Eq. (1.6c)). The average grain size (d) used in the simulation was fixed to 10 nm, whereas s was varied from 5 to 640. The value of $s = 640$ can be considered as a kind of maximum, because a further increase of s did not give a significant difference. However, larger values of s are also possible in different materials depending on temperature [Div01]. In fig. 4.24 the diffusion profiles calculated for varying s are depicted for fixed ratio $\Delta = 10^2$ and time $t = 10^6$ s. The length of the sample (geometry) was fixed to 2000 nm. The following property is reflected in fig. 4.24, the diffusion process with segregation is a nonlinear process going to some saturation, but never reaches it. In this sense, the situation is similar to the variation of t (fig. 4.21), i.e. the area under the curves varies with s .

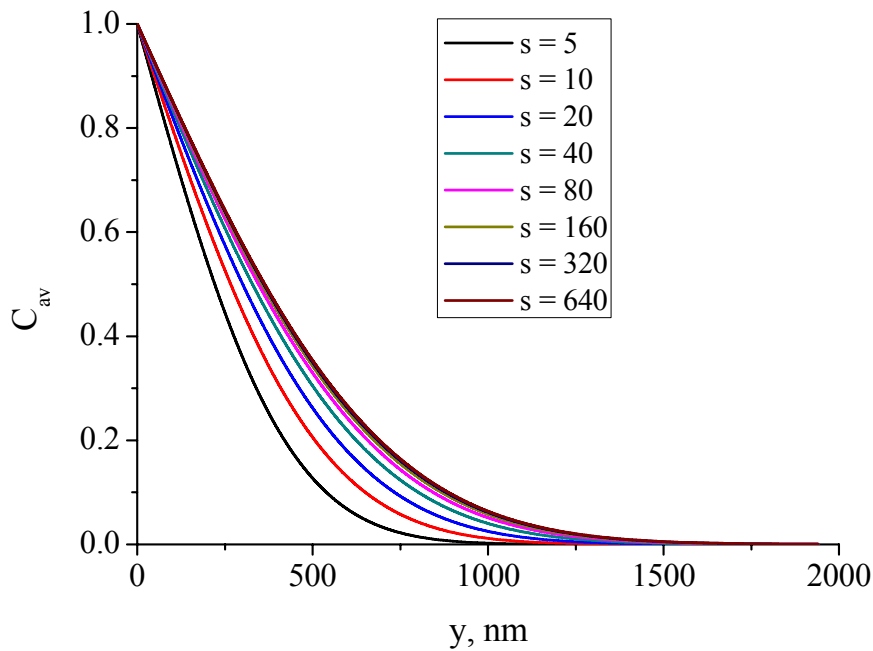


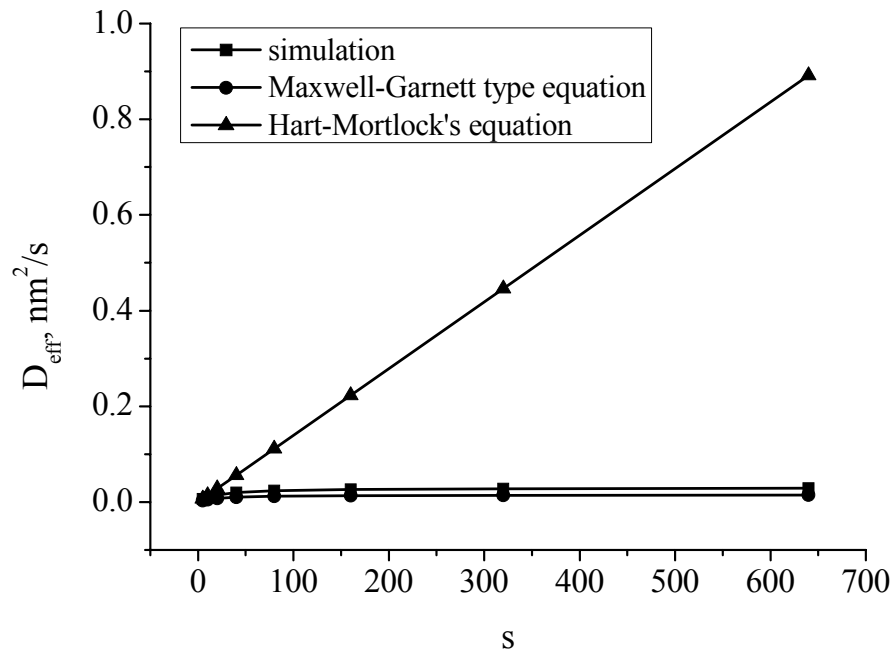
Fig. 4.24 Variation of C_{av} with y calculated for different segregation coefficients (s) for the model of square grains. The average grain size is 10 nm and $t = 10^6$ s.

Importantly, segregation suppresses the B-regime (Eqs. (1.10)-(1.11)) and gives larger values of L_{gb} (Eq. (1.12a)). Although, the rates of diffusion in the bulk are the same as in the case of diffusion without segregation. Segregation leads to larger values of β (Eq. (1.12b)) at the moment when the A-regime comes into play. This situation is similar to that for decreasing d . In both cases β can be very large even if $L_g \geq d$. It can be understood by the fact that segregation leads to an enhanced concentration within the GBs, because it restricts the contribution of GBs into the bulk (grain).

Following the procedure discussed in the preceding section, the diffusion profiles were fitted by a complementary error-function with the resulting D_{eff} being valid for a constant surface source as used in the simulation. Along with the fitting, the values of D_{eff} were estimated by using Hart-Mortlock's equation and Maxwell-Garnett's equation for each value of s . In fig. 4.25 the results of fitting are compared with those calculated by using the Hart-Mortlock and Maxwell-Garnett equations for the model of parallel boundaries as well as for the model of square grains. One can see the discrepancy that exists between the Hart-Mortlock equation and the simulation. The discrepancy increases with s , because the dependence of D_{eff} on s is linear in one case and nonlinear in another one. Contrary, Maxwell-Garnett's equation gives much more reasonable values for D_{eff} . This suggests that the linear

dependence supposed by the Hart-Mortlock equation is not valid even for the model of parallel boundaries when the Hart type equations are expected to be valid similarly to mixture rules [Nie78]. In fig. 4.26 the Maxwell-Garnett equation is compared separately with the simulation result. Interestingly, the deviation of Maxwell-Garnett's equation from the simulation is larger for the model of parallel boundaries. To estimate these deviations $D_{gb,app}$ was calculated by fitting the diffusion profiles by the complementary error-function with the Hart-Mortlock or Maxwell-Garnett type equations instead of a single D_{eff} , i.e. the fitting with respect to D_{gb} was done because all other parameters in the equations are known. The errors of determining D_{gb} were found from the fitting results and are summarized in table 4.4. The values of $D_{gb,app}$ are typically smaller than the true one ($D_{gb,true} = 2.95 \cdot 10^{-2} \text{ nm}^2/\text{s}$ or $2.95 \cdot 10^{-14} \text{ mm}^2/\text{s}$). Moreover, the errors vary with s in most cases. Very large errors were observed by using the Hart-Mortlock equation for the model of square grains, and smaller errors of applying this equation to the model of parallel boundaries were found for $s = 5-20$. However, the error increases up to $\sim 100\%$ for both the models applying the Hart-Mortlock equation, if $s = 640$. The Maxwell-Garnett type equation gives very small errors for the model of square grains. An error of 5% observed when this equation is applied to the model of square grains can have a numerical origin. Nevertheless, an error of 95% was observed for the model of parallel boundaries when using the Maxwell-Garnett type equation. Moreover, the Maxwell-Garnett type equation overestimates D_{gb} by a factor of 2, if applied to the model of parallel boundaries. By putting into Maxwell-Garnett's equation the value of g corresponding to the square grains and applying it again to the model of parallel boundaries, the error (improved $D_{gb,app}$ and error in table 4.4) was decreased to about 58% for $s = 40$. This was done according to the finding in the present work, that the diffusion profiles calculated for the model of parallel boundaries and the model of square grains are very similar at high t , i.e. in the A-regime in the case of self-diffusion (figs. 4.18 and 4.22). The decrease of the error indicates that the use of this equation requires g to be calculated for the model of square grains even if applied to the model of parallel boundaries. Similarly, the Hart type equation is supposed to be valid for the model of square grains if g is calculated as for the model of parallel boundaries. But this is valid only with $s = 1$. Segregation implies that the coincidence of the diffusion profiles for $s = 1$ does not longer exist in the case of $s > 1$. Accordingly, a significant error still remained for larger s even after using an appropriate g applying Maxwell-Garnett equation to the model of parallel boundaries. Additionally, there is a possible saturation of D_{eff} as a function of s . Therefore, at very large s the s -variation is close to steady-state with respect to that parameter.

a)



b)

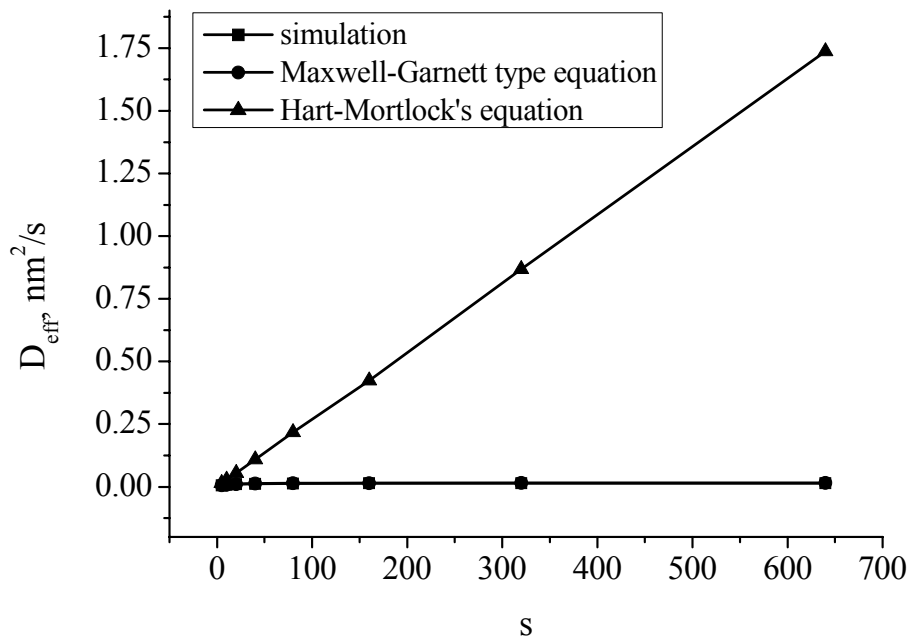
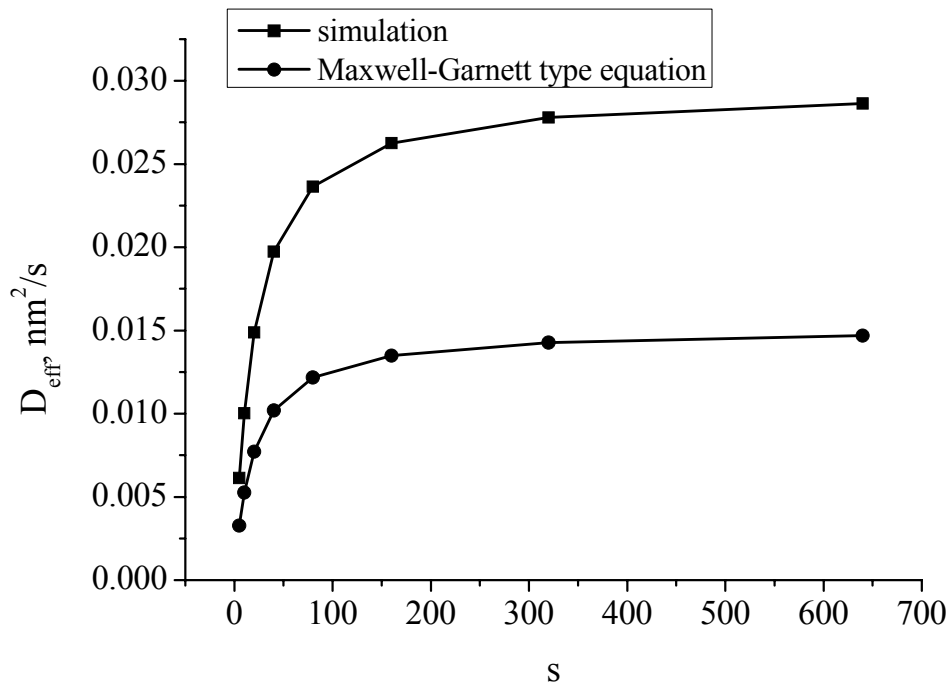


Fig. 4.25 Effective diffusivities obtained by fitting the simulated diffusion profiles to a complementary error-function for the model of parallel boundaries a) and the model of square grains b).

a)



b)

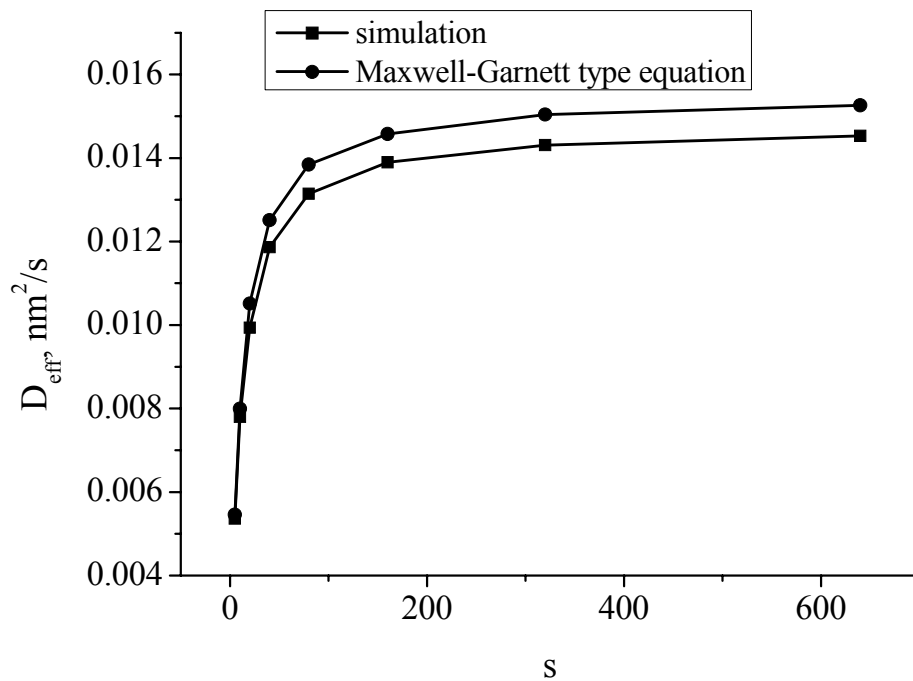


Fig. 4.26 A comparison of the simulation results with the Maxwell-Garnett type equation for the model of parallel boundaries a) and square grains b).

Table 4.4 The values of $D_{gb,app}$ and the errors of finding D_{gb} found from the simulated diffusion profiles by using the Maxwell-Garnett equation and the Hart-Mortlock equation for the model of parallel boundaries a) and the model of square grains b). $D_{gb,true} = 2.95 \cdot 10^{-2} \text{ nm}^2/\text{s}$.

a)

s	$D_{gb,app}$ due to Hart-Mortlock's eq., nm^2/s	Error in % due to Hart-Mortlock's eq.	$D_{gb,app}$ due to Maxwell-Garnett's eq., nm^2/s	Error in % due to Maxwell-Garnett's eq.	Improved $D_{gb,app}$ due to Maxwell-Garnett's eq., nm^2/s	Error in % due to improved Maxwell-Garnett's eq.
5	$2.48 \cdot 10^{-2}$	16	$5.74 \cdot 10^{-2}$	94	$3.33 \cdot 10^{-2}$	13
10	$2.07 \cdot 10^{-2}$	30	$5.75 \cdot 10^{-2}$	94	$3.72 \cdot 10^{-2}$	26
20	$1.56 \cdot 10^{-2}$	47	$5.75 \cdot 10^{-2}$	94	$4.20 \cdot 10^{-2}$	42
40	$1.05 \cdot 10^{-2}$	64	$5.75 \cdot 10^{-2}$	95	$4.67 \cdot 10^{-2}$	58
80	$6.42 \cdot 10^{-3}$	78	$5.75 \cdot 10^{-2}$	95	$5.05 \cdot 10^{-2}$	71
160	$3.70 \cdot 10^{-3}$	87	$5.76 \cdot 10^{-2}$	95	$5.31 \cdot 10^{-2}$	80
320	$2.10 \cdot 10^{-3}$	93	$5.76 \cdot 10^{-2}$	95	$5.46 \cdot 10^{-2}$	85
640	$1.23 \cdot 10^{-3}$	96	$5.76 \cdot 10^{-2}$	95	$5.54 \cdot 10^{-2}$	88

b)

s	$D_{gb,app}$ due to Hart-Mortlock's eq., nm^2/s	Error in % due to Hart-Mortlock's eq.	$D_{gb,app}$ due to Maxwell-Garnett's eq., nm^2/s	Error in % due to Maxwell-Garnett's eq.
5	$1.12 \cdot 10^{-2}$	62	$2.90 \cdot 10^{-2}$	2
10	$8.39 \cdot 10^{-3}$	72	$2.88 \cdot 10^{-2}$	2
20	$5.49 \cdot 10^{-3}$	81	$2.79 \cdot 10^{-2}$	5
40	$3.41 \cdot 10^{-3}$	88	$2.80 \cdot 10^{-2}$	5
80	$2.03 \cdot 10^{-3}$	93	$2.81 \cdot 10^{-2}$	5
160	$1.21 \cdot 10^{-3}$	96	$2.81 \cdot 10^{-2}$	5
320	$7.68 \cdot 10^{-4}$	97	$2.81 \cdot 10^{-2}$	5
640	$5.35 \cdot 10^{-4}$	98	$2.81 \cdot 10^{-2}$	5

Summary

The slope of the concentration profile ($\ln C_{av} = f(y^{6/5})$) increases as the average grain size decreases, and the grain boundaries orientations become important. Specifically, the ratio between the number of parallel and other diffusion paths is also very important in that sense. Accordingly, the slope also increases if the portion of parallel GBs is smaller than others. The increase of the slope suggests that D_{gb} can be underestimated when applying the conventional procedure, i.e. Le Claire's relation. Errors of the order of 50% are very possible (pure microstructure effect). The model of square grains, widely used in the literature, can represent an average microcrystalline structure, if the numbers of parallel and perpendicular diffusion paths are comparable. As the diffusion time grows, the role of perpendicular GBs vanishes, suggesting that the same criterion can be used for the transition from the B-regime to the A-regime for the models of square grains and parallel boundaries (for example, [Bel01]). In this case, the Hart-Mortlock equation is valid even for the model of square grains if the volume (area) fraction of GBs is calculated as for the model of parallel boundaries. However, segregation dictates new conditions for diffusion in polycrystalline materials. The diffusion profiles calculated for both models under these conditions differ, and the discrepancy increases with equilibrium segregation factors. The Maxwell-Garnett equation is not valid for the model of parallel boundaries, especially for large equilibrium segregation factors.

Chapter V. Space charge layer problems in grain boundary diffusion studies

Introduction

Space charge layer (SCL) effects are discussed in this chapter due to their importance in ionic and partly covalent materials. Unlike in materials where electrons are always available and fast, in ceramic systems there are typically two – oppositely charged – carriers the conductivity of which has to be taken into account [Duf86]. Because the individual defect formation energies differ, SCL arises and causes an electric potential difference between the surface, or GB, and the bulk interior [Leh53]. SCL affects considerably the properties of ionic materials and can in many cases be very significant [Mai95]. Despite this fact, conventional GB diffusion models typically neglect the space charge contribution. This seems to be due to two main reasons. First, the conventional models were applied historically to a large extent to metals, intermetallic compounds and alloys, in which the SCL does not exist. Preparation of ionic materials, like ceramic oxides, is much more complicated in comparison with metals and, that is why, diffusion data on these materials are still contradictory. However, nowadays one can find intensive literature on diffusion studies in oxides (for example, on diffusion in doped ZrO_2 : [Kil03a], [Kil03b], [Arg04], [Tay04], [Kil04], [Tay05], on diffusion in $\alpha\text{-Al}_2\text{O}_3$:

[Pro96a], [Pro96b], [Gal96], on diffusion in MgO: [Lib94], [Yoo02]). Second, it has been believed for a long time that the space charge contribution is negligible [Mis01], even at low temperatures. Indeed, the penetration profiles are treated by using Le Claire's relation for all the diffusion experiments based on penetration-depth profiles measurements without taking into account the SCLs at all. There are, however, intensive studies, e.g., in particular, on SrTiO₃, that show the drastic relevance of them as regard, transport [Leo99], [Gou01a].

There are several theoretical studies on discussion of the role of SCLs in diffusion studies. Yan *et al.* [Yan77] analyzed slightly enhanced diffusion near the boundaries, i.e. in the SCL, in doped and undoped KCl. Despite the fact, that this paper was not directly concerned the diffusion profiles measured by one of the appropriate techniques, Yan could suggest a model for diffusion analysis in ionic materials. Because of the SCL, the GB is to be considered as an inhomogeneous region, consisting of the GB core and the adjacent SCL. Accordingly, three diffusivities are used in Yan's model: in the bulk, SCL and GB core. The diffusivity within the SCL is suggested to be coordinate-dependent in Yan's model. Recently, Jamnik and Maier [Jam95], [Jam97a], [Jam01a] considered a similar model of the GBs in ionic materials. For this reason we distinguish here between the GB core and SCL. In this sense the GB core is the region which was supposed in the preceding chapters. The dependence of SCL diffusivity (D_{scl}) on coordinate was also taken into account in the derivations of Chung *et al.* [Chu00] on the basis of Gouy-Chapman model [Boc77]. The role of this dependence is discussed in this chapter on the basis of simulations by FEM and the program FLUX-EXPERT.

Contrary to the conclusion of Mishin and Gust on the importance of SCL [Mis01] (mostly based on the theoretical findings of Yan [Yan77]), Wang [WanR05] and De Souza [Sou05] took into account the SCL with the diffusivity different from that of the infinite bulk and surface, in order to analyze their experimental results properly. In both papers perovskite-like ABO₃ materials are concerned with SCL depleted of mobile charge carriers, *viz.* oxygen vacancies. Additionally, SrTiO₃ is recognized as a model electroceramic material with very different properties depending on experimental conditions [Sou03], [Mai04]. It could also be shown that SCLs can even overlap in nanocrystalline SrTiO₃ – the effect that we neglect in the following [Bal06]. Another important example of depleted SCL refers to ZrO₂. Here it can be mentioned that not only depth-profile measurements but also conductivity measurements provide important information on transport properties of ionic materials [Hei03]. By means of impedance spectroscopy Gou *et al.* [Gou01b], [Gou02] demonstrated the GB resistivity which was two to three orders of magnitude higher than in the bulk in yttria-doped ZrO₂ at low

temperatures. The effect was attributed to space charges and the results were successfully explained by the Mott-Schottky model [Mot39], [Scho39]. The blocking space charge effects were also observed in another fluorite structure material, namely doped nanocrystalline CeO₂ [Kim02]. The perpendicular GBs in this material lead to an additional semi-circle in the impedance spectra. The impact of those boundaries on impedance has already been discussed by Maier [Mai86]. Despite these facts, nobody has revealed the importance of SCLs adjacent to the GB cores studying oxygen in-diffusion in ZrO₂. In the following papers [Bro99b], [Knö03] on oxygen diffusion in doped and undoped nanocrystalline ZrO₂ the SCLs are completely ignored. Moreover, there are contradictions in the literature on the behavior of transport properties measured by impedance spectroscopy and depth-profiling methods [Man97], [Bro04]. Consequently, it is the purpose here to discuss the impact of SCL on diffusion in ionic materials in terms of conventional GB diffusion models.

As we are interested in fast GB transport we will focus on depletion layers between which the fast diffusing core is embedded. For simplicity's sake we again ignore the profiles within the GB core and characterize the SCL by a laterally constant effective transport coefficient. Also effects caused by electrical fields as discussed by Jamnik and Maier [Jam97b], [Jam01b] and Schmalzried *et al.* [Schm98] are neglected.

5.1 Mathematical model to describe diffusion in a polycrystal including space charge layers

Mathematically diffusion in polycrystalline materials can be described by means of differential equations, if both diffusion in the bulk and GBs obey Fick's law as it was explained in chapter I. The assumptions of an infinitely thin GB and a steplike change of the diffusion coefficient can be used for the SCL problem as well, leading to a system of three differential equations. The diffusivities are taken as time and concentration independent. The 2D case of this model suggests the following equations with C_g , C_{gb} and C_{scl} being the grain, GB and SCL concentrations, respectively

$$\begin{cases} \frac{\partial C_g(x, y, t)}{\partial t} = D_g \left(\frac{\partial^2 C_g(x, y, t)}{\partial x^2} + \frac{\partial^2 C_g(x, y, t)}{\partial y^2} \right) \\ \frac{\partial C_{scl}(x, y, t)}{\partial t} = D_{scl} \left(\frac{\partial^2 C_{scl}(x, y, t)}{\partial x^2} + \frac{\partial^2 C_{scl}(x, y, t)}{\partial y^2} \right) \\ \frac{\partial C_{gb}(y, t)}{\partial t} = D_{gb} \frac{\partial^2 C_{gb}(y, t)}{\partial y^2} + \frac{2D_{scl}}{\delta} \frac{\partial C_g(x, y, t)}{\partial x} \Big|_{|x|=\frac{\delta}{2}} \end{cases} \quad (5.1)$$

As usual the relevant equation in the grain is Fick's second law. The same is true for SCL as long as we ignore inhomogeneity effects and effects due to charge separation. For the GB we have to take the same form as in the Fisher system (Eq. (1.6a)). The main difference of this new model and the Fisher system is in fact, that the leakage of atoms exists from the GB to SCL. The term which controls this leakage is characterized by D_{scl} . Again, the problem is symmetrical with respect to $x = 0$. The relevant mathematical model corresponds to the geometrical model depicted in fig. 5.1. The thickness of SCL is denoted as δ_{scl} and is fixed to 1 nm along the calculations. The effective thickness δ_{scl} was employed in many theoretical considerations on space charges, leading to an abrupt variation of diffusion coefficients. However, there are contradictions in the literature with respect to this property. For example, in ZrO_2 δ_{scl} varies from 0.35 to 3 nm [Dij81], [Aok96]. Here the value was chosen as being the average of this range as well as from the point of view of numerical conveniences.

As before, the boundary conditions at the surface reflect a constant source and sufficiently fast surface reaction with zero initial concentration at $y > 0$:

$$\begin{cases} C_g(x, y, t) = C_{gb}(x, y, t) = 1 & \text{at } y = 0 \\ C_g(x, y, t) = C_{gb}(x, y, t) = 0 & \text{at } t = 0, y > 0 \end{cases} \quad (5.2a)$$

The continuity conditions and mass balance were used at interfaces: between GB and SCL, SCL and grain. Correspondingly, equal fluxes and concentrations were applied:

$$\begin{cases} C_{scl}(x, y, t) = C_{gb}(x, y, t) \\ J_{scl}(x, y, t) = J_{gb}(x, y, t) \end{cases}, \quad \text{if } |x| = \delta/2 \quad (5.2b)$$

and

$$\begin{cases} C_{\text{scl}}(x, y, t) = C_{\text{g}}(x, y, t) \\ J_{\text{scl}}(x, y, t) = J_{\text{g}}(x, y, t) \end{cases}, \quad \text{if } |x| = \frac{\delta}{2} + \delta_{\text{scl}}. \quad (5.2c)$$

Correspondingly, the equation describing diffusion along the GB core in Eq. (5.1) takes account of the relevant conditions at the interface between the GB and SCL (Eq. (5.2b)). The unity in Eq. (5.2a) means that the concentration is normalized with respect to the concentration at the surface. In the present study regarding the SCL problems the GB, or GB core is always assumed to represent a structurally disturbed region, i.e. we refer to the misorientation of grains. The question of the SCL to be the part of the GB or the bulk is not discussed here as it does not play a role given the above assumption. The system was numerically integrated with the flux boundary condition at the bottom of the sample used in the calculation is equal to zero (fig. 5.1). The role of this boundary condition was analyzed in the manner as discussed in chapter IV and estimated to be negligible, suggesting the obtained results correspond to the semi-infinite systems (see discussion below) and partly thin films in the sense that only the maximum of the derivative $\partial \ln C_{\text{av}} / \partial y^{6/5}$ determines D_{gb} . Importantly, all the conclusions made in chapter III are important for the SCL problems too.

The system of equations (Eq. (5.1)) was solved using FEM (FLUX-EXPERT, Simulog, France) as described in chapter II. Different kinetic regimes for different ratios of diffusivities Δ are covered, and different GB networks (parallel boundaries and square grains) are considered. In all the cases the calculated concentration distribution was numerically integrated parallel to the surface providing the average concentration (C_{av}). From the resulting concentration profiles D_{gb} values were deduced by using the conventional equations in order to compare them with the exact value (used in the simulation) and to estimate the error. In the calculations D_{g} and δ were fixed to $2.95 \cdot 10^{-4} \text{ nm}^2/\text{s}$ ($2.95 \cdot 10^{-16} \text{ mm}^2/\text{s}$) and 0.5 nm, respectively, whereas D_{gb} and D_{scl} were varied in order to have different ratios with respect to D_{g} . Accordingly, the ratio $\Lambda = D_{\text{g}}/D_{\text{scl}}$ was introduced for convenience.

5.2 Accuracy of the simulated diffusion profiles and effect of coordinate-dependent space charge layer diffusivity

5.2.1 The finite element mesh and diffusion barrier at the bottom of the geometrical model

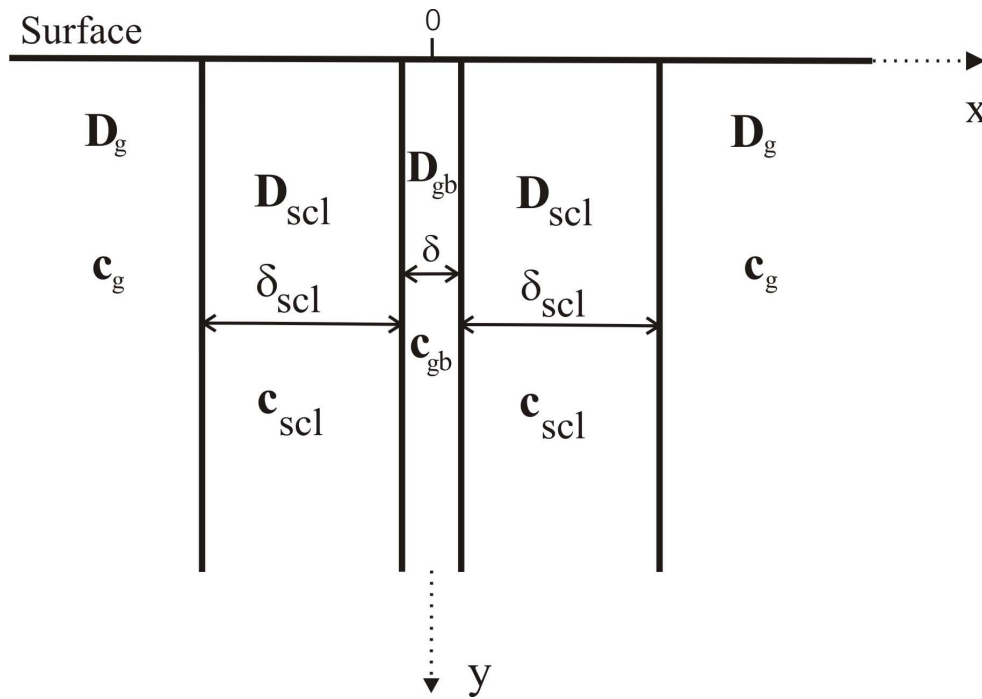


Fig. 5.1 Schematic representation of the geometrical model used for calculation including space charges.

The choice of an appropriate mesh for SCL diffusion problems is very critical due to the fact that D_{scl} differs from D_g . Different meshes (or, in other words, meshes of different densities) were tried, in order to find the most suitable one. Major emphasis was laid on optimizing the mesh in the SCL, because the problems of interest involve extremely small diffusivities in this region (blocking space charge effects). In fig. 5.2 a fragment of the mesh used for SCL diffusion is depicted. One can see a great difference between the densities of the mesh in the bulk and SCL. Such a mesh allows one to simulate diffusion in the type-B kinetics at very short t . The mesh in the SCL is homogenous as in the bulk, while close to the SCL the bulk mesh was inhomogeneous and adapted to the SCL-bulk transition. As a result, the number of triangle elements of the mesh in the SCL is about 87% of a whole number of the elements in the geometrical model (sample). However, the length of the sample was only 100 nm for simulating diffusion in the B-regime. Further increasing the mesh density did not allow D_{scl} to be more decreased, because the finite element problem with the higher density could not be solved even if the length of the sample was decreased. Consequently, the smallest value of D_{scl} used in the present study was $2.95 \cdot 10^{-7} \text{ nm}^2/\text{s}$ ($2.95 \cdot 10^{-19} \text{ mm}^2/\text{s}$), and, for comparison, $D_{gb} = 2.95 \cdot 10^{-2} \text{ nm}^2/\text{s}$ ($2.95 \cdot 10^{-14} \text{ mm}^2/\text{s}$). The interval between the nearest points of the mesh is about 0.03 nm and 0.5 nm in the SCL and bulk, respectively.

The mesh was also optimized for studying diffusion in the A-regime. The corresponding analysis will be given below.

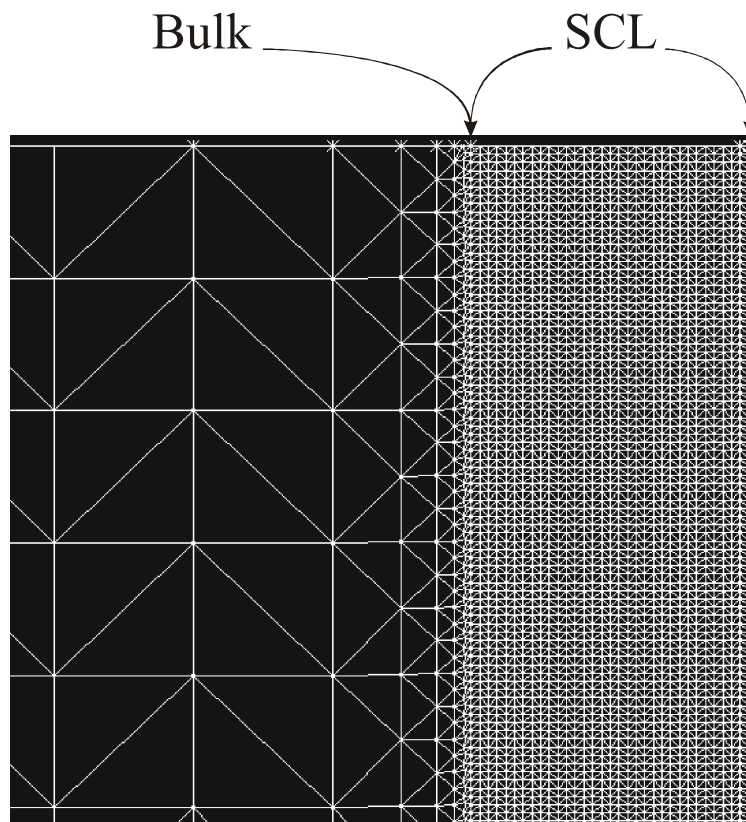


Fig. 5.2 A fragment of the mesh used to simulate diffusion in the B-regime ($\delta_{\text{scl}} = 1 \text{ nm}$). The red line represents the GB.

In order to prove that the obtained mesh is suitable for a diffusion study with various D_{scl} , the diffusion profile was calculated for the test case $D_{\text{scl}} = D_{\text{g}}$. This should give the same profile as obtained with mesh 1 described in chapter IV. The gradients of the corresponding profiles are compared in fig. 5.3. Obviously, there is a discrepancy between these profiles which increases along the depth indicating that the mesh density is not optimal, especially in the GB part. However, the gradients coincide at the maximum where the main interest of the present analysis lies.

Furthermore, it has to be noticed again that we are interested in small D_{scl} -values. The mesh shown in fig. 5.2 was also examined with respect to such small values. The diffusion profile was calculated for the sample comprised the SCL only in order to check the quality of the mesh. This means the bulk diffusion was simulated with the smallest D_{scl} . The corresponding diffusion profile is shown in fig. 5.4 and compared with the complementary error-function solution to diffusion equation. These profiles mostly coincide. This allowed us

to conclude that the relevant SCL mesh suffices for our purposes despite the deviations observed in fig. 5.3.

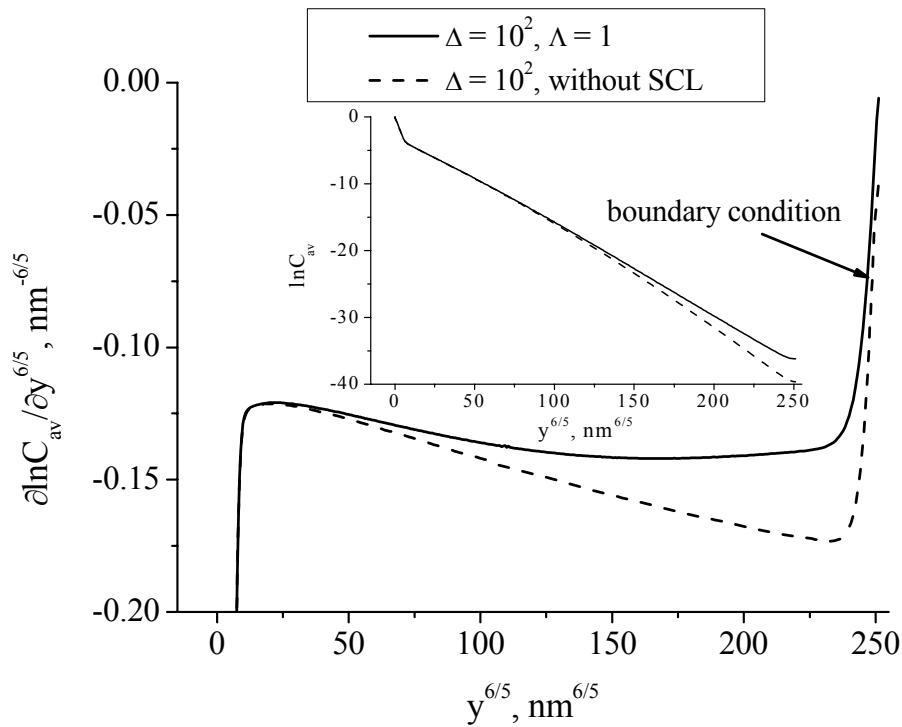


Fig. 5.3 A comparison of the mesh used for taking into account space charge effects with the mesh without the SCL having the same mesh density as for mesh 1 described in chapter IV. The profiles were calculated for the length of 100 nm at $t = 4700$ s. Also the $\ln C_{av} = f(y^{6/5})$ dependence is shown in inset.

Contrary to all the diffusion problems discussed so far, the meshes used for the SCL problems for simulation in the diffusion regimes of type-A and -B are very different. This is caused by extremely small diffusion lengths in the SCL under conditions of type-B kinetics. Two meshes were used to simulate the diffusion profiles in the A-regime. One mesh corresponds to simulations with $D_{scl} = 2.95 \cdot 10^{-7} \text{ nm}^2/\text{s}$ and another one to values $D_{scl} = 2.95 \cdot 10^{-5} \text{ nm}^2/\text{s}$ or larger. These meshes will also be analyzed with respect to the accuracy of the obtained results. In fig. 5.5 the diffusion profiles for the two values of D_{scl} are compared with the corresponding complementary error-function solutions. These calculations refer to SCL diffusion only as in fig. 5.3. The accuracy of the profile calculations is obvious, suggesting that these meshes can be used for simulating diffusion at long t . Interestingly, the density of the mesh in the SCL is 0.0625 and 0.125 for smaller and larger diffusivity, respectively. It is only double as large in the one case and four times larger in the other case

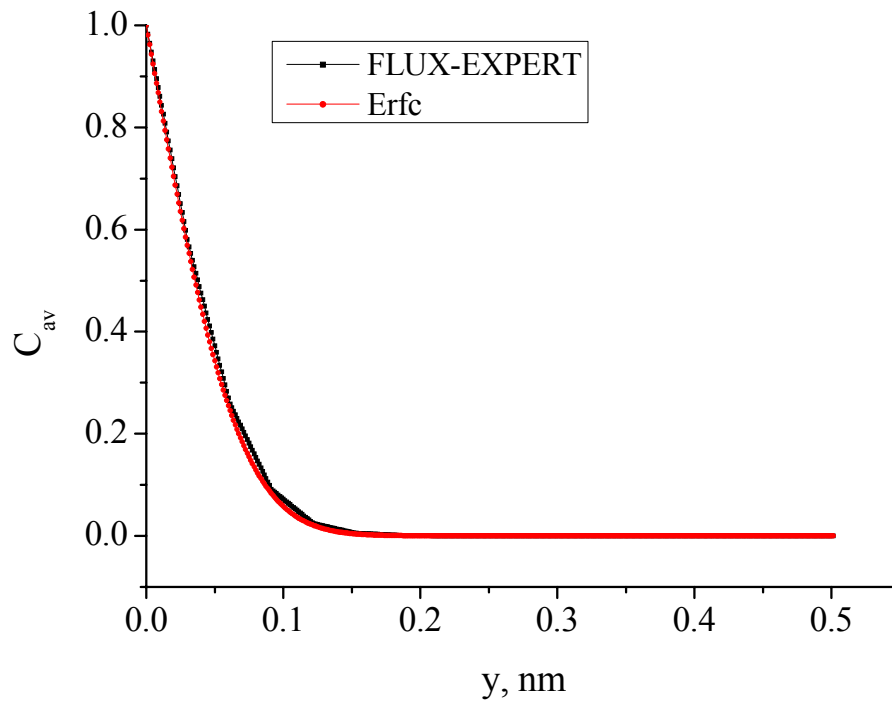


Fig. 5.4 A comparison of the bulk diffusion profiles obtained for $D_{\text{bulk}} = 2.95 \cdot 10^{-7} \text{ nm}^2/\text{s}$, representing D_{scl} , with the exact analytical solution to diffusion equation given by a complementary error-function (Erfc).

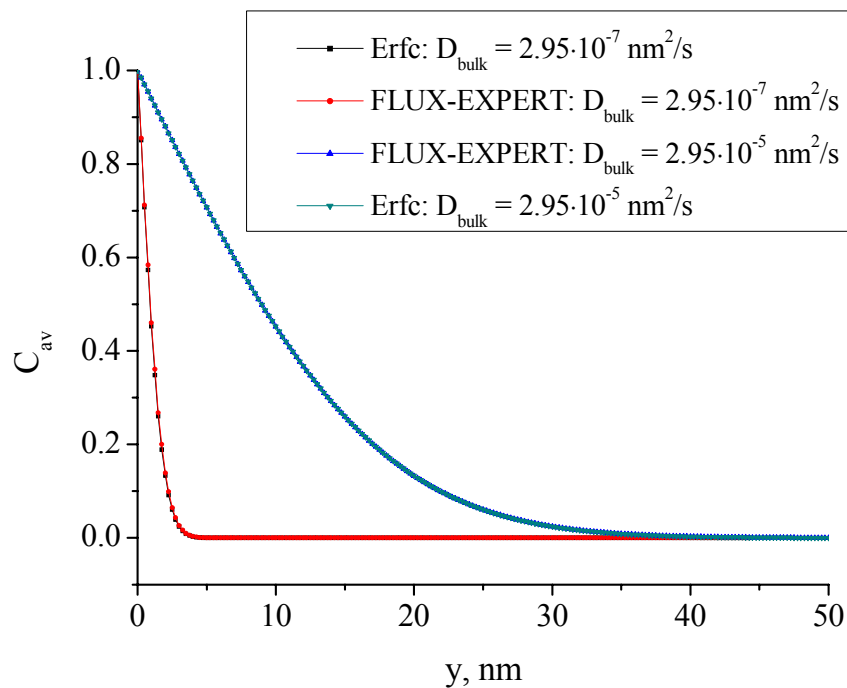


Fig. 5.5 A comparison of the two meshes (for different D_{bulk} , representing D_{scl} , see the text) used to simulate diffusion in the A-regime with the corresponding complementary error-function solutions (Erfc) at $t = 3 \cdot 10^6 \text{ s}$.

as for the mesh used for the B-regime. The density of the mesh in the bulk part of the geometrical model remains unchanged and is the same as used in all the calculations in the A-regime in the present study.

One can expect that the profiles calculated for the finite element model used are affected by the boundary condition at the bottom of the sample (geometrical model). This indeed plays an important role when simulating diffusion along the GBs accompanied by diffusion in the SCL with very small D_{scl} . Accordingly, one can plot the derivative of the profile calculated for the smallest D_{scl} . In fig. 5.6 such a derivative is shown (solid curve). As it was explained in chapter IV, the strong effect of the boundary condition is reflected in the extreme case that the maximum of the profile disappears, because the gradient goes to zero. This refers to the question of validity of the solutions for semi-infinite systems for the problem discussed here. As it is seen in fig. 5.6 the maximum is very well distinguishable and can be very easily estimated. The rest of the profile is affected by different factors, including the zero flux condition at the bottom. This also indicates that a sample length of 100 nm can be used to simulate diffusion in the B-regime.

5.2.2 The reason of using constant space charge diffusivity

First, it should be again noted that the main interest is related to the maximum of the derivative of the diffusion profile. This maximum gives the proper value of D_{gb} when deduced by using the conventional Le Claire relation. The constant D_{scl} used in the present simulation is questionable, since the concentration of defects varies with the distance perpendicular to the GB. That is why, for example, Chung *et al.* [Chu00] proposed the model of diffusion along the GBs with the adjacent SCLs based on the Gouy-Chapman model, in which D_{scl} is coordinate dependent. In order to check the effect of the coordinate dependent D_{scl} , the SCL thickness (δ_{scl}) was drastically reduced and a new model was developed.

Decreasing δ_{scl} from 1 nm to 0.03 nm, the SCL thickness was reduced to an unrealistically and infinitely thin region. However, the effect of blocking SCL is so strong, that the position of the maximum of the derivative is very similar to that for $\delta_{\text{scl}} = 1$ nm as fig. 5.6 shows. The values of the derivatives are also very close, suggesting that the maximum is determined by what happens in the first atomic layers close the GB core independent of thickness of the SCL and dependence of the diffusivity on coordinate. This means, that the maximum reflects directly the movement of the atoms from the GB core into the SCL. It is the same as the B-regime starts immediately when the leakage of diffusing atoms starts from

the GB into the grain. The beginning of this process determines the position of the maximum and its magnitude. To investigate further the insensitivity of the maximum on the coordinate dependence of D_{scl} , an additional calculation was performed. In the new calculation δ_{scl} was increased to 3 nm, and the SCL itself was divided into three regions with the thickness of 1 nm each. The diffusivities were different in all the three regions and varied from $2.95 \cdot 10^{-7} \text{ nm}^2/\text{s}$ in the first region directly adjacent to the GB core to $2.95 \cdot 10^{-5} \text{ nm}^2/\text{s}$ in the third region followed by the bulk (fig. 5.8). The concentration is enhanced in the first region due to the leakage from the GB core. This region is mostly filled by the diffusant at sufficiently long t such that it can lead to the flux of atoms to the second region. Interestingly, there is no leakage from the third region to the second one. The diffusion profiles calculated in this model are compared with those with the constant D_{scl} ($\delta_{\text{scl}} = 1 \text{ nm}$) at different t in fig. 5.7. There is no significant difference between the two models, indicating the overall result is determined by the region adjacent to the GB core even at long t . At shorter t the rest of the diffusion profiles becomes much more different depending on δ_{scl} and coordinate dependent D_{scl} (not shown here). Importantly, the maximum is not affected remaining the same under these quite different conditions. The fact that the diffusion profiles have two distinguishable parts at $t = 3 \cdot 10^6 \text{ s}$ will be discussed in the coming section.

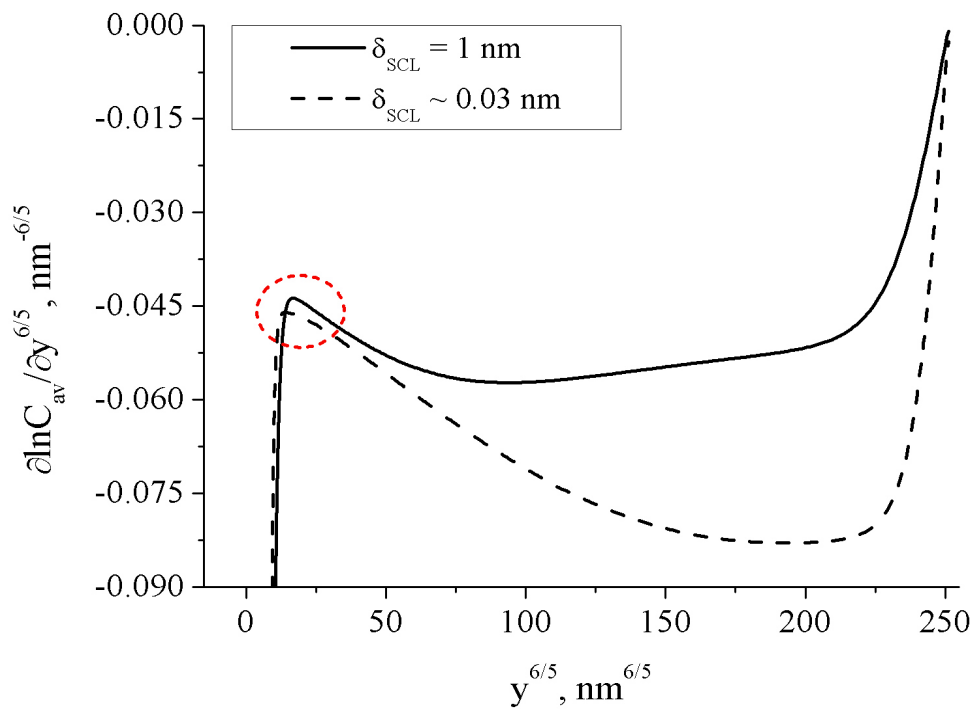


Fig. 5.6 Variation of the derivative $\partial \ln C_{\text{av}} / \partial y^{6/5}$ with $y^{6/5}$ calculated for two different SCL thicknesses for $\Delta = 10^2$.

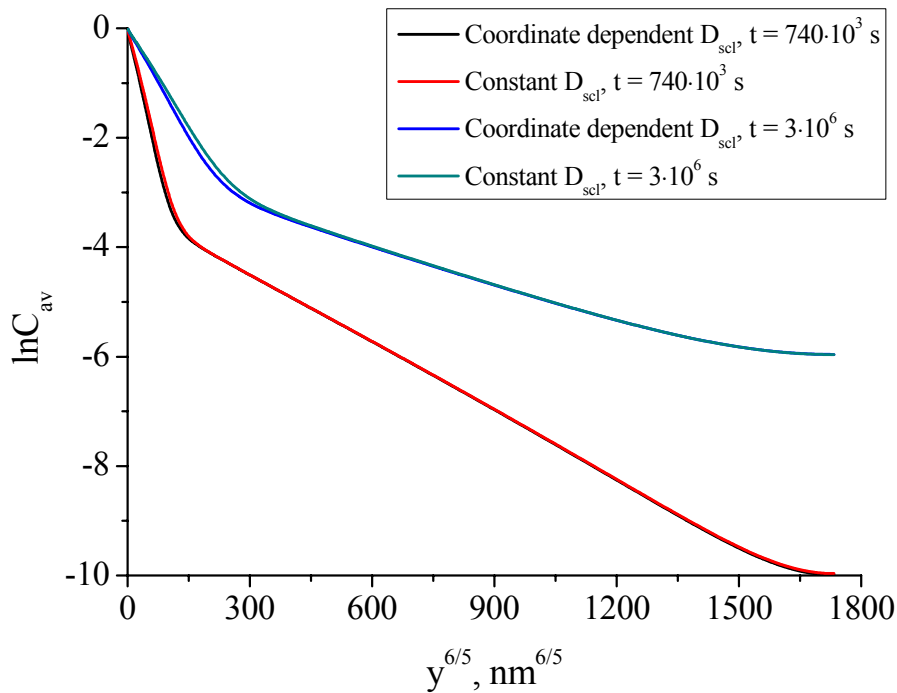


Fig. 5.7 Variation of $\ln C_{av}$ with $y^{6/5}$ calculated for the cases of constant and coordinate dependent D_{scl} for $\Delta = 10^2$.

5.3 How diffusion proceeds in the models of parallel boundaries and square grains

Two models were used to study diffusion in ionic materials, namely the model of parallel boundaries (or, isolated GB model, if $L_g < d/2$) and of square grains. As it was explained in chapter IV, these are the most important models, allowing diffusion to be characterized even in realistic polycrystalline microstructures. As usual, t and d were taken quite small, in order to reproduce situations in nanocrystalline materials. Emphasis is laid on the blocking effect recently observed in variety of ionic materials [see, for example, [Gou02]]. Consequently, the SCL diffusivities (D_{scl}) are supposed to be smaller than the grain diffusivities (D_g), whereas the GB diffusivity (D_{gb}) exceeds both. However, the situations when $D_{scl} > D_g$ are also discussed in order to analyze the whole trend of the ratio $D_{gb,app}/D_{gb,true}$ (here $D_{gb,app}$ is, as usual, an apparent GB diffusivity found by applying conventional models, and $D_{gb,true}$ is a true GB diffusivity used to simulate the diffusion profiles) as a function of $\Lambda = D_g/D_{scl}$. The latter is a new parameter which makes the analysis simpler. For both models and different diffusion regimes a recipe is given how to properly

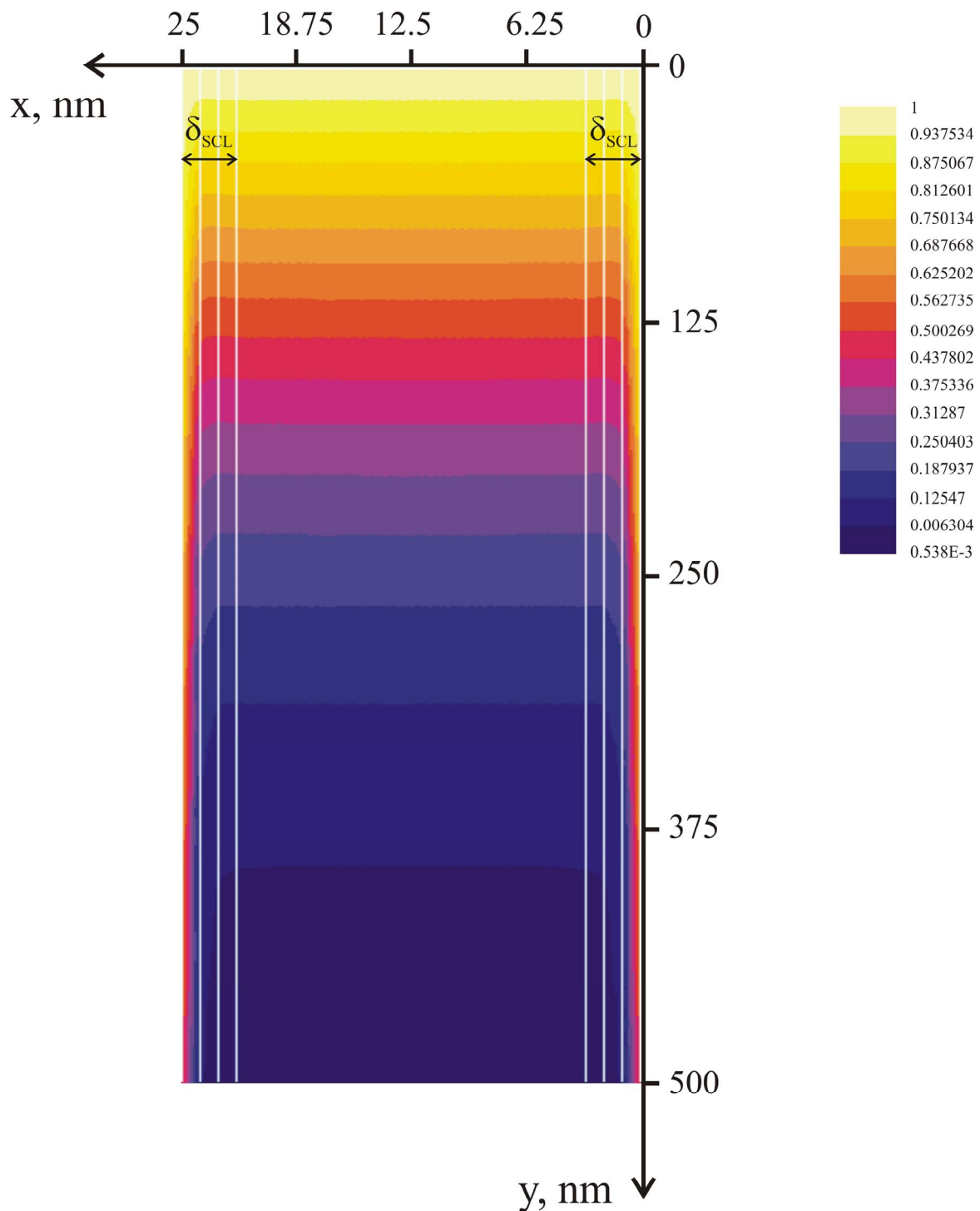


Fig. 5.8 Concentration distribution in the model of parallel boundaries with the SCL of the thickness 3 nm, comprising three parts with different diffusivities. The free surface is at $y = 0$ nm, whereas two neighboring parallel boundaries are at $x = 0$ and 25 nm, respectively. The result was obtained under conditions of the conventional A-regime, i.e. L_g is larger than the distance between the parallel boundaries. White lines show the borders of corresponding regions of different diffusivities. There is no a special physical property along white lines. Each color corresponds to certain value of the concentration, what is explained on a color pattern.

find D_{gb} . The suggestions which can be found in this chapter supplement the observations of the preceding chapters. Consequently, the problems of Le Claire's constant and the nonlinearity are also relevant here.

5.3.1 The model of parallel boundaries under conditions of type-B kinetics

It is important to note once more that both the model of parallel boundaries and the isolated GB model lead to the same results until $L_g > d/2$, where d is the average grain size or the distance between two neighboring parallel boundaries. In the present study for ionic materials the isolated GB model was used (what is caused by a very dense mesh used in the SCL) at extremely short t . Thus, only diffusion in the B-regime occurs. Consequently, the obtained results are valid for parallel boundaries as well. Trying various values for D_{scl} the diffusion profiles were calculated for fixed $D_g (= 2.95 \cdot 10^{-4} \text{ nm}^2/\text{s})$ and $D_{gb} (= 2.95 \cdot 10^{-2} \text{ nm}^2/\text{s})$. In fig. 5.9 the profiles are presented, with $\Lambda (= D_g/D_{scl})$ varying from 10^{-1} to 10^3 . According to the conventional procedure, the profiles represent dependences in the form $\ln C_{av} = f(y^{6/5})$. The smallest value of D_{scl} is $2.95 \cdot 10^{-7} \text{ nm}^2/\text{s}$, which corresponds to the diffusion length in the SCL $3.73 \cdot 10^{-2} \text{ nm}$ at $t = 4700 \text{ s}$. Such a value scales with the density of mesh used to simulate diffusion in the SCL, what also confirms the quality of obtained result. Additionally, a very small value of D_{scl} would mean a very small contribution of diffusion in the SCL. However, the slopes of diffusion profiles vary with Λ (fig. 5.9) which is usually unknown in the experiments. This is why, it became particularly important to estimate the errors of determining D_{gb} introduced by the SCL using the conventional procedures.

As one can see in fig. 5.9, the slope decreases as Λ increases, or as D_{scl} becomes smaller. The profile for $\Lambda = 1$ is also shown in fig. 5.9 and, it is possible, at least qualitatively, to state that D_{gb} found from such profiles by applying the Le Claire relation is overestimated, if $\Lambda > 1$. On the other hand, the slopes of the profiles calculated for $\Lambda < 1$ increase, what leads to opposite trend in the $D_{gb,app}$ behavior. Because of these two trends, one has to distinguish diffusion under different conditions: $\Lambda < 1$ or $\Lambda > 1$. The purpose of this distinction is to emphasize different physical situations, but the procedure to deduce D_{gb} is the same. The difference between the two situations is demonstrated in fig. 5.10. In this figure fragments of the concentration fields are shown at $t = 4700 \text{ s}$. If $\Lambda > 1$, diffusion is prolonged in the bulk and along the GB core, and one can immediately see, that there are fluxes from the GB core to the SCL and from the grain (bulk) to the SCL. The concentration field around the GB core is exactly what is expected for the non-overlapping fluxes from the neighboring parallel

diffusion paths. Such a contribution of the SCL is also similar to the situation, when diffusing atoms cannot move inside the material from the source due to the surface reaction, but because of the fast surface diffusion the atoms move along the surface (or along the GB core, if it is concerned). The blocking effect is reflected by the drastically reduced concentration within the SCL, and the question arises how this can affect the diffusion profile. Contrary, there is a flux from the SCL into the grain, if $\Lambda < 1$ (fig. 5.10b). Here the question about the overlapping within the SCL is not relevant, and the SCL can be filled by the diffusant in a very short time. It looks like the GB has increased its thickness due to the SCL, especially at higher diffusion times. However, it is also a matter of parameters, like the thickness δ_{scl} and diffusivity D_{gb} . It can be mentioned, that the overall process is not prolonged under conditions of $\Lambda < 1$. This is clear, as prolongation is only caused by great difference in the diffusivities in the two adjacent regions. Such a prolongation is more typical for diffusion for $\Lambda > 1$. One can see that the isoconcentration lines in fig. 5.10a are almost parallel to the GB core, i.e. the angle between them is very small – a situation typical for large values β and short t .

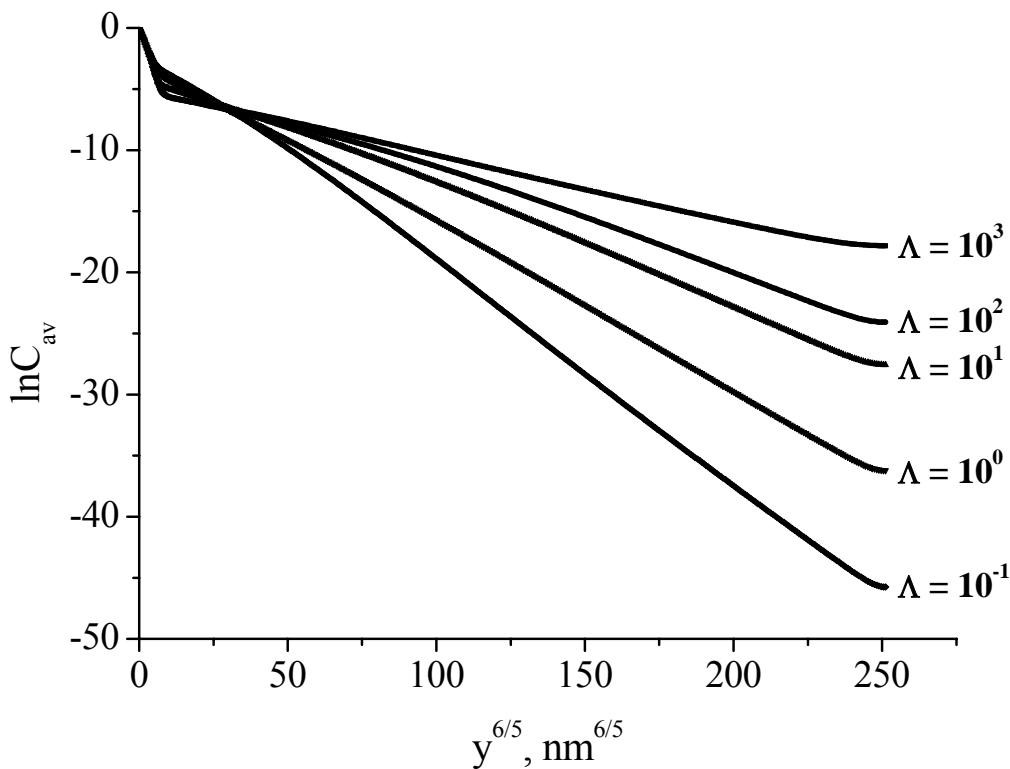
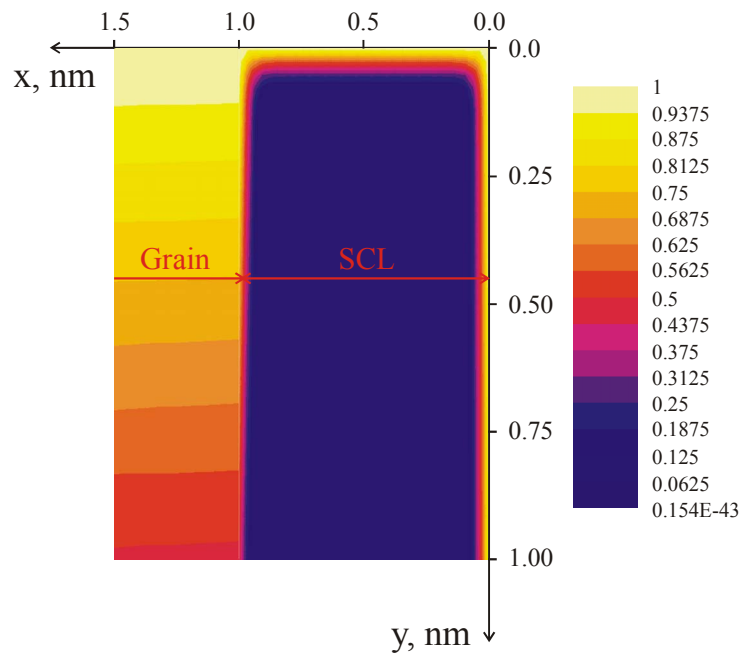


Fig. 5.9 Variation of $\ln C_{av}$ with $y^{6/5}$ calculated at $t = 4700$ s for $\Delta = 10^2$ and various Λ .

a)



b)

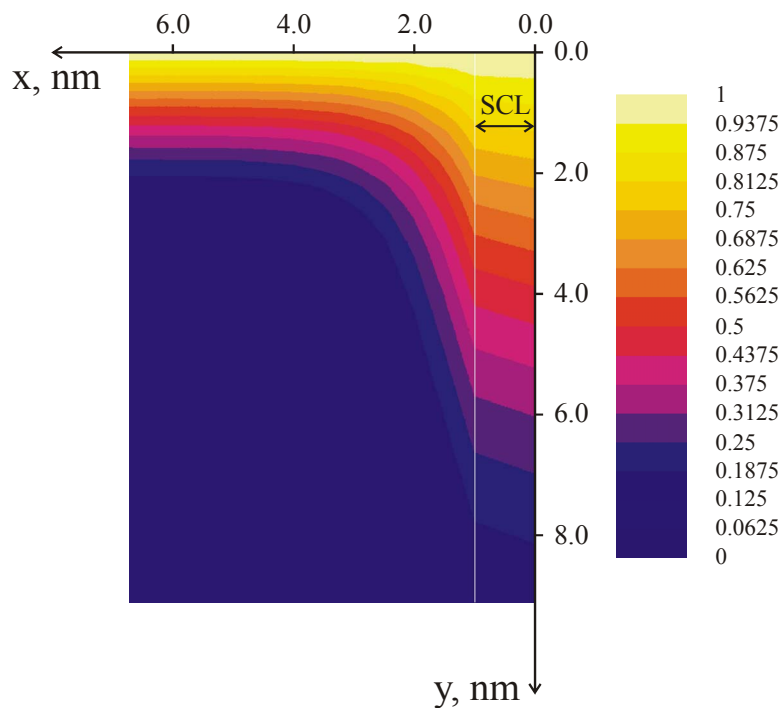


Fig. 5.10 A fragment of the concentration distribution in the model of isolated GB (the GB core is sitting exactly at $x = 0$ nm) with the adjacent SCL of the thickness 1 nm. As usual, a free surface is situated at $y = 0$ nm. Parameters: a) $\Lambda = 10^3$, $\Delta = 10^2$, $t = 4700$ s and b) $\Lambda = 10^{-1}$, $\Delta = 10^2$, $t = 4700$ s. The color patterns have their usual meaning.

The errors of using Le Claire's relation are demonstrated in fig. 5.11. Three curves are shown corresponding to three different procedures of deducing D_{gb} . First, $D_{gb,app}$ was calculated by using the standard Le Claire relation with a constant of 1.322 (Eq. (1.16)). The corresponding errors are shown as circles in fig. 5.11. This means that fitting the calculated diffusion profiles to the straight line was applied. In this case $D_{gb,app}$ is larger than the true one by a factor of about 3 at $\Lambda = 10^3$. Then the maximum of the derivative $\partial \ln C_{av} / \partial y^{6/5}$ was taken and used in Le Claire's relation (squares in fig. 5.11). In chapter III it was shown that this maximum gives the more accurate value for D_{gb} when Le Claire's relation is used. Taking the maximum leads to even larger errors in comparison with the errors of the standard fit, and D_{gb} is overestimated by a factor of 4 at $\Lambda = 10^3$. Moreover, the ratio $D_{gb,app}/D_{gb,true}$ is not unity at $\Lambda = 1$ in both cases. Obviously, this is related to the constant of 1.322. According to the findings of chapter III, the derivative $\partial \ln C_{av} / \partial w^{6/5}$ should be calculated properly depending on the parameter α ($=\delta/2L_g$). Finally, the improved derivative $\partial \ln C_{av} / \partial w^{6/5}$ was calculated by using Eq. (2.1) and put into the original Le Claire relation (Eq. (1.14)) instead of the constant 1.322. The latter is caused by very short t involved in the simulation, and all the discussions of chapter III are relevant here too. The parameter α is about 0.21 at $t = 4700$ s for $D_g = 2.95 \cdot 10^{-4}$ nm²/s. Following this improved procedure, the ratio $D_{gb,app}/D_{gb,true}$ was recalculated and finally achieved unity at $\Lambda = 1$ (triangles in fig. 5.11). But, the errors in finding D_{gb} increase further even after applying the improved procedures, giving D_{gb} overestimated by a factor of about 6 at $\Lambda = 10^3$. Interestingly, the attempts to reduce the errors by using the improved procedures make the discrepancy between the apparent and true diffusivities larger. This is related to the fact that the equations used for calculating D_{gb} completely ignore the third diffusivity involved in the process, namely D_{scl} . One has to pay attention that the flux of atoms moving from the GB core into the SCL is determined by D_{scl} and, therefore, the maximum of the derivative as being determined by this motion, should reveal something close to the ratio of diffusivities D_{gb}/D_{scl} . This ratio is obviously larger than Δ and Λ for the blocking SCL, because $D_g > D_{scl}$. However, this expectation should be clarified.

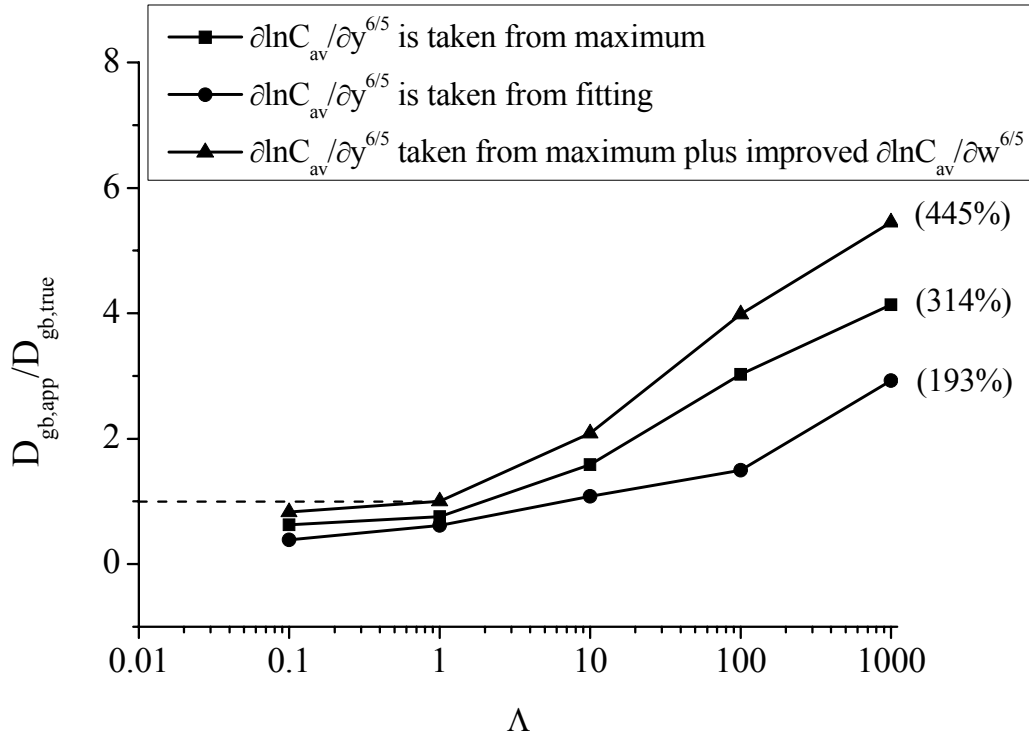


Fig. 5.11 Errors in calculating D_{gb} by using the conventional Le Claire equation and the improved procedures discussed in chapter III. The calculated profiles correspond to $\Delta = 10^2$ and $t = 4700$ s. Errors were estimated according to $\left(\left| D_{gb,app} - D_{gb,true} \right| / D_{gb,true} \right) \cdot 100\%$.

The blocking SCLs are accompanied by two processes. One is related to diffusion from the GB core into the SCL and another one is related to diffusion from the grain into the SCL. These processes are taken into account by the continuity conditions at the corresponding interfaces (Eq. (5.2a) and (5.2b)). In order to clarify, which process really determines the maximum of the derivatives, the plots $\partial \ln C_{av} / \partial y^{6/5} = f(y^{6/5})$ were analyzed and the equations derived in chapter III applied. The corresponding maxima for the SCL problem are rather small (fig. 5.12) and comparable to those in figs. 3.8a or 3.8b, i.e. for non-space-charge problems with $\Delta = 10^2$ or 10^3 . However, the calculations differ by values of the diffusivities in the region adjacent to the GB core (i.e., D_g for the results in fig. 3.8 and D_{scl} in fig. 5.12). For $\Delta = 10^3$ and $D_{scl} = 2.95 \cdot 10^{-7} \text{ nm}^2/\text{s}$ the ratio D_{gb}/D_{scl} equals 10^5 . The same ratio was realized in chapter III with $D_g = 2.95 \cdot 10^{-4} \text{ nm}^2/\text{s}$ and $D_{gb} = 2.95 \cdot 10^1 \text{ nm}^2/\text{s}$. However, the values of the corresponding maxima differ by two orders of magnitude. Generally, increasing Δ with fixed D_g leads to smaller values of the maxima. But, increasing Δ ($=D_{gb}/D_{scl}$ for the SCL problem) with fixed D_{gb} leads to much smaller deviations in the derivatives for different ratios in

comparison with the results in fig. 3.8, from -0.12 for $\Lambda = 10^0$ ($D_{gb}/D_{scl} = 10^2$) to -0.04 for $\Lambda = 10^3$ ($D_{gb}/D_{scl} = 10^5$). Probably, the latter effect depends on the absolute value of D_{scl} . It is difficult to expect the ratio between the diffusivities knowing only the absolute value of the derivative at the maximum. A new procedure should be used in order to extract this ratio. Moreover, in the SCL problems a third diffusivity is involved (D_{scl}) which is also unknown. However, this diffusivity determines the value of the maximum.

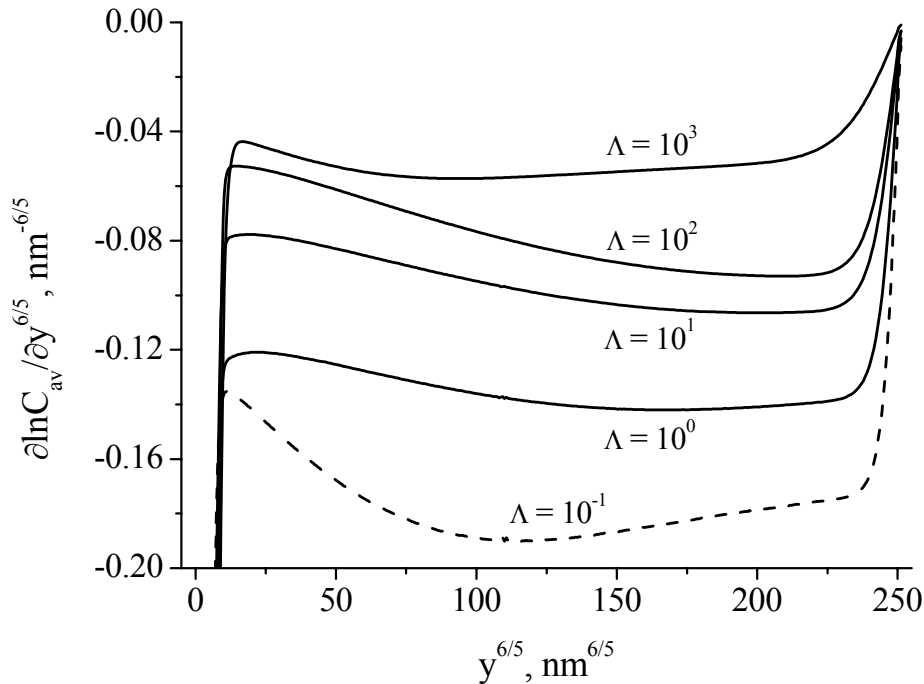


Fig. 5.12 Variation of the derivative at $t = 4700$ s for $\Delta = 10^2$.

In fig. 5.13 the derivatives are compared with the results of Whipple's solution integration (Eq. (1.9a)) which were obtained by fixing D_{gb} and varying D_g and D_{scl} , respectively. In the integration the same ratios of diffusivities were used as for the SCL problem, i.e. Δ in the integration equals D_{gb}/D_{scl} in the simulation (Δ in fig. 5.13 indicates the ratio used in the simulation). One can easily see that the derivatives simulated for the SCL problem are very close to those obtained by the integration, despite the fact that there is a flux of atoms from the grain into the SCL. This confirms that the maximum of the derivative is determined mostly by what happens between the GB core and the SCL. In fig. 5.13 the positions of maxima of the SCL problem slightly differ in comparison with Whipple's solution integration. The maximum is shifted to larger values of $y^{6/5}$ in the case of the SCL problem (red curves), especially for larger Λ .

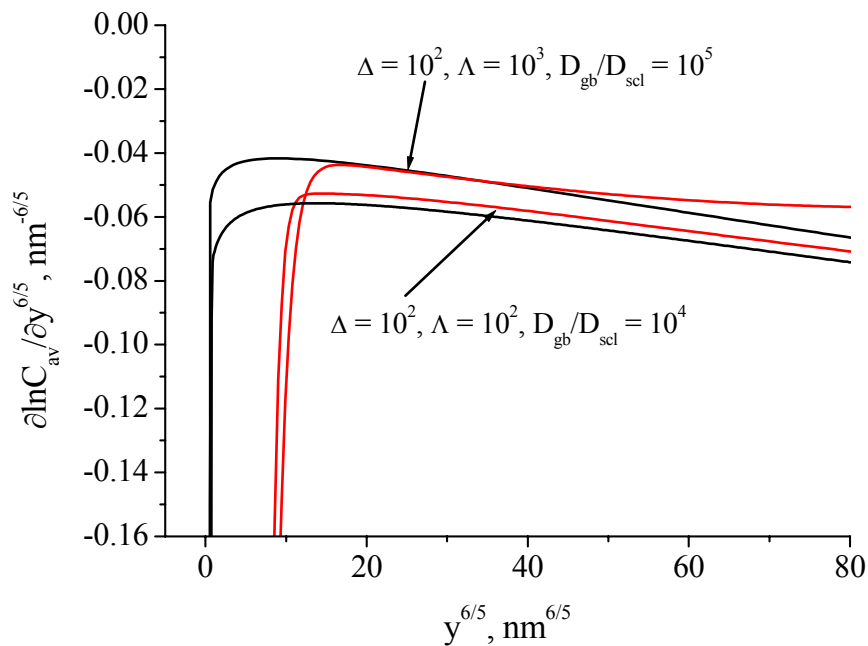


Fig. 5.13 A comparison of Whipple's solution and the simulation result of the SCL problem at $t = 4700$ s. The black curves correspond to Whipple's solution, whereas the red curves are responsible for the simulation.

Interestingly, the contribution of bulk diffusion can be observed at very short t . In fig. 5.14 different profiles simulated for the SCL problem are compared, and the complementary error-function solution is shown for D_g . The bulk diffusion is responsible for the process in the near-surface part of the profile for the smaller D_{scl} . However, this contribution becomes less pronounced, if Λ decreases. It means that, in principle, D_g can be still extracted even for blocking SCL, how it is done in the experiments [Sou05]. The bulk diffusion part is quite short and is followed by the part determined by the ratio D_{gb}/D_{scl} . Since D_g is smaller than D_{gb} , the process along the GB in the blocking SCL problem is characterized by even smaller slopes that one could expect to give a larger diffusivity. It should also be noticed that the profiles in fig. 5.14 are intersecting at $y^{6/5} \approx 30 \text{ nm}^{6/5}$. For $y^{6/5} < 30 \text{ nm}^{6/5}$ the area under these curves or the total amount of material entering the sample is larger for the smallest ratio $\Lambda = 0.1$. For $y^{6/5} > 30 \text{ nm}^{6/5}$ the opposite situation is observed. Nevertheless, it was found out that in the whole range of $y^{6/5}$ the total area is increased for $\Lambda = 0.1$. Consequently, the blocking SCLs decrease the total amount of material in the sample, at least at short t .

In order to improve the determination of D_{gb} , the new equation, discussed in chapter III (Eq. (3.7)), was used instead of Le Claire's relation. This equation relates the maximum of

the derivative $\partial \ln C_{av} / \partial y^{6/5}$ and the ratio Δ , or specifically for the SCL problem, the ratio D_{gb}/D_{scl} . Thus, Eq. (3.7) can be rewritten in the following form

$$\left| \frac{\partial \ln C_{av}}{\partial y^{6/5}} \right|_{\max} = C \cdot \left(\frac{D_{gb}}{D_{scl}} \right)^F \cdot t^B. \quad (5.3)$$

One of the ideas which can automatically arise is the fitting experimental data to Eq. (5.3). However, this equation cannot be used for real fitting, since consisting of two multiplied unknown parameters, i.e. C and Δ^F (here Δ means the ratio D_{gb}/D_{scl} as well). By using the fitting one can only find the prefactor to t^B , i.e. the whole term $C(D_{gb}/D_{scl})^F$. So the application of this equation requires knowledge of the unknowns C , F and B . As it was mentioned in chapter III the unknown parameter C is dependent on D_g and can strongly vary. Because of the problem of fitting, these parameters were estimated by integrating Whipple's solution for the diffusivities used to simulate diffusion for the SCL problem. The results are summarized in table 5.1. The integration was performed fixing D_{scl} and varying D_{gb} , i.e. to guarantee D_{gb}/D_{scl} to be 10^2 and 10^5 in order to have extremely different ratios. For each ratio D_{gb}/D_{scl} two very different t were realized, namely $2 \cdot 10^3$ s and 10^6 s, providing the quantities B , C and F . Consequently, this procedure was applied for each D_{scl} and Δ used. The absolute value of B slightly decreases with increasing Δ , C varies significantly with Δ , whereas F remains constant. The apparent GB diffusivity ($D_{gb,app}$) was calculated according to

$$D_{gb,app} = \frac{4}{(D_{gb}/D_{scl}) t \delta^2} \left(-\frac{\partial \ln C_{av}}{\partial w^{6/5}} \right)^{10/3} \left(-\frac{\partial \ln C_{av}}{\partial y^{6/5}} \right)^{-10/3}, \quad (5.4)$$

where the ratio D_{gb}/D_{scl} is known from Eq. (5.3) and the derivative $\partial \ln C_{av} / \partial w^{6/5}$ is found according to the improved procedure. The errors in finding D_{gb} were decreased by applying Eqs. (5.3) and (5.4) in comparison with Le Claire's relation (table 5.1). Still remaining errors can be attributed to deviations of the corresponding maxima from the result of integration of Whipple's solution (fig. 5.13). Consequently, Eq. (5.4) may be used to find $D_{gb,app}$. The disadvantage of this relation is in fact that it requires knowledge of all the parameters involved: C , B , F . Here a hint can be given for future research. It is particularly important to find a procedure to deduce D_{gb} in ionic materials. Eq. (5.3) seems to be a suitable candidate to improve the determination of D_{gb} . Further evaluations using Whipple's solution could help to correlate the maxima and ratios and all the other parameters.

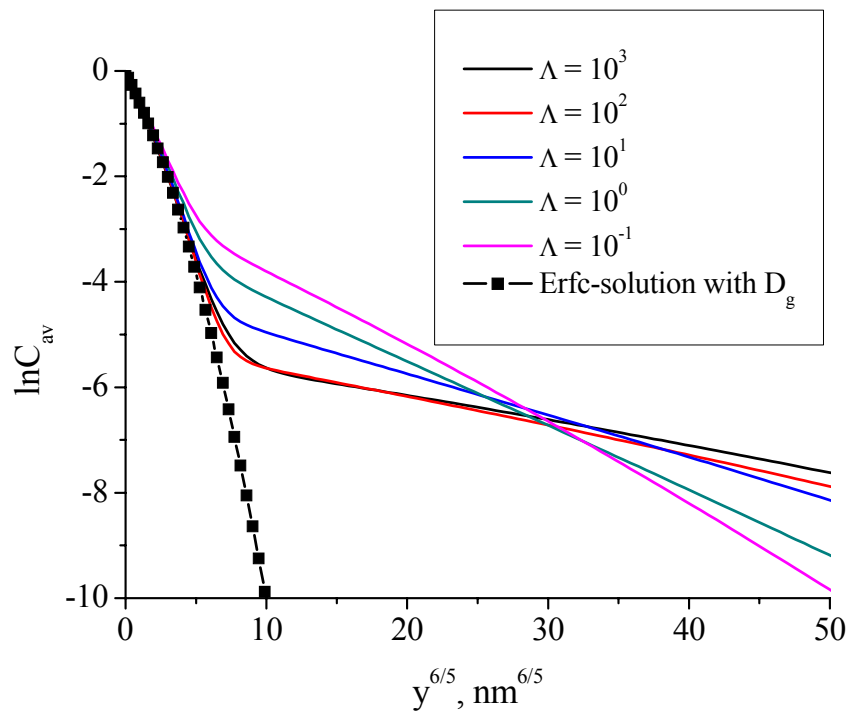


Fig. 5.14 A comparison of the profiles for different Λ and a complementary error function solution (Erfc-solution) in the region of very small depths.

Table 5.1 The parameters obtained to evaluate Eq. (5.3) and apparent GB diffusivities found by using Eq. (5.4) for $t = 4700$ s. As usual the errors were found due to $\left(\left| D_{gb,app} - D_{gb,true} \right| / D_{gb,true} \right) \cdot 100\%$.

Λ	B	C	F	$D_{gb,app}, \text{nm}^2/\text{s}$	Error in %
10^3	-0.47	2540	-0.61	$9.11 \cdot 10^{-4}$	97
10^2	-0.43	562.65	-0.60	$4.03 \cdot 10^{-3}$	86
10^1	-0.38	134	-0.60	$1.09 \cdot 10^{-2}$	63

5.3.2 The model of square grains under conditions of type-B kinetics

The model of square grains was used here to analyze the effect of blocking GBs under realistic conditions. The results obtained for this model with space charge effects included were compared with those obtained for the model of parallel boundaries and the model of square grains without SCLs. The importance of blocking SCLs lies in the channeling of transport. In other words, the reduced diffusivities in the regions adjacent to the GBs suggest an enhanced β -parameter (Eq. (1.9d)) and, as a result of this, increased penetrations. Indeed, the increased ratios between the diffusivities lead to smaller slopes, as it was shown in the

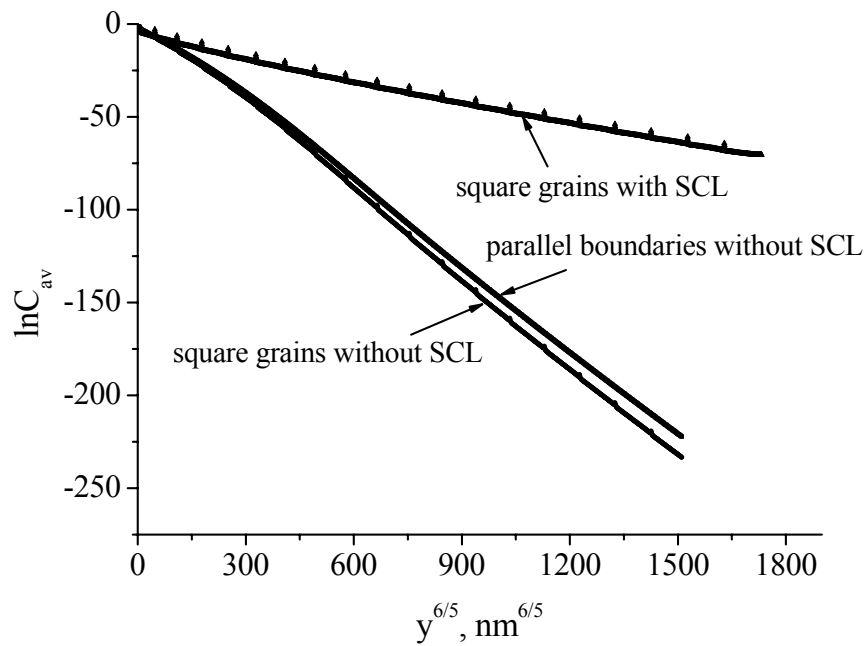
preceding section (fig. 5.12). If the perpendicular GB comes into play, the slope is changed the more strongly, the shorter diffusion time or the larger ratio between the diffusivities. The profile calculated for $\Lambda = 10^2$ and $\Delta = 10^2$ for the model of square grains is compared with that for the model of parallel boundaries and square grain without the SCL (fig. 5.15a). Because the ratio of diffusivities Δ is small, there are no corresponding contributions of perpendicular GBs in the model of square grains without SCL (see, for example, fig. 4.9). This makes the profile for the square grains without the SCL very comparable to the profile for the parallel boundaries without SCLs. Despite such a role of perpendicular GBs for the small ratio Δ , the slopes of the profiles for the square grains with the SCL are very different in comparison with the slopes of those profiles obtained without the SCL. Consequently, the role of GBs surrounded by the blocking SCLs is very specific and important. Moreover, the slope of the profile with the SCL decreases with Λ . It can make $D_{gb,app}$ larger applying the conventional equations, whereas the slope is increased in the problems without the SCL (fig. 4.9). This, obviously, yields one more specific role of the blocking SCL. Some diffusion profiles were also calculated for larger Δ . According to fig. 5.15b the contribution of perpendicular GBs is reflected in the larger slope in comparison with the situation when only parallel boundaries contribute. It is very clearly seen in fig. 5.15b that the slope of the profile is decreased by the influence of the blocking SCLs. Because the effects in the problems with and without the SCLs have opposite trends in the slope behavior, the question is only which of them dominates. In the case of the SCL problems, the contribution is directly determined by the ratio Λ . Obviously, the larger Λ , the smaller the slope. Since the results in figs. 5.15a and 5.15b have the same Λ , these are also comparable. The profile for larger Δ is characterized by typical spikes which are very tiny in comparison with the profiles without the SCLs. Surely, this is due to diffusion confined within the GBs in the SCL problem, i.e. there is no significant diffusion from the GBs to the adjacent SCLs.

5.3.3 The model of parallel boundaries and the model of square grains under conditions of type-A kinetics

According to fig. 1.5 the increase of t should finally lead to the A-regime. As far as the overall process is determined to a great extent by the ratio of the GB and SCL diffusivities, the A-regime is met when the diffusion length in the SCL is comparable to that in the grain and GB. It can be understood in the way that three different processes should have similar diffusion lengths, leading to a homogeneous situation. If this is not the case, and the processes

are still separable, the homogeneous solutions, such as Hart' equation (Eq. (1.17a)) lead to significant errors. The diffusion time needed to reach the homogenous situation can be extremely long, giving unrealistic values of several tens of millions seconds. In order to emphasize these points, the concentration distribution is shown in the model of parallel boundaries in fig. 5.16 at $t = 3 \cdot 10^6$ s for $\Lambda = 10^3$. At such a high t nominally the A-regime is valid, as being determined by the condition $L_g > d$ ($L_g \approx 30$ nm, $d = 25$ nm). In the region of SCL the concentration differs from that in the bulk. The contribution from GBs enhances the concentration within the SCL at high t despite a very small diffusivity D_{scl} . The role of SCLs is not the same as it was at short t . The contribution to the grain comes partly from the combined SCL-GB system. In this sense both the regions, the SCL and GB, represent one part of the sample. This is similar to what was discussed in section 5.2.2. Because of the blocking effect, first, some time is needed to fill the SCL by the diffusant, and then the contribution would continue from the SCL-GB into the grain. As a result, the diffusion profiles obtained under the nominal A-regime conditions comprise two distinguishable parts. In fig. 5.17 the diffusion profile calculated for the model of parallel boundaries with the SCL at high t is compared with that without SCL. Two interesting cases are also compared in fig. 5.17, namely $\Lambda = 10$ and $\Lambda = 10^3$. If the ratio Λ is small enough, the corresponding profile strongly differs from that for larger Λ and is close to the profile without the SCL, also shown fig. 5.17. The latter difference arises at very low concentrations due to the changed kinetics. However, if the larger Λ occurs, the two parts of the profile arise. Consequently, it would be necessary to apply the conventional procedure used for the B-regime. On the other hand, the A-regime is relevant. The problem, of course, deals with the conditions (Eqs. (1.9), (1.10), (1.11)) which do not take into account the third diffusivity involved in the process. The Hart equation, being the equation for the A-regime, was used to find $D_{gb,app}$, and the errors were indeed observed (fig. 5.18). The errors in finding D_{gb} are high, suggesting that it is underestimated, if the conventional equation is used. The error increases with Λ , reaching 88% at $\Lambda = 10^3$. The shorter t the larger the error (in the A-regime). For $\Lambda = 10^2$, $t = 50 \cdot 10^6$ s is sufficient to reach the ratio $D_{gb,app}/D_{gb,true} \approx 1$. On the other hand, applying Le Claire's relation gives even larger error. Because the profile with the two distinguishable parts is observed for large Λ , the procedure discussed in the preceding section can be applied, if one believes that the slope of the profile reflects the process between the GB and the SCL at $t = 3 \cdot 10^6$ s. Accordingly, the quantities B, C and F were taken from table 5.1 for $\Lambda = 10^3$ and Eqs. (5.3) and (5.4) were used

a)



b)

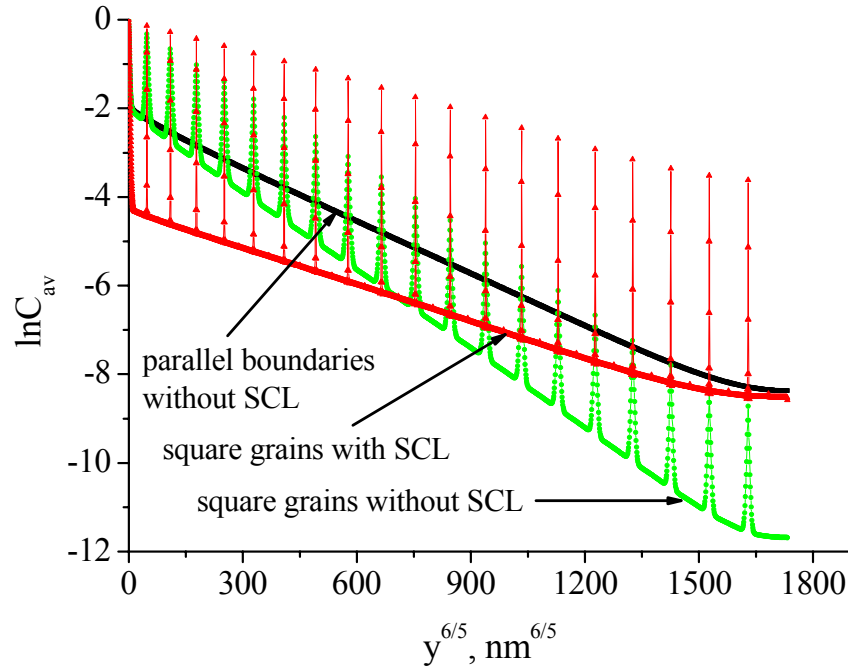


Fig. 5.15 Variation of $\ln C_{av}$ with $y^{6/5}$ calculated for the model of square grains with the GBs surrounded by the blocking SCLs compared with those for the square grains and parallel boundaries without SCLs for $\Lambda = 10^2$ and a) $\Delta = 10^2$, b) $\Delta = 2.2 \cdot 10^4$ at $t = 8200$ s.

to find $D_{gb,app}$. The error in finding D_{gb} was reduced to 44%, indicating the importance and validity of Eq. (5.3) for SCL problems.

The perpendicular GBs surrounded by the SCLs play a crucial role as it was also discussed in the preceding section. These lead to opposite trends when using the conventional models for the SCL problems and the non-space-charge problems in the B-regime. The concentration distribution is shown in fig. 5.19 for the model of square grains at long t . It is clearly seen that the role of the first grain is very specific. This grain is filled completely by the diffusant, whereas other grains are characterized by much smaller concentrations. The concentration is also enhanced within the GBs. One can expect that the effect of perpendicular GBs with the SCLs is to increase the concentration along the depth, in comparison with the model of parallel boundaries, which is due to deep penetrations. Consequently, the sample can be filled by the diffusant at long t , if each separate grain is filled. However, the perpendicular GBs with the SCLs do not allow the diffusant to proceed further into the next grain. The concentration is drastically reduced due to these GBs (fig. 5.20). An abrupt change of the kinetic regimes occurs along the depth. Again the effect is more pronounced for increasing Λ . Very similar effects due to the blocking SCLs were observed experimentally on different systems [Leo99], [Sou05], and [WanR05]. However, while studying diffusion in polycrystalline materials, it is very difficult to exclude such effects.

At longer t the concentration within the grains increases, and the step between the concentrations in two nearest grains vanishes. It is very well seen in figs. 5.21 and 5.22 for $\Lambda = 10^2$. Nevertheless, the effect of perpendicular GBs is so strong that resolving the problem of SCL by varying t is impossible. In a bicrystal one can estimate at least the role of SCL by plotting $\ln C_{av} = f(y^{6/5})$ even under conditions of the A-regime. In this case the use of Eq. (5.2) is very important, since both the Hart equation and Le Claire's relation yield significant errors. In polycrystals, either high temperature is needed to completely exclude the role of SCL or high gradients are needed to restrict analysis to the process close to the surface, in order to apply the improved procedure for the B-regime discussed in the present study.

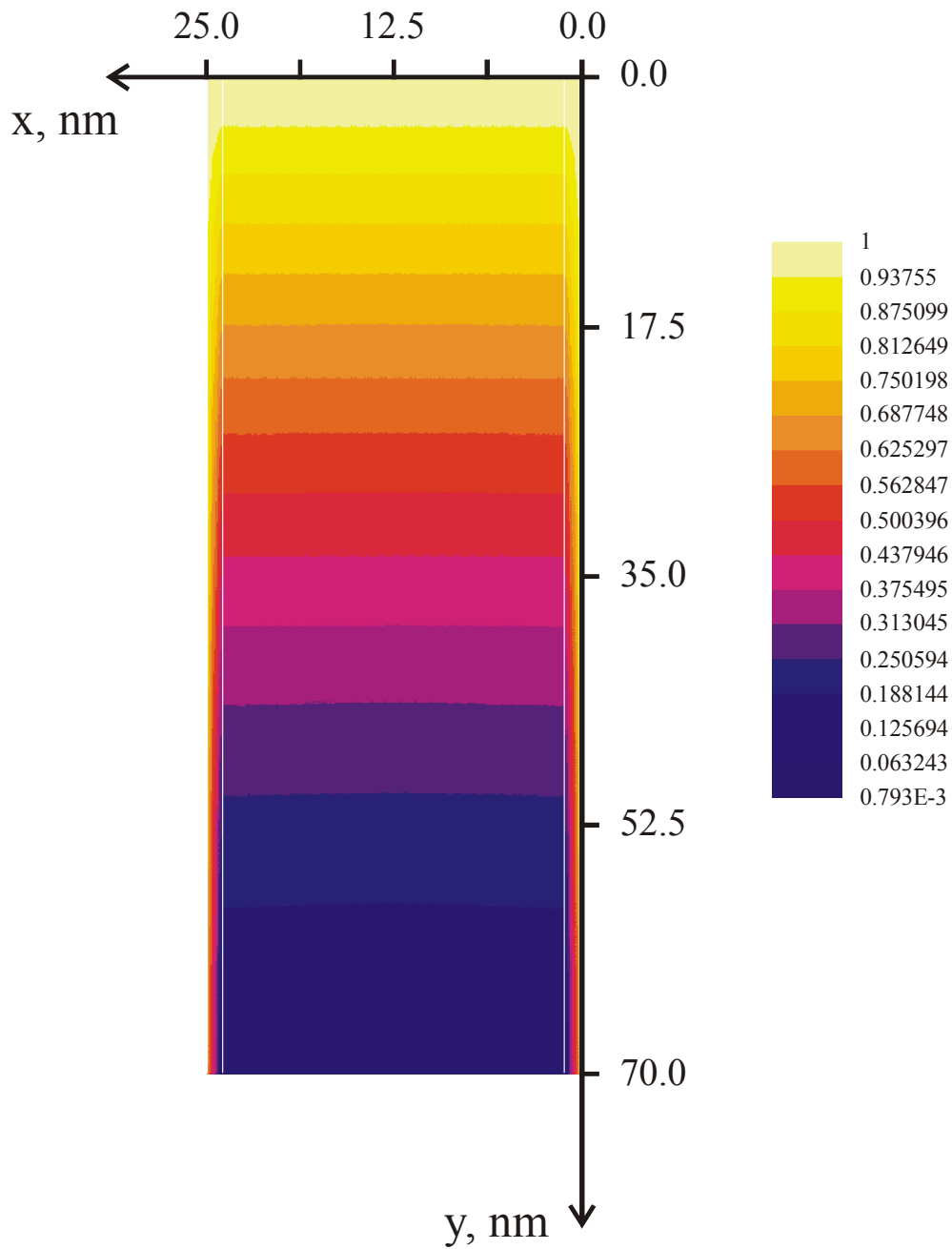


Fig. 5.16 Concentration distribution in the model of parallel boundaries at $t = 3 \cdot 10^6$ s. The GBs are used at $x = 0.0$ and 25.0 nm, whereas white lines correspond to the SCL/grain interface.

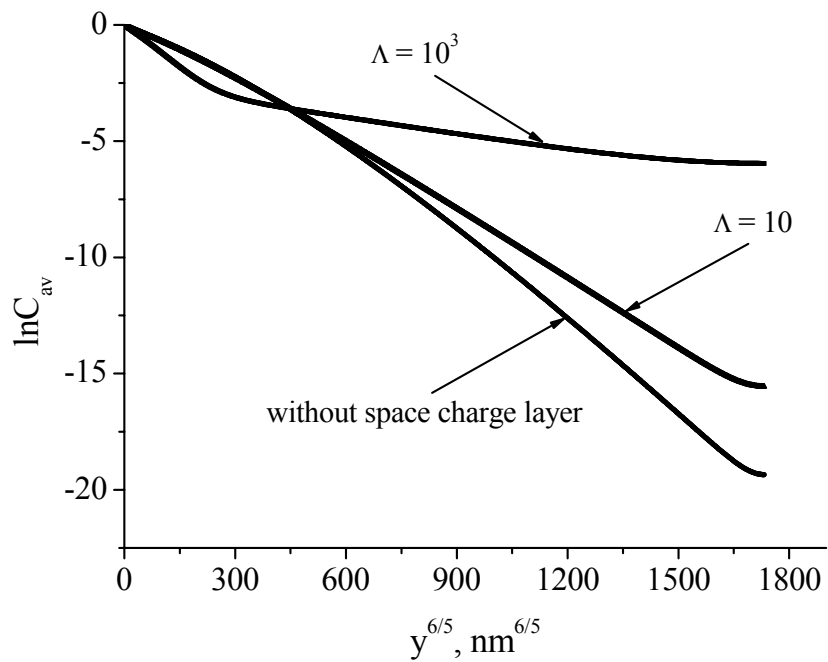


Fig. 5.17 Variation of $\ln C_{av}$ with $y^{6/5}$ calculated for $\Lambda = 10^3$ and $\Lambda = 10$. The diffusion profiles are compared with that without SCL at $t = 3 \cdot 10^6$ s. The ratio Δ is 10^2 .

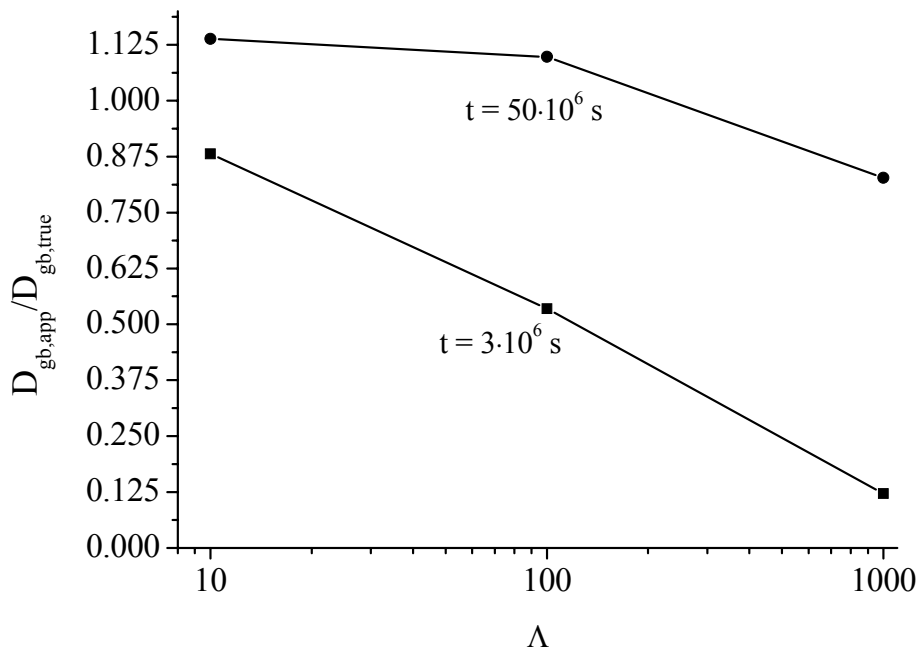


Fig. 5.18 Errors in determining D_{gb} by using conventional Hart's equation.

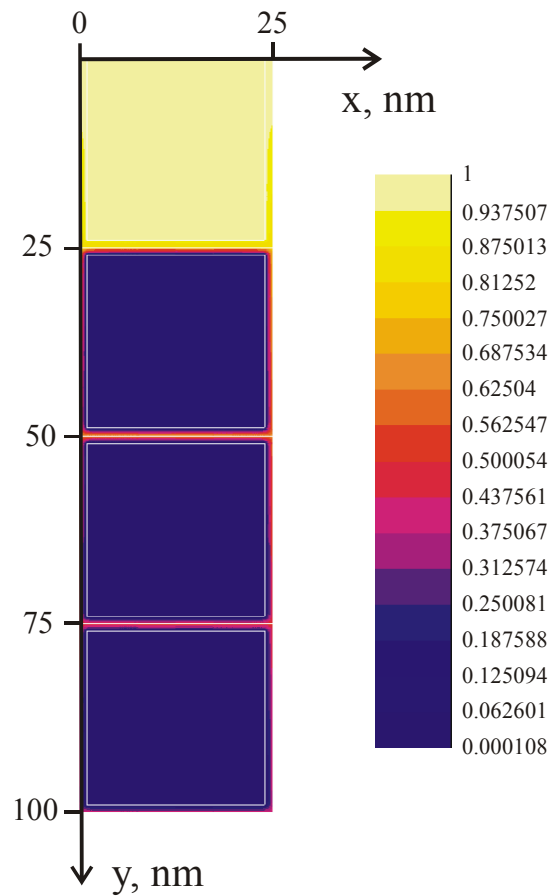


Fig. 5.19 A fragment of the concentration distribution in the model of square grains at $t = 3 \cdot 10^6$ s. The parameters used are the same as in fig. 5.16. The GBs are situated at $x = 0.0$ and 25.0 nm, $y = 25, 50, 75$ and 100 nm.

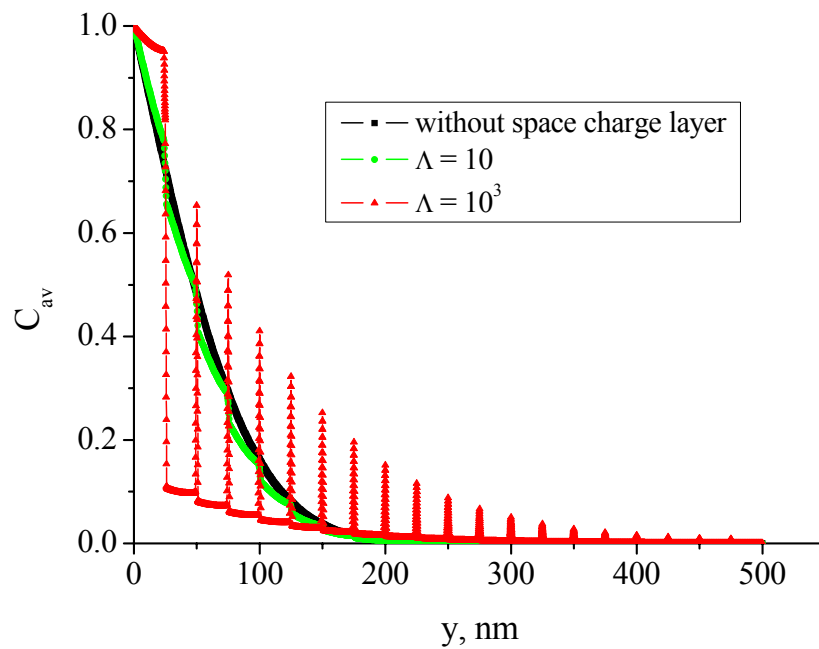


Fig. 5.20 Variation of C_{av} with y calculated at $t = 3 \cdot 10^6$ s for different Λ .

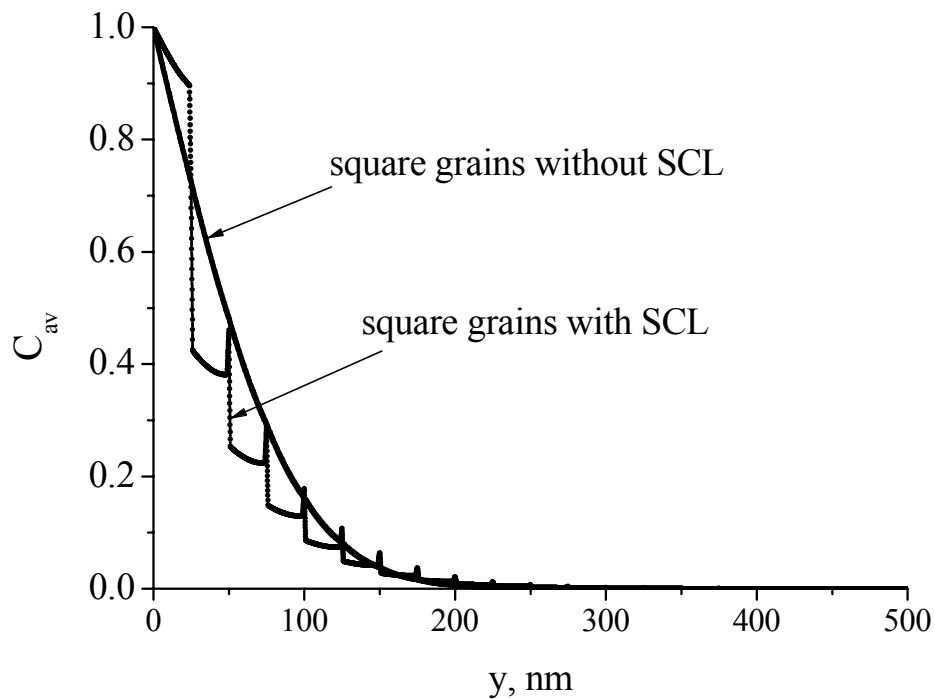


Fig. 5.21 Variation of the diffusion profiles with y calculated for $\Lambda = 10^2$ and $\Delta = 10^2$ at $t = 3 \cdot 10^6$ s are compared with the model without the SCL.

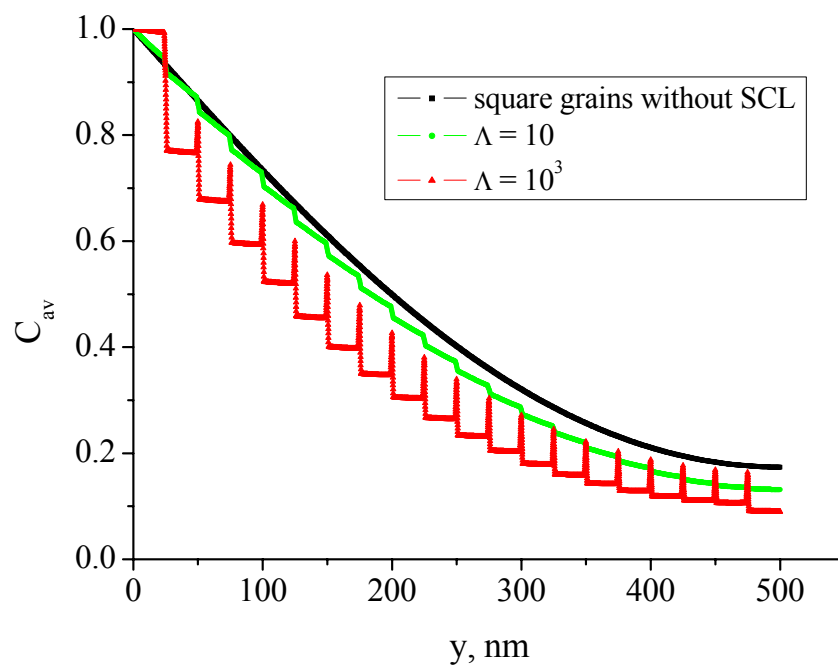


Fig. 5.22 Variation of C_{av} with y calculated for $\Lambda = 10^3$ and $\Lambda = 10$ in the model of square grains. The profiles are compared with that for the model of square grains without SCL for $\Delta = 10^2$ at $t = 50 \cdot 10^6$ s.

Summary

The effects of blocking SCLs were analyzed by simulating the diffusion profiles by means of the finite element approach. The kinetic regimes of type-A and -B were considered and the models of square grains and parallel boundaries applied. A very strong contribution of blocking effects was observed in both the kinetic regimes. This means that space charge effects should definitely be taken into account when deducing D_{gb} from the diffusion profiles measured in ionic materials. In the B-regime D_{gb} is overestimated, and the error increases with the ratio $\Lambda = D_g/D_{scl}$. Importantly, a relation is suggested to find the ratio D_{gb}/D_{scl} from the slopes measured in the B-regime on the basis of equations derived in chapter III. It is proposed how to find D_{gb} by using these new relations. In the A-regime D_{gb} is typically underestimated, and the errors increase with decreasing diffusion time. Again the use of a newly proposed procedure reduced the errors. This confirms the importance of those equations.

Strong concentration drops were observed in microstructure, what is also consistent with the experimental findings. In these cases the main suggestion is to analyze the diffusion profiles close to the surface.

Conclusions

I. In this dissertation diffusion in polycrystalline materials was studied under conditions of short diffusion times and, as a consequence, high concentration gradients in the type-B kinetics. The conventional models were tested for such conditions against the calculated diffusion profiles, in order to estimate corresponding errors in the evaluation of the grain boundary (GB) diffusivities (D_{gb}) as well to develop improved evaluation procedures. It was found that:

1) The application of Le Claire's method (Eq. (1.16)) can lead to substantial errors, when applied to the calculated diffusion profiles.

2) One reason for the large errors is related to the nonlinearity of diffusion profiles in $\ln C_{av} = f(y^{6/5})$ plot, where C_{av} is the average concentration measured by one of the depth profiling methods and y is the penetration depth. An improved procedure is proposed for using Le Claire's relation:

Conclusions

- a) *The derivative of the diffusion profile should be plotted, in order to estimate the effect of profile nonlinearity.*
- b) *The maximum value of the derivative should be used instead of fitting the profile to a straight line.*

3) If Le Claire's method is to be applied, the derivative $\partial \ln C_{av} / \partial w^{6/5}$ should not be necessarily constant (w is the dimensionless coordinate) depending on the dimensionless parameter α (Eq. (1.9d)). Consequently, Le Claire's constant should be replaced by an improved value calculated by the following relation, giving the maximum value of $\partial \ln C_{av} / \partial w^{6/5}$ at fixed diffusion time:

$$\left(\frac{\partial \ln C_{av}}{\partial w^{6/5}} \right)_{\max} = -0.77 - 0.71\alpha .$$

The dimensionless parameter α (Eq. (1.9d)) should be larger than 0.02, otherwise Le Claire's constant (≈ 0.78) may be safely used. This parameter can be easily estimated in the experiment, if the grain diffusivity (D_g) and the GB thickness (δ) are known.

4) For the dependence of the position of the maximum of the derivative $\partial \ln C_{av} / \partial y^{6/5}$ on the diffusion time the following empirical expression was found

$$y_{\max}^{6/5} = K \cdot t^H ,$$

where H is around 0.60, K is a function of grain diffusivity (D_g) and D_{gb} and t the diffusion time. The expression requires the condition $\beta > 10$ (Eq. (1.9d)) to be fulfilled.

5) The maximum value of the derivative $\partial \ln C_{av} / \partial y^{6/5}$ can be found by using the following expression

$$\left| \frac{\partial \ln C_{av}}{\partial y^{6/5}} \right|_{\max} = C \cdot \Delta^F \cdot t^B ,$$

where the ratio of diffusivities Δ equals D_{gb}/D_g , C depends on diffusion time and D_g , B and F are almost constants and given by -0.61 and -0.34 , respectively.

Conclusions

II. The conventional models ignore the GBs orientations with respect to the diffusion direction. Realistic microcrystalline structures were used, in order to estimate these effects. For this purpose three general geometrical models were developed which are directly comparable with the popular model of square grains and parallel boundaries. It was observed that the relevant effects manifest themselves:

1) Steeper diffusion profiles with concentrations smaller than compared to the situation when only parallel GB diffusion paths are present. Consequently,

This increases the slope of the diffusion profile with decreasing grain sizes, and, as a result of this, the use of Le Claire's relation underestimates D_{gb} .

2) General geometries with similar numbers of perpendicular and parallel paths are very well comparable with the model of square grains. Consequently,

This makes the model of square grains as a good approximation of the polycrystalline microstructure also for instationary diffusion.

3) Negligible role of perpendicular GB diffusion paths in the model of square grains, if the diffusion time increase guarantees the A-regime of diffusion. Consequently,

It was observed that the concentration profiles in both the model of parallel boundaries and the model of square grains almost coincide at very long diffusion times.

Additionally, the effects of impurity segregation were taken into account when analyzing diffusion in realistic microstructures. Very small and very large segregation coefficients (s) were used, allowing the conventional equations to be compared for different situations. The following conclusions were made:

1) The Hart-Mortlock (Eq. (1.17b)) equation is not valid when deducing D_{gb} with s larger than 20 even in the model of parallel boundaries. The use of this equation gives increasing errors with s . For example, errors of the order of 90% can be observed for $s = 160 - 640$.

Conclusions

2) The Hart-Mortlock equation is correct for finding D_{gb} in the model of square grains, if the volume (area) fraction of GBs is taken as it is in the model of parallel boundaries, and segregation is negligible. This conclusion refers to the negligible role of perpendicular GB diffusion paths at long diffusion times.

3) The Maxwell-Garnett type equation (Eq. (1.18b)) for segregation is not valid in the model of parallel boundaries under conditions of strong segregations and may be only applied in the model of square grains. Consequently,

Inappropriate use of the Maxwell-Garnett type equation increases the errors of finding D_{gb} . The error increases with s and can reach 90% and larger for $s \geq 640$.

III. The existence of depleted space charge layers (SCL) in ionic materials was taken into account. A special model was proposed in which constant space charge layer diffusivity (D_{scl}) is introduced. The diffusion profiles were simulated by the finite element method in the B- as well as A-regime varying the ratio $\Lambda = D_g/D_{scl}$. The main results are summarized in the following:

1) The depleted space charge layer leads to diffusion profiles with slopes different from those without space charge layers. Namely, the slope of the profile decreases with the ratio $\Lambda = D_g/D_{scl}$. Consequently,

The conventional Le Claire relation (Eq. (1.16)) overestimates D_{gb} by a factor of 6, if $\Lambda = 10^3$ at very short diffusion times.

2) The maximum of the derivative of the profile measured in the B-regime is determined by the transport process between the GB and SCL. Using the new equation for the maximum (Eq. (2.7) or I.5) of the derivative allows the ratio D_{gb}/D_{scl} to be obtained and, as a result of this, D_{gb} according to modified original Le Claire's relation (Eq. (1.14))

$$D_{gb,app} = \frac{4}{(D_{gb}/D_{scl}) t \delta^2} \left(-\frac{\partial \ln C_{av}}{\partial w^{6/5}} \right)^{10/3} \left(-\frac{\partial \ln C_{av}}{\partial y^{6/5}} \right)^{-10/3},$$

where $\partial \ln C_{av} / \partial w^{6/5}$ is determined by Eq. (1.14) or is -0.78 depending on α (see also I.3).

Conclusions

3) The kinetic regimes are shifted in time if the blocking space charge effects play a role. In this case, the diffusion profiles should be plotted in nonlinear scale according to $\ln C_{av} = f(y^{6/5})$ even if the nominal A-regime conditions are satisfied, in order to qualitatively estimate the effect of blocking SCLs. Consequently,

In the nominal A-regime strongly blocking SCLs may lead to a severe underestimation of D_{gb} by using a conventional analysis.

4) The role of perpendicular GB paths increases, if these are surrounded by blocking space charge regions. Consequently,

a) Crossing GBs with SCLs lead to the drop and significant decrease of concentration in the model of square grains.

b) Crossing GBs (square grains) with SCLs lead to further blocking effects and even for long diffusion times (nominal A-regime) modified profiles with two distinguishable parts and varying slopes may result.

IV. Moreover, along with the computer calculations, a procedure was developed for proper simulations of diffusion in polycrystalline materials by means of the finite element method. The procedure considers simulation of diffusion in a semi-infinite solid and the main aspects are summarized as follows:

1) Simulating diffusion in the B-regime, a special attention should be paid to the finite element mesh. Consequently,

a) The derivatives of diffusion profiles can be calculated for different mesh densities, in order to find the optimal mesh with respect to the initial time and the diffusion times of interest.

b) The denser mesh the shorter diffusion times for which profiles can be obtained.

2) The derivatives allow one also to estimate the effect of the boundary at the bottom of the geometrical model (sample) used, e.g., the condition of zero flux. Consequently,

Conclusions

If the maximum of the profile is not distinguishable, the length of the geometrical model should be increased and, if necessary, the density of mesh should be decreased.

3) The length of the geometrical model should be at least $4\sqrt{D_{\text{eff}}t}$ (D_{eff} is the effective diffusivity which reflects the homogeneous character of diffusion in the A-regime and can be obtained by using the Hart or Maxwell-Garnett equation) for properly simulating the diffusion profiles in the A-regime, otherwise the effect of the boundary condition becomes significant.

4) The simulation mesh density in the A-regime can be significantly reduced in comparison with the B-regime. However, the time increment can be increased. It means that some adaptive procedure with respect to the time increment is useful when simulating the diffusion profiles in the B-regime and A-regime simultaneously.

Kurzfassung der Dissertation in deutscher Sprache

1. Einführung

Viele anorganische Materialien in der Natur wie auch in technischen Anwendungen sind polykristallin. Die Struktur und die Chemie der Korngrenzen in den Materialien unterscheiden sich von Volumeneigenschaften, was die Ursache veränderter Transporteigenschaften der Korngrenzen ist. Erhöhte Diffusionskoeffizienten längs der Korngrenze erweisen sich als sehr relevant für die Anwendungen in vielen polykristallinen Materialien. Die Bedeutung der Korngrenzen erhöht sich weiter, wenn nanokristalline Materialien mit hoher Grenzflächendichte betrachtet werden. So befasst sich eine große Anzahl von experimentellen Arbeiten mit der Messung von erhöhten Korngrenzendiffusionskoeffizienten sowohl in Metallen als auch in keramischen Materialien.

Viele dieser Messungen beruhen auf der Bestimmung des Diffusionsprofils bei verschiedenen Temperaturen und/oder Zeiten. Das gemessene Profil spiegelt gewöhnlich die mittlere Diffusantkonzentration C_{av} parallel zur Oberfläche als Funktion der Eindringtiefe wider und kann zum Beispiel durch die Methode der Sekundärionen-Massenspektroskopie (SIMS) bestimmt werden. Je nach experimentellen Bedingungen existieren verschiedene Gleichungen, um den Diffusionskoeffizient der Korngrenze (D_{gb}) aus diesen Profilen zu bestimmen [Mis97]. Das bekannteste Modell nach Harrison [Harr61] betrachtet drei idealisierte Typen der Korngrenzdifffusion, die mit Typ A, Typ B und Typ C bezeichnet werden. In dieser Klassifikation bestimmt die Diffusionslänge im Volumen (oder innerhalb eines Kornes) $L_g = \sqrt{D_g t}$ die Kinetik, hierbei bezeichnet D_g den Diffusionskoeffizient im Korn. Im Bereich der Typ-B-Kinetik ist die Diffusionslänge L_g größer als die Korngrenzdicke (δ), aber viel kleiner als die durchschnittliche Korngröße (d). In diesem Fall kann Diffusion in einem polykristallinen Material in erster Näherung durch die Modellgeometrie, die in Bild 1 dargestellt ist, beschrieben werden, d.h. durch eine isolierte Korngrenze senkrecht zur Oberfläche.

Fisher [Fis51] hat ein erstes analytisches Modell, das die Korngrenzdifffusion beschreibt und als Fishers Modell bekannt ist, veröffentlicht und auch eine annähernde Lösung vorgeschlagen. Seitdem versuchten viele Autoren, die Bestimmung der Diffusionskoeffizienten der Korngrenzen ausgehend von experimentellen Daten zu verbessern. Whipple [Whi54] hat eine exakte analytische Lösung des Fisher-Modells gefunden, die eine Integralform aufweist. Le Claire [Cla63] hat auf Grund der Erkenntnisse von Levine und MacCallum [Lev60] gezeigt, dass das Produkt δD_{gb} für bekannte D_g und δ aus dem Konzentrationsprofil gefunden werden kann. Das Le Claire-Modell wird in zahlreichen Experimenten benutzt, um Diffusionsprofile zu analysieren. Allerdings wird meist die Hauptnäherung des Le Claire-Modells nicht überprüft, insbesondere erweist sich ein konstanter Koeffizient, der von Le Claire eingeführt worden ist, für kleine Körner als kritisch. Die Le Claire-Gleichung lautet [Cla63]

$$\delta D_{gb} = 1.322 \sqrt{\frac{D_g}{t}} \left(-\frac{\partial \ln C_{av}}{\partial y^{6/5}} \right)^{-5/3} . \quad (1)$$

Abgesehen von Problemen bezüglich des Modells der isolierten Korngrenze existieren auch Fälle, die für nanokristallinen Materialien charakteristisch sind, in denen $L_{gb} \gg d$. Mishin [Mis95] hat zusätzliche kinetische Regimes eingeführt, in denen diese Bedingungen

berücksichtigen werden. Unter diesen Bedingungen kann die Korngrenzorientierung in Bezug auf Diffusionsrichtung eine wichtige Rolle spielen. In dieser Arbeit wurden realistische Geometrien der polykristallinen Struktur erörtert: ein Modell quadratischer Körner und so genannte Modelle mit allgemeiner Geometrie, die in Bild 2 und Bild 3 dargestellt werden. Ergebnisse der Diffusionssimulation mit diesen Modellen wurden mit Ergebnissen verglichen, die mit dem Modell paralleler Korngrenzen erhalten wurden. Die Diffusionszeit (t) wurde so variiert, dass eindeutig Typ B oder Typ A vorlag. In den Fällen des Typs B ($d \gg L_g \gg \delta$) wurde Le Claires Gleichung (1) angewendet, aber in den Fällen des Typs A ($L_g \gg d$) konnte nur ein effektiven Diffusionskoeffizient (D_{eff}) experimentell gefunden werden. In diesem Fall ließ sich D_{gb} durch die Anwendung der Hart-Gleichung [Hart57]

$$D_{\text{eff}} = gD_{\text{gb}} + (1-g)D_g \quad (2)$$

erhalten, wenn der Volumenanteil (oder Flächenanteil) der Korngrenzen (g) und D_g bekannt war. Für Störstellendiffusion musste die Hart-Gleichung durch die Hart-Mortlock-Gleichung ersetzt werden [Mor60]:

$$D_{\text{eff}} = sgD_{\text{gb}} + (1-sg)D_g \quad (3)$$

Hierbei muss der Segregationskoeffizient (s) bekannt sein, um D_{gb} zu finden. Vor kurzem wurde bereits gezeigt, dass die Hart-Gleichung (und damit auch die Hart-Mortlock-Gleichung) bei vergrößertem g und/oder s zu Fehlern führt [Bel03]. In diesem Fall ist es besser, die Maxwell-Garnett-Gleichung [MaxG04]

$$D_{\text{eff}} = \frac{sD_{\text{gb}} \left[(2-g)D_g + sgD_{\text{gb}} \right]}{(1-g+sg) \left[sD_{\text{gb}}(2-g) + gD_g \right]} \quad (4)$$

zu benutzen. Die Gründe, weswegen die Hart-Gleichung zu Fehlern führen kann, waren nicht sorgfältig untersucht worden, deshalb werden sie in dieser Arbeit besprochen.

Historisch wurde die grundlegende Diffusionstheorie der Korngrenzen für metallische Systeme entwickelt. Le Claires und Harts Gleichungen wurden für die Bestimmung der Korngrenz-Diffusionskoeffizienten sowohl in Metallen als auch in ionischen Materialien benutzt. Man muss jedoch in Betracht ziehen, dass sich die Korngreneigenschaften der

Materialien unterscheiden. Wegen der ionischen Natur der Bindung und der Anwesenheit geladener Teilchen in den betrachteten Materialien sind Korngrenzen im Allgemeinen geladen (z.B. durch geladene Leerstellen, die an Korngrenzen adsorbiert sind). Um insgesamt die Elektroneutralität im Material zu gewährleisten, bildet sich eine Raumladungszone in der Nähe der Korngrenzen aus. Die Eigenschaften des Materials in diesem Bereich unterscheiden sich von den Volumen- und Korngreneigenschaften. Das führte zur Notwendigkeit, die veränderten Transporteigenschaften in diesem Bereich zu berücksichtigen und einen neuen Diffusionskoeffizienten D_{scl} , s. z. B. [Yan77], einzuführen. Diffusionsprofile wurden mit den Modellen paralleler Korngrenzen und quadratischer Körner für unterschiedliche Verhältnisse $\Lambda = D_g/D_{scl}$ modelliert. Große Aufmerksamkeit wird Bedingungen geschenkt, unter der $\Lambda > 1$, d. h. $D_{scl} < D_g$ ist. Dies wird durch Korngrenzen, die an beweglichen Ladungsträgern verarmt sind, realisiert, wobei die Korngrenze aus Kernbereich und aus Raumladungsbereich besteht [Jam97] (dabei wird der Diffusionskoeffizient im Raumladungsbereich als unabhängig von der Ortskoordinate angenommen). Solche Korngrenzen kommen in ZrO_2 oder $SrTiO_3$ vor und verringern in hohem Maße die Leitfähigkeit der Materialien [Gou01a], [Gou01b]. In dieser Arbeit wurde diskutiert, zu welchen Veränderungen das Vorhandensein eines Bereichs mit einem im Vergleich zum Volumen verringerten Diffusionskoeffizient führt.

2. Physikalische und geometrische Modelle, die in der numerischen Untersuchung benutzt wurden

Wie schon erwähnt, hat Fisher das erste Modell der Korngrenzdifffusion vorgeschlagen, das bis heute ein Standardmodell ist. In diesem Modell wurde die Korngrenze als ideale isolierter Schicht, die senkrecht zur Oberfläche orientiert ist, dargestellt (Bild 1). Die Diffusionskoeffizienten D_g und D_{gb} werden von der Zeit, Konzentration und/oder Koordinaten unabhängig angenommen. An der freien Oberfläche befindet sich eine Diffusionsquelle. In der Arbeit wird nur der Fall einer unerschöpflichen Diffusionsquelle betrachtet. Außerdem wird hier ein halbunendliches System betrachtet. Die Diffusion im

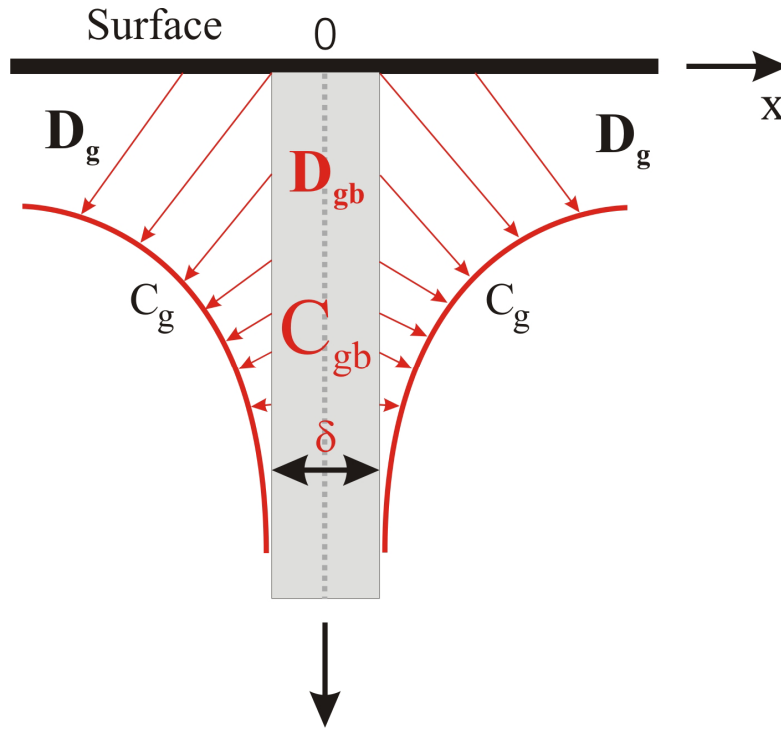


Bild 1 Isolierte Korngrenze.

Fisher-Modell kann mit zwei Diffusionsgleichungen beschrieben werden, d. h. mit den Fickschen Gleichungen unter folgenden Randbedingungen:

$$\begin{cases} C_g(x, y, t) = C_{gb}(x, y, t) \\ J_g(x, y, t) = J_{gb}(x, y, t) \end{cases}, \quad |x| = \delta/2. \quad (5)$$

Diese Randbedingungen stellen Gleichgewichtsbedingungen des Diffusionsverlaufs an der Grenzfläche zwischen zwei unterschiedlichen Phasen dar. Das Gleichungssystem kann jedoch nicht analytisch gelöst werden. Wenn man die Konzentration in der Korngrenze durch eine Taylor-Reihe, bezogen auf $x = 0$, ausdrückt und wenn man Glieder höherer Ordnung (d. h. $n \geq 3$) vernachlässigt, kann man das Gleichungssystem auf folgende Weise umschreiben [Kau95]:

$$\begin{cases} \frac{\partial C_g(x, y, t)}{\partial t} = D_g \left(\frac{\partial^2 C_g(x, y, t)}{\partial x^2} + \frac{\partial^2 C_g(x, y, t)}{\partial y^2} \right), & |x| \geq \delta/2 \\ \frac{\partial C_g(y, t)}{\partial t} = D_{gb} \frac{\partial^2 C_{gb}(y, t)}{\partial y^2} + \frac{2D_g}{\delta} \frac{\partial C_g(y, t)}{\partial x}, & |x| = \delta/2 \end{cases} \quad (6)$$

Die zweite Gleichung, die die Korngrenze beschreibt, ist die Randbedingung der ersten Gleichung; die Vernachlässigung der Korngrenzenkonzentration und der Korngrenzendicke wurden berücksichtigt. Die analytische Lösung dieses Gleichungssystems wurde von Whipple für eine unendliche Quelle vorgestellt [Whi54]:

$$C_g(\eta, \xi, \beta) = C_0 \operatorname{erfc}\left(\frac{\eta}{2}\right) + \frac{C_0 \eta}{2\pi^{1/2}} \int_1^{\Delta} \frac{d\sigma}{\sigma^{3/2}} \exp\left(-\frac{\eta^2}{4\sigma}\right) \operatorname{erfc}\left[\frac{1}{2}\left(\frac{\Delta-1}{\Delta-\sigma}\right)\left(\frac{\sigma-1}{\beta} + |\xi|\right)\right], \quad (7)$$

mit $\Delta = D_{gb}/D_g$. Die numerische Integration der Whipple-Lösung wurde mit Hilfe der Programmiersprache „MatLab“ ausgeführt, die numerische Integration des Gleichungssystems (6) durch die Finite-Element-Methode wurde für komplizierte geometrische und physikalische Modelle in dieser Arbeit benutzt, um die Effekte auf kleinen Längenskalen zu analysieren.

Das Gleichungssystem (6) muss umgeschrieben werden, wenn Fremdstoffdiffusion modelliert wird. Dabei ist es notwendig, die folgende Randbedingung zu berücksichtigen:

$$C_{gb}(x = \pm\delta/2, y, t) = sC_g(x = \pm\delta/2, y, t),$$

mit s - Segregationskoeffizient. Dann wird das System von Fisher umgeformt [Gib66]:

$$\begin{cases} \frac{\partial C_g(x, y, t)}{\partial t} = D_g \left(\frac{\partial^2 C_g(x, y, t)}{\partial x^2} + \frac{\partial^2 C_g(x, y, t)}{\partial y^2} \right), & x \geq \delta/2 \\ \frac{\partial C_g(y, t)}{\partial t} = D_{gb} \frac{\partial^2 C_{gb}(y, t)}{\partial y^2} + \frac{2D_g}{s\delta} \frac{\partial C_g(y, t)}{\partial x}, & |x| = \delta/2 \end{cases} \quad (8)$$

Das oben genannte Gleichungssystem wurde für Modellierung mit parallelen Korngrenzen und mit quadratischen Körnern nur im Diffusionsregime vom Typ A benutzt. In dieser Modellierung ist der Abstand zwischen den parallelen Korngrenzen, der gleich der Korngröße ist, $d = 10$ nm.

Es muss angemerkt werden, dass diese beiden Modelle (parallele Korngrenzen und quadratische Körner) die Standard-Mikrostrukturmodelle eines Polykristalls für die Modellierung sind, s. z. B. [Bel03]. Diese Modelle wurden für die Diffusionsanalyse sowohl im Typ B als auch im Typ A in Abwesenheit von Segregation benutzt. Ergebnisse im ersten Fall, die sich aus den Modellen ergaben, wurden mit realistischeren Mikrostrukturen (Bilder 3

und 4) verglichen und Bestimmungsfehler des Diffusionskoeffizienten D_{gb} abgeschätzt. Es ist wichtig festzustellen, dass die parallele Orientierung der Korngrenzen bei Herleitung der Hart-Gleichung angenommen wird [Hart57], [Bel03], im Fall der Maxwell-Gleichung jedoch kugelförmige Körner [Kal02].

Die Idee der Verwendung realistischer Mikrostrukturen bezieht sich drauf, dass in üblichen Korngrenzenmodellen angenommen wird, dass die Korngrenze parallel zur Diffusionsrichtung orientiert ist. Diese Näherung ist mit dem Wert des Parameters β verbunden, der den Sättigungsgrad des Diffusionsprozesses bestimmt. Das heißt, dass die Diffusion in nanokristallinen Materialien durch große Werte des Parameters β gekennzeichnet ist: große Werte β bedeuten tiefe Durchdringung. Dabei erhöht sich die Rolle der Korngrenzorientierung relativ zur Diffusionsrichtung.

Auf diese Weise ist das Modell der quadratische Körner die einfachste Näherung der Mikrostruktur. In dieser Arbeit wurden Diffusionsprofile für verschiedene Flächenanteile (g) modelliert, d. h. die durchschnittliche Korngröße variiert von 10 bis 100 nm.

Die Ergebnisse wurden mit dem Modell paralleler Korngrenzen sowohl im Typ B als auch im Typ A verglichen. Zusätzlich wurden für den Typ B drei so genannte allgemeine Modelle untersucht. Diese Modelle unterscheiden sich durch die Zahl der parallelen, senkrechten und sonstigen Korngrenzen. Das allgemeine Modell (Geometrie) 1 (Länge 250 nm, Breite 40 nm) umfasst 17 Korngrenzen (6 parallelen Korngrenzen, 11 sonstige); die durchschnittliche Korngröße im allgemeinen Modell 1 ist 30.5 nm.

Nummer des allgemeinen Modells	Zahl der parallelen Korngrenzen	Zahl der sonstigen Korngrenzen	Neigungswinkel in Grad	Durchschnittliche Korngröße
1	6	11	14 - 78.7	30.5
2	4	3	36 - 42	64
3	21	36	16 - 69.3	29.1

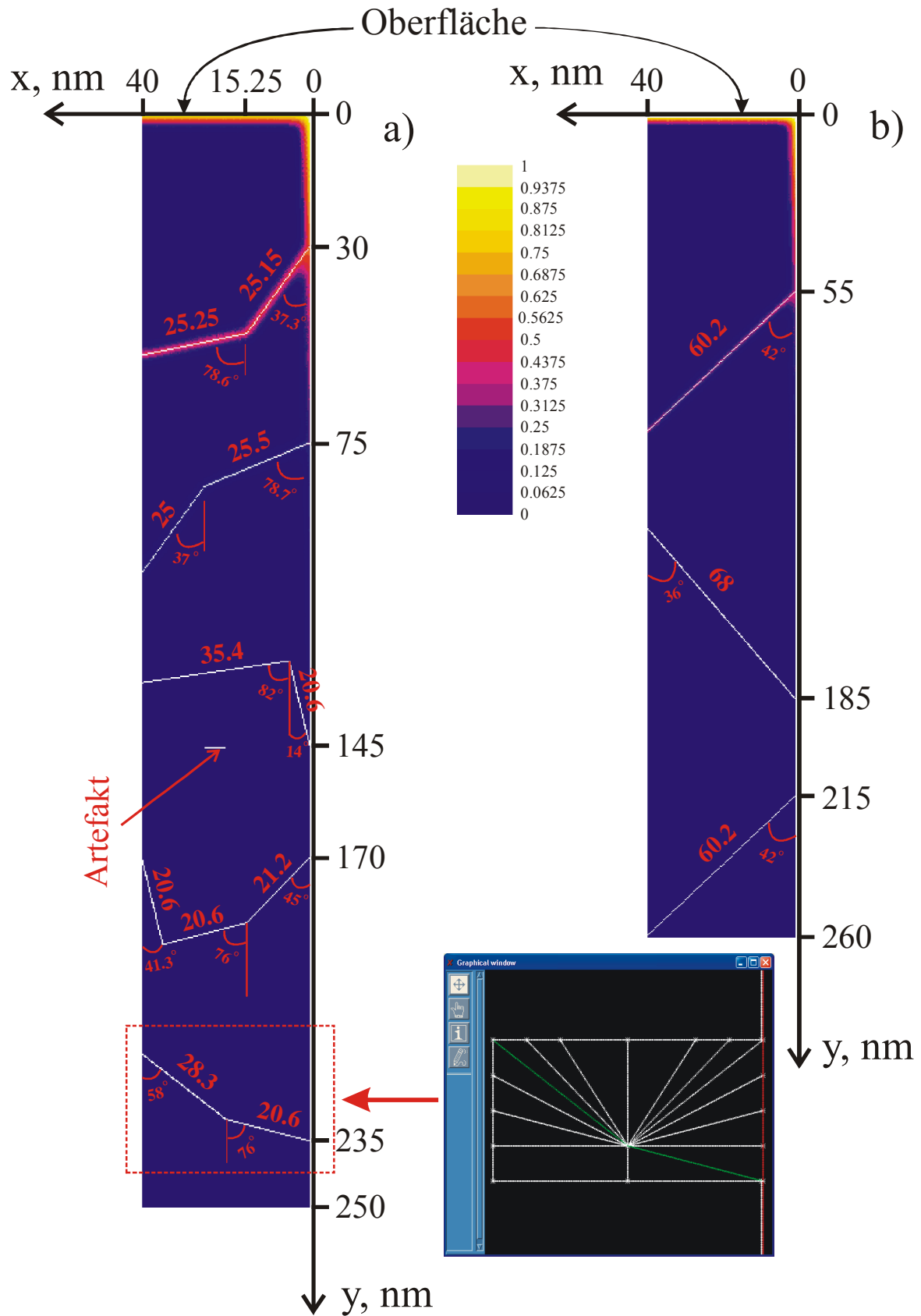


Bild 2 Allgemeines Modell 1 mit Konzentrationsverteilung (a) und allgemeines Modell 2 (b), in Farbe dargestellt. Alle weißen Linien sind Korngrenzen. Korngrenzenlängen und Neigungswinkel in Grad sind auch dargestellt.

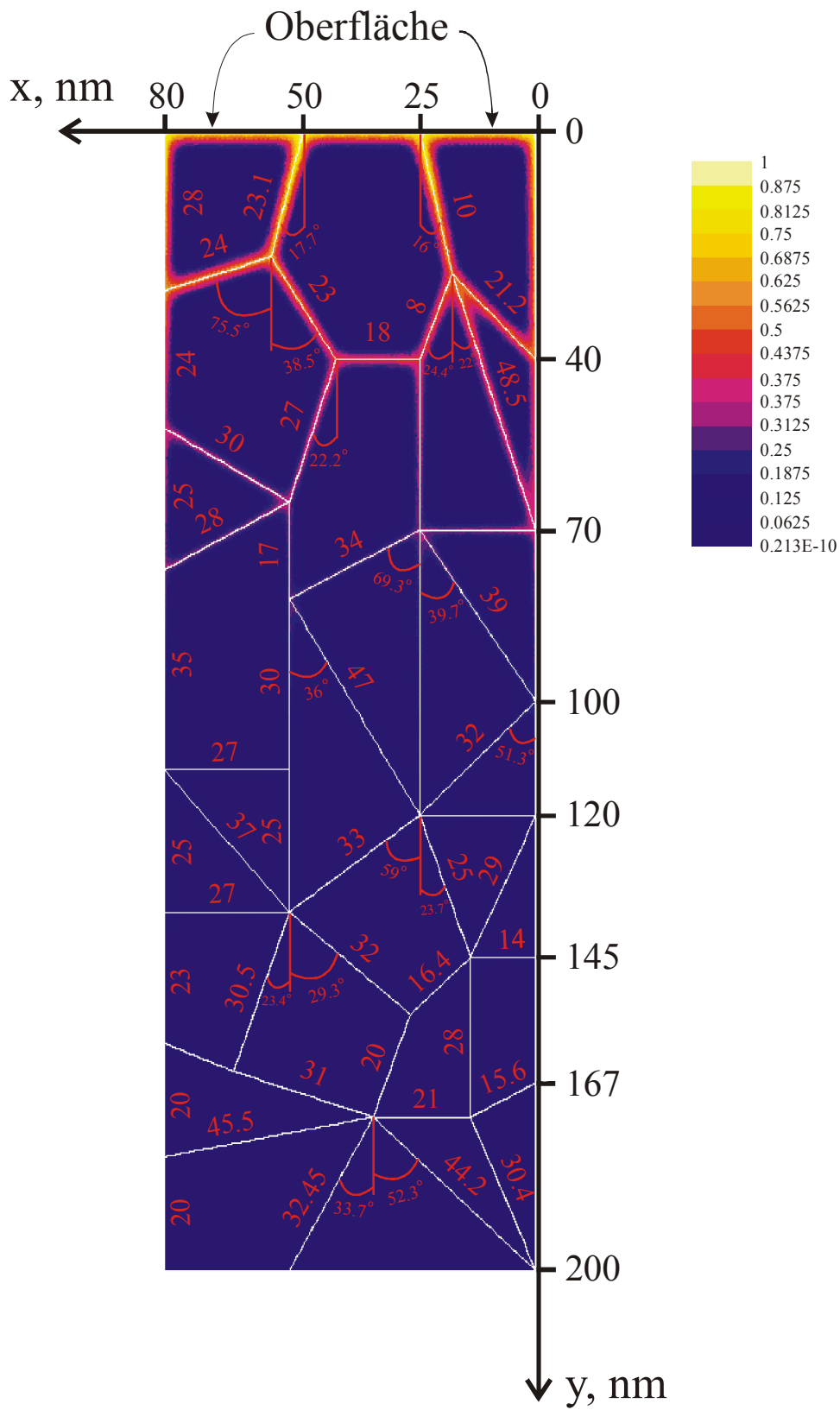


Bild 3 Die allgemeine Modell 3. Alle weißen Linien sind Korngrenzen. Korngrenzenlängen und Neigungswinkel in Grad sind auch dargestellt.

Die geometrischen Parameter der drei allgemeinen Modelle, die in dieser Arbeit benutzt wurden, sind in der Tabelle aufgeführt. Man sieht aus der Tabelle, dass zwei Modelle, nämlich Modell 1 und Modell 3, durch die gleiche durchschnittliche Korngröße aufweisen, aber sich stark in der Zahl der Korngrenzen und durch die Werte der Orientierungswinkel unterscheiden. Die durchschnittliche Korngröße wurde durch die Summe aller Korngrenzenlängen im Modell dividiert durch die Gesamtzahl der Korngrenzen abgeschätzt. Jedes Modell stellt ein Element dar, das dann in die Länge und/oder in die Breite gespiegelt wurde, um eine ausreichende Gesamtlänge der Geometrie zu gewährleisten.

3. Ergebnisse und Diskussion

3.1 Nichtlinearitätseffekt

Im Diffusionsregime vom Typ B wird der Diffusionskoeffizient D_{gb} durch das Le Claire – Verhältnis bestimmt, wenn der Diffusionskoeffizient D_g und die Korngrenzdicke bekannt sind. Das Verhältnis beruht darauf, dass die Abhängigkeit $\ln C_{av} = f(y^{6/5})$ (C_{av} ist eine Konzentration, die experimentell abgeschätzt) aus zwei Anteilen besteht: ein Volumenanteil (nahe an der Oberfläche) und ein Korngrenzanteil. Dabei soll der Korngrenzanteil des Profils eine lineare Funktion von $y^{6/5}$ sein. Es ist unmöglich, eine allgemeine lineare Beziehung aufzustellen. Dies ist eine Frage der Parameter und der Bedingungen. Es ist empirisch offensichtlich, dass der Korngrenzanteil mit der Abhängigkeit $\ln C_{av} = f(y^{6/5})$ bei hohen Diffusionstemperaturen und/oder bei langen Diffusionszeiten durch eine gerade Linie angenähert werden kann. In Nanomaterialien werden im Diffusionsregime vom Typ B sehr kurze Diffusionszeiten betrachtet. Dabei wird die Nichtlinearität des Korngrenzprofilanteils stärker ausgeprägt.

Die Diffusionsprofile wurden durch Integration der Whipple-Lösung (Gl. (3)) berechnet (das Verhältnis der Diffusionskoeffizienten Δ variiert von 10^2 bis 10^5 und die Diffusionszeit variiert von $2 \cdot 10^3$ s bis $1 \cdot 10^6$ s). Diese berechneten Profile wurden durch Gerade angenähert. Die erhaltenen Neigungswinkel können unmittelbar in die Le Claire-Gleichung eingesetzt werden und der Diffusionskoeffizient D_{gb} kann abgeschätzt werden. Die Anwendung der Le Claire-Lösung führt wegen der Nichtlinearität zu Fehlern in der Bestimmung von D_{gb} . In Bild 4 wird die Ableitung des Profils dargestellt, die für $\Delta = 2.2 \cdot 10^4$ und $t = 2000$ s berechnet wurde. Dieses Profil hat einen deutlich ausgeprägten

Nichtlinearitätseffekt. Die Fehler, die durch die Anwendung der Le Claire-Gleichung entstehen, werden in Abhängigkeit von der Zeit für unterschiedliche Verhältnisse Δ (schwarze Linie) in Bild 5 dargestellt. Es ist interessant, dass das Profil durch an Maximum charakterisiert ist. Dieses Maximum entspricht unmittelbar dem Diffusionsregime vom Typ B, während die Nichtlinearität des Profils durch die Veränderungen des Diffusionsregimes in der Tiefe y hervorgerufen wird. Die Fehler der Bestimmung von D_{gb} können erheblich verringert werden, indem die Maxima der Ableitung in der Le Claire-Gleichung (rote Linien in Bild 2) verwendet wurden.

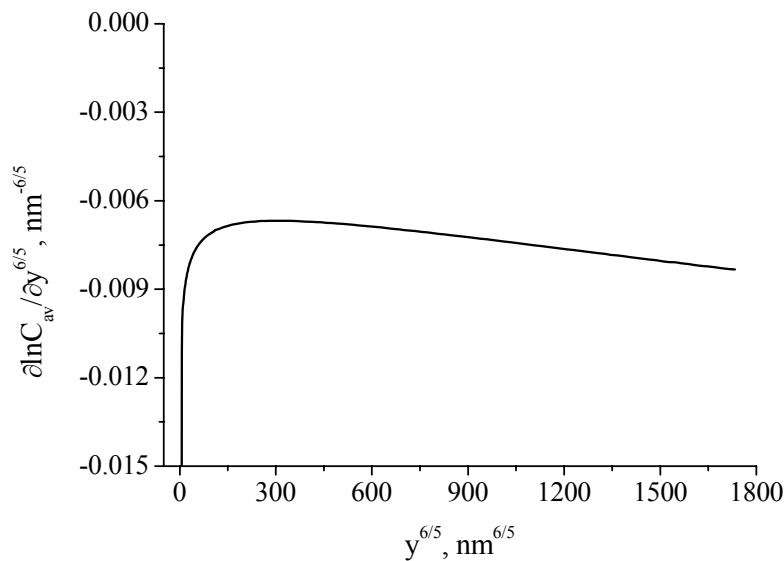


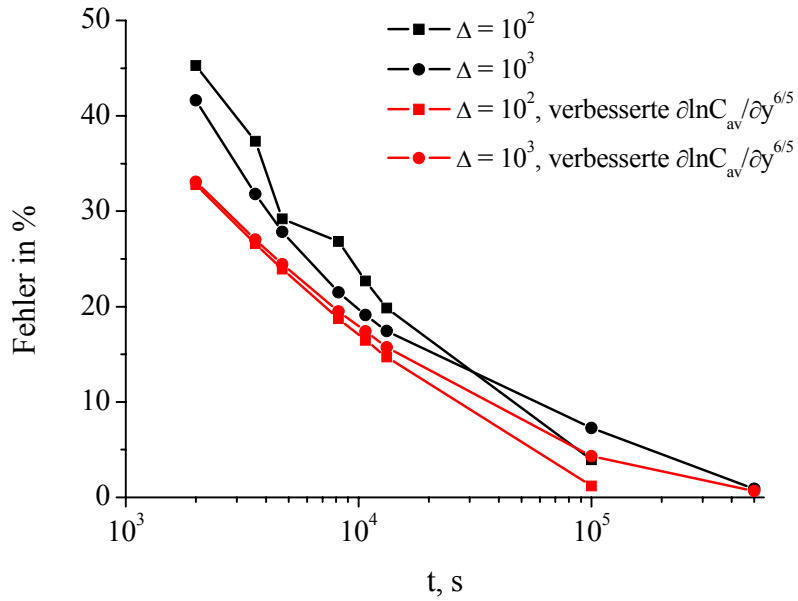
Bild 4 Ableitung des Profils: $\Delta = 2.2 \cdot 10^4$, $t = 2000$ s.

Die Fehler waren trotzdem erheblich, und sogar für $\Delta = 2.2 \cdot 10^4$, 10^5 erhöht sich der Fehler bei längeren Diffusionszeiten. Für die Analyse des Effekts muss berücksichtigt werden, dass die Konstante in der Le Claire-Gleichung dem Wert

$$1.322 = 2 \left(-\frac{\partial \ln C_{av}}{\partial w^{6/5}} \right)^{5/3} \Rightarrow \frac{\partial \ln C_{av}}{\partial w^{6/5}} = -0.78 \quad (9)$$

entspricht. Die Ableitung von $\ln C_{av}$ nach dem dimensionslosen Parameter w ist von Δ unabhängig, aber sie ist zeitabhängig. Nur bei sehr langen Zeiten wird diese Ableitung konstant. In Bild 6 wird ein Beispiel der Abhängigkeit $\partial \ln C_{av} / \partial w^{6/5} = f(w^{6/5})$ für $\Delta = 2.2 \cdot 10^4$ gezeigt. So führt die Anwendung der Konstanten 1.322 auch in Bild 5 zu Fehlern. Es wurde herausgefunden, dass die Maxima der Ableitung $\partial \ln C_{av} / \partial w^{6/5} = f(w^{6/5})$ vom dimensionslosen

a)



b)

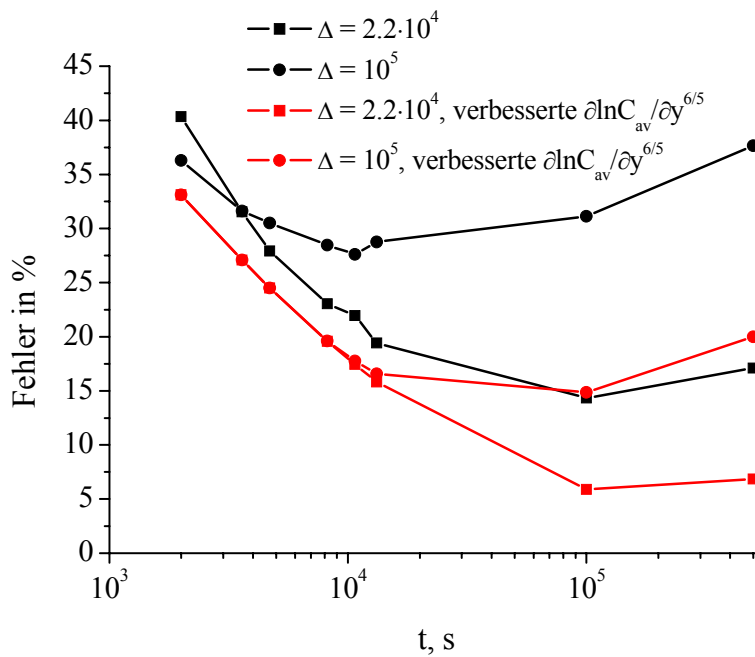


Bild 5 Bestimmungsfehler des Diffusionskoeffizienten D_{gb} für $\Delta = 10^2, 10^3$ a) und $\Delta = 2.2 \cdot 10^4, 10^5$ b).

Kurzfassung der Dissertation in deutscher Sprache

Parameter $\alpha = \delta/(2L_g)$ linear abhängig sind. Der folgende Ausdruck wird für eine genaue Bestimmung $\partial \ln C_{av} / \partial w^{6/5} = f(w^{6/5})$ vorgeschlagen:

$$\frac{\partial \ln C_{av}}{\partial w^{6/5}} = -0.77 - 0.71\alpha. \quad (10)$$

Außerdem ändert sich die Maximumlage der Abhängigkeit $\partial \ln C_{av} / \partial y^{6/5} = f(y^{6/5})$ mit der Zeit nach dem folgenden Potenzgesetz

$$y_{\max}^{6/5} = K \cdot t^H, \quad (11)$$

wobei K von den Diffusionsparametern abhängt. Schließlich können die Ableitungswerte im Maximum näherungsweise nach

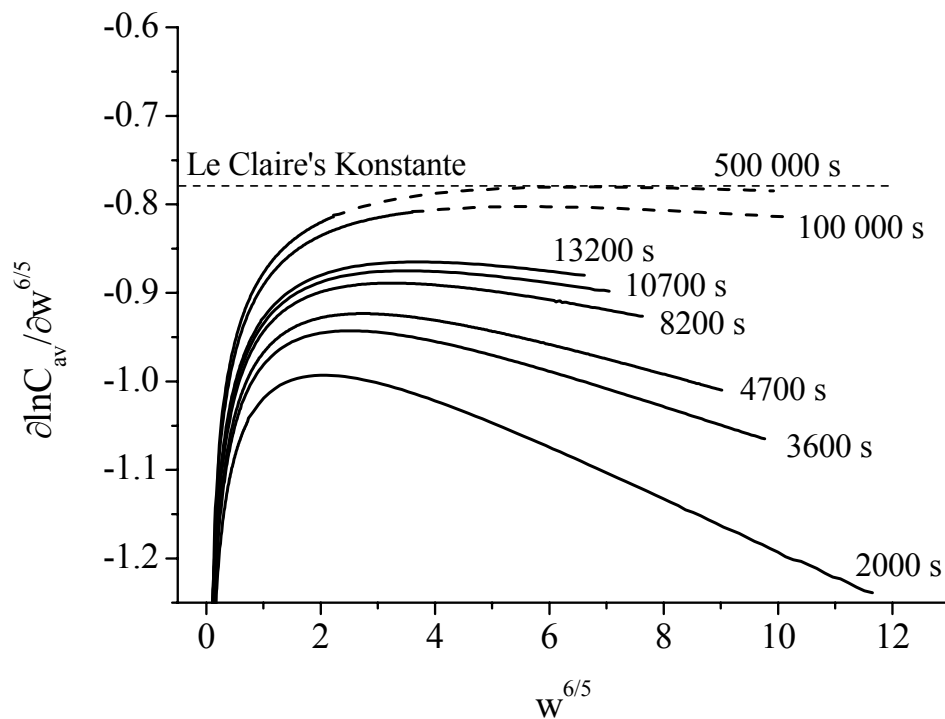


Bild 6 Ableitung von $\ln C_{av}$ nach dem dimensionslosen Parameter w bei fixiertem $\Delta = 2.2 \cdot 10^4$ für verschiedene Zeiten. Die durchgezogenen Linien entsprechen einer festen Geometrielänge von 500 nm. Die gepunkteten Linien entsprechen einer Längevergrößerung bis das Maximum erreicht.

$$\left| \frac{\partial \ln C_{av}}{\partial y^{6/5}} \right|_{\max} = C \cdot \Delta^F \cdot t^B, \quad (12)$$

bestimmt werden, wobei C ist Diffusionsparameter-Funktion und B den Wert -0.34 in einem breiten Bereich der Diffusionsparameter annehmen kann.

3.2 Realistische Mikrostrukturen

Sowohl das Diffusionsregime vom Typ B als auch das Diffusionsregime vom Typ A wurden für die Analyse des Orientierungseinflusses der Korngrenze relativ zur Diffusionsrichtung benutzt. Im Diffusionsregime vom Typ B wurden die Diffusionsprofile sowohl in allen drei allgemeinen Modellen (Tabelle) als auch im Modell quadratischer Körner berechnet. Die Verringerung der Korngröße im Modell quadratischer Körner führt zur Vergrößerung der Profilneigung (Bild 7). Der Diffusionskoeffizient D_{gb} kann durch die Anwendung der Le Claire-Gleichung unterschätzt werden. Wenn das allgemeine Mikrostrukturmodell eine stark unterschiedliche Zahl der parallelen und senkrechten Diffusionswege hat, können sowohl niedrige Konzentrationen als auch erhöhte Konzentrationen im Vergleich zum Modell quadratischer Körner entstehen. Diese Situation ist sehr schwer vorauszusagen. In Bild 8 werden die allgemeinen Modelle 1 und 3 mit dem entsprechenden Modell quadratischer Körner verglichen. Wenn die Zahl der Pfade miteinander vergleichbar ist, dann ist das Modell quadratischer Körner eine gute Näherung des Polykristalls.

Im Diffusionsregime vom Typ A wurden die Diffusionsprofile sowohl im Modell quadratischer Körner als auch im Modell paralleler Korngrenzen mit $d = 10$ nm modelliert. Der Segregationskoeffizient wurde von 5 bis 640 variiert. Sowohl die Hart-Mortlock-Gleichung (Gl. 3) als auch Maxwell-Garnett-Gleichung (Gl. 4) wurden mit der Modellierung verglichen. In Bild 9 werden die entsprechenden Ergebnisse gezeigt. Die Hart-Mortlock-Gleichung kann für die Bestimmung von D_{gb} nicht einmal für das Modell paralleler Korngrenzen verwendet werden, da sie zu Fehlern von 90 Prozent führt. Im Gegensatz dazu kann jedoch die Maxwell-Garnett-Gleichung für das Modell quadratischer Körner eingesetzt werden.

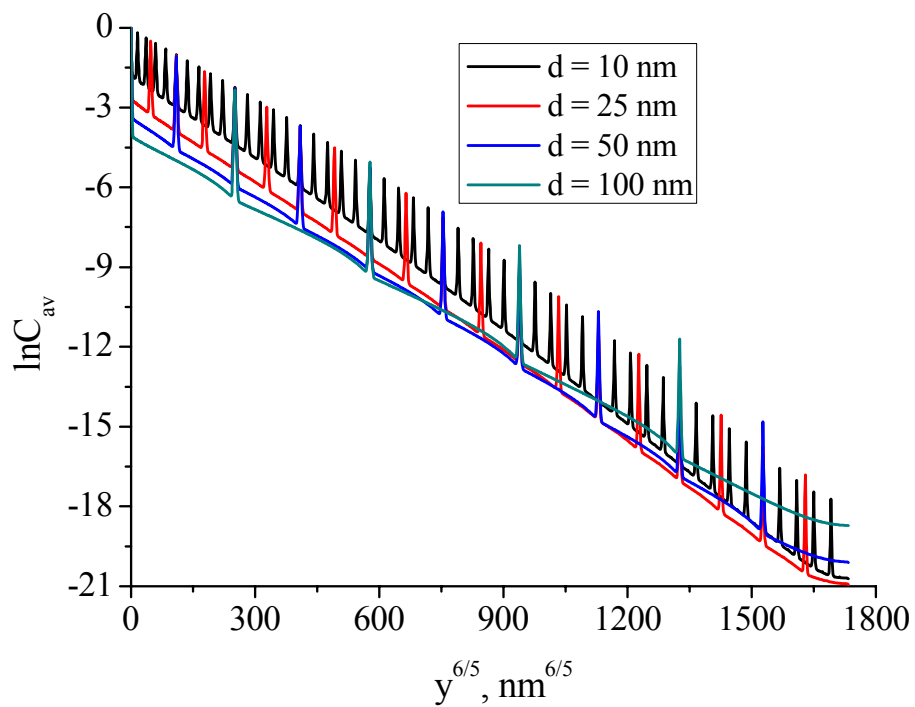


Bild 7 Diffusionsprofile für quadratische Körner unterschiedlicher Korngrößen.

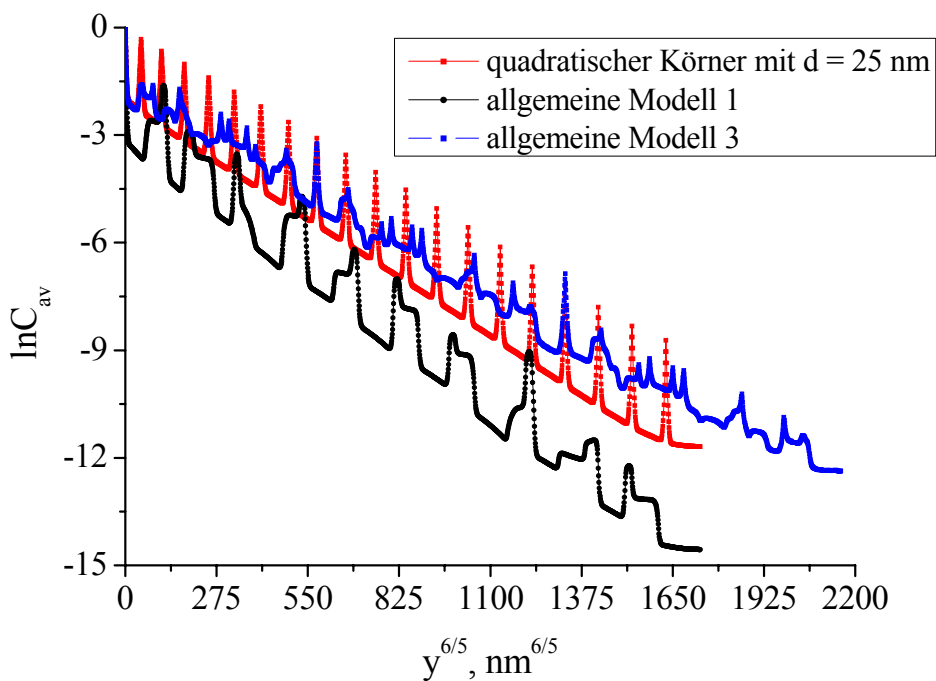


Bild 8 Diffusionsprofile für quadratische Körner und für die allgemeinen Modelle 1 und 3.

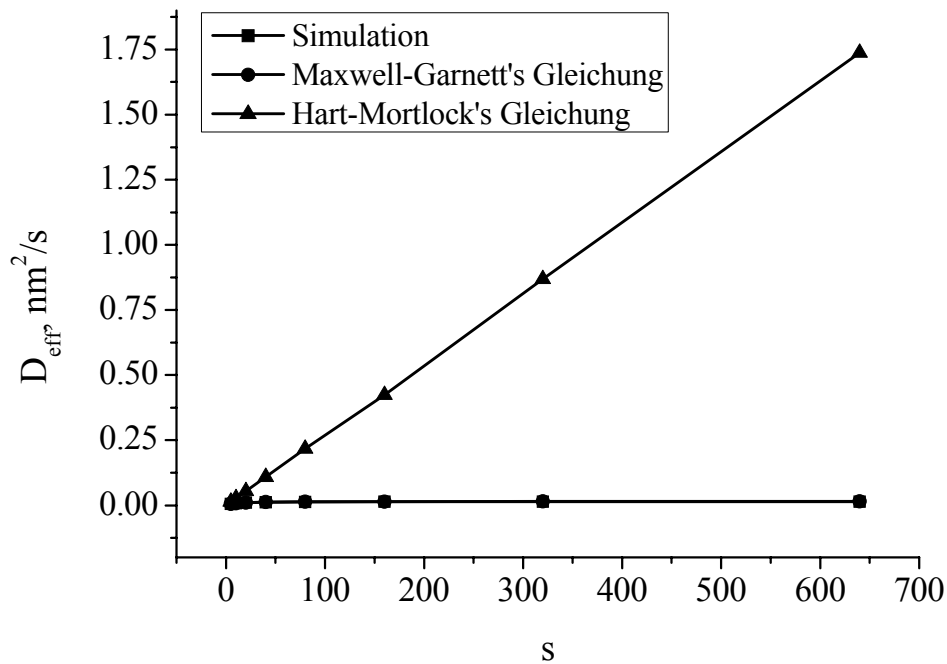


Bild 9. Vergleich der Simulation der Maxwell-Garnett-Gleichung mit der Hart-Mortlock-Gleichung.

3.3 Probleme durch Raumladungszonen

Vor kurzem wurde experimentell gezeigt [Sou05], dass die Verarmungsrandschichten der Raumladung eine sehr wichtige Rolle bei der Bestimmung des Diffusionskoeffizienten in ionischen Materialien spielen. In dieser Arbeit wurden die Diffusionsprofile für $\Delta = 10^2$ mit unterschiedlichen Verhältnissen Λ ($= D_g/D_{\text{scI}}$) sowohl im Regime vom Typ B als auch im Regime vom Typ A berechnet. In Bild 10 werden die Abhängigkeiten $\ln C_{\text{av}} = f(y^{6/5})$ für $t = 4700$ s dargestellt. Es muss angemerkt werden, dass sich die Neigung des Korngrenzanteils mit Veränderung von Λ ändert. Das bedeutet, dass, wenn die entsprechende Neigung in die Le Claire-Gleichung eingesetzt wird, D_{gb} stark überschätzt werden kann. Bei dem größten $\Lambda = 10^3$ ist D_{gb} sechsfach überschätzt. Diese große Überschätzung ist auch dann möglich, wenn verbesserte Ableitungswerte der Gleichung $\partial \ln C_{\text{av}} / \partial w^{6/5} = f(w^{6/5})$ und die Maxima der Abhängigkeit $\partial \ln C_{\text{av}} / \partial w^{6/5} = f(y^{6/5})$ benutzt werden. Auch die Ableitung der berechneten Profile wurde analysiert. Um zu verstehen, welchem Verhältnis der Diffusivitäten das Maximum der Ableitung entspricht, wurde Gleichung 12 benutzt.

Die Modellierung der Diffusionsprofile im Regime vom Typ A hat gezeigt, dass der Raumladungsbereich zur Verschiebung des kinetischen Regimes in der Zeit führt. Eine

Profilstruktur, die für das Regime vom Typ A, d. h. $L_g > d$ und $\ln C_{av} = f(y^{6/5})$ berechnet wurde, zeigt, dass das Profil zwei unterschiedliche Anteile besitzen kann: einen Korngrenzanteil und einen Volumenanteil. In Bild 11 ist ein solches Profil für $\Lambda = 10^3$ bei $t = 3 \cdot 10^6$ s dargestellt. Außerdem zeigt sich die starke Konzentrationsänderung im Modell quadratischer Körner wegen der senkrechten Korngrenzen, die von der Raumladungszone mit $D_g > D_{scl}$ (Bild 12) umgeben sind. Diese Ergebnisse zeigen, dass die Diffusion in der Raumladungszone durch die Einführung des dritten Diffusionskoeffizienten D_{scl} berücksichtigt werden muss. Die Bestimmungsfehler in D_{gb} durch die üblichen Auswertungsmethoden sind im Regime vom Typ A für das Modell paralleler Korngrenzen in

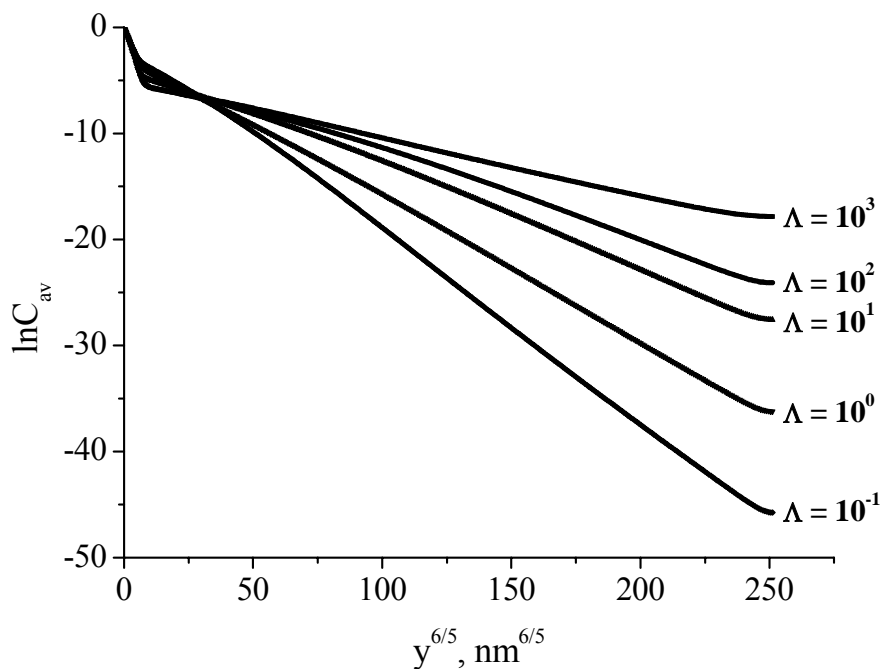


Bild 10 Diffusionsprofile für unterschiedliche Verhältnisse Λ für $\Delta = 10^2$ und $t = 4700$ s.

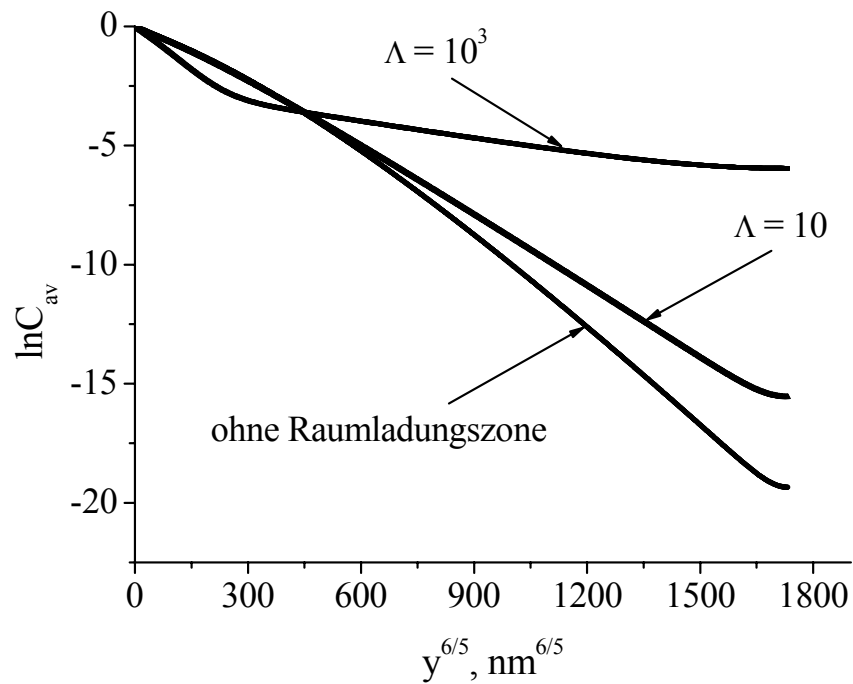


Bild 11 Vergleich der Diffusionsprofile bei unterschiedlichen Verhältnissen Λ und der Diffusionsprofile ohne Raumladungsschicht im Regime von Typ A für parallele Korngrenzen für $t = 3 \cdot 10^6$ s.

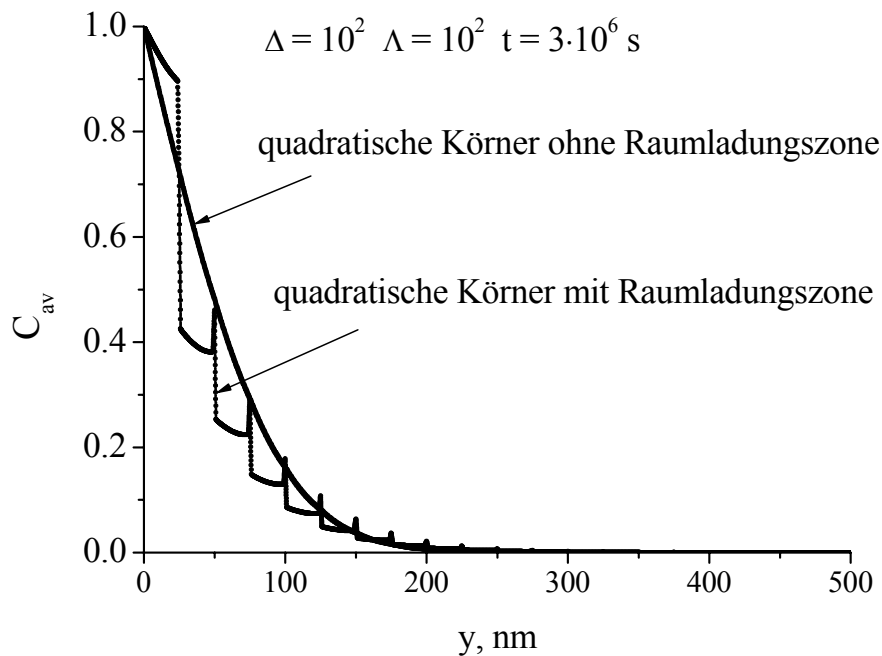


Bild 12 Vergleich der Diffusionsprofile mit und ohne Raumladungsschicht im Regime von Typ A für quadratische Körner.

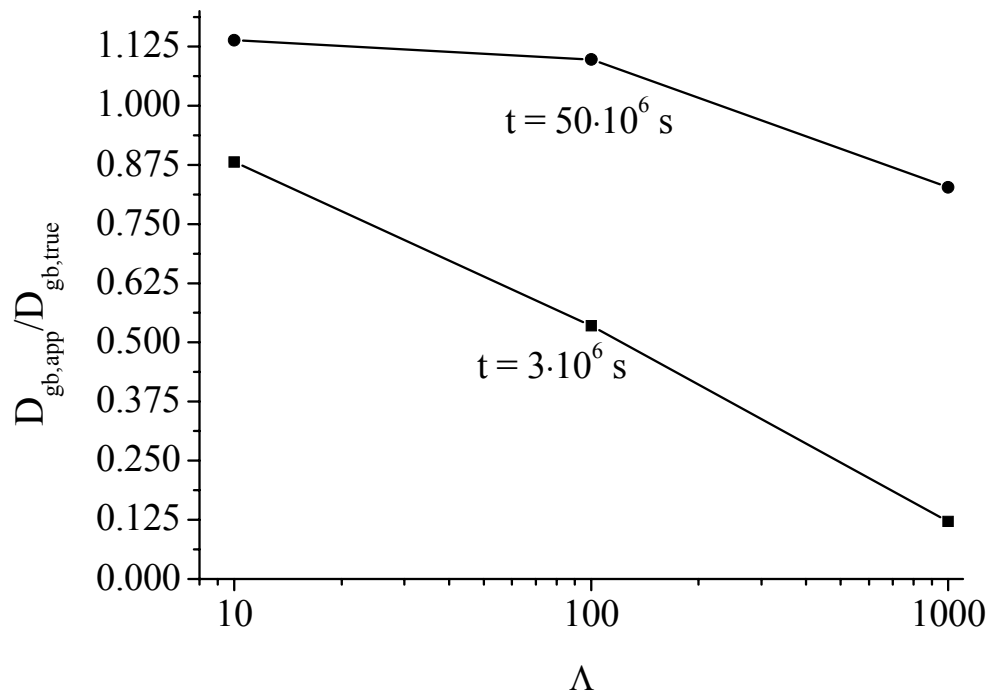


Bild 13 Bestimmungsfehler in D_{gb} durch die üblichen Auswertungsmethoden im Regime vom Typ A für das Modell paralleler Korngrenzen.

4. Zusammenfassung

In dieser theoretischen Arbeit wurden drei Effekte untersucht:

- 1) Der Effekt verschiedener Näherungen und Werte des Diffusionskoeffizienten bei kurzen Zeiten im Regime vom Typ B
- 2) Der Effekt großer und kleiner Segregationskoeffizienten im Regime vom Typ A
- 3) Der Effekt einer an beweglichen Ladungsträgern verarmten Raumladungszone, sowohl im Regime vom Typ B als auch im Regime vom Typ A

Alle drei Effekte wurden im Modell paralleler Korngrenzen (oder im Modell isolierter Grenzen) und im Modell quadratischer Körner analysiert. Außerdem wurde die Rolle der Korngrenzorientierung relativ zur Diffusionsrichtung bei kleinen Diffusionszeiten abgeschätzt.

Die Nichtlinearität der Diffusionsprofile zeigt sich bei kleinen Diffusionszeiten besonders stark und führt zu Fehlern in der Bestimmung des Korngrenzdifusionskoeffizienten (D_{gb}), falls die Le Claire-Gleichung angewendet wird. In diesem Fall wird vorgeschlagen, die Ableitung des Konzentrationsprofils zu betrachten. Die Auswertung des Maximums der Ableitung führt zur Verringerung des Fehlers in D_{gb} . Die Le Claire - Konstante kann auch der Grund der Fehler bei kleinen Diffusionszeiten sein. Die Gleichung für die Ableitung $\frac{d \ln C_{av}}{dw^{6/5}}$ in Abhängigkeit vom Wert des Parameters α lautet:

$$\frac{\partial \ln C_{av}}{\partial w^{6/5}} = -0.77 - 0.71\alpha, \text{ wenn } \alpha > 0.02.$$

Falls $\alpha < 0.02$ ist, kann die Le Claire-Konstante benutzt werden.

Folgende analytische Abhängigkeiten wurden für die Position der Maximumableitung und für seinen Wert bestimmt

$$y_{\max}^{6/5} = K \cdot t^H,$$

$$\left. \frac{\partial \ln C_{av}}{\partial y^{6/5}} \right|_{\max} = C \cdot \Delta^F \cdot t^B,$$

wobei C und K eine Funktion von Diffusionsparameter sind und B den Wert -0.34 in einem breiten Bereich der Diffusionsparameter annehmen kann.

Korngrenzen Senkrecht zur Diffusionsrichtung führen zu steilen Diffusionsprofilen, zur Vergrößerung des Neigungswinkels und zur Unterschätzung vom D_{gb} . Wenn sich die Zahl paralleler Korngrenzen der Zahl anderer Orientierungen in der realistischen Mikrostruktur nähert, ist das Modell quadratischer Körner eine gute Näherung der Mikrostruktur. Es ist interessant, dass sich die Rolle senkrechter Korngrenzen für große Zeiten verringert. So fallen im Regime vom Typ A die Diffusionsprofile, die im Modell paralleler Korngrenzen und im Modell quadratischer Körner gemessen wurden, zusammen.

Im Fall der Selbstdiffusion kann die Hart-Gleichung unabhängig von der Mikrostruktur verwendet werden, wenn die Volumendichte der Korngrenzen dem Modell paralleler Korngrenzen entspricht. Die Erhöhung des Segregationskoeffizienten führt zu einem starken Unterschied der Modelle. Die Hart-Mortlock-Gleichung kann nicht einmal für das Modell paralleler Grenzen verwendet werden, außer wenn der Segregationskoeffizient

kleiner als 20 ist. Die Maxwell-Garnett-Gleichung kann ausschließlich für das Modell quadratischer Körne angewendet werden.

Die an beweglichen Ladungsträgern verarmte Raumladungszone führt zur Transportbehinderung. Der Blockierungseffekt zeigt sich in der Verkleinerung der Profilneigung und in der Unterschätzung des D_{gb} , falls die Le Claire-Gleichung benutzt wird. Es wurde gefunden, dass das Maximum der Ableitung des Profils vom D_{gb} in der Korngrenze und D_{scl} in der Raumladungszone abhängig ist. Folglich lässt die neue Gleichung (Gl. 12) für das Maximum der Ableitung das Verhältnis D_{gb}/D_{scl} bestimmen, aber die Le Claire-Gleichung ergibt D_{gb} . Der Blockierungseffekt zeigt sich auch in der Regimeverschiebung mit der Zeit. Selbst wenn die Bedingungen des Typ A Regimes erfüllt sind, kann das Diffusionsprofil aus zwei unterschiedlichen Teilen (Volumen und Korngrenzanteile) bestehen.

References

- [Aok96] M. Aoki, Y.-M. Chiang, I. Kosacki, J.-R. Lee, H. Tuller, Y. Liu (1996), *J. Am. Ceram. Soc.*, 79 (5), 1169
- [Arg04] Ch. Argirusis, M. A. Taylor, M. Kilo, G. Borchardt, F. Jomard, B. Lesage, O. Kaitasov (2004), *Phys. Chem. Chem. Phys.*, 6, 3650
- [Ask70] J. Askill (1960), *Tracer Diffusion Data for Metals, Alloys, and Simple Oxides* (IFI/Plenum, New York)
- [Atk79] A. Atkinson, R. I. Taylor (1979), *Phil. Mag. A*, 39 (5), 581
- [Bak02] T. Bak, J. Nowotny, K. Prince, M. Rekas, C. Sorrel (2002), *J. Am. Ceram. Soc.*, 85 (9), 2244
- [Bal06] P. Balaya, J. Jamnik, J. Maier (2006), *Appl. Phys. Lett.*, 88, 062109
- [Bar05] B. Baretzky, M. D. Baro, G. P. Grabovetskaya, J. Gubisza, M. B. Ivanov, Yu. R. Kolobov, T.G. Langdon, J. Lebdvai, A.G. Lipnitskii, A. A. Mazilkin, A. A. Nazarov, J. Noguez, I. A. Ovidko, S. S. Protasova, G. I. Raab, A. Revesz, N. V. Skiba, J. Sort, M. J. Starink, B. B. Straumal, S. Surinach, T. Ungar, A. P. Zhilyaev (2005), *Rev. Adv. Mater. Sci.*, 9, 45
- [Bau85] Y. Baudon, S. Brassard, Ph. Masse (1985), *IEEE Trans. Magn.*, 21 (6), 2563
- [Bed05] K. Bedu-Amissah, J. M. Rickman, H. M. Chan, M. P. Harmer (2005), *J. Appl. Phys.*, 98, 063511
- [Bee03] R. J. Beerends, H. G. ter Morsche, J. C. van den Berg, E. M. van de Vrie (2003), *Fourier and Laplace Transforms* (Cambridge University, Cambridge)
- [Bek04] D. L. Beke, Z. Erdelyi, I. A. Szabo, G. A. Langer, G. Katona, C. Cserhati (2004), *Arc. Metall. Mater.*, 49 (2), 219
- [Bel01] I. V. Belova, G. E. Murch (2001), *Phil. Mag.*, 81 (10), 2447
- [Bel03] I. V. Belova, G. E. Murch (2003), *J. Phys. Chem. Solids*, 64, 873
- [Bel04] I. V. Belova, G. E. Murch (2004), *J. Metas. Nanocrys. Mater.*, 19, 25
- [Boc77] J. O'M. Bockris, A. K. N. Reddy (1977), *Modern Electrochemistry* (Plenum, New York)
- [Bok58] B. S. Bokshtein, I. A. Magidson, I. L. Svetlov (1958), *Fiz. Metal. Metall.*, 6 (6), 1040
- [Bro99a] U. Brossman, U. Södervall, R. Würschum, H.-E. Schaefer (1999), *NanoStr. Mater.*, 12, 871

References

- [Bro99b] U. Brossman, R. Würschum, U. Södervall, H.-E. Schaefer (1999), *J. Appl. Phys.*, 85 (11), 7646
- [Bro04] U. Brossman, G. Knöner, H.-E. Schaefer, R. Würschum (2004), *Rev. Adv. Mater. Sci.*, 6, 7
- [Cab91] J. Cabane, F. Cabane (1991), in *Interface Segregation and Related Processes*, J. Nowotny (ed.), (Trans. Tech, Zürich)
- [Chu96a] Y.-C. Chung, B. J. Wuensch (1996), *J. Appl. Phys.*, 79 (11), 8323
- [Chu96b] Y.-C. Chung, B. J. Wuensch (1996), *Mater. Lett.*, 28, 47
- [Chu00] Y.-C. Chung, C. K. Kim, B. J. Wuensch (2000), *J. Appl. Phys.*, 87 (6), 2747
- [Cla63] A. D. Le Claire (1963), *Brit. J. Appl. Phys.*, 14, 351
- [Com94] G. Comini, S. D. Guidice, C. Nonino (1994), *Finite Element Method in Heat Conduction* (Taylor&Francis, Washington)
- [Cur03] W. A. Curtin, R. E. Miller (2003), *Model. Simul. Mater. Sci. Eng.*, 11, R33
- [Def66] R. Defay, I. Prigogine (1966), *Surface Tension and Adsorption* (Longmans, London)
- [Dij81] T. van Dijk, A. J. Burggraaf (1981), *Phys. Stat. Sol. (a)*, 63, 229
- [Div01] S. Divinski, M. Lohman, Chr. Herzig (2001), *Acta Mater.*, 49, 249
- [Duf86] D. M. Duffy (1986), *J. Phys. C: Solid State Phys.*, 19, 4393
- [Eva97] J. W. Evans (1997), *J. Appl. Phys.*, 82 (2), 628
- [Fic55] A. Fick (1855), *Phil. Mag. S. 4*, 10, 30
- [Fis51] J. C. Fisher (1951), *J. Appl. Phys.*, 22 (1), 74
- [Flu92a] Handbook on Finite Element Method and FLUX-EXPERT (DT2i) (1992), *Introduction to the Finite Element Method*, Version 1.6
- [Flu92b] Handbook on Finite Element Method and FLUX-EXPERT (DT2i) (1992), *Generation of an Equation Using Flux-Expert*, Version 1.6
- [Flu92c] Handbook on Finite Element Method and FLUX-EXPERT (DT2i) (1992), *System Construction*, Version 1.6
- [Flu92d] Handbook on Finite Element Method and FLUX-EXPERT (DT2i) (1992), *Training-Generator Exercises*, Version 1.6
- [Flu92e] Handbook on Finite Element Method and FLUX-EXPERT (DT2i) (1992), *Exercise in Heat Conduction*, Version 1.6

References

- [Flu99] FLUX-EXPERT® (Simulog) (1999), *MANUEL METIER Thermique*
- [Flu00] FLUX-EXPERT® (Simulog) (2000), *User Manual*, Version 3.1
- [For60] G. E. Forsythe, W. R. Wasow (1960), *Finite-Difference Methods for Partial Differential Equations* (Wiley, New York)
- [Gal96] M. Le Gall, A. M. Huntz, B. Lesage (1996), *Phil. Mag. A*, 73 (4), 919
- [Gan00] W. Gander, W. Gautschi (2000), *BIT Num. Math.*, 40 (1), 84
- [Gar95] E. J. Garbozi, L. M. Schwartz, D. P. Bentz (1995), *Advn. Cem. Bas. Mat.*, 2, 169
- [Ger03] N. Gershenfeld (2003), *The Nature of Mathematical Modeling* (Cambridge University, Cambridge)
- [Ghe88] R. Ghez (1988), *A Primer of Diffusion Problems* (Wiley, New York)
- [Gib66] G. B. Gibbs (1966), *Phys. Stat. Sol.*, 16, K27
- [Gil76] G. H. Gilmer, H. H. Farrel (1976), *J. Appl. Phys.*, 47 (10), 4373
- [Gle89] H. Gleiter (1989), *Prog. Mater. Sci.*, 33, 223
- [Gou01a] X. Gou, J. Fleig, J. Maier (2001), *J. Electrochem. Soc.*, 148 (9), J50
- [Gou01b] X. Gou, J. Maier (2001), *J. Electrochem. Soc.*, 148 (3), E121
- [Gou02] X. Gou, W. Sigle, J. Fleig, J. Maier (2002), *Solid State Ionics*, 154-155, 555
- [Gry05] D. Gryaznov, J. Fleig, J. Maier (2005), *Defect Diff. Forum*, 237-240, 1043
- [Gug40] E. A. Guggenheim (1940), *Trans. Faraday Soc.*, 36, 397
- [Güt93] F. Güthoff, Y. Mishin, Chr. Herzig (1993), *Z. Metallk.*, 84 (8), 584
- [Harr61] L. G. Harrison (1961), *Trans. Faraday Soc.*, 57, 1191
- [Hart57] E. W. Hart (1957), *Acta Metall.*, 5, 597
- [Harte04] T. Harter, Chr. Knudby (2004), *Advn. Wat. Res.*, 27, 1017
- [Hei03] P. Heitjans, S. Indris (2003), *J. Phys.: Cond. Matter*, 15, R1257
- [Her03] Chr. Herzig, S. Divinski (2003), *Mater. Trans.*, 44 (1), 14
- [Her05] Chr. Herzig, Y. Mishin (2005), in *Diffusion in Condensed Matter*, P. Heitjans, J. Kärger (eds), (Springer, Berlin)
- [Höc94] T. Höche, P. R. Kenway, H.-J. Kleebe, M. Rühle, P. Morris (1994), *J. Am. Ceram. Soc.*, 77 (2), 339

References

- [Hun02] P. Hunter, A. Pullan (2002), *FEM/BEM Notes* (www.bioeng.auckland.ac.nz/cmiss/fembemnotes/fembemnotes.pdf, University of Auckland)
- [Jam95] J. Jamnik, M. Leonhardt, J. Maier (1995), *Solid State Ionics*, 80, 19
- [Jam97a] J. Jamnik, J. Maier (1997), *Solid State Ionics*, 94, 189
- [Jam97b] J. Jamnik, J. Maier (1997), *Ber. Bunsenges. Phys. Chem.*, 101 (1), 23
- [Jam01a] J. Jamnik, M. Leonhardt, J. Maier (2001), *Defect Diff. Forum*, 194, 1001
- [Jam01b] J. Jamnik, J. Maier (2001), *Phys. Chem. Chem. Phys.*, 3, 1668
- [Jam06] J. Jamnik, J. R. Kalnin, E. A. Kotomin, J. Maier (2006), *Phys. Chem. Chem. Phys.*, 8, 1310
- [Kab05] V. V. Kabanov, K. Zagar, D. Mihailovic (2005), *J. Exp. Theor. Phys.*, 100 (4), 715
- [Kal01] J. R. Kalnin, E. A. Kotomin, V. N. Kuzovkov (2001), *Defect Diff. Forum*, 194-199, 163
- [Kal02] J. R. Kalnin, E. A. Kotomin, J. Maier (2002), *J. Phys. Chem. Sol.*, 63, 449
- [Kau95] I. Kaur, Y. Mishin, W. Gust (1995), *Fundamentals of Grain and Interface Boundary Diffusion* (Wiley, Chichester West Sussex)
- [Kil03a] M. Kilo, C. Argirusis, G. Borchardt, R. Jackson (2003), *Phys. Chem. Chem. Phys.*, 5, 2219
- [Kil03b] M. Kilo, M. A. Taylor, Ch. Argirusis, G. Borchardt, B. Lesage, S. Weber, S. Scherrer, H. Scherrer, M. Schroeder, M. Martin (2003), *J. Appl. Phys.*, 94 (12), 7547
- [Kil04] M. Kilo, M. A. Taylor, Ch. Argirusis, G. Borchardt, S. Weber, H. Scherrer, R. A. Jackson (2004), *J. Chem. Phys.*, 121 (11), 5482
- [Kim02] S. Kim, J. Maier (2002), *J. Electrochem. Soc.*, 149 (10), J73
- [Kiu05] J. Kiussalaas (2005), *Numerical Methods in Engineering with MATLAB* (Cambridge University, Cambridge)
- [Klin99] L. Klinger, E. Rabkin (1999), *Acta Metall.*, 47, 725
- [Kne74] Z. Knesl, J. Jinoch, Z. Bilek (1974), *Czech. J. Phys. B*, 24, 347
- [Knö03] G. Knöner, K. Reimann, R. Röwer, U. Södervall, H.-E. Schaefer (2003), *Proc. Nat. Ac. Sci.*, 100 (7), 3870
- [Kop98] A. Kopylow, D. Heineman, D. Kolb (1998), *J. Phys. B: At. Mol. Opt. Phys.*, 31, 4743

References

- [Kor68] G. A. Korn, T. M. Korn (1968), *Mathematical Handbook for Scientists and Engineers* (McGraw-Hill, New York)
- [Kow00] K. Kowalski, A. Bernasik, A. Sadowski (2000), *J. Europ. Ceram. Soc.*, 20, 951
- [Lan78] R. Landauer (1978), *AIP Conf. Proc.*, 40 (1), 2
- [Lea57] D. McLean (1957), *Grain Boundaries in Metals* (Clarendon, Oxford)
- [Leh53] K. Lehovc (1953), *J. Chem. Phys.*, 21 (7), 1123
- [Leo99] M. Leonhardt, J. Jamnik, J. Maier (1999), *Electrochem. Solid State Lett.*, 2 (7), 333
- [Lep98] A. M. Lepi (1998), *Practical Guide to Finite Elements* (Marcel Dekker, New York)
- [Lev60] H.S. Levine and C.J. MacCallum (1960), *J. Appl. Phys.*, 31 (3), 595
- [Lew96] R. W. Lewis, K. Morgan, H. R. Thomas, K. N. Seetharamu (1996), *The Finite Element Method in Heat Transfer Analysis* (Wiley, Chichester West Sussex)
- [Lib94] M. Liberatore, B. J. Wuensch, I. G. Slorzano (1994), J. B. Vander Sande, *Mat. Res. Soc. Symp. Proc.*, 318, 637
- [Liu02] C.-Li Liu, Z. X. Jiang, R. I. Hedge, D. D. Sieloff, R. S. Rai, D. C. Gilmer, C. C. Hobbs, P. J. Tobin, S. Lu (2002), *J. Appl. Phys.*, 81 (8), 1441
- [Mai86] J. Maier (1986), *Ber. Bunsenges. Phys. Chem.*, 90, 26
- [Mai95] J. Maier (1995), *Prog. Solid State Chem.*, 23, 171
- [Mai03] J. Maier (2002), *Solid State Ionics*, 157, 327
- [Mai04a] J. Maier (2004), *Solid State Ionics*, 175, 7
- [Mai04b] J. Maier (2004), *Solid State Ionics*, 173, 1
- [Man97] P. S. Manning, J. D. Sirman, R. A. De Souza, J. A. Kilner (1997), *Solid State Ionics*, 100, 1
- [Mas84] P. Masse (1984), *IEEE Trans. Mag.*, 20 (5), 1885
- [Mat03] Optimization Toolbox. For Use with MatLab® (2003). *User's Guide* (The Mathworks, Inc), Version 2
- [Mat04] MatLab®. The Language of Technical Computing (2004). *Mathematics* (The Mathworks, Inc), Version 7
- [Mat06] Optimization Toolbox. For Use with MatLab® (2006). *User's Guide* (The Mathworks, Inc), Version 3

References

- [Max54] J. C. Maxwell (1954), *A Treatise on Electricity and Magnetism* (Dover Publications, New York)
- [MaxG04] J. C. Maxwell Garnett (1904), *Phil. Trans. R. Soc. London*, 203, 385
- [Meh05] H. Mehrer (2005), in *Diffusion in Condensed Matter*, P. Heitjans, J. Kärger (eds), (Springer, Berlin)
- [Mis92a] Yu. M. Mishin, I. M. Razumovski (1992), *Acta Metall. Mater.*, 40 (3), 597
- [Mis92b] Yu. M. Mishin (1992), *Phys. Stat. Sol. (a)*, 133, 259
- [Mis92c] Yu. M. Mishin (1992), *Phys. Stat. Sol. (b)*, 174, 335
- [Mis95] Y. Mishin, Chr. Herzig (1995), *NanoStr. Mat.*, 6, 859
- [Mis97] Y. Mishin, Chr. Herzig, J. Bernardini, W. Gust (1997), *Int. Mater. Rev.*, 42 (4), 155
- [Mis99] Y. Mishin, Chr. Herzig (1999), *Mater. Sc. Eng. A.*, 260, 55
- [Mis01] Y. Mishin, W. Gust (2001), *Ionics*, 7, 247
- [Mor60] A. J. Mortlock (1960), *Acta Metall.*, 8, 132
- [Mot39] N. F. Mott (1939), *Proc. R. Soc. London*, 171, 27
- [Moy91] E. G. Moya, F. Moya, J. Nowotny (1991) in *Interface Segregation and Related Processes*, J. Nowotny (ed.), (Trans. Tech, Zürich)
- [Nak98] A. Nakano, M. E. Bachlechner, T. J. Campbell, R. K. Kalia, A. Omeltchenko, K. Tsuruta, P. Vashishta, S. Ogata, I. Ebbsjö, A. Madhukar (1998), *IEEE Comp. Sc. Eng.*, 5 (4), 68
- [Nie78] L. E. Nielsen (1978), *Predicting the Properties of Mixtures* (Marcel Dekker, New York)
- [Prei05] W. Preis, W. Sitte (2005), *J. Appl. Phys.*, 97, 093504
- [Pres02] W. L. Press, S. A. Teukolsky, W. T. Vetterling, B. P. Flannery (2002), *Numerical Recipes in C++: The Art of Scientific Computing* (Cambridge University, Cambridge)
- [Pro96a] D. Prot, C. Monty (1996), *Phil. Mag. A*, 73 (4), 899
- [Pro96b] D. Prot, M. Le Gall, B. Lesage, A. M. Huntz, C. Monty (1996), *Phil. Mag. A*, 73 (4), 935
- [Qu03] F. Qu, A. M. Alcable, C. G. Almeida, N. O. Dantas (2003), *J. Appl. Phys.*, 94 (5), 3462
- [Sak90] T. Sakiyama, Y. Matsushita, Y. Shiinoki, T. Yano (1990), *J. Food Eng.*, 11, 317

References

- [Schm98] H. Schmalzried, S. Smolin (1998), *Ber. Bunsenges. Phys. Chem.*, 102 (12), 1740
- [Scho39] W. Schottky (1939), *Z. Phys.*, 113, 367
- [She63] P. G. Shewmon (1963), *Diffusion in Solids* (McGraw-Hill, New York)
- [Sha98] D. Shaw, T. L. Shaw (1998), *J. Appl. Phys.*, 84 (7), 3586
- [Sima95] SIMAIL (Simulog) (1995), *Getting Started*, Version 6.0-5
- [Sima97] SIMAIL (Simulog) (1995), *User's Manual*, Version 6.2
- [Simu02] FLUX-EXPERT® (Simulog) (2002), Documentation on diffusion equation DIFFUS_2D.EQU supplied together with the main installation files
- [Simu06] <http://www.simulog.fr> (2006)
- [Sou03] A. De Souza, J. Fleig, R. Merkle, J. Maier (2003), *Z. Metallkd.*, 94, 3
- [Sou04] R. A. De Souza, M. Martin (2004), *Arch. Metal. Mat.*, 49(2), 431
- [Sou05] R. A. De Souza, J. Zehnpfenning, M. Martin, J. Maier (2005), *Solid State Ionics*, 176, 1465
- [Sut95] A. P. Sutton, R. W. Balluffi (1995), *Interfaces in Crystalline Materials* (Clarendon, Oxford)
- [Suz61] T. Suzuoka (1961), *Trans. Jap. Inst. Metals*, 2, 25
- [Swi97] T. P. Swiler, V. Tikare, E. A. Holm (1997), *Mater. Sci. Eng. A*, 238, 85
- [Sza90] I. A. Szabo, D. L. Beke, F. J. Kedves (1990), *Phil. Mag.*, 62 (2), 227
- [Szt92] P. Sztulzaft, P. Masse, Y. Du Terrail (1992), *IEEE Trans. Magn.*, 28 (2), 1785
- [Tay04] M. A. Taylor, Chr. Argirusis, M. Kilo, G. Borchardt, K.-D. Luther, W. Assmus (2004), *Solid State Ionics*, 173, 51
- [Tay05] M. A. Taylor, M. Kilo, G. Borchardt, S. Weber, H. Scherrer (2005), *J. Eur. Ceram. Soc.*, 25, 1591
- [Tho97] H. R. Thomas, Z. Thou (1997), *Int. J. Num. Meth. Eng.*, 40, 3865
- [WanJ04] J. Y. Wang, E. J. Mittemeijer (2004), *J. Mater. Res.*, 19 (11), 3389
- [WanR05] R.-V. Wang, P. C. MacIntyre (2005), *J. Appl. Phys.* 97, 023508
- [Wei65] H. F. Weinberger (1965), *A First Course in Partial Differential Equations* (Ginn and Company, Massachusetts)
- [Whi54] R. T. P. Whipple (1954), *Phil. Mag.*, 45, 1225

References

- [Wür03] R. Würschum, S. Herth, U. Brossman (2003), *Adv. Eng. Mater.*, 5 (5), 365
- [Yan77] M. F. Yan, R. M. Cannon, H. K. Bowen, R. L. Coble (1977), *J. Am. Ceram. Soc.*, 60 (3-4), 120
- [Yas97] I. Yasuda, K. Ogasawara, M. Hishinuma (1997), *J. Am. Ceram. Soc.*, 80 (12), 3009
- [Yoo02] H.-I. Yoo, B. J. Wuensch, W. T. Peturskey (2002), *Solid State Ionics*, 150, 207
- [Zhu01] J. Zhu, L.-Q. Chen, J. Shen, V. Tikare (2001), *Comp. Mater. Sci.*, 20, 37

Curriculum Vitae

Name: Denis Gryaznov

Date of birth: 05.03.1977

Place of birth Riga, Latvia

Work experience

Baltic Scientific Instruments Ltd., Riga, Latvia 1998-2002

Research Assistant

Responsibility: Preparation and measurements of electrical properties of semiconductor x- and γ -ray radiation detectors

Education

1) Max Planck Institute for Solid State Research, Stuttgart 2002-2006

PhD Student

Dissertation: *Simulation of Diffusion in Nanocrystalline Materials: Continuum Approach*

2) Transport and Telecommunication Institute 1999-2001

Masters Degree

3) Riga Aviation University 1995-1999

Bachelors Degree

Publications

D. Gryaznov, J. Fleig, J. Maier, *Numerical Study of Grain Boundary Diffusion in Nanocrystalline Materials*, Defect and Diffusion Forum, Vols. 237-240 (2005), pp. 1043-148

D. Gryaznov, J. Fleig, J. Maier, *Numerical Study of Grain Boundary Diffusion in Nanocrystalline Materials Including Blocking Space Charges*, Solid State Ionics, Vol. 177 (2006), pp. 1583-1586

D. Gryaznov, J. Fleig, J. Maier, *Numerical Study of Grain Boundary Diffusion: Size Effects*, Diffusion Fundamentals, Vol. 2 (2005), pp. 49 (<http://www.uni-leipzig.de/diffusion/journal/>)

R. A. Evarestov, E. A. Kotomin, Yu. A. Mastrikov, **D. Gryaznov**, E. Heifets, J. Maier, *Comparative DFT LCAO and plane wave calculations of LaMnO₃ surfaces*, Phys. Rev. B, Vol. 72 (2005), pp. 214411

D. Fuks, L. Bakaleinikov, E. A. Kotomin, J. Felsteiner, A. Gordon, R. A. Evarestov, **D. Gryaznov**, J. Maier, *Thermodynamics Stability and Disorder in La_cSr_{1-c}MnO₃ solid solutions*, Solid State Ionics, Vol. 177 (2006), pp. 217-222

A. Schröder, J. Fleig, **D. Gryaznov**, J. Maier, W. Sitte, *Quantitative Model of Electrochemical Ostwald Ripening and Its Application to the Time-Dependent Electrode Potential of Nanocrystalline Metals*, J. Phys. Chem. B, Vol. 110 (2006), pp. 12274-12280